STUDIES OF THE EQUATION OF STATE AND ELASTICITY OF MANTLE MINERALS

Thesis by
Emily A. Hamecher

In Partial Fulfillment of the Requirements for the
Degree of
Doctor of Philosophy

CALIFORNIA INSTITUTE OF TECHNOLOGY
Pasadena, California
2013
(Defended January 31, 2013)

DEDICATION

This thesis is dedicated to my late father, Thomas L. Hamecher, who inspired my love and appreciation of the natural world, and my passion and curiosity for understanding how things work.

ACKNOWLEDGEMENTS

I wish to thank the members of my thesis advisory committee: First, my thesis advisor, Paul Asimow, who has been an extremely patient and understanding supervisor. I thank Jennifer Jackson for her encouragement and mentorship through good times and bad, for always having time to take me for coffee at Peet's, and, most of all, for her friendship. I thank George Rossman for his passion for mineralogy and teaching, and for his guidance in both academic and career matters. I thank Jason Saleeby for his enthusiasm and expertness in the field and for interesting conversations.

I wish to thank Paula Antoshechkina for all of her hard work, patience, and understanding; this thesis would not have been possible without her.

I thank my parents for kindling my love of the outdoors, camping, and geology as a small child. I thank my mother for her continuing love and support.

I have made many wonderful friends while at Caltech. I thank them all for making grad school bearable. I thank June Wicks for being an awesome office mate and always having a hug for me when I needed one. I thank Melanie Channon for her friendship and commiseration. I thank Aaron Wolf for all of the laughs, and all of the patient explanations of things I didn't understand. I thank Frank and Karl for their love and encouragement. Finally, I thank all of the friends I've made while living in the L.A. area; you have helped me keep things in perspective.

ABSTRACT

Because the Earth's upper mantle is inaccessible to us, in order to understand the chemical and physical processes that occur in the Earth's interior we must rely on both experimental work and computational modeling. This thesis addresses both of these geochemical methods. In the first chapter, I develop an internally consistent comprehensive molar volume model for spinels in the oxide system FeO-MgO-Fe_2O_3-Cr_2O_3-Al_2O_3-TiO_2. The model is compared to the current MELTS spinel model with a demonstration of the impact of the model difference on the estimated spinel-garnet lherzolite transition pressure. In the second chapter, I calibrate a molar volume model for cubic garnets in the system SiO_2-Al_2O_3-TiO_2-Fe_2O_3-Cr_2O_3-FeO-MnO-MgO-CaO-Na_2O. I use the method of singular value analysis to calibrate excess volume of mixing parameters for the garnet model. The implications the model has for the density of the lithospheric mantle are explored. In the third chapter, I discuss the nuclear inelastic X-ray scattering (NRIXS) method, and present analysis of three orthopyroxene samples with different Fe contents. Longitudinal and shear wave velocities, elastic parameters, and other thermodynamic information are extracted from the raw NRIXS data.

TABLE OF CONTENTS

Dedication iii

Acknowledgements iv

Abstract v

Table of Contents vi

List of Tables and Figures vii

Introduction 1

Chapter 1: The molar volume of FeO-MgO-Fe_2O_3-Cr_2O_3-Al_2O_3-TiO_2 spinels 5

Supplement 1 57

Supplement 2 59

Supplement 3 90

Supplement 4 120

Supplement 5 121

Supplement 6 122

Chapter 2: The molar volume of cubic garnets in the system SiO_2-Al_2O_3-TiO_2-Fe_2O_3-Cr_2O_3-FeO-MnO-MgO-CaO-Na_2O 131

Supplement 1 191

Supplement 2 198

Supplement 3 227

Supplement 4 229

Chapter 3: Nuclear inelastic X-ray scattering of (Mg,Fe)SiO_3 orthoenstatites 230

LIST OF TABLES AND FIGURES

Chapter 1

Table 1. Summary data table 39

Table 2. Standard state end-member molar volume 40

Table 3. Standard state end-member coefficient of thermal expansion 40

Table 4. Standard state end-member bulk modulus and pressure derivative 41

Table 5. Model parameters 42

Figure 1. Compositional coverage of the data used in model calibration 47

Figure 2. Compositional coverage of the data used in model calibration 48

Figure 3. Order-dependence of observed volume vs. ordering term 49

Figure 4. Model volume vs. measured volume 50

Figure 5. Model residuals vs. measured volume 51

Figure 6. Model volumes and data in the $MgAl_2O_4$-$MgCr_2O_4$-$FeCr_2O_4$-$FeAl_2O_4$ reciprocal square 52

Figure 7. Excess model volume in the $MgAl_2O_4$-$MgFe_2O_4$-Fe_3O_4-$FeAl_2O_4$ reciprocal square and along the $MgAl_2O_4$ – Fe_3O_4 binary 53

Figure 8. Excess model volume along the Fe_3O_4 – Fe_2TiO_4 binary 54

Figure 9. Model volume along the $FeCr_2O_4$ – Fe_3O_4 binary 55

Figure 10. Order variable s_0 vs. temperature for pure $MgFe_2O_4$ data 56

Chapter 2

Table 1. Model components 172

Table 2. Summary data table 173

Table 3. Standard state end-member properties 175

Table 4. Model parameters 176

Figure 1. Previous models along grossular-pyrope binary 181

Figure 2. Thermal pressure fitting 182

Figure 3. K_{oT} vs. R_x/R_y 183

Figure 4. Debye temperature vs. R_x/R_y 183

Figure 5. C_{vm} vs. R_x/R_y 184

Figure 6. V_o vs. R_x/R_y 184

Figure 7. Excess volume models and data along binary joins 185

Figure 8. Model residuals vs. measured volume 186

Figure 9. Excess volume models and data on grossular-pyrope join 187

Figure 10. Excess volume models and data on grossular-almandine join 187

Figure 11. Density comparisons with pMELTS 188

Figure 12. Density comparisons with Klemme et al. (2009) 189

Figure 13. Density comparisons with Stixrude and Lithgow-Bertelloni (2011) 189

Figure 14. Density comparisons with Stixrude and Lithgow-Bertelloni (2011) 190

Chapter 3

Table 1. Debye sound velocities and elastic parameters 247

Table 2. Thermodynamic parameters 248

Figure 1. Experimental set-up 252

Figure 2. Raw NRIXS energy spectra 253

Figure 3. Partial phonon density of states 254

Figure 4. Debye velocity fitting 255

Figure 5. Velocity vs. density..... 256

Figure 6. Elastic moduli vs. density 257

Figure 7. Select thermodynamic parameters extracted from PDOS 258

Figure 8. Energy dependence on mean force constant..... 259

Figure 9. Energy dependence of vibrational contribution to specific heat..... 260

INTRODUCTION

Thermodynamic modeling of mineral solid solutions facilitates calculations of phase equilibrium in the Earth's mantle. Mantle melting models include constraints from phase equilibria experiments, calorimetry, and crystal chemistry to indirectly explore mantle processes, as well as the physical properties of solid and liquid phases as a function of pressure, temperature, and composition. MELTS (Ghiorso and Sack 1995; Ghiorso et al. 2002; Asimow et al. 2004) is a software package that models mantle melting. The xMELTS model (Ghiorso et al. 2007) extends the capabilities of MELTS to pressures and temperatures commensurate with those at the base of the transition zone in the Earth's mantle. Future work on xMELTS will incorporate a comprehensive thermodynamic model for garnet and pyroxene solid solutions. The goal is to create a model that reproduces phase relations for temperature and pressure conditions at depths from the shallow crust to the top of the lower mantle, for all compositions of natural magma and coexisting solids.

Garnet is a particularly important phase involved in partial melting of the upper mantle because it controls partitioning of major and minor elements at pressures greater than 3 GPa. Chromium is a minor but significant component of mantle rocks because its presence increases the spinel stability field relative to the garnet and pyroxene stability fields at high pressures. Models incorporating Cr into garnet solid solutions have been missing from MELTS, requiring that simulations only be performed for Cr-free bulk compositions and preventing the modeling of the spinel-garnet phase transition. This type of model is needed to provide constraints on the energetics of mixing in garnet, and to extend the model to conditions found at the base of the transition zone. Additional minor

elements (e.g., Ti and Na) should also be included in a thermodynamic model for mantle garnets and pyroxenes.

Internally consistent molar volume models are required before the full activity-composition models for garnet and pyroxene can be recalibrated. Because most constraints on the activity of garnet and pyroxene at high-*P* are derived from experiments with coexisting spinel, we must be confident in the ability of our spinel model to realistically reproduce thermodynamic behavior over all applicable compositions. Additionally, producing a spinel molar volume model calibrated with recent in situ high-*P, T* diffraction data is crucial to our ability to accurately model the spinel–garnet transition in Earth's upper mantle. A new garnet volume model calibrated with recent in situ high-*P*, *T* diffraction data is also critical for accurately modeling key mineralogical transitions in the mantle, e.g., the spinel–garnet transition and the mantle transition zone. Above 5 GPa a majorite component is an essential part of any thermodynamic model of mantle garnets, which to be useful must accurately predict garnet stability with respect to spinel, pyroxene, perovskites, and melt.

Mineral physics experiments give us insight into the elastic behavior of mantle minerals. Determinations of sound velocities of mantle minerals, such as orthopyroxene, allow us to map chemical and thermal properties of the Earth's interior to seismic observations. Ultrasonic and Brillouin scattering measurements often disagree with each other and offer a limited amount of information about the material being studied. Newer synchrotron-based spectroscopic methods, like nuclear resonant inelastic X-ray scattering (NRIXS), allow us to nondestructively probe the properties of very small samples of

material, and offer the added benefit of providing additional thermodynamic information about the material.

In this thesis I explore the physical and chemical properties of three upper mantle minerals—spinel, garnet, and orthopyroxene. In the first chapter, I develop a comprehensive model of molar volume for spinels in the oxide system FeO-MgO-Fe_2O_3-Cr_2O_3-Al_2O_3-TiO_2. In the second chapter, I calibrate a model of molar volume for cubic garnets in the system SiO_2-Al_2O_3-TiO_2-Fe_2O_3-Cr_2O_3-FeO-MnO-MgO-CaO-Na_2O. In the final chapter, I analyze NRIXS data for three samples of orthopyroxene with variable amounts of Fe, and determine longitudinal and shear wave velocity and additional thermodynamic parameters.

REFERENCES

Asimow PD, Dixon JE, Langmuir CH (2004) A hydrous melting and fractionation model for mid-ocean ridge basalts: Application to the Mid-Atlantic Ridge near the Azores. Geochem Geophys Geosyst 5. doi:10.1029/2003GC000568

Ghiorso MS, Sack RO (1995) Chemical mass transfer in magmatic processes IV. A revised and internally consistent thermodynamic model for the interpolation and extrapolation of liquid-solid equilibria in magmatic systems at elevated temperatures and pressures. Contrib Mineral Petrol 119:197–212

Ghiorso MS, Hirschmann MM, Reiners PW, Kress III VC (2002) The pMELTS: A revision of MELTS for improved calculation of phase relations and major element partitioning related to partial melting of the mantle to 3 GPa. Geochem Geophys Geosyst 3. doi:10.1029/2001GC000217

Ghiorso MS, Hirschmann MM, Grove TL (2007) xMELTS: A thermodynamic model for the estimation of magmatic phase relations over the pressure range 0-30 GPa and at temperatures up to 2500 °C. Eos Trans Am Geophys Union 88(52), Fall Meet Suppl Abstr V31C-0608

Chapter 1

THE MOLAR VOLUME OF FeO-MgO-Fe_2O_3-Cr_2O_3-Al_2O_3-TiO_2 SPINELS

Emily A. Hamecher

Paula M. Antoshechkina

Mark S. Ghiorso

Paul D. Asimow

This chapter has been published as: Hamecher EA, Antoshechkina PM, Ghiorso MS, Asimow PD (2013) The molar volume of FeO-MgO-Fe_2O_3-Cr_2O_3-Al_2O_3-TiO_2 spinels. Contrib Mineral Petrol 165:25-43. doi:10.1007/s00410-012-0790-0

ABSTRACT

We define and calibrate a new model of molar volume as a function of pressure, temperature, ordering state, and composition for spinels in the supersystem $(Mg,Fe^{2+})(Al,Cr,Fe^{3+})_2O_4 – (Mg,Fe^{2+})_2TiO_4$. We use 832 X-ray and neutron diffraction measurements performed on spinels at ambient and in situ high-*P*, *T* conditions to calibrate end-member equations of state and an excess volume model for this system. The effect on molar volume of cation ordering over the octahedral and tetrahedral sites is captured with linear dependence on Mg^{2+}, Al^{3+}, and Fe^{3+} site occupancy terms. We allow standard state volumes and coefficients of thermal expansion of the end members to vary within their uncertainties during extraction of the mixing properties, in order to achieve the best fit. Published equations of state of the various spinel end members are analyzed to obtain optimal values of the bulk modulus and its pressure derivative, for each explicit end member. For any spinel composition in the supersystem, the model molar volume is obtained by adding excess volume and cation order-dependent terms to a linear combination of the five end-member volumes, estimated at pressure and temperature using the high-*T* Vinet equation of state. The preferred model has a total of nine excess volume and order-dependent parameters and fits nearly all experiments to within 0.02 J/bar/mol, or better than 0.5% in volume. The model is compared to the current MELTS spinel model with a demonstration of the impact of the model difference on the estimated spinel–garnet lherzolite transition pressure.

INTRODUCTION

Spinel-group minerals are commonly found in igneous and metamorphic rocks in the Earth's crust and upper mantle and are frequently used as petrogenetic indicators (Buddington and Lindsley 1964; Sack 1982; Dick and Bullen 1984; Ghiorso and Sack 1991; Ghiorso and Evans 2008). Spinel is a significant reference phase for high-pressure thermodynamic solution models of melts and of other solid phases, because it contains several key components of upper mantle assemblages at appreciable concentrations and because high-quality activity-composition models for spinels have been constructed (Sack 1982; Nell and Wood 1989; Sack and Ghiorso 1991a, b; Kessel et al. 2003). Beyond their petrologic significance, natural and synthetic spinel-group phases have numerous applications in the material sciences (e.g., Taberna et al. 2006; Yang et al. 2007).

The prevalence of spinels can be partly explained by the variety of cations of different valence that can be accommodated within the structure. While the spinel structure is quite simple, its solid solution behavior is complex. Cubic spinels (space group *Fd3m*) have the stoichiometry AB_2O_4, where A and B are cations with, most often, 2+ and 3+ charge, respectively, although substitution toward end members where A is 4+ and B is 2+ can occur. Additional complexity arises due to the existence of two distinct cation coordination environments and the ability of a wide array of cations to distribute themselves over the octahedral and tetrahedral crystallographic sites. "Normal" spinels are defined as having the A ion in the tetrahedral site and both B ions in the two identical octahedral sites. Perfectly "inverse" spinels have one B ion per formula unit occupying the tetrahedral site, with one A and one B ion residing in the octahedral sites. For many

choices of A and B, spinel solid solutions can adopt ordering states at any point along this continuum. A number of models have described the extent of such ordering in spinels (Callen et al. 1956; O'Neill and Navrotsky 1983, 1984; Sack and Ghiorso 1991a) in terms of the energetics of the cation ordering reactions.

Molar volume is an important thermodynamic quantity at high pressures, both when using spinels to infer petrogenetic information from high-pressure rocks and particularly when using spinels from high-pressure experiments to define chemical potentials in coexisting phases. Because pressures of interest in spinel-bearing experiments range up to at least 3 GPa (3×10^4 bar), differences in volume of only 0.03 J/bar/mol (i.e., 0.3 cm^3/mol, or ≤1% of typical spinel molar volumes) yield differences of 1 kJ/mol in chemical potentials, which is often the accuracy level sought in calibrations of solid- and liquid-solution models. A model of spinel volumes with the necessary accuracy needs to account not only for equations of state of pure end members and considerable deviation from ideal mixing of compositions, but also for significant effects of ordering state on the volume (O'Neill and Navrotsky 1983; Hazen and Navrotsky 1996). Differences in ionic size, charge, and/or coordination environment can contribute to non-ideal behavior (O'Neill and Navrotsky 1984). Pressure, in addition to temperature and composition, can strongly affect cation-ordering state, which in turn affects physical properties, including the elastic moduli (Hazen and Navrotsky 1996). The complexities due to cation ordering over distinct crystallographic sites, along with the wide range of stable compositions of spinels, create difficulties in modeling their thermodynamic behavior, including molar volume (Sack and Ghiorso 1991a). Generally, studies are restricted to subsystems of spinels, e.g., along a solid-solution binary. While

limiting the system of interest usually allows one to recover the data used in calibration, discrepancies exist between various end-member models; i.e., a particular spinel end member may be assigned different model volumes in fits to adjacent subsystems. Hence currently available models are inadequate for modeling of volumes over the full compositional range of spinels formed in the Earth's upper mantle. It is necessary to devise a comprehensive model applicable to the entire chemical system of the upper mantle.

In this work, we present a model of molar volumes of stoichiometric spinels containing the oxide components FeO-MgO-Fe_2O_3-Cr_2O_3-Al_2O_3-TiO_2; the cations in this system account for at least 98% of the compositional range of natural spinels (Sack 1982). Our chosen set of independent compositional model end members is spinel sensu stricto ($MgAl_2O_4$), hercynite ($FeAl_2O_4$), magnetite (Fe_3O_4), chromite ($FeCr_2O_4$), and ulvöspinel (Fe_2TiO_4). Dependent end members in this system—magnesiochromite ($MgCr_2O_4$), magnesioferrite ($MgFe_2O_4$), and qandilite (Mg_2TiO_4)—are formed from linear combinations of the independent end members. As written, these are *compositional* end members only, and the order in which the cations are written should not be taken to imply an ordering state over tetrahedral and octahedral sites. Within the MELTS software, end-member thermodynamic quantities are calculated for the standard state structural arrangement, and mixing properties are referenced to the end-member values. For calibration of the volume, we are therefore obliged to use end members with the ordering states adopted by Sack and Ghiorso (1991a, b), i.e., normally ordered $FeCr_2O_4$ and Fe_2TiO_4, almost perfectly normal $MgAl_2O_4$ and $FeAl_2O_4$, and near-perfect inversely ordered Fe_3O_4. Note that this constraint did not apply to Sack and Ghiorso's formulation

of the activity-composition models, as the adopted end-member heat capacity functions (taken from the internally consistent database of Berman 1988) were independent of ordering state. In fact, the Sack and Ghiorso (1991a, b) model was calibrated using perfectly inverse ordered components; normally ordered and standard state values for the compositional components were inferred from the fitted parameters.

Our primary motivation in this work is to develop a comprehensive spinel molar volume model for use in calibration of activity-composition models of garnet and pyroxene solid solutions. The thermodynamic models, along with a new silicate liquid equation of state (Ghiorso 2004a, 2004b, 2004c; Ghiorso and Kress 2004), will be incorporated into the next generation MELTS (Ghiorso and Sack 1995; Ghiorso et al. 2002; Asimow et al. 2004) model, xMELTS (Ghiorso et al. 2007). The new solid solution models will include some minor components, including Ti^{4+} and Cr^{3+}. Because most constraints on the activity of garnets and pyroxenes at high-*P* are derived from experiments with coexisting spinels, we must be confident in the ability of our spinel model to realistically reproduce thermodynamic behavior over the entire applicable range of compositions. Additionally, producing a spinel molar volume model calibrated with recent in situ high-*P, T* X-ray and neutron diffraction data is crucial to our ability to accurately model the spinel–garnet transition in Earth's upper mantle. For example, we recently calibrated Cr-Al exchange equilibria for garnet and spinel (Hamecher et al. 2009). When this new calibration is used with the current MELTS model, a region of garnet–spinel coexistence in lherzolites is predicted with width in pressure comparable to experimental constraints. The transition occurs, however, at the unexpectedly low pressure of ~1.7 GPa, though this is not entirely due to the introduction of Cr to the

system, as discussed below. The improved model of spinel molar volume presented here will enable coupled recalibration of the garnet and pyroxene models to match both the absolute pressure and width of this key transition in mantle lithology.

In this chapter, we first discuss previous models of spinel molar volume, with attention to the ranges of composition they cover and inconsistencies among the models. We then present the X-ray and neutron diffraction and ultrasonic data used in our calibration, and the formulation of our model in terms of the components and ordering variables of the spinel solid solution model of Sack and Ghiorso (1991a, b). The calibration strategy we used to estimate the parameters of the model and assess goodness of fit to the data is outlined. Finally, we compare the final model to models from the literature and present an estimate of the magnitude of the impact of the new model on MELTS calculations and other high-pressure thermodynamic inferences.

PREVIOUS MODELS

Several models for the molar volume of spinel group minerals have been proposed. However, most of these models are restricted to binary subsystems. Furthermore, there are discrepancies between models with corresponding end members. In this section we present examples of previous models of spinel molar volume.

The current molar volume model for spinels in MELTS and pMELTS covers the same compositional range as our proposed model. There is no mention of volume in Sack and Ghiorso (1991a) or Sack and Ghiorso (1991b) and, indeed, initially the entire system was assumed to have zero volume of mixing. However, before being put to use for calculation or calibration of other phases, the model was modified to include asymmetric

excess volume of mixing terms along the Fe_3O_4–Fe_2TiO_4 join (Ghiorso 1990; Ghiorso and Sack 1991): an excess model of the form $-0.1250X^2_{Fe3O4}X_{Fe2TiO4} + 0.1018X_{Fe3O4}X^2_{Fe2TiO4}$ J/bar/mol was fitted to the molar volume data of Lindsley (1965). This excess term was used in calibration of subsequent models including the pyroxene family (Sack and Ghiorso 1994b), the MELTS liquid model (Ghiorso and Sack 1995), and the pMELTS liquid model (Ghiorso et al. 2002) and is present in all currently supported versions of the MELTS code. As part of the provisional xMELTS liquid model calibration, the spinel volume model was extended to higher pressures by fitting the formula for the high-T Vinet equation of state (see Eq. 6 below) for $MgAl_2O_4$ and Fe_3O_4 to the Berman (1988) polynomial equation of state (see Ghiorso 2004b). Since standard state volume data for other spinel components are not given in Berman (1988), P- and T-coefficients for $MgAl_2O_4$ or Fe_3O_4 were assigned to the remaining end members. There is now an opportunity to simultaneously optimize both standard state and mixing terms in order to form an internally consistent general spinel-system volume model for use in future calibration and calculation efforts. Our recalibration includes refinement of the asymmetric terms along the Fe_3O_4–Fe_2TiO_4 join alongside consideration of all other possible binary excess terms in the composition space.

Oka et al. (1984) fit their molar volume data along the $MgAl_2O_4$–$MgCr_2O_4$ binary to an asymmetric regular solution model $W_{AlAlCr}(1 - X_{Cr})^2X_{Cr} + W_{AlCrCr}(1 - X_{Cr})X_{Cr}^2$ (where X_{Cr} is mole fraction $MgCr_2O_4$ for this binary). For their best-characterized data, synthesized at 1250 °C, they obtained excess volume parameters $W_{AlAlCr} = 0.0524(91)$ and $W_{AlCrCr} = 0.0040(92)$ J/bar/mol. On the other hand, average parameters for fits to three different sets of synthesis temperatures are $W_{AlAlCr} = 0.0504$ and $W_{AlCrCr} =$

0.0182 J/bar/mol (uncertainties not stated). Both versions of the model show positive deviation from ideality along the entire binary.

Doroshev et al. (1997) also investigated the molar volume of the $MgAl_2O_4$–$MgCr_2O_4$ subsystem. Phase equilibria experiments containing Cr-rich garnets were performed, and the multiphase products were analyzed by electron microprobe and X-ray diffraction. Doroshev et al. also adopted an asymmetric regular-solution excess volume model, with the largest deviation from ideality in the Al-rich part of the join. Contrary to the previous study, however, Doroshev et al. found negative deviation from ideality in the Cr-rich region. The excess volume parameters are $W_{\mathrm{AlAlCr}} = 0.0722(90)$ and $W_{\mathrm{AlCrCr}} = -0.0483(75)$ J/bar/mol. The authors attribute the difference between the models to a more thorough characterization of the Cr-rich samples.

Brey et al. (1999) performed similar experiments to Doroshev et al. (1997), but in the larger system FeO-MgO-Al_2O_3-SiO_2-Cr_2O_3. The explicit spinel end members in the Brey et al. model are $MgAl_2O_4$, $FeCr_2O_4$, and $MgCr_2O_4$. After considering a possible non-zero volume of reaction for the reciprocal (cross-site) reaction, Brey et al. discard this term. They retain an excess mixing volume due to exchange of Mg^{2+} and Fe^{2+} cations, fit by a symmetric model with the parameter $W_{\mathrm{FeMg}} = -0.020(7)$ J/bar/mol. Also, like Doroshev et al., Brey et al. use an asymmetric excess volume model for the Cr^{3+}-Al^{3+} exchange with parameters (recast into common form with above models) $W_{\mathrm{AlCrCr}} = 0.034(18)$ and $W_{\mathrm{AlCrCr}} = -0.014(12)$ J/bar/mol. This fit retains a negative deviation from ideality for Cr-rich compositions, but this result is only marginally significant, and does not fit the pure Fe-free data of Doroshev et al. and Oka et al. (1984) especially well.

Mattioli et al. (1987) derived a model of the volume of the ternary spinel system $MgAl_2O_4$-Fe_3O_4-$\gamma Fe_{8/3}O_4$. The volumes of the Fe_3O_4–$\gamma Fe_{8/3}O_4$ and $MgAl_2O_4$–$\gamma Fe_{8/3}O_4$ edges of this ternary system are treated as ideal. The $MgAl_2O_4$–Fe_3O_4 join is modeled as an asymmetric regular solution model, of the same form discussed above, with excess volume parameters $W_{\text{mt-mt-sp}} = 0.075(17)$ and $W_{\text{mt-sp-sp}} = 0.18(5)$ J/bar/mol, where mt = Fe_3O_4 and sp = $MgAl_2O_4$. In our final model, we find that an asymmetric excess volume term along the $MgAl_2O_4$–Fe_3O_4 binary is not justified by the data at ambient pressure, and thus treat this join as symmetric.

Three choices of solid solution model for spinel, each one based on the thermodynamic dataset of Holland and Powell (1998), are included in the modeling package THERMOCALC (e.g., Powell et al. 1998; currently hosted at http://www.metamorph.geo.uni-mainz.de/thermocalc/). None of the models incorporate any excess volume terms. The latest version of the thermodynamic database (Holland and Powell 2011) uses a modified equation of state that may be more easily extrapolated to very high pressures than the Murnaghan equation of state used in Holland and Powell (1998). Updated solid solution models have yet to be released. The Perple_X modeling package (e.g., Connolly 2009) offers the potential to adopt a wide variety of solid solution models, including several of those mentioned above (see http://www.perplex.ethz.ch/). All of the spinel models treat the $MgAl_2O_4$–$FeAl_2O_4$ join as ideal in volume. Only one of the available thermodynamic databases includes a chrome-bearing component for spinel (Klemme et al. 2009). The corresponding solution model for MgO-FeO-Al_2O_3-Cr_2O_3 spinels adopts the formulation of Oka et al. (1984) for asymmetric excess volume due to Al^{3+}-Cr^{3+} exchange.

DATA SOURCES

The American Mineralogist Crystal Structure Database (AMCSD) (Downs and Hall-Wallace 2003) provides a comprehensive collection of published X-ray and neutron diffraction refinements of cell volume and site occupancy; we fit the entire database of spinels with *Fd3m* space group symmetry in the system FeO-MgO-Fe_2O_3-Cr_2O_3-Al_2O_3-TiO_2 (Figs. 1, 2). The very oldest studies (Bragg 1915; Passerini 1930; Verwey and Heilmann 1947) and all other spinels in the database — e.g., tetragonal spinels, franklinites, trevorites, and maghemites — were excluded. In addition, we found these data sources for refined site occupancy data not in the AMCSD: Carbonin et al. (1996), Della Giusta et al. (1996), Princivalle et al. (1999), and Levy et al. (2004). Furthermore, a few sources are available that provide cell parameter based on powder XRD and electron microprobe analysis of an experimental charge (Doroshev et al. 1997; Brey et al. 1999; Girnis et al. 2003). We used these data by assuming the specimen was quenched from an equilibrium ordering state at experimental conditions and applying the ordering model built into MELTS (Sack and Ghiorso 1991a, b). This approximation introduces two potential sources of error: (a) the temperature recorded by the true ordering state may be lower than the experimental one and (b) there is an inherent uncertainty associated with the MELTS ordering model (e.g., a consequence of the simplistic spinel volume model in MELTS is that the predicted ordering state is independent of pressure). Both errors are probably systematic, and the restricted compositional and *P*-*T* ranges mean that the data are likely to be affected to a similar degree. Hence, although the measurements were given slightly less weight during the regression than those with accompanying site-

occupancy data, their inclusion is reasonable and the model fit is not substantially affected by absence of measured site occupancies.

Our final model is calibrated using a total of 832 experiments. The compositional and *P-T* coverage of the data is summarized in Table 1. All references for data used in model calibration are listed in Supplementary Material 1. Experimental conditions, observed cell parameters, and cation site occupancies are given in Supplementary Material 2. There are a number of compositional gaps in the volume calibration database. Some are due to immiscibility (Barnes and Roeder 2001; Pascal et al. 2011) and some correspond to spinels found in lunar samples too precious for analysis by XRD (Haggerty 1971). Still others are filled by studies of binary spinels for which site occupancies were not characterized (Golla-Schindler et al. 2005; Mattioli et al. 1987; Muan et al. 1972; Robbins et al. 1971; Wechsler et al. 1984; Woodland et al. 2009; Zhao et al. 1998). Unlike the experimental studies discussed above, none of these measurements could be incorporated into the calibration data set. Either the equilibration temperature could not be estimated sufficiently accurately or the measured volume trend disagreed with a reliable data source for one or other pure phase end member, even when ordering state could not be a factor. Hence inclusion of these studies would have had a detrimental effect on the calibrated standard state volumes. Nevertheless, the data were useful for comparison and (once allowance was made for any discrepancies in the end-member volume contributions) provided a valuable independent test of the newly calibrated model.

We assume that all Ti^{4+} (Wechsler et al. 1984; Sack and Ghiorso 1991a; Bosi et al. 2009) and all Cr^{3+} (Dunitz and Orgel 1957; Sack and Ghiorso 1991b) cations occupy

the octahedral site in spinels. This choice is supported by the calibration data set: of the data considered, only one $MgCr_2O_4$ (Tabira and Withers 1999), one Fe_2TiO_4 (Stout and Bayliss 1980), and one Mg_2TiO_4 (O'Neill et al. 2003) are reported as having 2% or more of Ti^{4+} or Cr^{3+} partitioned onto the tetrahedral site. Thus, we assigned any reported tetrahedral Ti^{4+} and Cr^{3+} to the octahedral site, moving Mg^{2+} as needed to compensate for site occupancy and charge. For example:

$$
\begin{aligned}
{}^{[4]}X_{Mg^{2+}} &= {}^{[4]}X'_{Mg^{2+}} + {}^{[4]}X'_{Cr^{3+}} \\
{}^{[6]}X_{Mg^{2+}} &= {}^{[6]}X'_{Mg^{2+}} - \tfrac{1}{2}\,{}^{[4]}X'_{Cr^{3+}} \\
{}^{[6]}X_{Cr^{3+}} &= {}^{[6]}X'_{Cr^{3+}} + \tfrac{1}{2}\,{}^{[4]}X'_{Cr^{3+}}
\end{aligned}
\quad , \qquad (1)
$$

where left superscript [4] denotes the tetrahedral site, [6] denotes the octahedral site, and *X'* represents the proportion of the indicated cation before the adjustment is made. The same relationships hold for the substitution of Ti^{4+} by replacing Cr^{3+} with Ti^{4+} in Eq. 1. Elements not included in our system were projected onto major cations of similar size and charge: Mn^{2+} and Mn^{3+} were assigned to Fe^{2+} and Fe^{3+}, respectively; the divalent cations Zn^{2+}, Ni^{2+}, and Co^{2+} were distributed proportionally over Mg^{2+} and Fe^{2+}; V^{3+} was projected onto Fe^{3+}; and Si^{4+} was cast into Ti^{4+}.

To limit the data used to fit the model to those spinels that are applicable to terrestrial or lunar mafic and ultramafic rocks, we developed a set of exclusion criteria. All experiments that contained vacancies on either crystallographic site were excluded. Likewise, experiments that contained Ca^{2+} were not included in the calibration, because even very small amounts of octahedral Ca^{2+} produced systematic errors in the model. We established a 5% site occupancy threshold for the other minor elements, i.e., we rejected experiments that reported greater than 5% occupancy in either site of Mn^{2+}, Mn^{3+}, Ni^{2+},

Zn^{2+}, Co^{2+}, V^{3+}, or Si^{4+}. We noted no evidence that Jahn-Teller distortion affects the volume at the level of Mn^{3+} substitution allowed (Ishii et al. 1972). In order that the projected composition of all calibrated spinels conform to the stoichiometry of the chosen model end members, within a reasonable tolerance, we filtered out any site occupancy data with reported site totals differing from unity by more than ±0.01 and any data with total cation charge greater than +8.03 or less than +7.97 per formula unit.

One drawback with the chosen data set is the lack of reliable error estimates for the observed and modeled molar volumes, which makes it difficult to weight the calibration data in any meaningful way. Errors on lattice parameters are estimated when data are curated in the AMCSD and suggest that the measurement precision values reported in the original sources can be misleadingly small. Room temperature fluctuations have a negligible effect on the total error, naturally, but interlaboratory differences can be significant for in situ experiments at high *P* and *T*; several of the high-*T* and high-*P* measurements have no reported bounds. Uncertainties associated with site occupancy determinations are almost never quantified but must vary depending on the type of sample (synthetic or natural), composition (end-member, binary, etc.), and measurement procedure. O'Neill and Dollase (1994) compared the effect of different refinement procedures on the final site occupancy distributions and several authors (e.g., Mattioli et al. 1987; O'Neill et al. 1992) have studied the effect of stoichiometry, or lack thereof, on molar volume. Given that it was impossible to come up with an automated strategy for assigning error estimates, we instead weighted all data equally but paid more attention to end-member and binary compositions when deciding between conflicting data or identifying outliers. This approach was later modified slightly to use weighted

nonlinear least squares, where all data were assigned the same nominal standard error except those requiring the MELTS ordering model (Doroshev et al. 1997; Brey et al. 1999; Girnis et al. 2003) which were given a doubled value. Reasons and details are given above and in the appendix (Supplementary Material 3).

MODEL FORMULATION

For fitting molar volume data to our model, the data must first be recast in a consistent manner into the representation of composition and ordering state we adopted. Most of the data we use are given in the AMCSD in the form of cation mole fractions on the tetrahedral and octahedral sites. For this kind of data, we first transformed the molar cation proportions into the following set of linearly independent compositional variables:

$$X_{\mathrm{sp}} = {}^{[4]}X_{\mathrm{Mg}^{2+}} + 2\,{}^{[6]}X_{\mathrm{Mg}^{2+}} \tag{2a}$$

$$X_{\mathrm{ch}} = {}^{[6]}X_{\mathrm{Cr}^{3+}} \tag{2b}$$

$$X_{\mathrm{uv}} = 2\,{}^{[6]}X_{\mathrm{Ti}^{4+}} \tag{2c}$$

$$X_{\mathrm{mt}} = \tfrac{1}{2}\left({}^{[4]}X_{\mathrm{Fe}^{3+}} + 2\,{}^{[6]}X_{\mathrm{Fe}^{3+}}\right), \tag{2d}$$

plus the dependent closure variable

$$X_{\mathrm{hc}} = 1 - X_{\mathrm{sp}} - X_{\mathrm{ch}} - X_{\mathrm{uv}} - X_{\mathrm{mt}}\ , \tag{2e}$$

where sp = $MgAl_2O_4$, ch = $FeCr_2O_4$, uv = Fe_2TiO_4, mt = Fe_3O_4, and hc = $FeAl_2O_4$. The cation ordering variables are

$$s_0 = {}^{[4]}X_{\mathrm{Mg}^{2+}} - 2\,{}^{[6]}X_{\mathrm{Mg}^{2+}} \tag{3a}$$

$$s_1 = \tfrac{1}{2}\left(2\,{}^{[6]}X_{Al^{3+}} - {}^{[4]}X_{Al^{3+}}\right) \quad (3b)$$

$$s_2 = \tfrac{1}{2}\left(2\,{}^{[6]}X_{Fe^{3+}} - {}^{[4]}X_{Fe^{3+}}\right). \quad (3c)$$

Sack and Ghiorso (1991a) tabulate the relationships between these compositional and ordering parameters for various end-member and binary spinels. See the spinel volume web tool (http://magmasource.caltech.edu/calculator/) described below for more general bounds that the composition of a spinel implies for the range of possible values of the order parameters. Note that Sack and Ghiorso (1991a, b) originally included an order parameter for Cr that was later abandoned and that they numbered the order parameters 1 through 4; their s_4 corresponds to our s_2. Although general dependence of volume on order state was considered, in practice only $MgAl_2O_4$-rich, $MgFe_2O_4$-rich, and $FeAl_2O_4$-rich compositions show order dependence of volumes at fixed composition.

Taking into account the site occupancy restrictions:

$$1 = {}^{[4]}X_{Fe^{2+}} + {}^{[4]}X_{Mg^{2+}} + {}^{[4]}X_{Al^{3+}} + {}^{[4]}X_{Fe^{3+}} \quad (4a)$$

$$1 = {}^{[6]}X_{Fe^{2+}} + {}^{[6]}X_{Mg^{2+}} + {}^{[6]}X_{Al^{3+}} + {}^{[6]}X_{Fe^{3+}} + {}^{[6]}X_{Ti^{4+}} + {}^{[6]}X_{Cr^{3+}}, \quad (4b)$$

expressions mapping mole fractions of cations into our chosen compositional and ordering variables may be readily derived.

The previously mentioned experiments of Doroshev et al. (1997), Brey et al. (1999), and Girnis et al. (2003) were quenched with an unknown ordering state. In order to use this data, we converted the reported oxide wt% into moles of cations. Note that the Fe^{2+}/Fe^{3+} ratio is calculated based on stoichiometry for this type of data, i.e., the total anion charge is −8, so the total charge of the cations must equal +8. We assumed the

experimental *P, T*-conditions represented conditions corresponding to equilibrium ordering state, and applied the MELTS ordering model (Sack and Ghiorso 1991b). Once we recast the electron microprobe data into the site occupancy model, we are able to calculate Eqs. 2a–e, and proceed as above. Measurements not included in the calibration dataset but used for comparison (e.g., Golla-Schindler et al. 2005) were treated in a similar way; reported synthesis conditions or annealing temperatures were used if available and, where necessary, forward models were repeated for a range of plausible equilibrium temperatures.

Standard state end-member properties included in our model are molar volume at reference pressure P_o = 1 bar and reference temperature T_o = 298.15 K (V^o), coefficient of thermal expansion (α), isothermal bulk modulus (K_{oT}), and the pressure derivative of the bulk modulus (K'). The general expression for the molar volume of a crystalline solid is $V = V_{ideal} + V_{excess}$, where excess volume of mixing is determined by an appropriate mixing model. The expression for V_{ideal} as a function of pressure, temperature, and composition is

$$V_{\text{ideal}} = \sum_i X_i V_i(P, T) \quad , \tag{5}$$

where i = [sp, ch, uv, mt, hc]. $V_i(P, T)$ is found by using Newton's method to search along the high-T Vinet equation of state,

$$P = 3K_{\text{oT},i}\left(\frac{V_i}{V_i^{\text{o}}}\right)^{-2/3}\left[1-\left(\frac{V_i}{V_i^{\text{o}}}\right)^{1/3}\right]\exp\left\{\frac{3}{2}\left(K_i'-1\right)\left[1-\left(\frac{V_i}{V_i^{\text{o}}}\right)^{1/3}\right]\right\}+\alpha_i K_{\text{oT},i}\left(T-T_{\text{o}}\right) \quad . \tag{6}$$

The Vinet formalism is applied to each end-member composition at the P and T of interest, and the resulting volumes are mixed to construct the ideal term. Initial estimates

of V^o, α, K_{oT}, and K' for each end member came from the provisional xMELTS spinel volume model (Ghiorso 2004b) except that K_{oT} values were taken from ultrasonic studies where available.

During model calibration, we considered excess volume terms of the symmetric regular solution form $W_{ij}X_iX_j$, asymmetric regular solution form $W_{ij}X_iX_j + dW_{ij}X_iX_j(X_i - X_j)$, and special terms dependent on ordering parameters. We allowed terms to depend on P and T as a way to encode non-ideal mixing of compressibility or thermal expansion without resorting to use of explicitly P, T-dependent expressions for K_{oT}, K', or α. Ultimately, however, we found that such P- and T-dependent parameters were not justified by the data.

Although it can be used in any context where a model of spinel molar volume is required, the present model is designed to be compatible with the activity-composition and ordering model of Sack and Ghiorso (1991a, b), which accounts for the standard state, exchange, reciprocal, and excess energies among the same set of independent and dependent end members adopted here and computes equilibrium site occupancy by Gibbs energy minimization. In formulating an extension to describe molar volumes we begin of course by adopting the Sack and Ghiorso set of independent end members to define the standard state contribution to the volume as a function of pressure and temperature. However, in modeling the excess and ordering volumes we have a choice. We might adopt a parameter set strictly parallel to the parameters of the Sack and Ghiorso enthalpy model, or we might formulate a new model guided by the volume data available. The former approach has some theoretical justification in that non-ideal enthalpy and volume of solutions both arise from the same microscopic effect, namely mismatch of ionic radii

of substituting cations. However, the Sack and Ghiorso enthalpy model has 32 parameters, which turns out to be many more than are needed to describe the non-ideal component of volume behavior. The formulation of the enthalpy model may not yield a stable minimum set of parameters when fit to the volume data in a conservative way. In practice, the volume data set can be fit with a much smaller set of parameters with a minimum of parameter correlation if we choose a different formulation for excess volumes and volumes of ordering. Since our interest is in creating the most useful and reliable model for use in macroscopic thermodynamic applications, we have therefore adopted a new formulation for the non-ideal parts of our volume model, not parallel to the formulation of the enthalpy and ordering model, even though the result may provide less insight into the microscopic origin of the excess volumes.

MODEL CALIBRATION SUMMARY

A full description of the strategy for calibration, including parameters deemed significant or negligible and data used or excluded, is provided in the appendix (Supplementary Material 3). In summary, the standard state end-member properties, ordering terms, and contributions to selected symmetric regular solution terms were first calibrated to ambient, high-T, and high-P data for all end members, including the dependent end members $MgCr_2O_4$, $MgFe_2O_4$, and Mg_2TiO_4. The provisional regular solution terms accounted for the volume of reaction for the formation of the dependent end members by Fe-Mg exchange and were constructed in a way that was consistent with the data for binary and ternary spinels. Then the remaining ambient pressure and temperature data were used to calibrate additional contributions to V_{excess} as a function of composition.

Finally, the small number of high-T and high-P data for intermediate compositions were checked to see if they required any revisions to the model, which they did not.

We have developed a calibration scheme that is able to directly query a MySQL database containing phase equilibrium, site occupancy, and volume data. The calibration scheme is written in MATLAB™ and uses the MATLAB-MySQL interface written by Robert Almgren (http://www.mathworks.com/matlabcentral/fileexchange/8663-mysql-database-connector). For the database, we adapted the schema from the Library of Experimental Phase Relations (LEPR) (Hirschmann et al. 2008) to incorporate the cell parameters and site occupancy data, with suitable metadata, and made a number of internal changes that reflect the different ways in which the two databases are updated and accessed. The MATLAB-generated MySQL queries allow us to test the effect of including or excluding a particular data source or type of experiment (e.g., heated in situ vs. annealed and quenched) with minimal effort and without the need for intermediate files.

Three terms describe the observed linear volume dependence on each of the cation ordering variables s_0, s_1, and s_2 (Fig. 3). The adopted standard states for $MgAl_2O_4$ and $FeAl_2O_4$ are sufficiently close to normally ordered (e.g., $s_1 = 0.99998$ for $FeAl_2O_4$) that we assume them to be perfectly so. In order for the s_0-dependent term to vanish at Mg-free compositions, we used the form $(s_0 - 1)/2$, multiplied by X_{sp}, as this represents total Mg cations per formula unit. Likewise, we multiplied the s_1-dependent term by total Al, given by $2(X_{sp} + X_{hc})$. End member Fe_3O_4 is approximated as perfectly inversely ordered and the s_2 term is multiplied by total Fe^{3+}, which is simply $2X_{mt}$ (see Eq. 7 below). The resulting ordering-composition cross-terms account for nearly all the excess

volume along several key binaries: notably Fe_3O_4–Fe_2TiO_4 (Bosi et al. 2009) and $MgAl_2O_4$–$FeAl_2O_4$ (Andreozzi and Lucchesi 2002).

That no additional excess volume terms were required on the $MgAl_2O_4$-$FeAl_2O_4$ join was particularly fortuitous as it meant that the Cr^{3+}-, Fe^{3+}-, and Ti^{4+}-bearing spinel subsystems could be considered separately when choosing between candidate parameters. This process is described in more detail in the appendix. Briefly, we chose the minimum number of parameters that could reasonably describe the ordering-adjusted volume surface for each reciprocal square (e.g., $MgAl_2O_4$-$MgCr_2O_4$-$FeCr_2O_4$-$FeAl_2O_4$) before moving our attention to other joins, such as Fe_3O_4–Fe_2TiO_4 and Fe_3O_4–$FeCr_2O_4$, and to multicomponent spinels.

When calibrating the independent and dependent end-member data we were careful not to activate excess volume terms along joins, such as $FeCr_2O_4$–$MgCr_2O_4$ (Lenaz et al. 2004), which showed little or no deviation from ideality once any ordering effects were subtracted. This strategy meant that certain combinations of solution parameters (e.g., $W_{\text{mt-sp}} - W_{\text{mt-hc}}$) were constrained by the end-member data. In the second stage calibration, end-member properties and ordering parameters were fixed; instead we adjusted the existing excess volume terms (i.e., $W_{\text{sp-ch}}$, $W_{\text{hc-ch}}$, $W_{\text{mt-sp}}$, and $W_{\text{mt-hc}}$) and introduced two new terms ($dW_{\text{sp-ch}}$ and $W_{\text{ch-mt}}$) in a way that did not disturb the fit for the dependent end members.

We used the Bayesian information criterion (BIC) (Schwarz 1978), along with analysis of the reduced χ^2 statistic, to measure how efficiently our parameterized model predicts the data. Since we do not have information on measurement error for site occupancies, we are required to estimate the error in observed volume for calculating

reduced χ^2. The BIC assigns a penalty term that is based on the complexity, or number of parameters, of the model. The formula is BIC = $-2\ln(L) + k\ln(n)$, where $\ln(L)$ is the optimized log-likelihood function associated with a particular model, k is the number of model parameters, and n is the number of observations associated with $\ln(L)$. By applying the BIC iteratively to the excess volume parameters and analyzing reduced χ^2, for example, all excess terms involving X_{uv} were found to be insignificant.

In all stages of the model, each of the five explicit end members has a pure component equation of state described by four parameters: V^o, α, K_{oT}, and K' (Tables 2–4). The additional parameters of the preferred final model include six excess terms along compositional binaries and three order-dependent terms. The values of the excess volume and order-dependent parameters are given in Table 5. The full expression of the model is:

$$\begin{aligned} V(\boldsymbol{X},T,P,\boldsymbol{s}) = & \sum_i X_i V_i(T,P) \\ & + W_{\text{hc-ch}} X_{\text{hc}} X_{\text{ch}} + W_{\text{ch-mt}} X_{\text{ch}} X_{\text{mt}} + \\ & W_{\text{sp-ch}} X_{\text{sp}} X_{\text{ch}} + dW_{\text{sp-ch}} X_{\text{sp}} X_{\text{ch}} (X_{\text{sp}} - X_{\text{ch}}) + \\ & W_{\text{mt-hc}} X_{\text{mt}} X_{\text{hc}} + W_{\text{mt-sp}} X_{\text{mt}} X_{\text{sp}} + \\ & \frac{(s_0 - 1)}{2} W_{s0} X_{\text{sp}} + 2(s_1 - 1) W_{s1} (X_{\text{sp}} + X_{\text{hc}}) + 2 s_2 W_{s2} X_{\text{mt}} \end{aligned} \qquad (7).$$

This model fits virtually all of the data to within 0.02 J/bar/mol, or better than 0.5% in volume (Figs. 4, 5), with a few exceptions for the studies of Antao et al. (2005a, 2005b), Finger et al. (1986), Haavik et al. (2000), and Méducin et al. (2004) (see appendix for exclusion criteria for these studies). The mean of the absolute values of the residuals for calibrated data is 0.0038 J/bar/mol and the root mean squared error is 0.0053 J/bar/mol. The goodness-of-fit of the model is displayed in Fig. 4, where observed molar volume is

plotted first against the volume model with asymmetric excess on the Fe_3O_4–Fe_2TiO_4 join used in current versions of MELTS (Fig. 4a), then against an ideal volume model using the refined end-member equation of state coefficients from Tables 2–4 (Fig. 4b), and finally against the model volume from the full form of Eq. 7 (Fig. 4c). When compared with the ideal model (Fig. 4b), data for dependent end members $MgCr_2O_4$ and $MgFe_2O_4$ show parallel trends with fixed offsets from the equiline that correspond to the quantities $2(W_{sp\text{-}ch} - W_{hc\text{-}ch})$ and $2(W_{mt\text{-}sp} - W_{mt\text{-}hc})$ respectively. The residuals in the final model are uncorrelated with observed molar volume and are nearly all ≤0.02 J/bar/mol for data accepted into the calibration set (Fig. 5). It is difficult to derive a more quantitative assessment of goodness-of-fit given uncertain knowledge of errors on composition, site occupancy, and molar volume in the calibration data.

Obtaining confidence bounds on the derived parameters is a separate issue from goodness-of-fit and can be addressed using bootstrap estimation (Efron 1982). Uncertainty bounds on each fitted parameter and a full correlation matrix for the parameter set derived from 50,000 bootstrap iterations are given in Supplementary Material 4 and 5. All parameters were varied, except those taken from ultrasonic studies or other sources (e.g., the Levy et al. (2003) fit of K_{oT} and K' for $MgAl_2O_4$). The end-member properties are generally independent of one another; those trade-offs that exist are understandable given that the high-T properties of Fe^{3+}-, and Ti^{4+}-bearing spinels were constrained by data for the dependent end members $MgFe_2O_4$ and Mg_2TiO_4 respectively. Likewise, there is some correlation between V^o and ordering parameters for certain end members. As expected (see the appendix), many of the purely compositional excess parameters are strongly correlated (e.g., $W_{sp\text{-}ch}$ with $W_{hc\text{-}ch}$, and $W_{mt\text{-}sp}$ with $W_{mt\text{-}hc}$)

and are well-defined only in a joint sense. These observations emphasize that the calibrated parameters should only be used in the context of the full model derived here and that they may not be optimal descriptions of subsystems if ideal and excess terms are separated. As noted above, the calibration data vary in coverage and quality, and full estimates of measurement uncertainties are sparse, which means confidence bounds calculated using random sampling are probably unrealistically wide. Large uncertainties in the fit parameters do not necessarily feed into large uncertainties in the volumes calculated using the calibrated model, once the high degree of correlation between parameters is accounted for properly (Powell and Holland 1985). However, as the Vinet equation must be solved iteratively at each stage of the calculation in this case, such sophisticated propagation of uncertainties is neither straightforward nor likely to be that informative. Instead, for comparison, we obtained a more conservative confidence bound for each parameter, again using the bootstrapping technique but holding all other parameters at their optimal values; these uncertainties are reported in Tables 2, 3, and 5.

A few aspects of the model remain underconstrained by data. There are neither ultrasonic velocities nor in situ high-*P* volume data for Ti-bearing compositions. We are forced to assume that the K_{oT} and K' for Fe_2TiO_4 are equal to those of Fe_3O_4 (Table 4). Given the low compressibility of spinels and the small Ti^{4+} concentrations in most spinels (and in particular in all the spinels that will be used for calibration of models of coexisting phases like garnet and pyroxene), this assumption is unlikely to have any significant effect on free energies within the pressure range of the spinel stability field. In addition, the value of α for $FeCr_2O_4$ was not varied during the calibration process. However, when the final model is used to calculate the effective α for a chromian spinel

with composition $MgAl_{0.8}Cr_{1.2}O_4$, the value agrees with the one obtained from the lower temperature measurements (i.e., the ones made below the blocking temperature) of Levy and Artioli (1998, see fig. 3a) to within 5.4×10^{-7} K^{-1}. In the absence of high-*T* structural refinements for $FeCr_2O_4$, we believe that the value of α adopted is the best estimate currently available.

DISCUSSION

Model comparison

A comparison between our model and the model of Brey et al. (1999) is shown in Fig. 6. The gray surface in Fig. 6a shows the excess volume of the Brey et al. model in the $MgAl_2O_4$-$MgCr_2O_4$-$FeCr_2O_4$-$FeAl_2O_4$ reciprocal square, i.e., the end-member contributions have been subtracted from the volume surface. The data plotted have also had the ideal end-member contributions to their volumes subtracted. The surface in Fig. 6b shows our proposed model in the same composition space as the Brey et al. model. Here, contributions from the end members and from our model ordering terms have been subtracted from model and data. That the data appear smoother in Fig. 6b than in Fig. 6a shows that there is a distinct ordering effect on the volume that cannot be mapped into a purely compositional term (cf. the Fe_3O_4–Fe_2TiO_4 join discussed below). Both models give similar fits to the data of Brey et al. and Doroshev et al. (1997) (diamonds), but the molar volume of $FeCr_2O_4$ is more tightly constrained in our model due to the availability of data from Lenaz et al. (2004). Unlike Brey et al., we explicitly account for the dependent end member ($MgCr_2O_4$ in our model; $FeAl_2O_4$ in theirs) so our model predicts a warped volume surface. Finally, by making the asymmetrical excess volume term a

function of X_{sp} and X_{ch}, rather than X_{Cr} and X_{Al}, our model is able to provide a much better fit to the rest of the data in the composition space (circles in Fig. 6).

The surface in Fig. 7a shows our model for spinels in $MgAl_2O_4$-$MgFe_2O_4$-Fe_3O_4-$FeAl_2O_4$ space; again, the end-member and ordering contributions have been subtracted from the model surface and the data. The model along the $MgAl_2O_4$–Fe_3O_4 binary is plotted in Fig. 7b, along with the model of Mattioli et al. (1987); the magnitudes of the positive, symmetric excess terms of the two models along this join are similar, and differences of up to ~0.004 J/bar are due to different standard state volumes for Fe_3O_4. The ordering state of Fe_3O_4 is particularly hard to quench, since it involves only electron exchange rather than cation mobility; hence in Fig. 7b we show curves with and without the modeled volume contribution due to ordering. A significant part of the asymmetry observed by Mattioli et al. on this join is apparently attributable to the composition-dependent closure temperature of the ordering reaction. Once these systematic differences in order state and measured volumes for compositions approaching pure Fe_3O_4 are accounted for, the data do not seem to justify an asymmetric excess volume term like the one used by Mattioli et al. The calibration data of Nakatsuka et al. (2004) ($MgAl_2O_4$–$MgFe_2O_4$) and the comparison data of Golla-Schindler et al. (2005) ($FeAl_2O_4$–Fe_3O_4) also support the simpler symmetric formalism (Fig. 7a).

The current spinel volume model formulation in MELTS and pMELTS includes asymmetric excess volume terms for the Fe_3O_4–Fe_2TiO_4 binary (Sack and Ghiorso 1991a), whereas in our model the asymmetry comes solely from the ordering contribution to the volume (Fig. 8). The asymmetry in the volume variation is subtle, though well resolved by the data. The strong preference of Ti^{4+} for the octahedral site limits the

configurational freedom along this join but the Mössbauer spectroscopic measurements of Bosi et al. (2009) indicate a sigmoidal variation in s_2 with X_{uv}. Deviations from the Akimoto (1954) ordering model (equivalent to setting $s_2 = 0$) have the same sense as the deviations from Vegard's Law, so it is not surprising that introducing an ordering dependence to the volume model may reduce the need for asymmetric interaction parameters. However, inasmuch as the ordering terms were calibrated only with data for pure $MgFe_2O_4$ (s_0 and s_2), $MgAl_2O_4$ (s_0 and s_1), and $FeAl_2O_4$ (s_1), the result that excess volume along the Fe_3O_4–Fe_2TiO_4 binary may be completely explained in this way is unexpected. Although we cannot properly constrain the nature of Ti^{4+} mixing in spinel, the notion that same-site substitution is nearly ideal for volume (i.e., excess volumes of mixing are due to ordering amongst the other cations) is supported by the few data available within the Ti-bearing subsystem.

The MELTS ordering model of Sack and Ghiorso (1991a, b) predicts a cation distribution that is independent of pressure because the accompanying volume model is ideal. As shown here, ordering effects can successfully explain all of the observed symmetric excess volumes of mixing on the $MgAl_2O_4$–$FeAl_2O_4$ join (Andreozzi and Lucchesi 2002), and the $MgAl_2O_4$–Mg_2TiO_4 and $FeAl_2O_4$–Fe_2TiO_4 binaries (Muan et al. 1972), as well as the aforementioned variation along Fe_3O_4–Fe_2TiO_4 (Bosi et al. 2009). The ordering parameters in our model also capture most of the mixing behavior along the Fe_3O_4–$FeCr_2O_4$ join (Robbins et al. 1971; Woodland et al. 2009) (Fig. 9). In our model the excess volume term along this join is symmetric and constrained by data elsewhere in the composition space; introduction of the s_2 ordering term accounts for the asymmetry in the data (which were not included in the calibration). Furthermore, when the MELTS

ordering model (Sack and Ghiorso 1991a, b) is updated to use our volume expression in the self-consistent calculation of ordering state by Gibbs energy minimization, it successfully predicts the high-*P*, *T* results of Antao et al. (2005b) for $MgFe_2O_4$ (Fig. 10). Note that the Antao et al. study was not included in the calibration data set (see appendix) but the observed variation in volume with *P* and *T* is nevertheless consistent with the model presented here. The general role of order-disorder reactions in mineral volumes and compressibilities has been discussed by Hazen and Navrotsky (1996) and illustrated for the highly order-sensitive spinel $CoFe_2O_4$ by O'Neill and Navrotsky (1983). Spinel molar volume is a specific function of the tetrahedral (A-O) and octahedral (B-O) bond distances. The volume is about twice as sensitive to the B-O distance as it is to the A-O distance. Given differences in the ionic radii of cations in different coordination environments and valence states it is therefore not surprising that spinel volumes are strongly order-dependent. Hazen and Navrotsky argue that such behavior is most pronounced when there are changes in ionic charge and coordination number, such that order-disorder reactions in minerals like olivine and orthopyroxene (mostly involving Fe^{2+} and Mg on crystallographically distinct octahedral sites) should show smaller effects than those documented here for spinel. The pyroxene model of Sack and Ghiorso (1994a) includes an ordering contribution to the volume.

Applications

Klemme (2004) presented experimental reversals for the garnet–spinel transition reaction $MgCr_2O_4 + 4\ MgSiO_3 = Mg_3Cr_2Si_3O_{12} + Mg_2SiO_4$. Klemme (2004) and Klemme et al. (2009) used the experimental brackets to extract enthalpy of formation and standard state

entropy for the garnet end member knorringite ($Mg_3Cr_2Si_3O_{12}$). Klemme's (2004) values were designed to be consistent with the thermodynamic data set of Holland and Powell (1990), whereas Klemme et al. (2009) used a later version (Holland and Powell 1998). When Hamecher et al. (2009) repeated the exercise using the provisional xMELTS thermodynamic data set (based on Berman 1988, but updated to use the Vinet equation of state) the recovered standard state entropy of $Mg_3Cr_2Si_3O_{12}$ was significantly lower than the values given by Klemme and co-workers. We tested the effect of our newly calibrated spinel model and found only a small difference with the result from Hamecher et al. (2009). We also used the expressions and thermodynamic data of Holland and Powell (1990, 1998) and retrieved essentially the same values as Klemme et al. (2009). We could reproduce the results of Klemme (2004) but only if we used the volume parameters taken from Klemme et al. (2009) for both $Mg_3Cr_2Si_3O_{12}$ and $MgCr_2O_4$, instead of those from Irifune et al. (1982) and Robie et al. (1979) (see table 3 in Klemme 2004). Hence, while the volume properties of $MgCr_2O_4$ spinel clearly influence the location of the spinel-garnet transition in the MgO-Cr_2O_3-SiO_2 system, a final volume model for Cr-bearing garnet is required in order to update the Hamecher et al. (2009) thermodynamic data for $Mg_3Cr_2Si_3O_{12}$.

In the meantime, we can gauge the effect that the new spinel volume model might have on MELTS calculations by extracting a typical lherzolite spinel composition from pMELTS, and comparing its molar volume before and after recalibration. At 1000 ºC and 3 GPa, in the Workman and Hart (2005) depleted mantle composition, pMELTS predicts a spinel of composition $Fe^{2+}_{0.42}Mg_{0.60}Fe^{3+}_{0.20}Al_{0.38}Cr_{1.40}Ti_{0.01}O_4$. The molar volume of this spinel at the applied conditions, calculated with the spinel molar volume model built

into all versions of MELTS to date, is $V(\boldsymbol{X}, T, P, \boldsymbol{s}) = 4.3285$ J/bar/mol, whereas the model proposed in this work yields $V(\boldsymbol{X}, T, P, \boldsymbol{s}) = 4.3564$ J/bar/mol, a difference $\delta V_{sp} = +0.0279$ J/bar/mol. Although a full internally consistent recalibration of all aspects of the MELTS model is needed to see all the consequences of such a difference, the following simple calculation gives a preliminary sense of the magnitude of possible effects.

The difference in spinel molar volume corresponds to a difference in the model Gibbs free energy of spinel at elevated pressure, and hence in the Gibbs free energy change of any reaction involving spinel. Keeping other quantities constant, the resulting displacement in pressure of an equilibrium boundary can be found by comparing the change in Gibbs energy of reaction to the volume change across the reaction. In this way, we can estimate, for example, what change in modeled pressure of the spinel–garnet transition will result when the current model is assimilated into MELTS. This is of some interest, because the match between experimental determinations of this boundary and MELTS calculations performed between 1995 and 2004 turned out to depend on an error in the implementation of the garnet solid solution model that was applied during model calibration (Berman and Koziol 1991). Since that error was fixed (Smith and Asimow 2005), the model is no longer self-consistent, and the spinel–garnet lherzolite reaction has been calculated at a pressure as much as 0.8 GPa lower than experimental constraints (Hamecher et al. 2009).

For simplicity, consider the spinel–garnet lherzolite reaction in the simple MgO-Al_2O_3-SiO_2 (MAS) system: $MgAl_2O_4 + 2Mg_2Si_2O_6 = Mg_3Al_2Si_3O_{12} + Mg_2SiO_4$. At

equilibrium, the Gibbs free energy of reaction (ΔG_{rxn}) is zero, and $\left.\frac{\partial \Delta G_{rxn}}{\partial P}\right|_T = \Delta V_{rxn}$. We make the approximation:

$$\delta P_T \approx \frac{\delta \Delta G_{rxn}}{\Delta V_{rxn}} = -\frac{\delta G_{\mathrm{sp}}}{\Delta V_{rxn}}, \tag{8}$$

where δ refers to the finite change between the two models, and $\delta \Delta G_{rxn} = -\delta G_{\mathrm{sp}}$ since we are not changing the properties of the other reactants or products. We can estimate the difference between models in the Gibbs free energy of spinel by making the approximation:

$$\delta G_{\mathrm{sp}} = \int_{P_{\mathrm{o}}}^{P} \delta V_{\mathrm{sp}}\, dP \approx \delta V_{\mathrm{sp}} \left(P - P_{\mathrm{o}}\right), \tag{9}$$

which, for $\delta V_{\mathrm{sp}} = +0.0279$ J/bar/mol and $P = 3$ GPa, gives $\delta G_{\mathrm{sp}} \sim 837$ J/mol. ΔV_{rxn} for the MAS reaction at 1000 ºC and 3 GPa is –0.8243 J/bar/mol (from the MELTS model, but substituting the new spinel model would make less than a 4% difference in this number). Hence, the approximate displacement in the equilibrium pressure of the reaction between the two models is $\delta P_T \approx +1015$ bars = +0.1 GPa. This difference is in the right direction to address the error in the current MELTS model, but is not enough to explain the entire discrepancy. Recovering a self-consistent model that matches experimental constraints on the pressure of the spinel-garnet lherzolite reaction will require a full recalibration of the garnet and pyroxene activity-composition models, with the best available molar volume models built into the calibration.

Web tool

There may be many applications of a molar volume model for spinel solid solutions beyond the MELTS-based calculations discussed herein. However, the formulation of the present model in terms of MELTS end members and ordering variables may be an impediment to its wide application. Hence we have provided an online tool (http://magmasource.caltech.edu/calculator/) whereby users may input a spinel either as site occupancy data (that is, both composition and ordering state are measured) or as electron probe data with specified P and T (that is, composition is measured but ordering state is not) or as mole fractions of end members (including dependent ones) with P and T. The data are processed in the same manner as the calibration data herein and assigned to MELTS end members. If site occupancy is not given, the updated MELTS ordering model (i.e., based on Sack and Ghiorso (1991a, b) but with the volume model presented here) is used to estimate site occupancy by Gibbs energy minimization. Much like annealed samples within the calibration data set, there is an option to specify one set of P-T conditions for the equilibrium ordering state (P_S, T_S) and another for calculation of the measureable volume (P_V, T_V). The web tool automatically converts between the various input options, such as wt% oxides and site occupancy, and displays the results. Finally, V_{ideal} (as a function of P_V and T_V), V_{excess} (calculated with site occupancy data, or with the MELTS ordering model using P_S and T_S), and V_{total} (i.e., $V_{\text{ideal}} + V_{\text{excess}}$) and, where appropriate, their derivatives with the relevant P and T are returned to the user.

Future prospects

Many of the assumptions made in our model were required due to the lack of published full structural refinements for certain regions of composition, temperature, and pressure space. There is a dearth of data available for the volume of Ti- and Cr-bearing spinels: we found only one in situ high-*T* study for Ti-bearing spinel, Mg_2TiO_4 (O'Neill et al. 2003), and not a single in situ high-*P* (at ambient or elevated-*T*) data set. Likewise, the Martignago et al. (2003) in situ high-*T* study of three natural samples along the $MgAl_2O_4$–$MgCr_2O_4$ binary is the only full refinement we currently have for Cr-bearing spinels measured at elevated conditions. As detailed in our discussion of Haavik et al. (2000), Méducin et al. (2004), and Antao et al. (2005a, b) (see the appendix), there are some substantial disagreements in the literature even among compositions that have been more widely studied, e.g., $MgAl_2O_4$ and Fe_3O_4, and some hints that the behavior of spinel at simultaneous high-*P*, *T* may by more complex than at high-*P* or high-*T* conditions alone. On the other hand, recent systematic measurements of the site occupancy and volume of binary spinels (Andreozzi and Lucchesi 2002; Bosi et al. 2009) allowed us to calibrate the effect of ordering on volume in a way not possible when the MELTS spinel model was originally developed (Sack and Ghiorso 1991a). It is our hope that with the current advances in X-ray and neutron diffraction methods, more high-quality data will become available for these spinel compositions, particularly at simultaneous very high-*P* and -*T*, enabling us to improve upon our model assumptions in future calibrations.

Acknowledgements

We wish to thank Peter Luffi for identifying the garnet solid solution error in the original MELTS code, Ashley Nagle for pointing out the anomalously low spinel-garnet transition pressures obtained when the corrected garnet model is used, and Aaron Wolf for helpful discussions regarding statistical analysis. Comments by Associate Editor Jon Blundy are greatly appreciated, as are the reviews of two anonymous reviewers. This work was supported by the National Science Foundation and the American Recovery and Reinvestment Act through award 0838244.

TABLES

Table 1. Summary table of data coverage in composition, *P*, and *T*

Composition	Total Experiments	Ambient-*P*, *T*	High-*P*	*P* Range (GPa)	High-*T*	*T* Range (ºC)
End members						
$MgAl_2O_4$	151	48	21	0.6 - 29	82	132 - 1600
$FeCr_2O_4$	1	1	0	-	0	-
Fe_2TiO_4	2	2	0	-	0	-
Fe_3O_4	55	9	46	0.02 - 11.11	0	-
$FeAl_2O_4$	40	23	0	-	17	200 - 1150
$MgCr_2O_4$	6	6	0	-	0	-
$MgFe_2O_4$	69	24	28	0.11 - 34.39	17	100 - 1200
Mg_2TiO_4	53	2	0	-	51	70 - 1416
Binaries						
$MgAl_2O_4$-$FeAl_2O_4$	14	14	0	-	0	-
$FeAl_2O_4$-Fe_3O_4	1	1	0	-	0	-
$FeTi_2O_4$-Fe_3O_4	18	18	0	-	0	-
$MgAl_2O_4$-$MgFe_2O_4$	68	15	4	1 - 4	49	200 - 1050
$MgAl_2O_4$-$MgCr_2O_4$	194	87	34	4.4 - 8.03	73	200 - 1000
$FeCr_2O_4$-$MgCr_2O_4$	13	13	0	-	0	-
Fe_3O_4-$MgFe_2O_4$	1	1	0	-	0	-
Multi-component	146	146	0	-	0	-
Total	832	410	133		289	

Table 2. Optimized standard state end-member molar volume for given ordering state

	V^o (J/bar/mol)	$1\sigma^*$	Ordering State	[s_0, s_1, s_2]	a (Å)	ρ (kg m^{-3})
$MgAl_2O_4$	3.9722	1.7×10^{-4}	normal	[1, 1, 0]	8.0808	3582
$FeCr_2O_4$	4.4243	3.9×10^{-4}	normal	[0, 0, 0]	8.3765	5059
Fe_2TiO_4	4.6873	3.1×10^{-4}	normal	[0, 0, 0]	8.5393	4769
Fe_3O_4	4.4553	5.5×10^{-4}	inverse	[0, 0, 0]	8.3960	5197
$FeAl_2O_4$	4.0871	2.0×10^{-4}	normal	[0, 1, 0]	8.1580	4253

*Bootstrap estimation of s.d. for V^o, holding other parameters at optimal values

Table 3. Standard state end-member coefficient of thermal expansion

	α(10^{-5}) (K^{-1})	$1\sigma^*$
$MgAl_2O_4$	2.4413	3.8×10^{-8}
$FeCr_2O_4$[a]	2.1691	-
Fe_2TiO_4	3.3458	4.3×10^{-8}
Fe_3O_4	3.3376	2.1×10^{-7}
$FeAl_2O_4$	2.6431	2.7×10^{-8}

*Bootstrap estimation of s.d. for α, holding other parameters at optimal values

[a]Value of α was held constant (see text)

Table 4. Bulk moduli and pressure derivatives of end members

	K_{oT} (GPa)	K'
$MgAl_2O_4$	190.8[a]	6.77[a]
$FeCr_2O_4$	203.3[b]	6.5[c]
Fe_2TiO_4	181[d]	5.5[d]
Fe_3O_4	181[e]	5.5[e]
$FeAl_2O_4$	210.3[f]	5.5[d]

[a] From Levy et al. (2003)

[b] From Doraiswami (1947)

[c] Constrained using data of Fan et al. (2008) (see appendix)

[d] Assumed to be equal to that of Fe_3O_4 (see text)

[e] From Nakagiri et al. (1986)

[f] From Wang and Simmons (1972)

Table 5. Model parameters

		$1\sigma^*$	
$W_{hc\text{-}ch}$	0.0108	0.018	(J/bar/mol)
$W_{ch\text{-}mt}$	0.0715	0.19	
$W_{sp\text{-}ch}$	0.0578	0.014	
$dW_{sp\text{-}ch}$	0.0489	0.063	
$W_{mt\text{-}hc}$	0.0833	0.025	
$W_{mt\text{-}sp}$	0.1020	0.025	
W_{s0}	-0.0692	0.00049	
W_{s1}	0.0264	0.00049	
W_{s2}	0.1035	0.0019	

*Bootstrap estimation of s.d. for each parameter, holding all other parameters at optimal values

FIGURE CAPTIONS

Fig. 1 Compositional coverage of the data used in model calibration. Diamonds are experiments measured at ambient conditions, circles are experiments measured at high-*T*, squares are data measured at high-*P*. Triangles are data not included in calibration due to lack of measured site occupancies, and are used only for comparison to model results below. **a** Mg# ($Mg/[Mg + Fe^{2+}]$) vs. $Ti^{4+}/(Ti^{4+} + Cr^{3+} + Fe^{3+} + Al^{3+})$; **b** Mg# vs. $Cr^{3+}/(Ti^{4+}+ Cr^{3+} + Fe^{3+} + Al^{3+})$; **c** Mg# vs. $Fe^{3+}/(Ti^{4+} + Cr^{3+} + Fe^{3+} + Al^{3+})$.

Fig. 2 Compositional coverage of the data used in model calibration. Symbols the same as in Fig. 1. **a** Ti^{4+} - Fe^{3+} - Al^{3+} ternary; **b** Cr^{3+} - Fe^{3+} - Al^{3+} ternary.

Fig. 3 Order-dependence of observed volume vs. ordering term for **a** s_0, **b** s_1, and **c** s_2. The order-dependence for s_0, for example, is calculated by subtracting the model V_{ideal} and all other model terms not dependent on s_0 from the observed volume, V_{obs}. The linearity of the data shows the simple form of the order-dependence of the data and the slope of the linear trend is proportional to the W_{s0} parameter (see Eq. 7). The corresponding calculations were done for s_1 and s_2. The solid lines are the model order-dependences, plotted over the relevant range of ordering states.

Fig. 4 Model volume vs. measured volume. **a** Model results using spinel volume model currently implemented in MELTS (shown in box); **b** Ideal model volume results after

fitting of end members. Model results from **a** shown grayed out; **c** Final model results. Model results from **a** shown grayed out.

Fig. 5 Model residuals vs. measured volume. Gray diamonds are samples measured at ambient-*P*, *T*, open circles are samples measured at high-*T* in situ, and black squares are samples measured at high-*P* in situ.

Fig. 6 Model volumes and data in the $MgAl_2O_4$-$MgCr_2O_4$-$FeCr_2O_4$-$FeAl_2O_4$ reciprocal square. End members are labeled at the corners. **a** Gray surface is the model of Brey et al. (1999) with end-member contributions subtracted. Diamonds are the data of Brey et al. (1999) and Doroshev et al. (1997); open circles are the rest of the room-*T*, *P* calibration data set with <5% magnetite or ulvöspinel component; **b** Gray surface is the model presented in this work, with end-member and ordering contributions subtracted. Symbols are the same as in **a**.

Fig. 7 a Excess model volume in the $MgAl_2O_4$-$MgFe_2O_4$-Fe_3O_4-$FeAl_2O_4$ reciprocal square. End members are labeled at the corners. Gray surface is the model presented in this work, with end-member and ordering contributions subtracted. Open circles are the room-*T*, *P* calibration data with < 5% chromite or ulvöspinel component; diamonds are the data of Mattioli et al. (1987), only the most stoichiometric data (samples synthesized at 1400 °C and oxygen fugacity of 10^{-4} atm) are plotted; triangles are the data of Golla-Schindler et al. (2005) for an equilibration temperature of 1100 ºC (varying this value

within the stated range of annealing temperatures has little effect); squares are the data of Nakatsuka et al. (2004); data from Zhao et al. (1998) ($MgFe_2O_4$-Fe_3O_4) are not shown due to minor amounts of Ca in the analyses; **b** Excess model volumes along the $MgAl_2O_4$ – Fe_3O_4 binary. The upper solid line is the model excess volume along this join, including ordering states calculated with the MELTS ordering routine for the Mattioli et al. experimental temperature of 1400 °C. The lower solid line is the excess volume model plotted without additional ordering effects, i.e., the order is perfectly normal at spinel and perfectly inverse at magnetite. The dashed line is the excess volume model of Mattioli et al. (1987); gray circles are the data of Mattioli et al. (1987); open diamonds are calibration data for the magnetite end member, measured at ambient conditions; the optimized end-member contributions from this work have been subtracted from models and data.

Fig. 8 Excess model volume (black curve) along the Fe_3O_4 – Fe_2TiO_4 binary. The ordering state is calculated using the MELTS ordering routine at 1100 ºC; in other respects the volume is calculated for ambient conditions. Open circles are the data of Wechsler et al. (1984) and gray triangles are the data of Bosi et al. (2009). Optimized end-member contributions from this work have been subtracted from the data. The volume along this binary is treated as ideal in the present model; asymmetry along this join is captured in the model by the effect of ordering alone.

Fig. 9 Model volume (black curve) along the $FeCr_2O_4$ – Fe_3O_4 binary, plotted with the data of Robbins et al. (1971) (open circles) and Woodland et al. (2009) (gray circles). The model curve is calculated using the MELTS ordering routine and the volume model from this work at ambient conditions. This binary is modeled with a symmetric excess term. The asymmetry of the data, which were not included in the calibration, is captured by the s_2 ordering term.

Fig. 10 Order variable s_0 vs. temperature for pure $MgFe_2O_4$ data. The Levy et al. (2004) and Antao et al. (2005a, 2005b) data were measured at high-*T*, in situ. O'Neill et al. (1992) samples were annealed over a range of temperatures; the annealing *T* is plotted here. The solid lines are calculated using the updated MELTS ordering model at 1 bar, 3 GPa, 5 GPa, and 6 GPa for pure $MgFe_2O_4$.

FIGURES

Fig. 1

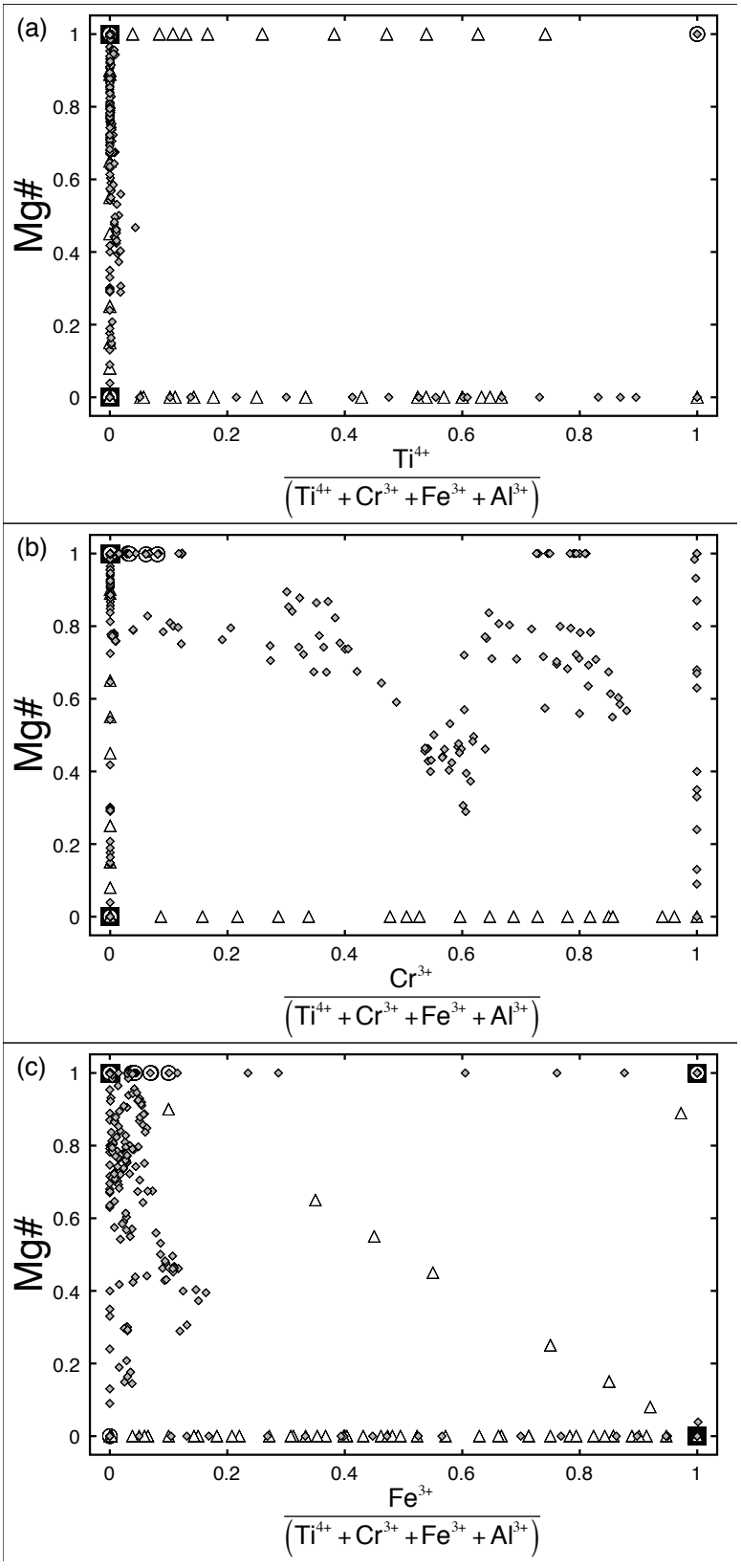

Fig. 2

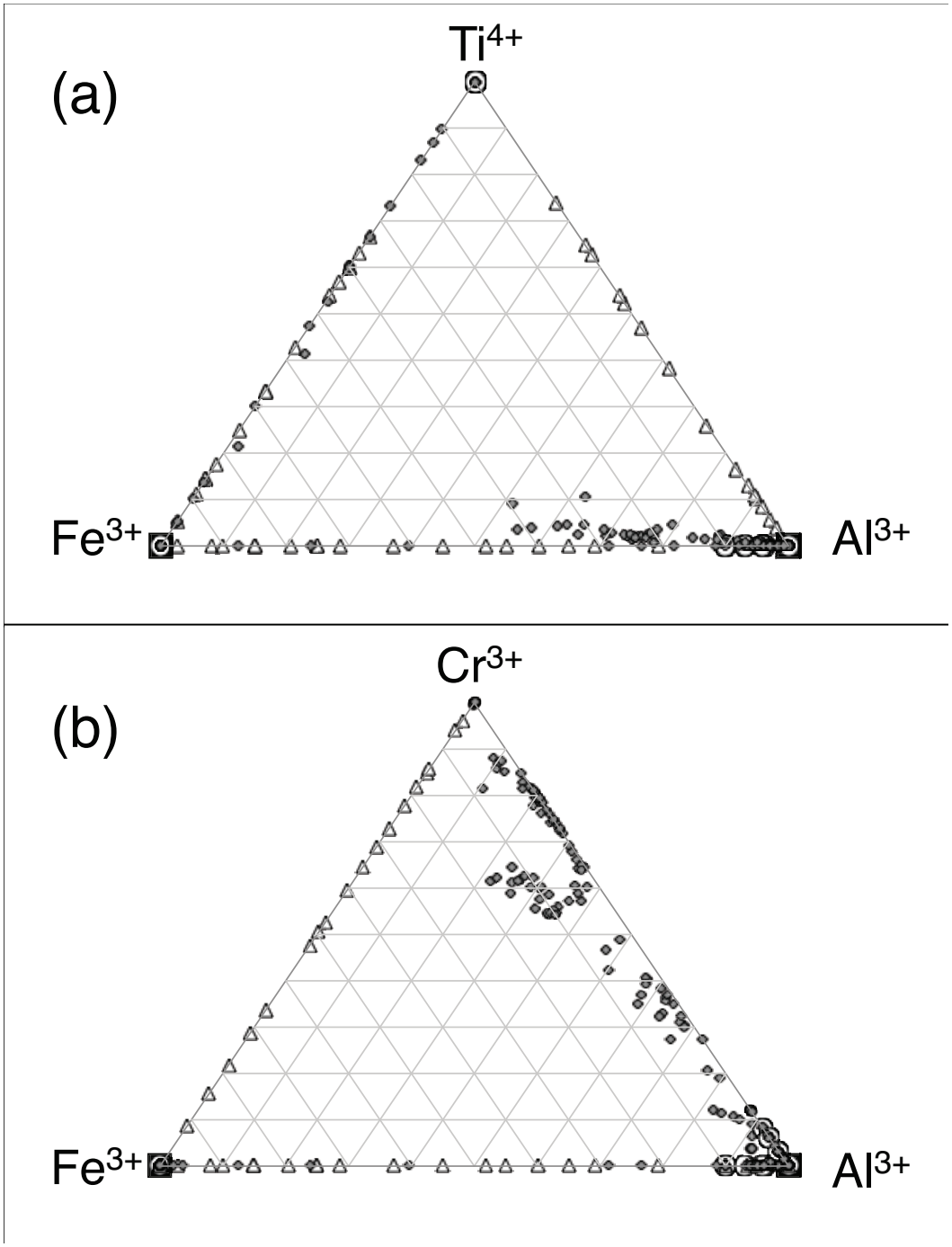

Fig. 3

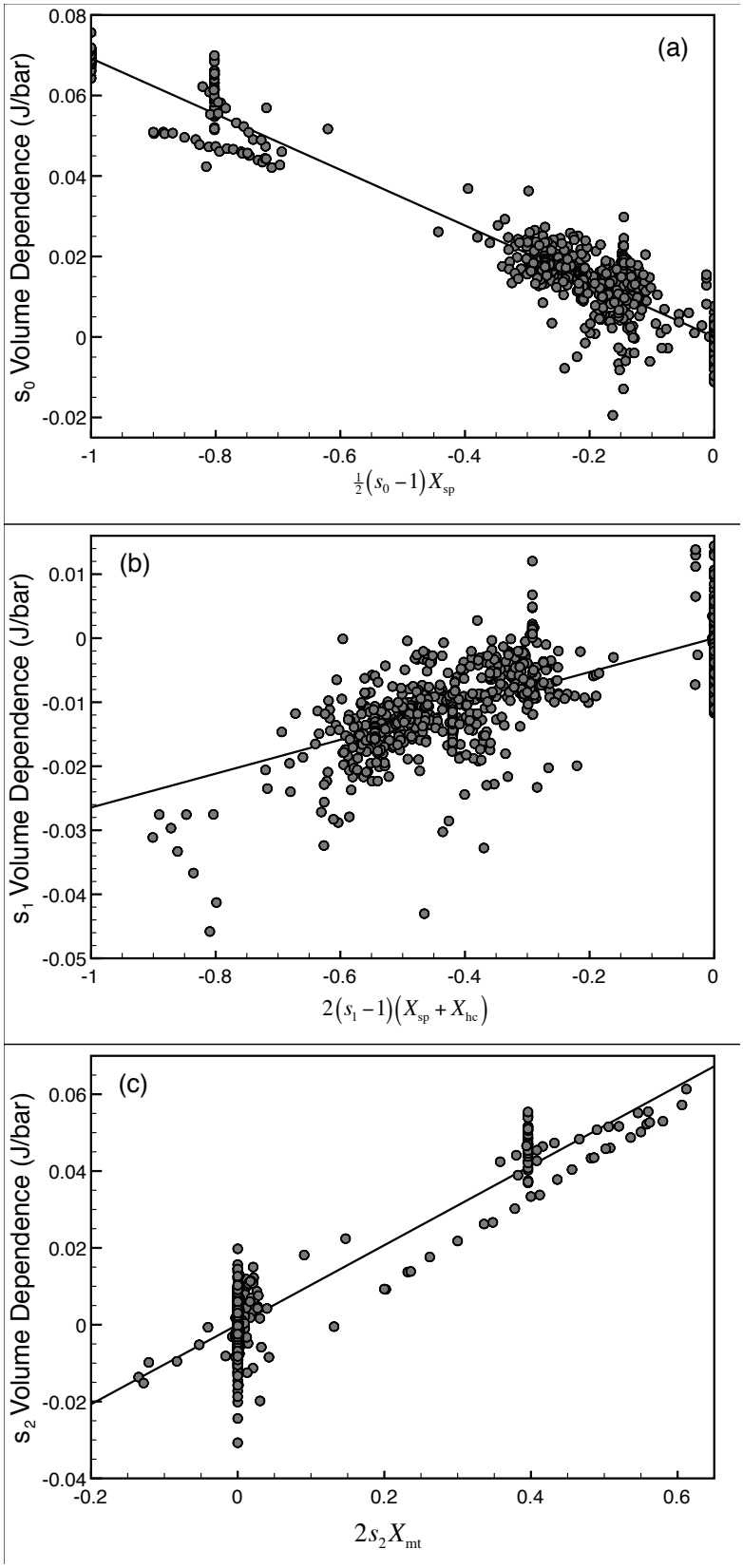
(a)
s_0 Volume Dependence (J/bar)
$\frac{1}{2}(s_0-1)X_{sp}$
(b)
s_1 Volume Dependence (J/bar)
$2(s_1-1)(X_{sp}+X_{hc})$
(c)
s_2 Volume Dependence (J/bar)
$2s_2X_{mt}$

Fig. 4

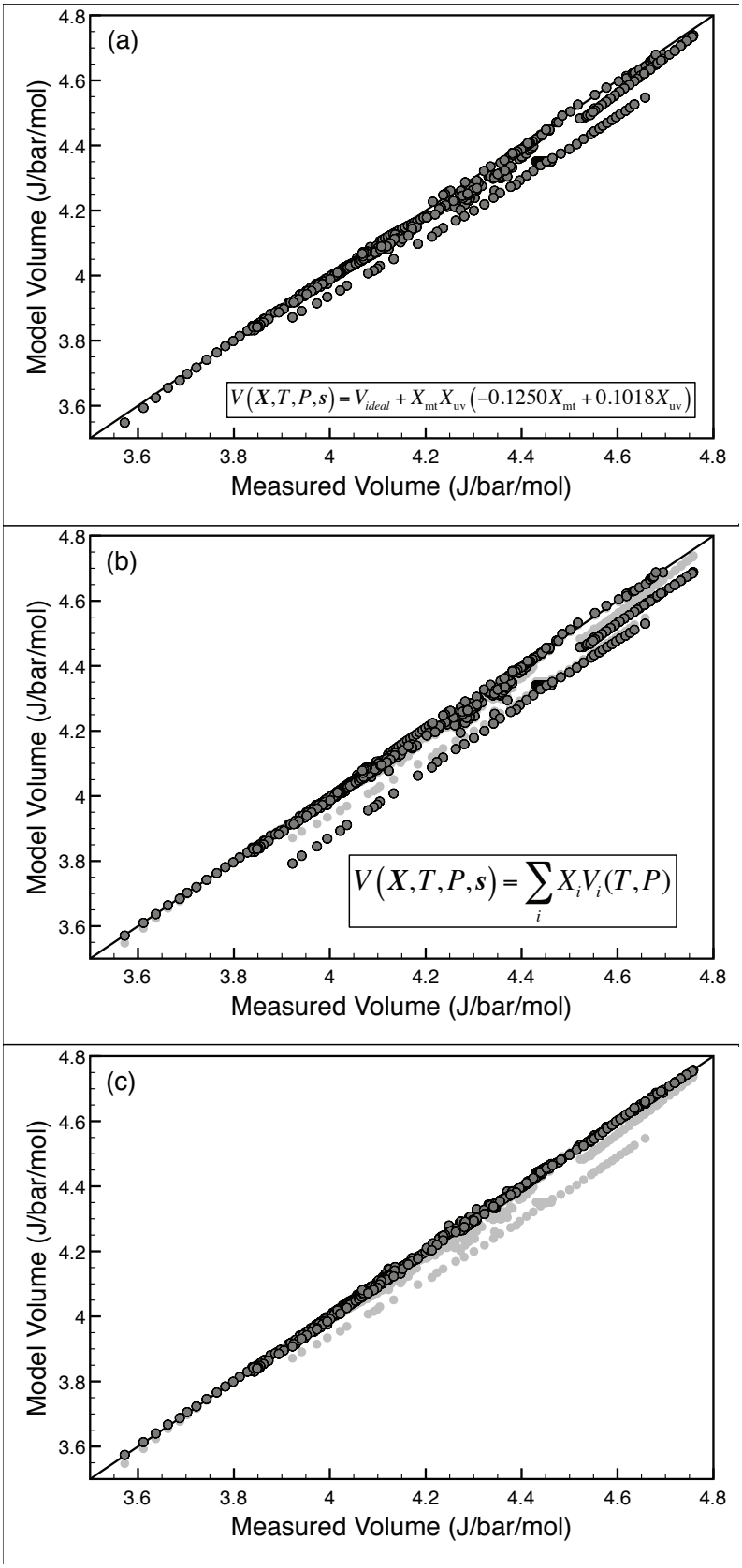
(a)
Model Volume (J/bar/mol)
Measured Volume (J/bar/mol)
$V(\boldsymbol{X},T,P,\boldsymbol{s}) = V_{ideal} + X_{\mathrm{mt}}X_{\mathrm{uv}}\left(-0.1250X_{\mathrm{mt}} + 0.1018X_{\mathrm{uv}}\right)$
(b)
Model Volume (J/bar/mol)
Measured Volume (J/bar/mol)
$V(\boldsymbol{X},T,P,\boldsymbol{s}) = \sum_i X_i V_i(T,P)$
(c)
Model Volume (J/bar/mol)
Measured Volume (J/bar/mol)
3.6
3.8
4
4.2
4.4
4.6
4.8

Fig. 5

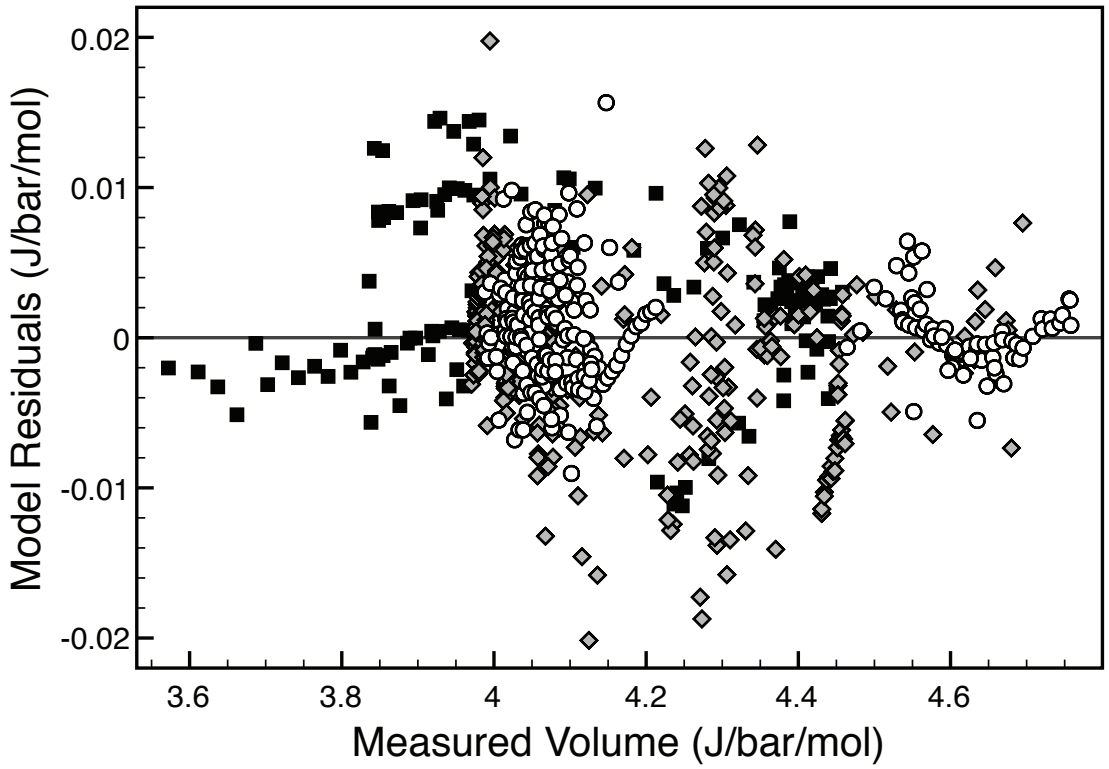
0.02
0.01
0
-0.01
-0.02
Model Residuals (J/bar/mol)
3.6
3.8
4
4.2
4.4
4.6
Measured Volume (J/bar/mol)

Fig. 6

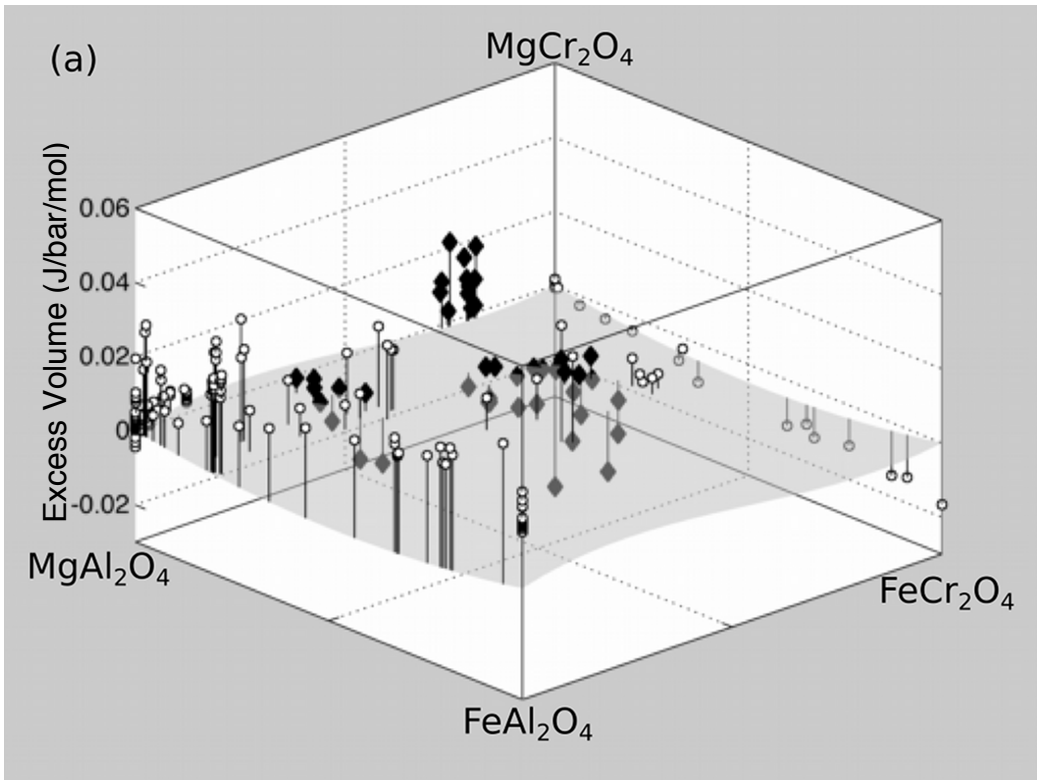
(a)
$MgCr_2O_4$
Excess Volume (J/bar/mol)
0.06
0.04
0.02
0
-0.02
$MgAl_2O_4$
$FeCr_2O_4$
$FeAl_2O_4$

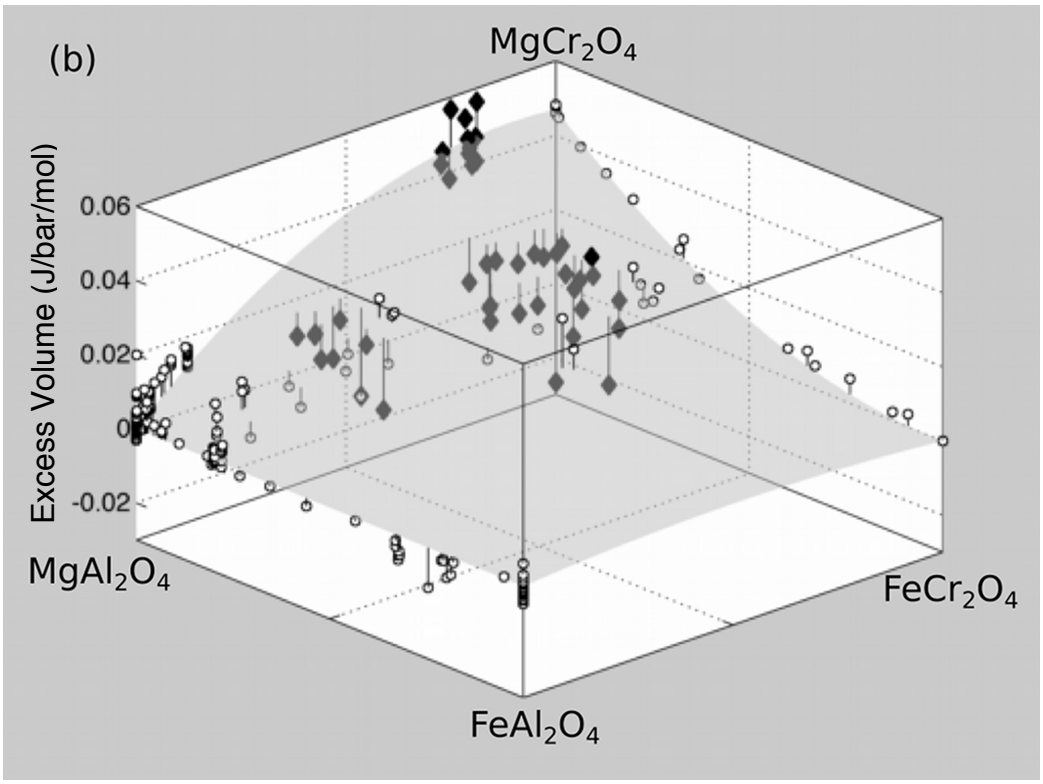
(b)
$MgCr_2O_4$
Excess Volume (J/bar/mol)
0.06
0.04
0.02
0
-0.02
$MgAl_2O_4$
$FeCr_2O_4$
$FeAl_2O_4$

Fig. 7

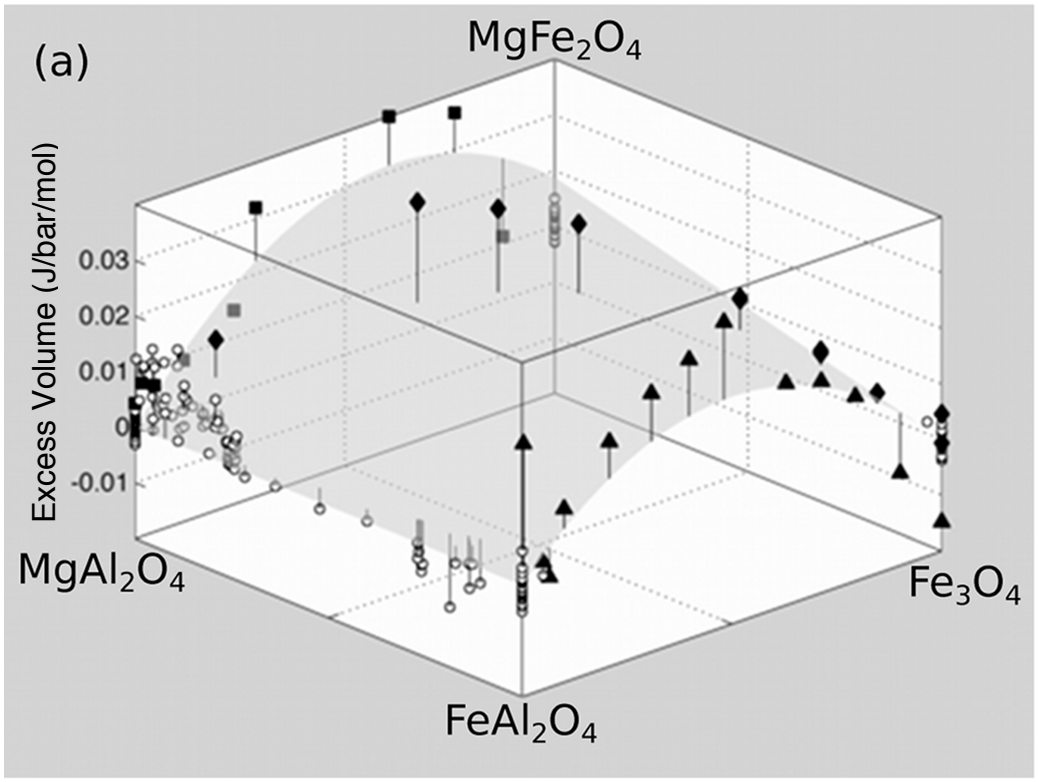
(a)
MgFe2O4
Excess Volume (J/bar/mol)
0.03
0.02
0.01
0
-0.01
MgAl2O4
Fe3O4
FeAl2O4

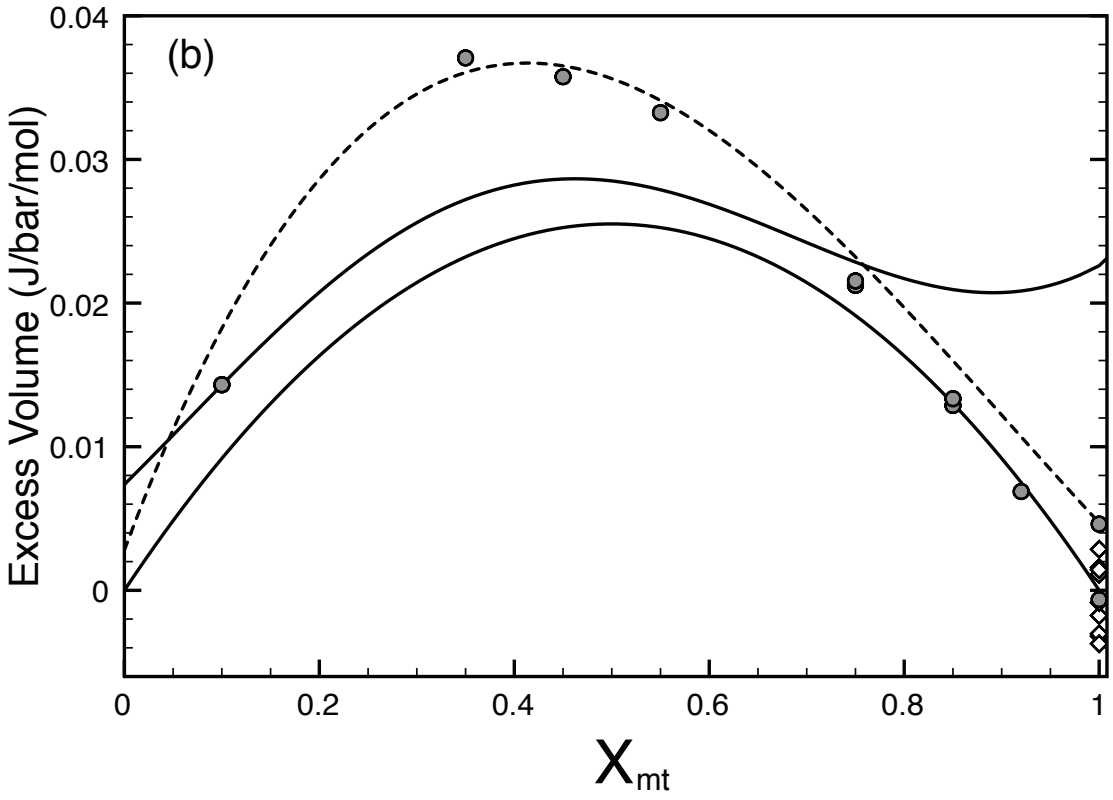
(b)
Excess Volume (J/bar/mol)
0.04
0.03
0.02
0.01
0
0
0.2
0.4
0.6
0.8
1
Xmt

Fig. 8

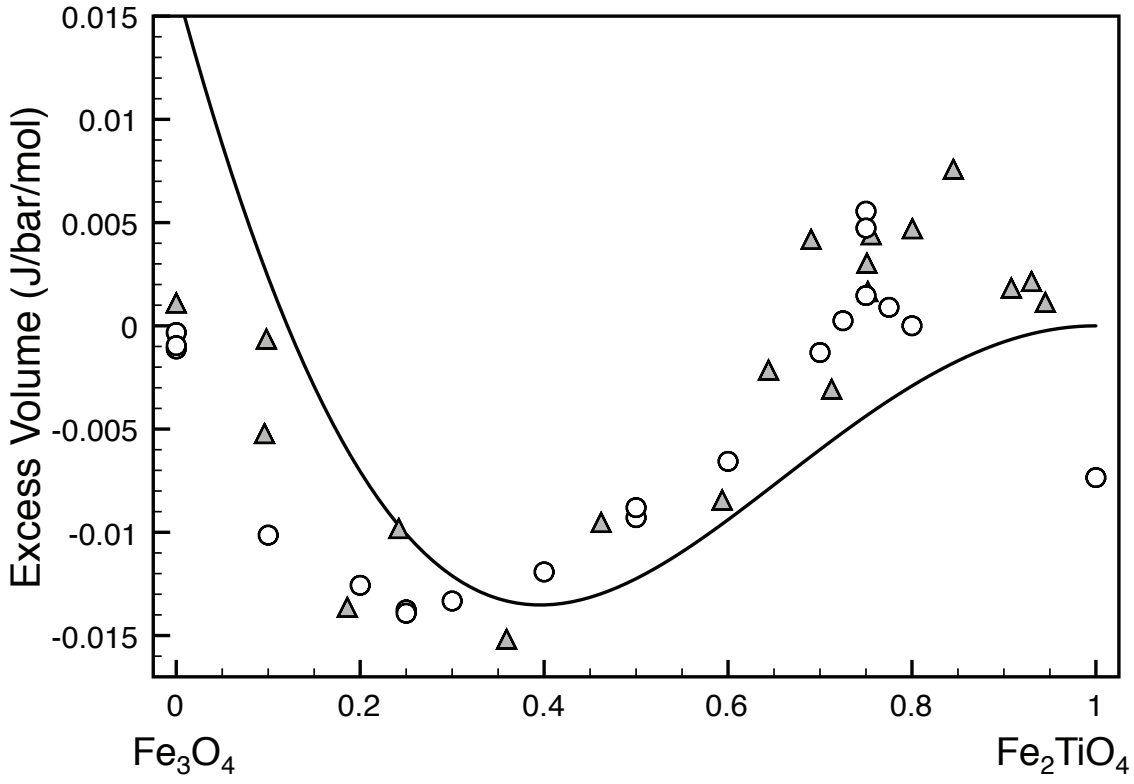
0.015
0.01
0.005
0
-0.005
-0.01
-0.015
Excess Volume (J/bar/mol)
0
0.2
0.4
0.6
0.8
1
Fe3O4
Fe2TiO4

Fig. 9

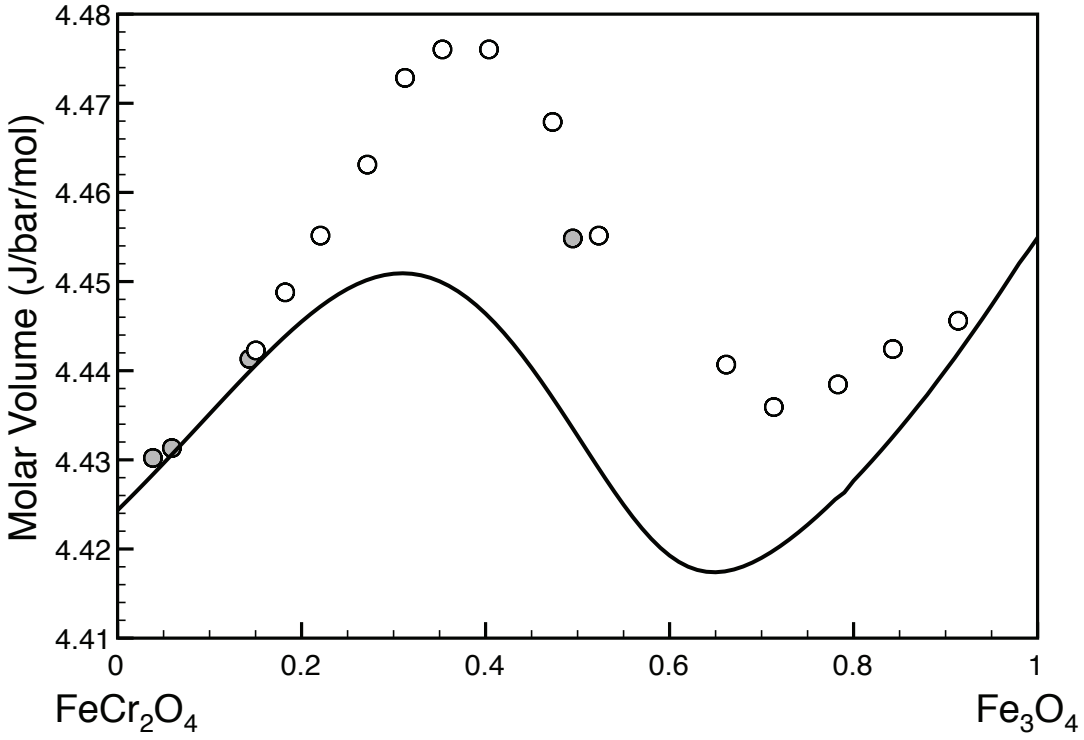
Molar Volume (J/bar/mol)
4.48
4.47
4.46
4.45
4.44
4.43
4.42
4.41
0
0.2
0.4
0.6
0.8
1
FeCr2O4
Fe3O4

Fig. 10

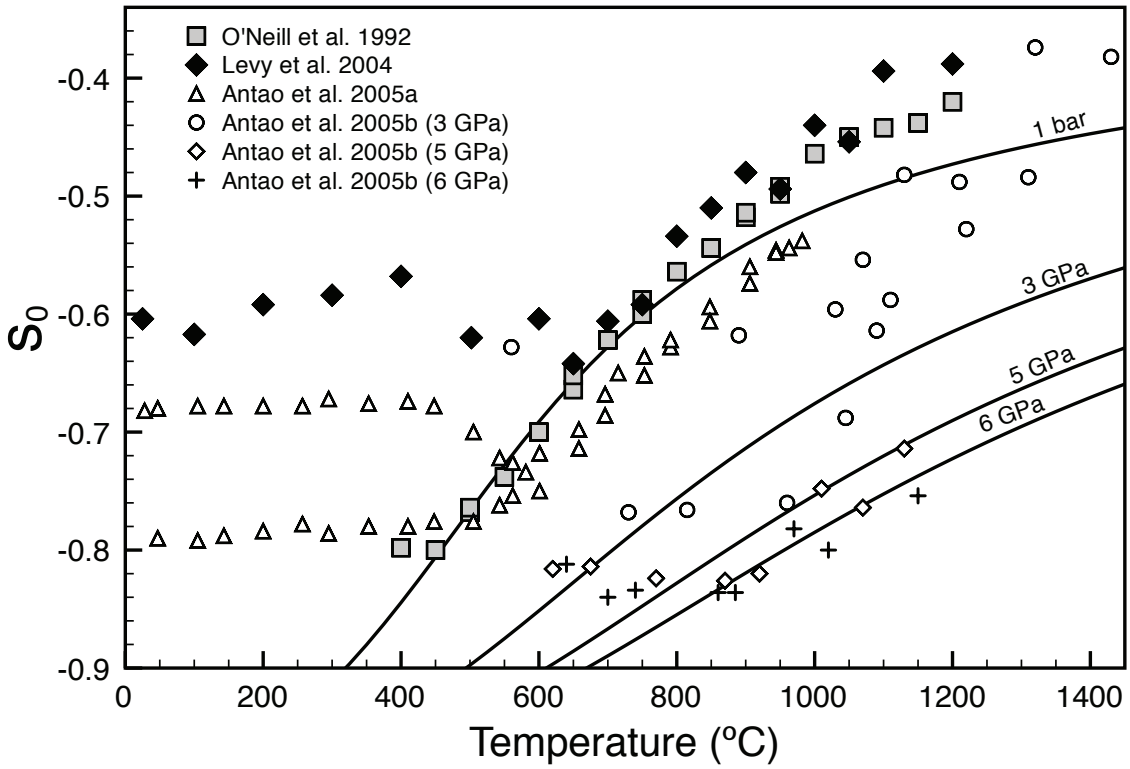
O'Neill et al. 1992
Levy et al. 2004
Antao et al. 2005a
Antao et al. 2005b (3 GPa)
Antao et al. 2005b (5 GPa)
Antao et al. 2005b (6 GPa)
1 bar
3 GPa
5 GPa
6 GPa
S0
-0.4
-0.5
-0.6
-0.7
-0.8
-0.9
0
200
400
600
800
1000
1200
1400
Temperature (ºC)

SUPPLEMENTARY MATERIAL

Supplement 1. Data sources used in model calibration

	Reference
1	Andreozzi, G.B. and Lucchesi, S. 2002
2	Andreozzi, G.B. and Princivalle, F. 2002
3	Andreozzi, G.B. et al. 2000
4	Andreozzi, G.B. et al. 2001
5	Bosi, F. et al. 2007
6	Bosi, F. et al. 2009
7	Brey, G.P. et al. 1999
8	Carbonin, S. et al. 1996
9	Carbonin, S. et al. 2002
10	Carraro, A. 2003
11	Della Giusta, A. et al. 1996
12	Doroshev, A.M. et al. 1997
13	Finger, L.W. et al. 1986
14	Fleet, M.E. 1981
15	Fleet, M.E. 1984
16	Gatta, G.D. et al. 2007
17	Girnis, A.V. et al. 2003
18	Harrison, R.J. et al. 1998
19	Hill, R.J. 1984
20	Ishii, M. et al. 1982
21	Larsson, L. et al. 1994
22	Lavina, B. et al. 2003
23	Lavina, B. et al. 2005
24	Lavina, B. et al. 2009
25	Lenaz, D. and Princivalle, F. 2005
26	Lenaz, D. et al. 2004
27	Lenaz, D. et al. 2007
28	Lenaz, D. et al. 2009
29	Levy, D. et al. 2003
30	Levy, D. et al. 2004
31	Lucchesi, S. et al. 1998
32	Martignago, F. et al. 2003
33	Martignago, F. et al. 2006
34	Menegazzo, G. and Carbonin, S. 1998
35	Millard, R.L. et al. 1995
36	Nakagiri, N. et al. 1986
37	Nakatsuka, A. et al. 2004
38	Nestola, F. et al. 2007
39	O'Neill, H.St.C. and Dollase, W.A. 1994
40	O'Neill, H.St.C. et al. 1992
41	O'Neill, H.St.C. et al. 2003

42 Peterson, R.C. et al. 1991
43 Princivalle, F. et al. 1999
44 Princivalle, F. et al. 2006
45 Redfern, S.A.T. et al. 1999
46 Sedler, I.K. et al. 1994
47 Tabira, Y. and Withers, R.L. 1999
48 Waerenborgh, J.C. et al. 1994
49 Wechsler, B.A. and Von Dreele, R.B. 1989
50 Wechsler, B.A. et al. 1984
51 Yamanaka, T. et al. 2001

Supplement 2. Data used in model calibration

AMCSD ID	Reference (see Supplement 1)	*a* (Å)	*V* (J/bar/mol)	*V residuals* (J/bar/mol)	*P* (GPa)	*T* (°C)	T site				M site					
							Al	Fe^{2+}	Fe^{3+}	Mg	Al	Fe^{2+}	Fe^{3+}	Mg	Cr	Ti
6033	25	8.2837(1)	4.2789	0.00703	0.0001	25	0.00100	0.51878	0.06500	0.41522	0.36100	0.02360	0.03000	0.01590	0.56250	0.00700
6034	25	8.2905(1)	4.2895	0.00831	0.0001	25	0.00500	0.49959	0.02700	0.46841	0.33900	0.00734	0.07150	0.02366	0.54350	0.01500
6037	25	8.3232(2)	4.3404	0.00683	0.0001	25	0.00100	0.51976	0.05700	0.42224	0.24562	0.02791	0.07654	0.04163	0.56678	0.04152
6036	25	8.2996(3)	4.3036	-0.00632	0.0001	25	-	0.51000	0.03900	0.45100	0.26900	-	0.08600	0.02550	0.61100	0.00850
6039	25	8.3039(2)	4.3103	-0.01347	0.0001	25	-	0.53200	0.02500	0.44300	0.24350	0.00567	0.10250	0.01133	0.62850	0.00850
6041	25	8.3011(1)	4.3059	0.01077	0.0001	25	0.02000	0.50754	0.03600	0.43646	0.28850	0.01251	0.07700	0.02399	0.59050	0.00750
6042	25	8.3004(4)	4.3049	0.00880	0.0001	25	0.02700	0.52600	0.01500	0.43200	0.28700	0.01054	0.08150	0.01896	0.59350	0.00850
6035	25	8.3171(1)	4.3309	-0.01287	0.0001	25	0.00100	0.58700	0.02800	0.38400	0.22450	0.01424	0.14600	0.00876	0.59350	0.01300
6038	25	8.3191(2)	4.3340	-0.00918	0.0001	25	-	0.60300	0.03900	0.35800	0.22511	0.01925	0.12806	0.01176	0.60080	0.01501
6040	25	8.2829(1)	4.2777	0.01261	0.0001	25	0.02600	0.56700	0.01200	0.39500	0.36182	0.00316	0.03698	0.02633	0.56272	0.00900
6043	25	8.2822(2)	4.2766	0.00498	0.0001	25	0.03600	0.56700	0.01000	0.38700	0.34400	0.01115	0.03400	0.02335	0.57650	0.01100
6044	25	8.3250(1)	4.3432	0.00603	0.0001	25	0.00200	0.70719	0.02800	0.26281	0.24350	0.00585	0.11500	0.02715	0.59050	0.01800
6045	25	8.3269(1)	4.3462	0.01282	0.0001	25	0.00800	0.68342	0.02700	0.28158	0.24900	0.02600	0.10350	0.00900	0.59450	0.01800
7226	27	8.2913(1)	4.2907	0.00930	0.0001	25	0.03000	0.55917	0.01200	0.39883	0.33600	0.01176	0.08650	0.01924	0.53650	0.01000
7227	27	8.2942(2)	4.2952	0.00908	0.0001	25	0.02500	0.57000	0.01600	0.38900	0.32750	0.00639	0.08700	0.02611	0.54150	0.01150
7228	27	8.2944(2)	4.2955	0.00997	0.0001	25	0.03900	0.53800	0.00700	0.41600	0.32000	0.00877	0.10450	0.02523	0.53100	0.01050
7229	27	8.2950(1)	4.2965	0.00864	0.0001	25	0.02300	0.53767	0.01200	0.42733	0.32250	0.00548	0.10250	0.02302	0.53550	0.01100
7230	27	8.2902(1)	4.2890	0.00504	0.0001	25	0.02900	0.53067	0.01700	0.42333	0.32800	0.00842	0.09600	0.02358	0.53450	0.00950
7231	27	8.2900(2)	4.2887	0.00953	0.0001	25	0.03400	0.51862	0.00700	0.44038	0.33250	0.01364	0.09600	0.01636	0.53250	0.00900
7232	27	8.2994(2)	4.3033	-0.00198	0.0001	25	-	0.57863	0.08300	0.33837	0.31034	0.01987	0.08096	0.03660	0.53623	0.01599
7233	27	8.3013(3)	4.3063	-0.02300	0.0001	25	0.00100	0.60589	0.03600	0.35711	0.27000	0.00164	0.12400	0.02736	0.55950	0.01750
7234	27	8.2929(2)	4.2932	-0.01383	0.0001	25	-	0.54757	0.04500	0.40743	0.29100	0.00444	0.08350	0.02556	0.58450	0.01100
7235	27	8.2963(3)	4.2985	0.00175	0.0001	25	-	0.53600	0.03700	0.42700	0.30950	0.00711	0.08750	0.02189	0.56300	0.01100
7236	27	8.3577(2)	4.3946	0.00086	0.0001	25	-	0.60000	-	0.40000	-	-	-	-	1.00000	-
7237	27	8.3620(1)	4.4014	0.00407	0.0001	25	-	0.65000	-	0.35000	-	-	-	-	1.00000	-

7238	27	8.3613(2)	4.4003	0.00152	0.0001	25	-	0.67000	-	0.33000	-	-	-	-	1.00000	-
7239	27	8.3672(2)	4.4096	0.00418	0.0001	25	-	0.76000	-	0.24000	-	-	-	-	1.00000	-
7240	27	8.3710(1)	4.4156	0.00173	0.0001	25	-	0.87000	-	0.13000	-	-	-	-	1.00000	-
7241	27	8.3739(2)	4.4202	0.00316	0.0001	25	-	0.91000	-	0.09000	-	-	-	-	1.00000	-
7242	27	8.3765(2)	4.4243	0.00000	0.0001	25	-	1.00000	-	-	-	-	-	-	1.00000	-
7243	27	8.15579(6)	4.08375	-0.00332	0.0001	25	-	1.00000	-	-	1.00000	-	-	-	-	-
7244	27	8.14578(3)	4.08606	0.00614	0.0001	25	0.13500	0.86500	-	-	0.93250	0.06750	-	-	-	-
7245	27	8.15612(3)	4.10158	0.00240	0.0001	25	0.13400	0.86600	-	-	0.93300	0.06700	-	-	-	-
8912	26	8.16949(3)	4.12169	-0.00016	0.0001	25	0.13400	0.86600	-	-	0.93300	0.06700	-	-	-	-
8913	26	8.17298(3)	4.12696	-0.00075	0.0001	25	0.13300	0.86700	-	-	0.93350	0.06650	-	-	-	-
8914	26	8.17657(3)	4.13237	-0.00124	0.0001	25	0.13200	0.86800	-	-	0.93400	0.06600	-	-	-	-
8915	26	8.18021(3)	4.13787	-0.00203	0.0001	25	0.12500	0.87500	-	-	0.93750	0.06250	-	-	-	-
8916	26	8.18390(3)	4.14345	-0.00310	0.0001	25	0.11200	0.88800	-	-	0.94400	0.05600	-	-	-	-
8917	26	8.18781(3)	4.14937	-0.00268	0.0001	25	0.12200	0.87800	-	-	0.93900	0.06100	-	-	-	-
8918	26	8.19177(3)	4.15537	-0.00224	0.0001	25	0.13200	0.86800	-	-	0.93400	0.06600	-	-	-	-
8903	26	8.19571(3)	4.16134	-0.00183	0.0001	25	0.14300	0.85700	-	-	0.92850	0.07150	-	-	-	-
8904	26	8.19988(3)	4.16767	-0.00118	0.0001	25	0.15300	0.84700	-	-	0.92350	0.07650	-	-	-	-
8905	26	8.20404(3)	4.17399	-0.00044	0.0001	25	0.16600	0.83400	-	-	0.91700	0.08300	-	-	-	-
8906	26	8.20826(3)	4.18041	0.00012	0.0001	25	0.17500	0.82500	-	-	0.91250	0.08750	-	-	-	-
8907	26	8.21252(3)	4.18689	0.00074	0.0001	25	0.18500	0.81500	-	-	0.90750	0.09250	-	-	-	-
8908	26	8.21680(3)	4.19341	0.00096	0.0001	25	0.19300	0.80700	-	-	0.90850	0.09150	-	-	-	-
8909	26	8.22103(3)	4.19987	0.00156	0.0001	25	0.20100	0.79900	-	-	0.89950	0.10050	-	-	-	-
8910	26	8.22525(3)	4.20631	0.00172	0.0001	25	0.20700	0.79300	-	-	0.89650	0.10350	-	-	-	-
8911	26	8.22939(3)	4.21264	0.00201	0.0001	25	0.21900	0.78100	-	-	0.89050	0.10950	-	-	-	-
958	19	8.0895(3)	3.9850	0.00282	0.0001	25	0.23900	0.04600	-	0.71500	0.88050	-	-	0.11950	-	-
2031	18	8.0937(3)	3.9912	0.00066	0.0001	25	0.24900	0.11100	-	0.64000	0.87500	-	-	0.12500	-	-
2032	18	8.1006(3)	4.0014	0.00013	0.0001	200	0.22400	0.18800	-	0.58800	0.88300	-	0.00350	0.11350	-	-
2033	18	8.1071(3)	4.0110	-0.00209	0.0001	400	0.21400	0.27200	-	0.51400	0.88406	0.00200	0.00750	0.10645	-	-

2034	18	8.1134(3)	4.0204	-0.00159	0.0001	450	0.21900	0.34700	-	0.43400	0.88056	0.00400	0.00800	0.10745	-	-
2035	18	8.1221(3)	4.0334	-0.00385	0.0001	500	0.19400	0.42400	0.01600	0.36600	0.88356	0.01749	0.01000	0.08896	-	-
2036	18	8.1306(3)	4.0460	-0.00222	0.0001	550	0.19200	0.53100	0.01000	0.26700	0.88556	0.02699	0.01099	0.07646	-	-
2037	18	8.1406(3)	4.0610	-0.00415	0.0001	600	0.16800	0.63000	0.01700	0.18500	0.88456	0.03598	0.02049	0.05897	-	-
2038	18	8.1494(4)	4.0742	-0.00493	0.0001	650	0.15200	0.71300	0.03400	0.10100	0.88656	0.05697	0.01849	0.03798	-	-
2039	18	8.1646(3)	4.0970	-0.00348	0.0001	700	0.13300	0.84900	0.01800	-	0.88250	0.07650	0.04100	-	-	-
2040	18	8.1517(2)	4.0776	-0.00179	0.0001	750	0.14500	0.85500	-	-	0.92750	0.07250	-	-	-	-
2041	18	8.1516(2)	4.0775	0.00055	0.0001	800	0.19200	0.80800	-	-	0.90400	0.09600	-	-	-	-
2042	18	8.1514(2)	4.0772	0.00051	0.0001	850	0.19700	0.80300	-	-	0.90150	0.09850	-	-	-	-
2043	18	8.1511(2)	4.0767	0.00043	0.0001	900	0.20400	0.79600	-	-	0.89800	0.10200	-	-	-	-
2044	18	8.1501(2)	4.0752	-0.00165	0.0001	950	0.19300	0.80700	-	-	0.90350	0.09650	-	-	-	-
2045	18	8.1513(2)	4.0770	-0.00472	0.0001	1000	0.10100	0.89900	-	-	0.94950	0.05050	-	-	-	-
2046	18	8.1518(2)	4.0778	-0.00381	0.0001	1050	0.10400	0.89600	-	-	0.94800	0.05200	-	-	-	-
2047	18	8.1522(2)	4.0784	-0.00247	0.0001	1100	0.11800	0.88200	-	-	0.94100	0.05900	-	-	-	-
2048	18	8.1521(2)	4.0782	-0.00225	0.0001	1150	0.12500	0.87500	-	-	0.93750	0.06250	-	-	-	-
2873	1	8.1522(2)	4.0784	-0.00109	0.0001	25	0.14400	0.85600	-	-	0.92800	0.07200	-	-	-	-
2874	1	8.1525(2)	4.0788	-0.00048	0.0001	25	0.14700	0.85300	-	-	0.92650	0.07350	-	-	-	-
2875	1	8.1523(2)	4.0785	-0.00031	0.0001	25	0.15600	0.84400	-	-	0.92200	0.07800	-	-	-	-
2876	1	8.1526(2)	4.0790	0.00110	0.0001	25	0.17400	0.82600	-	-	0.91300	0.08700	-	-	-	-
2877	1	8.1522(2)	4.0784	0.00076	0.0001	25	0.17900	0.82100	-	-	0.91050	0.08950	-	-	-	-
2878	1	8.1522(2)	4.0784	0.00118	0.0001	25	0.18700	0.81300	-	-	0.90650	0.09350	-	-	-	-
2879	1	8.1523(2)	4.0785	0.00096	0.0001	25	0.18000	0.82000	-	-	0.91000	0.09000	-	-	-	-
2880	1	8.1520(2)	4.0781	0.00094	0.0001	25	0.18800	0.81200	-	-	0.90600	0.09400	-	-	-	-
2881	1	8.1507(2)	4.0761	-0.00123	0.0001	25	0.18400	0.81600	-	-	0.90800	0.09200	-	-	-	-
2882	1	8.1507(2)	4.0761	-0.00149	0.0001	25	0.17900	0.82100	-	-	0.91050	0.08950	-	-	-	-
2872	1	8.1547(3)	4.0821	0.00219	0.0001	25	0.13500	0.86500	-	-	0.93250	0.06750	-	-	-	-
6509	21	8.1546(3)	4.0820	0.00315	0.0001	25	0.15600	0.84400	-	-	0.92200	0.07800	-	-	-	-
6510	21	8.1396(1)	4.0595	-0.00582	0.0001	25	0.18000	0.62000	0.02000	0.18000	0.88000	0.04000	0.02000	0.06000	-	-

6511	21	8.1388(1)	4.0583	-0.00774	0.0001	25	0.18000	0.62000	0.02000	0.18000	0.88000	0.04500	0.02000	0.05500	-	-
6512	21	8.1384(1)	4.0577	-0.00797	0.0001	25	0.18182	0.61616	0.01010	0.19192	0.88000	0.04500	0.02500	0.05000	-	-
6513	21	8.1380(1)	4.0571	-0.00635	0.0001	25	0.16000	0.60000	0.03000	0.21000	0.89000	0.05500	0.01000	0.04500	-	-
6514	21	8.1380(1)	4.0571	-0.00920	0.0001	25	0.17000	0.61000	0.02000	0.20000	0.89000	0.04500	0.02000	0.04500	-	-
6515	21	8.2367(5)	4.2065	-0.00397	0.0001	25	0.03400	0.39856	0.03000	0.53744	0.46950	0.00609	0.00850	0.02741	0.48650	0.00200
6516	21	8.2892(1)	4.2874	0.00275	0.0001	25	0.01800	0.43482	0.02400	0.52318	0.30500	0.02349	0.07350	0.01151	0.57450	0.01200
6517	21	8.2453(2)	4.2197	0.00153	0.0001	25	0.05600	0.36017	0.01700	0.56683	0.44400	0.00052	0.04750	0.04248	0.45800	0.00750
6518	21	8.2701(2)	4.2579	-0.00163	0.0001	25	0.04100	0.41630	0.00100	0.54170	0.33700	0.00750	0.03700	0.01500	0.60100	0.00250
6519	21	8.3341(2)	4.3575	0.00105	0.0001	25	-	-	-	1.00000	-	-	-	-	1.00000	-
6520	21	8.3342(2)	4.3577	0.00120	0.0001	25	-	-	-	1.00000	-	-	-	-	1.00000	-
6521	21	8.3339(2)	4.3572	0.00073	0.0001	25	-	-	-	1.00000	-	-	-	-	1.00000	-
6522	21	8.3327(4)	4.3553	-0.00115	0.0001	25	-	-	-	1.00000	-	-	-	-	1.00000	-
6523	21	8.3329(1)	4.3556	-0.00084	0.0001	25	-	-	-	1.00000	-	-	-	-	1.00000	-
6524	21	8.3328(5)	4.3555	-0.00099	0.0001	25	-	-	-	1.00000	-	-	-	-	1.00000	-
6525	21	8.3340(1)	4.3573	-0.00047	0.0001	25	-	0.01600	-	0.98400	-	-	0.00400	-	0.99600	-
6526	21	8.3352(1)	4.3592	-0.00119	0.0001	25	-	0.06800	-	0.93200	-	-	0.00200	-	0.99800	-
6527	21	8.3379(3)	4.3635	-0.00020	0.0001	25	-	0.13000	-	0.87000	-	-	-	-	1.00000	-
7893	48	8.3415(2)	4.3691	0.00137	0.0001	25	-	0.20000	-	0.80000	-	-	-	-	1.00000	-
7897	48	8.3462(1)	4.3765	0.00143	0.0001	25	-	0.32000	-	0.68000	-	-	-	-	1.00000	-
8938	23	8.3490(1)	4.3809	0.00521	0.0001	25	-	0.33000	-	0.67000	-	-	-	-	1.00000	-
8939	23	8.3465(1)	4.3770	-0.00127	0.0001	25	-	0.37000	-	0.63000	-	-	-	-	1.00000	-
8940	23	8.3805(3)	4.4307	-0.01171	0.0001	25	-	-	0.89900	0.10100	-	-	0.55050	0.44950	-	-
8941	23	8.3806(3)	4.4308	-0.01141	0.0001	25	-	-	0.90000	0.10000	-	-	0.55000	0.45000	-	-
8942	23	8.3827(3)	4.4342	-0.01028	0.0001	25	-	-	0.88400	0.11600	-	-	0.55800	0.44200	-	-
7767	39	8.3827(3)	4.4342	-0.01056	0.0001	25	-	-	0.88200	0.11800	-	-	0.55900	0.44100	-	-
7768	39	8.3845(3)	4.4370	-0.00949	0.0001	25	-	-	0.86900	0.13100	-	-	0.56550	0.43450	-	-
7769	39	8.3863(3)	4.4399	-0.00925	0.0001	25	-	-	0.85000	0.15000	-	-	0.57500	0.42500	-	-
7771	39	8.3883(3)	4.4431	-0.00856	0.0001	25	-	-	0.83200	0.16800	-	-	0.58400	0.41600	-	-

8365	47	8.3883(3)	4.4431	-0.00938	0.0001	25	-	-	0.82600	0.17400	-	-	0.58700	0.41300	-	-
1484	40	8.3899(3)	4.4456	-0.00891	0.0001	25	-	-	0.81100	0.18900	-	-	0.59450	0.40550	-	-
1485	40	8.3914(3)	4.4480	-0.00804	0.0001	25	-	-	0.80000	0.20000	-	-	0.60000	0.40000	-	-
1486	40	8.3914(3)	4.4480	-0.00886	0.0001	25	-	-	0.79400	0.20600	-	-	0.60300	0.39700	-	-
1487	40	8.3934(3)	4.4512	-0.00733	0.0001	25	-	-	0.78200	0.21800	-	-	0.60900	0.39100	-	-
1488	40	8.3946(3)	4.4531	-0.00680	0.0001	25	-	-	0.77200	0.22800	-	-	0.61400	0.38600	-	-
1489	40	8.3959(3)	4.4552	-0.00652	0.0001	25	-	-	0.75900	0.24100	-	-	0.62050	0.37950	-	-
1490	40	8.3959(3)	4.4552	-0.00680	0.0001	25	-	-	0.75700	0.24300	-	-	0.62150	0.37850	-	-
1491	40	8.3970(3)	4.4569	-0.00656	0.0001	25	-	-	0.74600	0.25400	-	-	0.62700	0.37300	-	-
1492	40	8.3970(3)	4.4569	-0.00615	0.0001	25	-	-	0.74900	0.25100	-	-	0.62550	0.37450	-	-
1493	40	8.3981(3)	4.4587	-0.00674	0.0001	25	-	-	0.73200	0.26800	-	-	0.63400	0.36600	-	-
1494	40	8.3987(3)	4.4596	-0.00675	0.0001	25	-	-	0.72500	0.27500	-	-	0.63750	0.36250	-	-
1495	40	8.3998(3)	4.4614	-0.00555	0.0001	25	-	-	0.72100	0.27900	-	-	0.63950	0.36050	-	-
1496	40	8.4000(3)	4.4617	-0.00550	0.0001	25	-	-	0.71900	0.28100	-	-	0.64050	0.35950	-	-
1497	40	8.3998(3)	4.4614	-0.00706	0.0001	25	-	-	0.71000	0.29000	-	-	0.64500	0.35500	-	-
1498	40	8.2796(5)	4.2726	0.00875	0.0001	25	0.09000	-	0.53000	0.38000	0.35000	-	0.34000	0.31000	-	-
1499	40	8.3252(4)	4.3436	0.00717	0.0001	25	0.05051	-	0.66667	0.28283	0.21000	-	0.43000	0.36000	-	-
1500	40	8.3422(5)	4.3702	-0.01410	0.0001	25	-	-	0.81000	0.19000	0.11000	-	0.48000	0.41000	-	-
1501	40	8.4716(4)	4.5768	-0.00645	0.0001	25	-	0.57900	0.42100	-	0.01400	0.50350	0.19000	-	-	0.29250
1502	40	8.4875(4)	4.6026	-0.00185	0.0001	25	-	0.64000	0.36000	-	-	0.50200	0.17600	-	-	0.32200
1503	40	8.4972(5)	4.6184	-0.00237	0.0001	25	-	0.70000	0.30000	-	-	0.50600	0.13750	-	-	0.35650
1504	40	8.4975(4)	4.6189	0.00010	0.0001	25	-	0.75500	0.24500	-	-	0.46800	0.18700	-	-	0.34500
1505	40	8.5052(5)	4.6314	-0.00148	0.0001	25	-	0.81300	0.18700	-	-	0.46950	0.15450	-	-	0.37600
8861	37	8.5059(5)	4.6326	0.00107	0.0001	23	-	0.78900	0.21100	-	-	0.48100	0.14350	-	-	0.37550
8862	37	8.5079(4)	4.6358	0.00317	0.0001	23	-	0.77900	0.22100	-	-	0.48800	0.13400	-	-	0.37800
8863	37	8.5139(5)	4.6457	0.00188	0.0001	23	-	0.86900	0.13100	-	-	0.46573	0.13407	-	-	0.40020
a	37	8.5220(4)	4.6589	0.00466	0.0001	23	-	0.93600	0.06400	-	-	0.45450	0.12300	-	-	0.42250
a	37	8.5274(5)	4.6678	0.00008	0.0001	23	-	1.00000	-	-	-	0.45400	0.09200	-	-	0.45400

a	37	8.5307(4)	4.6732	0.00113	0.0001	23	-	1.00000	-	-	-	0.46500	0.07000	-	-	0.46500
a	37	8.5322(4)	4.6757	0.00051	0.0001	23	-	1.00000	-	-	-	0.47250	0.05500	-	-	0.47250
a	37	8.44183(3)	4.52867	0.00185	0.0001	23	-	-	-	1.00000	-	-	-	0.50000	-	0.50000
a	37	8.4376(5)	4.5219	-0.00496	0.0001	23	-	-	-	1.00000	-	-	-	0.50000	-	0.50000
4822	6	8.3967(3)	4.4564	0.00111	0.0001	25	-	-	1.00000	-	-	0.50000	0.50000	-	-	-
4823	6	8.4067(5)	4.4724	0.00021	0.0001	25	-	0.06700	0.93300	-	-	0.51450	0.43750	-	-	0.04800
4824	6	8.4095(5)	4.4768	0.00352	0.0001	25	-	0.07600	0.92400	-	-	0.51150	0.43950	-	-	0.04900
4825	6	8.4145(5)	4.4848	0.00035	0.0001	25	-	0.10300	0.89700	-	-	0.54150	0.36550	-	-	0.09300
4826	6	8.4250(5)	4.5016	0.00273	0.0001	25	-	0.16200	0.83800	-	-	0.54000	0.33900	-	-	0.12100
4827	6	8.4348(5)	4.5174	-0.00191	0.0001	25	-	0.26700	0.73300	-	0.01500	0.54300	0.26500	-	-	0.17700
4828	6	8.4569(4)	4.5530	-0.00095	0.0001	25	-	0.38500	0.61500	-	-	0.53850	0.23050	-	-	0.23100
4829	6	8.3949(3)	4.4536	-0.00176	0.0001	25	-	-	1.00000	-	-	0.50000	0.50000	-	-	-
4830	6	8.3970(1)	4.4569	0.00159	0.0001	25	-	-	1.00000	-	-	0.50000	0.50000	-	-	-
4831	6	8.3940(10)	4.4521	-0.00319	0.0001	25	-	-	1.00000	-	-	0.50000	0.50000	-	-	-
4832	6	8.3950(5)	4.4537	-0.00085	0.0001	25	-	-	1.00000	-	-	0.50000	0.50000	-	-	-
4833	6	8.3941(7)	4.4523	-0.00303	0.0001	25	-	-	1.00000	-	-	0.50000	0.50000	-	-	-
4815	6	8.3969(8)	4.4567	0.00143	0.0001	25	-	-	1.00000	-	-	0.50000	0.50000	-	-	-
4816	6	8.3975(7)	4.4577	0.00146	0.0001	25	-	-	0.98700	0.01300	-	0.48000	0.50700	0.01300	-	-
4817	6	8.08435(7)	3.97737	0.00042	0.0001	25	0.32000	-	-	0.68000	0.84000	-	-	0.16000	-	-
4818	6	8.07975(5)	3.97059	-0.00310	0.0001	25	0.12000	-	-	0.88000	0.94000	-	-	0.06000	-	-
4819	6	8.08360(6)	3.97627	0.00039	0.0001	25	0.21800	-	-	0.78200	0.89100	-	-	0.10900	-	-
4820	6	8.08360(6)	3.97627	0.00172	0.0001	25	0.14300	-	-	0.85700	0.92850	-	-	0.07150	-	-
4821	6	8.1154(3)	4.0234	-0.00102	0.0001	25	0.18182	-	0.09291	0.72527	0.80890	-	0.05403	0.13707	-	-
6568	46	8.1082(6)	4.0127	0.00321	0.0001	25	0.20721	-	0.06106	0.73173	0.81900	-	0.03950	0.14150	-	-
1746	35	8.0937(5)	3.9912	-0.00586	0.0001	25	0.24068	-	0.03625	0.72306	0.83950	-	0.02450	0.13600	-	-
9832	49	8.0889(2)	3.9841	0.00356	0.0001	25	0.14300	-	-	0.85700	0.91350	-	-	0.07150	0.01500	-
953	50	8.0889(2)	3.9841	0.00358	0.0001	25	0.14200	-	-	0.85800	0.91400	-	-	0.07100	0.01500	-
7389	13	8.0889(2)	3.9841	0.00355	0.0001	25	0.14400	-	-	0.85600	0.91300	-	-	0.07200	0.01500	-

7390	13	8.0888(2)	3.9839	0.00340	1	25	0.14400	-	-	0.85600	0.91300	-	-	0.07200	0.01500	-
7391	13	8.0889(1)	3.9841	0.00348	2	25	0.14800	-	-	0.85200	0.91100	-	-	0.07400	0.01500	-
7392	13	8.0888(2)	3.9839	0.00328	3	25	0.15100	-	-	0.84900	0.90950	-	-	0.07550	0.01500	-
7393	13	8.0889(2)	3.9841	0.00334	4	25	0.15600	-	-	0.84400	0.90700	-	-	0.07800	0.01500	-
7418	36	8.0887(1)	3.9838	0.00299	0.0001	25	0.15900	-	-	0.84100	0.90550	-	-	0.07950	0.01500	-
7419	36	8.0888(1)	3.9839	0.00300	0.63	25	0.16700	-	-	0.83300	0.90150	-	-	0.08350	0.01500	-
7420	36	8.0865(1)	3.9805	-0.00217	1.55	25	0.27100	-	-	0.72900	0.84950	-	-	0.13550	0.01500	-
7421	36	8.0862(1)	3.9801	-0.00239	2.09	25	0.25800	-	-	0.74200	0.85600	-	-	0.12900	0.01500	-
7422	36	8.0863(1)	3.9803	-0.00223	2.76	25	0.25700	-	-	0.74300	0.85650	-	-	0.12850	0.01500	-
7423	36	8.0876(2)	3.9822	0.00022	3.67	25	0.22600	-	-	0.77400	0.87200	-	-	0.11300	0.01500	-
7424	36	8.0881(1)	3.9829	0.00135	4.44	25	0.20300	-	-	0.79700	0.88350	-	-	0.10150	0.01500	-
b	36	8.0883(2)	3.9832	0.00165	1.42	25	0.20300	-	-	0.79700	0.88350	-	-	0.10150	0.01500	-
b	36	8.0882(2)	3.9831	0.00155	2	25	0.20000	-	-	0.80000	0.88500	-	-	0.10000	0.01500	-
b	36	8.0882(2)	3.9831	0.00155	2.62	25	0.20000	-	-	0.80000	0.88500	-	-	0.10000	0.01500	-
b	36	8.0882(1)	3.9831	0.00159	3.14	25	0.19800	-	-	0.80200	0.88600	-	-	0.09900	0.01500	-
b	36	8.0928(1)	3.9899	0.00409	3.67	25	0.13500	-	-	0.86500	0.90400	-	-	0.06750	0.02850	-
b	36	8.0907(1)	3.9868	-0.00131	0.74	25	0.26400	-	-	0.73600	0.83950	-	-	0.13200	0.02850	-
b	36	8.0907(1)	3.9868	-0.00130	1.51	25	0.26300	-	-	0.73700	0.84000	-	-	0.13150	0.02850	-
b	36	8.0908(1)	3.9869	-0.00100	2.52	25	0.25500	-	-	0.74500	0.84400	-	-	0.12750	0.02850	-
b	36	8.0909(1)	3.9870	-0.00080	0.76	25	0.25200	-	-	0.74800	0.84550	-	-	0.12600	0.02850	-
b	36	8.0918(1)	3.9884	0.00071	1.02	25	0.24200	-	-	0.75800	0.85050	-	-	0.12100	0.02850	-
b	36	8.0919(1)	3.9885	0.00091	1.14	25	0.23900	-	-	0.76100	0.85200	-	-	0.11950	0.02850	-
b	36	8.0919(1)	3.9885	0.00093	1.21	25	0.23800	-	-	0.76200	0.85250	-	-	0.11900	0.02850	-
b	36	8.0919(1)	3.9885	0.00098	1.45	25	0.23500	-	-	0.76500	0.85400	-	-	0.11750	0.02850	-
b	36	8.1180(1)	4.0272	0.00485	1.71	25	0.11300	-	-	0.88700	0.82150	-	-	0.05650	0.12200	-
b	36	8.1176(1)	4.0267	0.00421	1.83	25	0.11500	-	-	0.88500	0.82050	-	-	0.05750	0.12200	-
b	36	8.1175(1)	4.0265	0.00406	1.99	25	0.11500	-	-	0.88500	0.82050	-	-	0.05750	0.12200	-
b	36	8.1174(1)	4.0264	0.00364	2.03	25	0.12700	-	-	0.87300	0.81450	-	-	0.06350	0.12200	-

b	36	8.1175(1)	4.0265	0.00374	2.11	25	0.12900	-	-	0.87100	0.81350	-	-	0.06450	0.12200	-
b	36	8.1174(1)	4.0264	0.00327	2.23	25	0.14300	-	-	0.85700	0.80650	-	-	0.07150	0.12200	-
b	36	8.1174(1)	4.0264	0.00313	2.31	25	0.14900	-	-	0.85100	0.80350	-	-	0.07450	0.12200	-
b	36	8.1173(1)	4.0262	0.00308	2.36	25	0.14500	-	-	0.85500	0.80550	-	-	0.07250	0.12200	-
b	36	8.1171(1)	4.0259	0.00269	2.53	25	0.14900	-	-	0.85100	0.80350	-	-	0.07450	0.12200	-
b	36	8.1174(1)	4.0264	0.00311	2.84	25	0.15000	-	-	0.85000	0.80300	-	-	0.07500	0.12200	-
b	36	8.1163(1)	4.0247	0.00006	3.08	25	0.21200	-	-	0.78800	0.77200	-	-	0.10600	0.12200	-
b	36	8.1162(2)	4.0246	0.00012	3.31	25	0.20300	-	-	0.79700	0.77650	-	-	0.10150	0.12200	-
b	36	8.1166(1)	4.0252	0.00101	4.06	25	0.19000	-	-	0.81000	0.78300	-	-	0.09500	0.12200	-
b	36	8.1174(1)	4.0264	0.00295	0.72	25	0.15700	-	-	0.84300	0.79950	-	-	0.07850	0.12200	-
b	36	8.1178(1)	4.0269	0.00377	0.65	25	0.14700	-	-	0.85300	0.80450	-	-	0.07350	0.12200	-
b	36	8.1177(1)	4.0268	0.00374	0.02	25	0.14200	-	-	0.85800	0.80700	-	-	0.07100	0.12200	-
b	36	8.1176(1)	4.0267	0.00359	0.0001	25	0.14200	-	-	0.85800	0.80700	-	-	0.07100	0.12200	-
8502	51	8.1176(1)	4.0267	0.00355	0.0001	25	0.14400	-	-	0.85600	0.80600	-	-	0.07200	0.12200	-
9110	16	8.1166(1)	4.0252	0.00044	0.0001	20	0.21500	-	-	0.78500	0.77050	-	-	0.10750	0.12200	-
9110	16	8.1166(1)	4.0252	0.00044	4.99	20	0.21500	-	-	0.78500	0.77050	-	-	0.10750	0.12200	-
9111	16	8.1160(1)	4.0243	-0.00036	9.21	20	0.21100	-	-	0.78900	0.77250	-	-	0.10550	0.12200	-
b	16	8.1160(1)	4.0243	0.00021	0.0001	20	0.18600	-	-	0.81400	0.78500	-	-	0.09300	0.12200	-
b	16	8.1160(1)	4.0243	0.00041	1.66	20	0.17700	-	-	0.82300	0.78950	-	-	0.08850	0.12200	-
b	16	8.0883(3)	3.9832	0.00444	2.98	20	0.23400	0.00300	0.00300	0.76000	0.87856	0.00150	0.00300	0.11694	-	-
b	16	8.0965(5)	3.9953	0.01000	3.05	20	0.22777	0.01299	0.00300	0.75624	0.87200	0.01100	0.01250	0.10450	-	-
b	16	8.0888(1)	3.9839	0.00896	5.69	20	0.14515	-	-	0.85485	0.92650	-	-	0.07250	0.00100	-
b	16	8.0961(2)	3.9947	0.01976	7.54	20	0.14515	-	-	0.85485	0.92650	-	-	0.07250	0.00100	-
b	16	8.0849(1)	3.9782	0.00113	9.06	20	0.27200	-	-	0.72800	0.86350	-	-	0.13550	0.00100	-
b	16	8.0899(2)	3.9856	0.00851	9.65	20	0.27200	-	-	0.72800	0.86350	-	-	0.13550	0.00100	-
b	16	8.2339(2)	4.2022	-0.00780	9.82	20	0.05100	0.31700	0.05500	0.57700	0.46850	0.00666	0.04450	0.05484	0.41650	0.00900
b	16	8.1947(1)	4.1425	-0.00634	11.11	20	0.08900	0.22826	0.03200	0.65074	0.58250	0.01586	0.02800	0.04914	0.32050	0.00400
9740	14	8.2134(2)	4.1709	-0.00803	0.0001	25	0.04500	0.31236	0.08200	0.56064	0.55050	0.00939	0.00600	0.06111	0.36550	0.00750

9994	15	8.1904(3)	4.1360	-0.01582	0.0001	25	0.13100	0.27100	0.01800	0.58000	0.56650	0.00413	0.02450	0.07337	0.32600	0.00550
9995	15	8.1256(1)	4.0386	-0.00540	0.0001	25	0.10300	0.21574	0.01700	0.66426	0.84400	-	0.00400	0.06050	0.09000	0.00150
1398	42	8.1513(3)	4.0770	-0.00641	0.0001	20	0.09300	0.23705	0.00700	0.66295	0.74700	-	0.01150	0.05000	0.19050	0.00100
1399	42	8.1115(2)	4.0176	-0.00174	0.0001	20	0.19172	0.11209	0.05691	0.63928	0.84455	0.00010	0.03041	0.12424	0.00010	0.00060
1400	42	8.1103(3)	4.0158	-0.00171	0.0001	600	0.19522	0.13228	0.04560	0.62690	0.85126	-	0.02756	0.12049	0.00020	0.00050
1401	42	8.1088(3)	4.0136	-0.00034	0.0001	650	0.19201	0.08175	0.06357	0.66267	0.84905	0.00390	0.02281	0.12404	0.00020	-
1402	42	8.1011(3)	4.0021	-0.00076	0.0001	700	0.20084	0.09455	0.04181	0.66280	0.87105	-	0.00805	0.12084	0.00005	-
1403	42	8.0991(3)	3.9992	-0.00072	0.0001	700	0.21034	0.09067	0.03211	0.66688	0.87130	-	0.00780	0.12070	0.00010	0.00010
1404	42	8.1061(3)	4.0096	-0.00129	0.0001	750	0.20454	0.07022	0.05681	0.66843	0.84618	-	0.02231	0.13071	0.00005	0.00075
1405	42	8.0996(2)	3.9999	-0.00011	0.0001	800	0.20973	0.06116	0.04193	0.68719	0.86338	-	0.01096	0.12566	-	-
1406	42	8.1041(3)	4.0066	-0.00029	0.0001	800	0.22424	0.04391	0.04911	0.68274	0.83857	-	0.01706	0.14017	-	0.00420
1407	42	8.1057(3)	4.0090	-0.00104	0.0001	850	0.21164	0.04459	0.05131	0.69246	0.83880	-	0.01561	0.13813	-	0.00745
1408	42	8.1067(3)	4.0105	-0.00180	0.0001	900	0.20884	0.05759	0.04821	0.68536	0.83878	-	0.01456	0.13726	-	0.00940
1409	42	8.1093(4)	4.0143	-0.00263	0.0001	900	0.20124	0.12186	0.05171	0.62519	0.84754	-	0.02531	0.12640	0.00030	0.00045
1410	42	8.1111(3)	4.0170	-0.00125	0.0001	1000	0.19686	0.10753	0.06025	0.63536	0.84390	0.00315	0.02736	0.12524	0.00035	-
1411	42	8.1130(4)	4.0198	-0.00145	0.0001	1000	0.19128	0.14293	0.05212	0.61367	0.84775	-	0.03026	0.12154	0.00045	-
2106	45	8.1141(3)	4.0214	-0.00364	0.0001	26	0.18401	0.15144	0.05363	0.61091	0.84527	-	0.03627	0.11846	-	-
2144	45	8.1150(4)	4.0228	-0.00294	0.0001	25	0.19744	0.15999	0.05531	0.58726	0.84041	0.00135	0.03246	0.12523	-	0.00055
2107	45	8.1085(3)	4.0131	-0.00030	0.0001	410	0.19314	0.08054	0.06191	0.66441	0.84895	-	0.02296	0.12754	-	0.00055
2108	45	8.1103(3)	4.0158	0.00050	0.0001	434	0.19962	0.08602	0.05441	0.65995	0.84265	-	0.02581	0.12894	0.00025	0.00235
2109	45	8.0978(3)	3.9973	0.00183	0.0001	493	0.20912	0.01502	0.04950	0.72635	0.86253	-	0.00675	0.12966	-	0.00105
2110	45	8.1001(4)	4.0007	0.00690	0.0001	564	0.17270	0.00211	0.03720	0.78799	0.87776	-	0.01145	0.10753	0.00015	0.00310
2111	45	8.1017(4)	4.0030	0.00567	0.0001	630	0.16832	0.00050	0.04070	0.79048	0.87199	-	0.01516	0.10835	-	0.00450
2112	45	8.1077(3)	4.0119	0.00043	0.0001	696	0.16583	0.05471	0.05531	0.72414	0.85967	-	0.01776	0.11596	0.00035	0.00625
2113	45	8.0855(2)	3.9791	0.00300	0.0001	762	0.23600	-	-	0.76400	0.88200	-	-	0.11800	-	-
2114	45	8.1174(3)	4.0264	0.00186	0.0001	827	0.18100	-	0.09100	0.72800	0.80850	-	0.05550	0.13600	-	-
2115	45	8.0903(8)	3.9862	0.00682	0.0001	891	0.13213	-	-	0.86787	0.92200	-	-	0.06550	0.01250	-
2116	45	8.0940(4)	3.9916	0.00493	0.0001	955	0.13100	-	-	0.86900	0.90495	-	-	0.06403	0.03102	-

2117	45	8.0981(7)	3.9977	0.00612	0.0001	1018	0.12600	-	-	0.87400	0.89450	-	-	0.06200	0.04350	-
2118	45	8.1020(10)	4.0035	0.00534	0.0001	1082	0.12613	-	-	0.87387	0.87744	-	-	0.06253	0.06003	-
2119	45	8.1044(5)	4.0070	0.00638	0.0001	1145	0.12200	-	-	0.87800	0.87344	-	-	0.06003	0.06653	-
2120	45	8.1091(8)	4.0140	0.00687	0.0001	1208	0.12200	-	-	0.87800	0.85607	-	-	0.06097	0.08296	-
2121	45	8.1172(3)	4.0261	0.00574	0.0001	1271	0.11400	-	-	0.88600	0.82991	-	-	0.05403	0.11606	-
2122	45	8.1358(6)	4.0538	0.00278	0.0001	1333	0.14400	0.17900	0.03800	0.63900	0.79650	0.00627	0.00700	0.08723	0.10250	0.00050
2123	45	8.1394(5)	4.0592	0.00210	0.0001	1371	0.13100	0.17764	0.04200	0.64936	0.79000	0.01152	0.01300	0.07698	0.10800	0.00050
2124	45	8.1470(9)	4.0706	0.00143	0.0001	1389	0.12900	0.20173	0.03700	0.63227	0.76500	0.00157	0.03000	0.08543	0.11600	0.00200
2125	45	8.1534(6)	4.0802	0.00094	0.0001	1377	0.11400	0.23411	0.04500	0.60689	0.75900	0.00793	0.03650	0.07407	0.12150	0.00100
2126	45	8.1572(4)	4.0859	-0.00601	0.0001	1322	0.11100	0.19145	0.03100	0.66655	0.71000	0.00683	0.01150	0.06517	0.20500	0.00150
2127	45	8.1940(10)	4.1414	0.00343	0.0001	1259	0.08300	0.27400	0.04600	0.59700	0.62600	0.01193	0.02800	0.05757	0.27300	0.00350
2128	45	8.2201(8)	4.1811	0.00600	0.0001	1195	0.05600	0.31800	0.03900	0.58700	0.54800	0.00628	0.04500	0.04872	0.34700	0.00500
2129	45	8.2140(20)	4.1718	0.00421	0.0001	1132	0.05900	0.24800	0.03200	0.66100	0.54100	0.00053	0.01350	0.04997	0.39150	0.00350
2130	45	8.2129(9)	4.1701	0.00122	0.0001	1005	0.06000	0.24983	0.03300	0.65717	0.53950	0.00788	0.00700	0.04262	0.39950	0.00350
2131	45	8.0806(5)	3.9718	-0.00037	0.0001	941	-	-	-	1.00000	1.00000	-	-	-	-	-
2132	45	8.0898(9)	3.9854	0.01199	0.0001	879	-	-	-	1.00000	0.98500	-	0.00250	0.01250	-	-
2133	45	8.1252(4)	4.0380	0.00208	0.0001	815	0.05599	0.17220	0.07688	0.69493	0.89151	0.01940	-	0.04859	0.03900	0.00150
2134	45	8.1233(5)	4.0351	-0.00204	0.0001	751	0.18420	0.16342	0.08170	0.57068	0.82547	0.02427	-	0.11002	0.03910	0.00115
2135	45	8.1218(3)	4.0329	-0.00290	0.0001	688	0.20048	0.15462	0.07699	0.56790	0.81921	0.02778	-	0.11251	0.03900	0.00150
2136	45	8.1259(3)	4.0390	0.00237	0.0001	625	0.17237	0.13613	0.05389	0.63762	0.81749	0.01841	-	0.09792	0.06359	0.00260
2137	45	8.0942(6)	3.9919	0.00503	0.0001	561	0.13000	-	-	0.87000	0.90350	-	0.00100	0.06500	0.03050	-
2138	45	8.0944(5)	3.9922	0.00542	0.0001	497	0.12500	-	-	0.87500	0.90600	-	0.00100	0.06250	0.03050	-
2139	45	8.0926(6)	3.9896	0.00117	0.0001	437	0.21300	-	-	0.78700	0.86200	-	0.00100	0.10650	0.03050	-
2140	45	8.0924(6)	3.9893	0.00003	0.0001	337	0.26000	-	-	0.74000	0.83850	-	0.00100	0.13000	0.03050	-
2141	45	8.0929(6)	3.9900	0.00158	0.0001	243	0.21500	-	-	0.78500	0.86100	-	0.00100	0.10750	0.03050	-
2142	45	8.0849(8)	3.9782	0.00200	0.0001	191	0.24300	-	-	0.75700	0.87850	-	-	0.12150	-	-
2143	45	8.0849(6)	3.9782	0.00198	0.0001	132	0.24400	-	-	0.75600	0.87800	-	-	0.12200	-	-
2145	45	8.0840(10)	3.9769	0.00085	0.0001	200	0.23200	-	-	0.76800	0.88400	-	-	0.11600	-	-

2146	45	8.0914(11)	3.9878	0.00042	0.0001	400	0.11900	0.00100	-	0.88000	0.90450	-	-	0.06250	0.03300	-
2147	45	8.0917(10)	3.9882	0.00087	0.0001	500	0.11900	0.00100	-	0.88000	0.90450	-	-	0.06250	0.03300	-
2148	45	8.1019(10)	4.0033	0.00445	0.0001	600	0.11300	0.00202	-	0.88498	0.87794	-	-	0.06053	0.06153	-
2149	45	8.1018(10)	4.0032	0.00430	0.0001	700	0.11300	0.00202	-	0.88498	0.87794	-	-	0.06053	0.06153	-
2150	45	8.1080(12)	4.0124	0.00584	0.0001	800	0.12300	0.00202	-	0.87498	0.85550	-	-	0.06350	0.08100	-
2151	45	8.1085(8)	4.0131	0.00658	0.0001	900	0.12300	0.00202	-	0.87498	0.85550	-	-	0.06350	0.08100	-
2152	45	8.0989(10)	3.9989	0.00667	0.0001	1000	0.13179	0.00101	0.00704	0.86016	0.89389	-	0.03654	0.06957	-	-
2153	45	8.0987(6)	3.9986	0.00637	0.0001	1100	0.13179	0.00101	0.00704	0.86016	0.89389	-	0.03654	0.06957	-	-
2154	45	8.5439(0)	4.6949	0.00763	0.0001	1200	-	1.00000	-	-	-	0.50000	-	-	-	0.50000
2155	45	8.0861(3)	3.9800	0.00434	0.0001	1300	0.22000	-	-	0.78000	0.89000	-	-	0.11000	-	-
2156	45	8.0926(3)	3.9896	0.00611	0.0001	1400	0.26000	-	0.01000	0.73000	0.85000	-	0.01000	0.14000	-	-
2157	45	8.0993(4)	3.9995	0.00191	0.0001	1500	0.24000	-	0.03000	0.73000	0.84000	-	0.03000	0.13000	-	-
2158	45	8.1211(4)	4.0319	-0.00154	0.0001	1600	0.27000	-	0.11000	0.62000	0.75000	-	0.06000	0.19000	-	-
4018	33	8.1576(3)	4.0865	-0.00453	0.0001	25	0.23762	-	0.20792	0.55446	0.65000	-	0.13000	0.22000	-	-
4031	33	8.1817(7)	4.1228	0.00952	0.0001	25	0.13000	-	0.26000	0.61000	0.64000	-	0.16000	0.20000	-	-
4045	33	8.2139(8)	4.1717	0.00153	0.0001	25	0.06900	0.24900	0.02900	0.65300	0.52900	0.00779	0.00900	0.04571	0.40550	0.00300
4019	33	8.0889(2)	3.9841	0.00356	0.0001	200	0.14300	-	-	0.85700	0.91350	-	-	0.07150	0.01500	-
4020	33	8.5348(2)	4.6799	-0.00735	0.0001	400	-	1.00000	-	-	-	0.50000	-	-	-	0.50000
4021	33	8.0776(5)	3.9674	0.01440	0.0001	450	-	0.35000	0.65000	-	0.04545	0.60586	-	0.02546	0.02020	0.30303
4022	33	8.0638(1)	3.9471	0.01374	0.0001	500	-	-	-	1.00000	0.98500	-	0.00250	0.01250	-	-
4023	33	8.0515(6)	3.9291	0.01462	0.0001	550	-	-	-	1.00000	0.98500	-	0.00250	0.01250	-	-
4024	33	8.0340(10)	3.9035	0.00731	0.0001	600	-	-	-	1.00000	0.98500	-	0.00250	0.01250	-	-
4025	33	8.3862(2)	4.4397	-0.00026	0.0001	650	-	-	1.00000	-	-	0.50000	0.50000	-	-	-
4026	33	8.3740(2)	4.4204	0.00219	0.0001	700	-	-	1.00000	-	-	0.50000	0.50000	-	-	-
4027	33	8.3656(2)	4.4071	0.00138	0.0001	800	-	-	1.00000	-	-	0.50000	0.50000	-	-	-
4028	33	8.3557(2)	4.3915	0.00093	0.0001	900	-	-	1.00000	-	-	0.50000	0.50000	-	-	-
4029	33	8.3440(2)	4.3730	0.00260	0.0001	1000	-	-	1.00000	-	-	0.50000	0.50000	-	-	-
4030	33	8.3332(2)	4.3561	0.00220	0.0001	1050	-	-	1.00000	-	-	0.50000	0.50000	-	-	-

4032	33	8.3198(8)	4.3351	-0.00657	0.0001	200	-	-	1.00000	-	-	0.50000	0.50000	-	-	-
4033	33	8.2634(8)	4.2475	-0.01120	0.0001	400	-	-	1.00000	-	-	0.50000	0.50000	-	-	-
4034	33	8.12501(5)	4.03769	0.00266	0.0001	450	0.23000	-	-	0.77000	0.88500	-	-	0.11500	-	-
4035	33	8.12508(5)	4.03779	-0.00222	0.0001	500	0.20000	-	-	0.80000	0.90000	-	-	0.10000	-	-
4036	33	8.13219(5)	4.04840	0.00203	0.0001	550	0.25000	-	-	0.75000	0.87500	-	-	0.12500	-	-
4037	33	8.12872(4)	4.04322	-0.00315	0.0001	600	0.25000	-	-	0.75000	0.87500	-	-	0.12500	-	-
4038	33	8.13235(5)	4.04864	-0.00365	0.0001	650	0.27000	-	-	0.73000	0.86500	-	-	0.13500	-	-
4039	33	8.13927(6)	4.05898	0.00103	0.0001	700	0.27000	-	-	0.73000	0.86500	-	-	0.13500	-	-
4040	33	8.13613(5)	4.05429	-0.00367	0.0001	800	0.27000	-	-	0.73000	0.86500	-	-	0.13500	-	-
4041	33	8.13991(5)	4.05994	-0.00407	0.0001	900	0.29000	-	-	0.71000	0.85500	-	-	0.14500	-	-
4042	33	8.14616(6)	4.06930	-0.00115	0.0001	1000	0.33000	-	-	0.67000	0.83500	-	-	0.16500	-	-
4043	33	8.14369(5)	4.06560	-0.00453	0.0001	1050	0.31000	-	-	0.69000	0.84500	-	-	0.15500	-	-
4046	33	8.15409(4)	4.08120	-0.00154	0.0001	200	0.36000	-	-	0.64000	0.82000	-	-	0.18000	-	-
4047	33	8.15090(5)	4.07641	-0.00600	0.0001	400	0.34000	-	-	0.66000	0.83000	-	-	0.17000	-	-
4048	33	8.11006(6)	4.01544	0.00125	0.0001	450	0.19600	-	-	0.80400	0.90200	-	-	0.09800	-	-
4049	33	8.11142(6)	4.01746	0.00105	0.0001	500	0.17800	-	-	0.82200	0.91100	-	-	0.08900	-	-
4050	33	8.11590(5)	4.02412	0.00128	0.0001	550	0.18900	-	-	0.81100	0.90550	-	-	0.09450	-	-
4051	33	8.12066(6)	4.03121	0.00083	0.0001	600	0.18400	-	-	0.81600	0.90800	-	-	0.09200	-	-
4052	33	8.12577(6)	4.03882	0.00151	0.0001	650	0.16900	-	-	0.83100	0.91550	-	-	0.08450	-	-
4053	33	8.13098(6)	4.04659	0.00237	0.0001	700	0.14600	-	-	0.85400	0.92700	-	-	0.07300	-	-
4054	33	8.13564(6)	4.05356	0.00171	0.0001	800	0.16000	-	-	0.84000	0.92000	-	-	0.08000	-	-
4055	33	8.13979(6)	4.05976	-0.00012	0.0001	900	0.19900	-	-	0.80100	0.90050	-	-	0.09950	-	-
4056	33	8.14426(6)	4.06645	-0.00119	0.0001	1000	0.22200	-	-	0.77800	0.88900	-	-	0.11100	-	-
4057	33	8.14888(6)	4.07338	-0.00150	0.0001	1050	0.20600	-	-	0.79400	0.89700	-	-	0.10300	-	-
4059	44	8.15365(6)	4.08054	-0.00229	0.0001	25	0.23400	-	-	0.76600	0.88300	-	-	0.11700	-	-
4060	44	8.15805(6)	4.08715	-0.00344	0.0001	25	0.23600	-	-	0.76400	0.88200	-	-	0.11800	-	-
4061	44	8.16360(6)	4.09549	-0.00303	0.0001	25	0.24900	-	-	0.75100	0.87550	-	-	0.12450	-	-
4062	44	8.16885(6)	4.10340	-0.00333	0.0001	25	0.27100	-	-	0.72900	0.86450	-	-	0.13550	-	-

4063	44	8.17402(6)	4.11119	-0.00346	0.0001	25	0.26800	-	-	0.73200	0.86600	-	-	0.13400	-	-
4064	44	8.17940(6)	4.11932	-0.00361	0.0001	25	0.28600	-	-	0.71400	0.85700	-	-	0.14300	-	-
4065	44	8.18326(6)	4.12515	-0.00286	0.0001	25	0.29400	-	-	0.70600	0.85300	-	-	0.14700	-	-
4066	44	8.18536(6)	4.12833	-0.00211	0.0001	25	0.29800	-	-	0.70200	0.85100	-	-	0.14900	-	-
4067	44	8.18455(6)	4.12710	-0.00173	0.0001	25	0.29600	-	-	0.70400	0.85200	-	-	0.14800	-	-
4068	44	8.17903(6)	4.11876	-0.00257	0.0001	25	0.27500	-	-	0.72500	0.86250	-	-	0.13750	-	-
4069	44	8.17360(6)	4.11056	-0.00272	0.0001	25	0.27700	-	-	0.72300	0.86150	-	-	0.13850	-	-
4070	44	8.16810(6)	4.10227	-0.00297	0.0001	25	0.27900	-	-	0.72100	0.86050	-	-	0.13950	-	-
4071	44	8.16459(6)	4.09698	0.00013	0.0001	25	0.24500	-	-	0.75500	0.87750	-	-	0.12250	-	-
4072	44	8.15030(6)	4.07551	-0.00544	0.0001	25	0.21400	-	-	0.78600	0.89300	-	-	0.10700	-	-
4073	44	8.14730(6)	4.07101	-0.00223	0.0001	25	0.20700	-	-	0.79300	0.89650	-	-	0.10350	-	-
4074	44	8.14249(6)	4.06380	-0.00212	0.0001	25	0.20200	-	-	0.79800	0.89900	-	-	0.10100	-	-
4075	44	8.13777(6)	4.05674	-0.00177	0.0001	25	0.19900	-	-	0.80100	0.90050	-	-	0.09950	-	-
4076	44	8.13316(6)	4.04985	-0.00135	0.0001	25	0.19600	-	-	0.80400	0.90200	-	-	0.09800	-	-
4077	44	8.12854(6)	4.04295	-0.00051	0.0001	25	0.15400	-	-	0.84600	0.92300	-	-	0.07700	-	-
4078	44	8.12390(6)	4.03603	-0.00013	0.0001	25	0.13200	-	-	0.86800	0.93400	-	-	0.06600	-	-
4079	44	8.11928(6)	4.02915	0.00003	0.0001	25	0.12700	-	-	0.87300	0.93650	-	-	0.06350	-	-
4080	44	8.11468(6)	4.02231	0.00007	0.0001	25	0.12600	-	-	0.87400	0.93700	-	-	0.06300	-	-
4081	44	8.11057(6)	4.01620	0.00009	0.0001	25	0.14000	-	-	0.86000	0.93000	-	-	0.07000	-	-
4082	44	8.10563(6)	4.00886	0.00329	0.0001	25	0.13300	-	-	0.86700	0.93350	-	-	0.06650	-	-
4083	44	8.09701(5)	3.99609	0.00001	0.0001	25	0.13900	-	-	0.86100	0.93050	-	-	0.06950	-	-
4084	44	8.09365(5)	3.99111	0.00031	0.0001	25	0.13700	-	-	0.86300	0.93150	-	-	0.06850	-	-
4085	44	8.09159(6)	3.98807	0.00303	0.0001	25	0.14300	-	-	0.85700	0.92850	-	-	0.07150	-	-
4086	44	8.09650(6)	3.99533	0.00362	0.0001	25	0.13700	-	-	0.86300	0.93150	-	-	0.06850	-	-
4087	44	8.11009(6)	4.01548	0.00301	0.0001	25	0.15500	-	-	0.84500	0.92250	-	-	0.07750	-	-
4088	44	8.11685(6)	4.02553	0.00267	0.0001	25	0.14500	-	-	0.85500	0.92750	-	-	0.07250	-	-
4089	44	8.12443(6)	4.03682	0.00341	0.0001	25	0.13100	-	-	0.86900	0.93450	-	-	0.06550	-	-
4090	44	8.13192(6)	4.04800	0.00347	0.0001	25	0.13700	-	-	0.86300	0.93150	-	-	0.06850	-	-

4091	44	8.13916(6)	4.05882	0.00261	0.0001	25	0.16300	-	-	0.83700	0.91850	-	-	0.08150	-	-
4092	44	8.14652(6)	4.06984	0.00161	0.0001	25	0.19400	-	-	0.80600	0.90300	-	-	0.09700	-	-
4093	44	8.15428(6)	4.08148	0.00128	0.0001	25	0.20500	-	-	0.79500	0.89750	-	-	0.10250	-	-
4094	44	8.16214(6)	4.09330	0.00061	0.0001	25	0.23000	-	-	0.77000	0.88500	-	-	0.11500	-	-
4095	44	8.17015(6)	4.10536	0.00020	0.0001	25	0.23600	-	-	0.76400	0.88200	-	-	0.11800	-	-
4096	44	8.17859(6)	4.11809	-0.00007	0.0001	25	0.25500	-	-	0.74500	0.87250	-	-	0.12750	-	-
4097	44	8.19804(6)	4.14754	0.01565	0.0001	25	0.29800	-	-	0.70200	0.85100	-	-	0.14900	-	-
4098	44	8.20091(6)	4.15190	0.00600	0.0001	25	0.33600	-	-	0.66400	0.83200	-	-	0.16800	-	-
4099	44	8.20857(6)	4.16355	0.00371	0.0001	25	0.34700	-	-	0.65300	0.82650	-	-	0.17350	-	-
4100	44	8.0864(4)	3.9804	0.01449	0.0001	25	0.14515	-	-	0.85485	0.92650	-	-	0.07250	0.00100	-
4101	44	8.0494(4)	3.9260	0.00848	0.0001	25	0.14515	-	-	0.85485	0.92650	-	-	0.07250	0.00100	-
4102	44	7.9996(3)	3.8536	0.01246	0.0001	25	0.14515	-	-	0.85485	0.92650	-	-	0.07250	0.00100	-
4103	44	7.9921(5)	3.8428	0.01261	0.0001	25	0.14515	-	-	0.85485	0.92650	-	-	0.07250	0.00100	-
4104	44	8.0801(3)	3.9711	0.00313	0.0001	25	0.27200	-	-	0.72800	0.86350	-	-	0.13550	0.00100	-
4105	44	8.0451(3)	3.9197	0.00012	0.0001	25	0.27200	-	-	0.72800	0.86350	-	-	0.13550	0.00100	-
4106	44	7.9928(3)	3.8438	0.00057	0.0001	25	0.27200	-	-	0.72800	0.86350	-	-	0.13550	0.00100	-
4107	44	7.9874(3)	3.8360	0.00376	0.0001	25	0.27200	-	-	0.72800	0.86350	-	-	0.13550	0.00100	-
4108	44	8.1256(2)	4.0386	-0.00372	0.0001	25	0.18300	-	0.09800	0.71900	0.80990	-	0.05053	0.13957	-	-
a	44	8.1399(4)	4.0599	-0.00342	0.0001	25	0.18719	-	0.09109	0.72172	0.80700	-	0.05400	0.13900	-	-
4260	5	8.1438(4)	4.0658	-0.00322	0.0001	25	0.18600	-	0.09000	0.72400	0.80750	-	0.05500	0.13750	-	-
4261	5	8.1482(3)	4.0724	-0.00217	0.0001	25	0.19000	-	0.08800	0.72200	0.80540	-	0.05603	0.13857	-	-
4464	38	8.1520(5)	4.0781	-0.00191	0.0001	25	0.18200	-	0.09300	0.72500	0.80990	-	0.05303	0.13707	-	-
4465	38	8.1564(5)	4.0847	-0.00072	0.0001	25	0.19281	-	0.07892	0.72827	0.80400	-	0.06050	0.13550	-	-
4470	38	8.1606(5)	4.0910	-0.00014	0.0001	25	0.18700	-	0.08100	0.73200	0.80700	-	0.05950	0.13350	-	-
4471	38	8.1643(5)	4.0965	-0.00133	0.0001	25	0.19680	-	0.09391	0.70929	0.80050	-	0.05350	0.14600	-	-
4466	38	8.1721(6)	4.1083	-0.00145	0.44	25	0.21179	-	0.08891	0.69930	0.79300	-	0.05600	0.15100	-	-
4467	38	8.1800(7)	4.1202	-0.00211	2.92	25	0.22877	-	0.08691	0.68432	0.78400	-	0.05750	0.15850	-	-
4468	38	8.1871(7)	4.1310	-0.00404	7.34	25	0.22900	-	0.09800	0.67300	0.78400	-	0.05150	0.16450	-	-

4469	38	8.1898(7)	4.1351	-0.00590	8.03	25	0.24400	-	0.08400	0.67200	0.77650	-	0.05850	0.16500	-	-
4472	38	8.1184(6)	4.0278	-0.00012	0.44	25	0.20521	-	0.06206	0.73273	0.81950	-	0.04050	0.14000	-	-
4473	38	8.1328(5)	4.0493	0.00029	2.92	25	0.20621	-	0.06507	0.72873	0.81941	-	0.03852	0.14207	-	-
4474	38	8.1365(7)	4.0548	0.00080	7.34	25	0.20721	-	0.05806	0.73473	0.81850	-	0.04200	0.13950	-	-
4475	38	8.1408(7)	4.0613	0.00165	8.03	25	0.21000	-	0.05900	0.73100	0.81750	-	0.04150	0.14100	-	-
b	38	8.1447(5)	4.0671	0.00195	0.0001	25	0.20600	-	0.06000	0.73400	0.81991	-	0.04102	0.13907	-	-
b	38	8.1489(7)	4.0734	0.00267	0.535	25	0.20921	-	0.05906	0.73173	0.81741	-	0.04152	0.14107	-	-
b	38	8.1529(7)	4.0794	0.00312	1.136	25	0.19000	-	0.06000	0.75000	0.82700	-	0.04150	0.13150	-	-
b	38	8.1571(9)	4.0857	0.00392	1.642	25	0.20400	-	0.06000	0.73600	0.82050	-	0.04050	0.13900	-	-
b	38	8.1648(9)	4.0973	0.00370	2.484	25	0.22022	-	0.06206	0.71772	0.81200	-	0.03900	0.14900	-	-
b	38	8.1727(9)	4.1092	0.00349	3.023	25	0.23676	-	0.05594	0.70729	0.80350	-	0.04250	0.15400	-	-
b	38	8.1802(9)	4.1205	0.00247	4.153	25	0.24800	-	0.05900	0.69300	0.79800	-	0.04050	0.16150	-	-
b	38	8.1841(9)	4.1264	0.00185	4.752	25	0.26200	-	0.06000	0.67800	0.79050	-	0.04000	0.16950	-	-
b	38	8.1039(3)	4.0063	-0.00549	5.961	25	0.24093	-	0.03327	0.72581	0.84585	-	0.02002	0.13413	-	-
b	38	8.1179(6)	4.0271	-0.00680	6.584	25	0.25605	-	0.02823	0.71573	0.83500	-	0.02550	0.13950	-	-
b	38	8.1219(6)	4.0331	-0.00613	6.975	25	0.25277	-	0.02820	0.71903	0.83692	-	0.02551	0.13757	-	-
b	38	8.1256(7)	4.0386	-0.00614	7.253	25	0.25378	-	0.02618	0.72004	0.83592	-	0.02701	0.13707	-	-
b	38	8.1292(6)	4.0439	-0.00497	7.374	25	0.25176	-	0.02920	0.71903	0.83950	-	0.02250	0.13800	-	-
b	38	8.1340(7)	4.0511	-0.00291	7.427	25	0.21652	-	0.03323	0.75025	0.85650	-	0.02050	0.12300	-	-
b	38	8.1386(8)	4.0580	-0.00252	0.0001	25	0.21551	-	0.03323	0.75126	0.85493	-	0.02251	0.12256	-	-
b	38	8.1423(8)	4.0635	-0.00260	0.535	25	0.22457	-	0.03424	0.74119	0.85050	-	0.02150	0.12800	-	-
b	38	8.1500(8)	4.0751	-0.00245	1.136	25	0.24270	-	0.03525	0.72205	0.84250	-	0.02000	0.13750	-	-
b	38	8.1581(7)	4.0872	-0.00517	1.642	25	0.26385	-	0.03726	0.69889	0.82600	-	0.02450	0.14950	-	-
b	38	8.1652(8)	4.0979	-0.00630	2.484	25	0.28571	-	0.03521	0.67907	0.81609	-	0.02449	0.15942	-	-
b	38	8.1678(8)	4.1018	-0.00904	3.023	25	0.28471	-	0.04024	0.67505	0.81550	-	0.02250	0.16200	-	-
b	38	8.1044(8)	4.0070	0.00287	4.153	25	0.13400	-	-	0.86600	0.90150	-	0.00100	0.06700	0.03050	-
b	38	8.1190(7)	4.0287	0.00427	4.752	25	0.12800	-	-	0.87200	0.90450	-	0.00100	0.06400	0.03050	-
b	38	8.1232(7)	4.0350	0.00534	5.961	25	0.12600	-	-	0.87400	0.90550	-	0.00100	0.06300	0.03050	-

b	38	8.1195(7)	4.0295	0.00507	6.584	25	0.12500	-	-	0.87500	0.90600	-	0.00100	0.06250	0.03050	-
b	38	8.1271(6)	4.0408	0.00586	6.975	25	0.12600	-	-	0.87400	0.90550	-	0.00100	0.06300	0.03050	-
b	38	8.1235(6)	4.0354	0.00576	7.253	25	0.12700	-	-	0.87300	0.90500	-	0.00100	0.06350	0.03050	-
b	38	8.1323(7)	4.0486	0.00837	7.374	25	0.12100	-	-	0.87900	0.90800	-	0.00100	0.06050	0.03050	-
b	38	8.1282(6)	4.0424	0.00752	7.427	25	0.12500	-	-	0.87500	0.90600	-	0.00100	0.06250	0.03050	-
6730	31	8.1362(6)	4.0544	0.00851	0.0001	25	0.13700	-	-	0.86300	0.90000	-	0.00100	0.06850	0.03050	-
6731	31	8.1441(7)	4.0662	0.00816	0.0001	25	0.20400	-	-	0.79600	0.86650	-	0.00100	0.10200	0.03050	-
6732	31	8.1516(8)	4.0775	0.00741	0.0001	25	0.24700	-	-	0.75300	0.84500	-	0.00100	0.12350	0.03050	-
6733	31	8.1592(8)	4.0889	0.00660	0.0001	25	0.28800	-	-	0.71200	0.82450	-	0.00100	0.14400	0.03050	-
6734	31	8.1510(8)	4.0766	0.00631	0.0001	25	0.25800	-	-	0.74200	0.83950	-	0.00100	0.12900	0.03050	-
6735	31	8.1510(8)	4.0766	0.00631	0.0001	25	0.25800	-	-	0.74200	0.83950	-	0.00100	0.12900	0.03050	-
6736	31	8.1431(7)	4.0647	0.00610	0.0001	25	0.23500	-	-	0.76500	0.85100	-	0.00100	0.11750	0.03050	-
6737	31	8.1350(6)	4.0526	0.00526	0.0001	25	0.21800	-	-	0.78200	0.85950	-	0.00100	0.10900	0.03050	-
6738	31	8.1271(6)	4.0408	0.00426	0.0001	25	0.21500	-	-	0.78500	0.86100	-	0.00100	0.10750	0.03050	-
6739	31	8.1183(8)	4.0277	0.00174	0.0001	25	0.21100	-	-	0.78900	0.86300	-	0.00100	0.10550	0.03050	-
6740	31	8.1036(8)	4.0059	0.00023	0.0001	25	0.21500	-	-	0.78500	0.86100	-	0.00100	0.10750	0.03050	-
6741	31	8.1525(8)	4.0788	0.00271	0.0001	25	0.26600	-	-	0.73400	0.83550	-	0.00100	0.13300	0.03050	-
6742	31	8.1025(8)	4.0042	-0.00225	0.0001	25	0.26200	-	-	0.73800	0.83750	-	0.00100	0.13100	0.03050	-
6743	31	8.1166(5)	4.0252	-0.00167	0.0001	25	0.26000	-	-	0.74000	0.83850	-	0.00100	0.13000	0.03050	-
6744	31	8.1247(6)	4.0372	-0.00011	0.0001	25	0.25900	-	-	0.74100	0.83900	-	0.00100	0.12950	0.03050	-
6745	31	8.1283(6)	4.0426	-0.00014	0.0001	25	0.26200	-	-	0.73800	0.83750	-	0.00100	0.13100	0.03050	-
6746	31	8.1320(9)	4.0481	0.00031	0.0001	25	0.24400	-	-	0.75600	0.84650	-	0.00100	0.12200	0.03050	-
6747	31	8.1413(6)	4.0620	0.00333	0.0001	25	0.23900	-	-	0.76100	0.84900	-	0.00100	0.11950	0.03050	-
6748	31	8.1488(7)	4.0733	0.00308	0.0001	25	0.25400	-	-	0.74600	0.84150	-	0.00100	0.12700	0.03050	-
6749	31	8.1563(9)	4.0845	0.00257	0.0001	25	0.27000	-	-	0.73000	0.83350	-	0.00100	0.13500	0.03050	-
6750	31	8.1480(8)	4.0721	0.00195	0.0001	25	0.25000	-	-	0.75000	0.84350	-	0.00100	0.12500	0.03050	-
6861	4	8.1407(8)	4.0611	0.00256	0.0001	25	0.23200	-	-	0.76800	0.85250	-	0.00100	0.11600	0.03050	-
6863	4	8.1329(7)	4.0495	0.00200	0.0001	25	0.22500	-	-	0.77500	0.85600	-	0.00100	0.11250	0.03050	-

6982	22	8.1248(8)	4.0374	0.00083	0.0001	25	0.21500	-	-	0.78500	0.86100	-	0.00100	0.10750	0.03050	-
6983	22	8.1172(8)	4.0261	0.00007	0.0001	25	0.21300	-	-	0.78700	0.86200	-	0.00100	0.10650	0.03050	-
6984	22	8.1031(7)	4.0051	-0.00048	0.0001	25	0.21300	-	-	0.78700	0.86200	-	0.00100	0.10650	0.03050	-
6985	22	8.0950(8)	3.9931	-0.00036	0.0001	25	0.24500	-	-	0.75500	0.87750	-	-	0.12250	-	-
6986	22	8.1092(9)	4.0142	0.00023	0.0001	25	0.24400	-	-	0.75600	0.87800	-	-	0.12200	-	-
6987	22	8.1169(8)	4.0256	0.00103	0.0001	25	0.25000	-	-	0.75000	0.87500	-	-	0.12500	-	-
6988	22	8.1095(9)	4.0146	0.00050	0.0001	25	0.25500	-	-	0.74500	0.87250	-	-	0.12750	-	-
7002	10	8.1204(9)	4.0308	0.00086	0.0001	25	0.25100	-	-	0.74900	0.87450	-	-	0.12550	-	-
7003	10	8.1251(9)	4.0378	0.00247	0.0001	25	0.25000	-	-	0.75000	0.87500	-	-	0.12500	-	-
7004	10	8.1336(9)	4.0505	0.00448	0.0001	25	0.22900	-	-	0.77100	0.88550	-	-	0.11450	-	-
7005	10	8.1407(9)	4.0611	0.00332	0.0001	25	0.26100	-	-	0.73900	0.86950	-	-	0.13050	-	-
7006	10	8.1485(9)	4.0728	0.00312	0.0001	25	0.28300	-	-	0.71700	0.85850	-	-	0.14150	-	-
7007	10	8.1516(9)	4.0775	0.00162	0.0001	25	0.30100	-	-	0.69900	0.84950	-	-	0.15050	-	-
7008	10	8.1474(8)	4.0712	0.00138	0.0001	25	0.28900	-	-	0.71100	0.85550	-	-	0.14450	-	-
7009	10	8.1395(9)	4.0593	0.00134	0.0001	25	0.27200	-	-	0.72800	0.86400	-	-	0.13600	-	-
7010	10	8.1391(10)	4.0587	0.00082	0.0001	25	0.26700	-	-	0.73300	0.86650	-	-	0.13350	-	-
7011	10	8.1316(12)	4.0475	0.00123	0.0001	25	0.24500	-	-	0.75500	0.87750	-	-	0.12250	-	-
7349	20	8.1233(9)	4.0351	0.00008	0.0001	25	0.23200	-	-	0.76800	0.88400	-	-	0.11600	-	-
8151	34	8.1192(8)	4.0290	-0.00061	0.0001	25	0.23200	-	-	0.76800	0.88400	-	-	0.11600	-	-
8152	34	8.1155(10)	4.0235	0.00981	0.0001	25	0.23100	-	-	0.76900	0.88450	-	-	0.11550	-	-
8153	34	8.1081(10)	4.0125	0.00923	0.0001	25	0.22600	-	-	0.77400	0.88700	-	-	0.11300	-	-
8158	34	8.0942(9)	3.9919	-0.00137	0.0001	25	0.23400	-	-	0.76600	0.88300	-	-	0.11700	-	-
8661	9	8.1018(11)	4.0032	-0.00126	0.0001	25	0.11300	0.00100	-	0.88600	0.90750	-	-	0.05950	0.03300	-
8666	9	8.1169(10)	4.0256	0.00040	0.0001	25	0.13400	0.00100	-	0.86500	0.89700	-	-	0.07000	0.03300	-
8682	9	8.1207(10)	4.0313	0.00111	0.0001	25	0.11800	0.00100	-	0.88100	0.90500	-	-	0.06200	0.03300	-
8684	9	8.1168(10)	4.0255	0.00025	0.0001	25	0.13400	0.00100	-	0.86500	0.89700	-	-	0.07000	0.03300	-
8699	9	8.1256(8)	4.0386	0.00288	0.0001	25	0.13200	0.00100	-	0.86700	0.89800	-	-	0.06900	0.03300	-
8700	9	8.1217(8)	4.0328	0.00246	0.0001	25	0.12600	0.00100	-	0.87300	0.90100	-	-	0.06600	0.03300	-

8703	9	8.1298(9)	4.0448	0.00404	0.0001	25	0.11900	0.00100	-	0.88000	0.90450	-	-	0.06250	0.03300	-
8721	9	8.1335(10)	4.0504	0.00412	0.0001	25	0.12200	0.00100	-	0.87700	0.90300	-	-	0.06400	0.03300	-
8662	9	8.1381(7)	4.0572	0.00542	0.0001	200	0.12900	0.00100	-	0.87000	0.89950	-	-	0.06750	0.03300	-
8663	9	8.1423(10)	4.0635	0.00449	0.0001	400	0.22300	0.00100	-	0.77600	0.85250	-	-	0.11450	0.03300	-
8664	9	8.1503(11)	4.0755	0.00466	0.0001	450	0.25700	0.00100	-	0.74200	0.83550	-	-	0.13150	0.03300	-
8665	9	8.1577(11)	4.0866	0.00383	0.0001	400	0.28300	0.00100	-	0.71600	0.82250	-	-	0.14450	0.03300	-
8667	9	8.1667(14)	4.1002	0.00545	0.0001	500	0.29300	0.00100	-	0.70600	0.81750	-	-	0.14950	0.03300	-
8668	9	8.1116(10)	4.0177	0.00193	0.0001	450	0.11700	0.00202	-	0.88098	0.87594	-	-	0.06253	0.06153	-
8669	9	8.1263(10)	4.0396	0.00330	0.0001	550	0.12700	0.00202	-	0.87098	0.87094	-	-	0.06753	0.06153	-
8670	9	8.1305(7)	4.0459	0.00446	0.0001	500	0.12200	0.00202	-	0.87598	0.87344	-	-	0.06503	0.06153	-
8671	9	8.1265(9)	4.0399	0.00360	0.0001	600	0.12700	0.00202	-	0.87098	0.87094	-	-	0.06753	0.06153	-
8672	9	8.1338(9)	4.0508	0.00422	0.0001	700	0.11700	0.00202	-	0.88098	0.87594	-	-	0.06253	0.06153	-
8673	9	8.1302(8)	4.0454	0.00397	0.0001	800	0.12400	0.00202	-	0.87398	0.87244	-	-	0.06603	0.06153	-
8674	9	8.1379(9)	4.0569	0.00497	0.0001	900	0.12000	0.00202	-	0.87798	0.87444	-	-	0.06403	0.06153	-
8675	9	8.1419(11)	4.0629	0.00546	0.0001	800	0.12600	0.00202	-	0.87198	0.87144	-	-	0.06703	0.06153	-
8676	9	8.1461(9)	4.0692	0.00599	0.0001	800	0.14300	0.00202	-	0.85498	0.86293	-	-	0.07554	0.06153	-
8677	9	8.1502(9)	4.0754	0.00550	0.0001	700	0.20200	0.00202	-	0.79598	0.83342	-	-	0.10505	0.06153	-
8678	9	8.1577(8)	4.0866	0.00492	0.0001	600	0.23600	0.00202	-	0.76198	0.81641	-	-	0.12206	0.06153	-
8679	9	8.1658(12)	4.0988	0.00516	0.0001	500	0.26300	0.00202	-	0.73498	0.80290	-	-	0.13557	0.06153	-
8680	9	8.1733(4)	4.1101	0.00469	0.0001	400	0.26700	0.00202	-	0.73098	0.80090	-	-	0.13757	0.06153	-
8681	9	8.1180(11)	4.0272	0.00368	0.0001	200	0.12000	0.00202	-	0.87798	0.85700	-	-	0.06200	0.08100	-
8683	9	8.1316(10)	4.0475	0.00395	0.0001	850	0.10700	0.00202	-	0.89098	0.86350	-	-	0.05550	0.08100	-
8685	9	8.1354(11)	4.0532	0.00435	0.0001	200	0.11100	0.00202	-	0.88698	0.86150	-	-	0.05750	0.08100	-
8686	9	8.1315(14)	4.0474	0.00380	0.0001	400	0.10700	0.00202	-	0.89098	0.86350	-	-	0.05550	0.08100	-
8687	9	8.1400(14)	4.0601	0.00602	0.0001	500	0.10900	0.00202	-	0.88898	0.86250	-	-	0.05650	0.08100	-
8688	9	8.1358(13)	4.0538	0.00520	0.0001	550	0.09900	0.00202	-	0.89898	0.86750	-	-	0.05150	0.08100	-
8689	9	8.1445(6)	4.0668	0.00762	0.0001	600	0.10100	0.00202	-	0.89698	0.86650	-	-	0.05250	0.08100	-
8690	9	8.1482(8)	4.0724	0.00760	0.0001	700	0.11100	0.00202	-	0.88698	0.86150	-	-	0.05750	0.08100	-

8691	9	8.1525(6)	4.0788	0.00826	0.0001	800	0.12900	0.00202	-	0.86898	0.85250	-	-	0.06650	0.08100	-
8692	9	8.1569(7)	4.0854	0.00820	0.0001	900	0.18700	0.00202	-	0.81098	0.82350	-	-	0.09550	0.08100	-
8693	9	8.1655(5)	4.0984	0.00964	0.0001	800	0.20400	0.00202	-	0.79398	0.81500	-	-	0.10400	0.08100	-
8694	9	8.1726(11)	4.1091	0.00857	0.0001	700	0.22200	0.00202	-	0.77598	0.80600	-	-	0.11300	0.08100	-
8695	9	8.1791(9)	4.1189	0.00631	0.0001	600	0.24200	0.00202	-	0.75598	0.79600	-	-	0.12300	0.08100	-
8696	9	8.1092(6)	4.0142	0.00385	0.0001	500	0.12689	0.00101	0.01309	0.85901	0.89685	-	0.03405	0.06910	-	-
8697	9	8.1239(6)	4.0360	0.00557	0.0001	400	0.12048	0.00101	0.01205	0.86646	0.89995	-	0.03352	0.06653	-	-
8698	9	8.1281(7)	4.0423	0.00611	0.0001	200	0.13166	0.00101	0.01106	0.85628	0.89389	-	0.03453	0.07157	-	-
8701	9	8.1243(6)	4.0366	0.00617	0.0001	200	0.12048	0.00101	0.01205	0.86646	0.89995	-	0.03352	0.06653	-	-
8702	9	8.1318(5)	4.0478	0.00612	0.0001	400	0.12362	0.00101	0.01508	0.86030	0.89840	-	0.03253	0.06907	-	-
8704	9	8.1280(6)	4.0421	0.00577	0.0001	500	0.11883	0.00101	0.01410	0.86606	0.89990	-	0.03353	0.06657	-	-
8705	9	8.1359(6)	4.0539	0.00629	0.0001	400	0.12374	0.00101	0.02314	0.85211	0.89790	-	0.02853	0.07357	-	-
8706	9	8.1403(7)	4.0605	0.00686	0.0001	550	0.14874	0.00101	0.02412	0.82613	0.88494	-	0.02801	0.08704	-	-
8707	9	8.1440(7)	4.0661	0.00587	0.0001	600	0.18090	0.00101	0.03015	0.78794	0.86793	-	0.02501	0.10705	-	-
8708	9	8.1469(7)	4.0704	0.00339	0.0001	700	0.22211	0.00101	0.03719	0.73969	0.84692	-	0.02151	0.13157	-	-
8709	9	8.1547(8)	4.0821	0.00330	0.0001	800	0.24297	0.00101	0.03614	0.71988	0.83684	-	0.02202	0.14114	-	-
8710	9	8.1627(9)	4.0941	0.00283	0.0001	900	0.26406	0.00101	0.03414	0.70080	0.82574	-	0.02404	0.15023	-	-
8711	9	8.1701(10)	4.1053	0.00184	0.0001	950	0.27811	0.00101	0.03213	0.68875	0.81782	-	0.02503	0.15716	-	-
8712	9	8.33273(8)	4.35535	0.00128	0.0001	900	-	0.41041	0.02202	0.56757	0.09500	0.01100	0.01700	-	0.87500	0.00200
8713	9	8.3264(3)	4.3454	-0.00078	0.0001	800	0.03904	0.37337	-	0.58759	0.09200	0.01100	0.02800	0.00700	0.86100	0.00100
8714	9	8.3266(3)	4.3457	-0.00402	0.0001	800	0.02603	0.41041	-	0.56356	0.09600	0.00400	0.02100	0.01300	0.86000	0.00600
8715	9	8.3249(2)	4.3431	0.00358	0.0001	700	0.01600	0.38100	0.01200	0.59100	0.11500	0.00236	0.02100	0.01064	0.85100	-
8716	9	8.3293(3)	4.3500	-0.00069	0.0001	600	-	0.44344	0.03704	0.51952	0.11400	0.00318	0.01600	0.01482	0.85000	0.00200
8717	9	8.3390(2)	4.3652	-0.00059	0.0001	550	0.02302	0.43944	0.01502	0.52252	0.09810	0.00722	0.06907	0.02681	0.78078	0.01802
8718	9	8.17149(7)	4.10738	-0.00120	0.0001	400	0.11000	0.24200	-	0.64800	0.66900	0.00633	-	0.05067	0.27200	0.00200
8719	9	8.1517(6)	4.0776	-0.00796	0.0001	300	0.14141	0.77778	0.02020	0.06061	0.88300	0.04400	0.02800	0.04300	-	0.00200
8720	9	8.1504(5)	4.0757	-0.00336	0.0001	200	0.18182	0.73737	0.02020	0.06061	0.87500	0.06200	0.01500	0.04500	-	0.00300
8765	32	8.1474(6)	4.0712	-0.00858	0.0001	25	0.16162	0.74747	0.02020	0.07071	0.88100	0.04951	0.02000	0.04749	-	0.00200

8770	32	8.1460(6)	4.0691	-0.00318	0.0001	25	0.11111	0.77778	0.01010	0.10101	0.92522	0.01894	0.01097	0.04487	-	-
8780	32	8.1451(5)	4.0677	-0.01322	0.0001	28	0.11000	0.76000	0.02000	0.11000	0.91700	0.01300	0.01800	0.04800	-	0.00400
8785	32	8.0844(1)	3.9774	0.00149	0.0001	28	0.22900	-	-	0.77100	0.88550	-	-	0.11450	-	-
8795	32	8.0845(1)	3.9776	0.00161	0.0001	25	0.23100	-	-	0.76900	0.88450	-	-	0.11550	-	-
8800	32	8.0841(1)	3.9770	0.00087	0.0001	25	0.24000	-	-	0.76000	0.88000	-	-	0.12000	-	-
8810	32	8.0840(1)	3.9769	0.00056	0.0001	25	0.25000	-	-	0.75000	0.87500	-	-	0.12500	-	-
8815	32	8.0838(1)	3.9766	0.00007	0.0001	25	0.26200	-	-	0.73800	0.86900	-	-	0.13100	-	-
8766	32	8.0835(1)	3.9761	-0.00051	0.0001	200	0.27000	-	-	0.73000	0.86500	-	-	0.13500	-	-
8767	32	8.0829(1)	3.9752	-0.00172	0.0001	400	0.29000	-	-	0.71000	0.85500	-	-	0.14500	-	-
8768	32	8.0837(1)	3.9764	-0.00015	0.0001	450	0.26600	-	-	0.73400	0.86700	-	-	0.13300	-	-
8769	32	8.0846(1)	3.9777	0.00177	0.0001	400	0.23000	-	-	0.77000	0.88500	-	-	0.11500	-	-
8771	32	8.0851(1)	3.9785	0.00287	0.0001	500	0.20800	-	-	0.79200	0.89600	-	-	0.10400	-	-
8772	32	8.0856(1)	3.9792	0.00406	0.0001	450	0.18000	-	-	0.82000	0.91000	-	-	0.09000	-	-
8773	32	8.0832(2)	3.9757	-0.00098	0.0001	550	0.27200	-	-	0.72800	0.86400	-	-	0.13600	-	-
8774	32	8.0832(3)	3.9757	-0.00104	0.0001	600	0.27500	-	-	0.72500	0.86200	-	-	0.13800	-	-
8775	32	8.0835(1)	3.9761	-0.00053	0.0001	650	0.27100	-	-	0.72900	0.86400	-	-	0.13600	-	-
8776	32	8.0835(2)	3.9761	-0.00034	0.0001	700	0.26000	-	-	0.74000	0.87000	-	-	0.13000	-	-
8777	32	8.0836(4)	3.9763	-0.00020	0.0001	800	0.26000	-	-	0.74000	0.87000	-	-	0.13000	-	-
8778	32	8.0838(2)	3.9766	0.00016	0.0001	900	0.25600	-	-	0.74400	0.87200	-	-	0.12800	-	-
8779	32	8.0837(2)	3.9764	0.00002	0.0001	1000	0.25500	-	-	0.74500	0.87200	-	-	0.12800	-	-
8781	32	8.0838(1)	3.9766	0.00020	0.0001	200	0.25400	-	-	0.74600	0.87300	-	-	0.12700	-	-
8782	32	8.0835(1)	3.9761	-0.00054	0.0001	400	0.27200	-	-	0.72800	0.86400	-	-	0.13600	-	-
8783	32	8.0834(1)	3.9760	-0.00061	0.0001	450	0.26700	-	-	0.73300	0.86600	-	-	0.13400	-	-
8784	32	8.0836(1)	3.9763	-0.00026	0.0001	400	0.26400	-	-	0.73600	0.86800	-	-	0.13200	-	-
8786	32	8.0840(1)	3.9769	0.00056	0.0001	500	0.25000	-	-	0.75000	0.87500	-	-	0.12500	-	-
8787	32	8.0843(1)	3.9773	0.00109	0.0001	450	0.24500	-	-	0.75500	0.87800	-	-	0.12200	-	-
8788	32	8.0844(1)	3.9774	0.00143	0.0001	550	0.23300	-	-	0.76700	0.88400	-	-	0.11600	-	-
8789	32	8.0846(1)	3.9777	0.00174	0.0001	600	0.23200	-	-	0.76800	0.88400	-	-	0.11600	-	-

8790	32	8.0845(1)	3.9776	0.00160	0.0001	650	0.23100	-	-	0.76900	0.88400	-	-	0.11600	-	-
8791	32	8.0846(1)	3.9777	0.00177	0.0001	700	0.23000	-	-	0.77000	0.88500	-	-	0.11500	-	-
8792	32	8.0832(2)	3.9757	-0.00098	0.0001	800	0.27200	-	-	0.72800	0.86400	-	-	0.13600	-	-
8793	32	8.0831(3)	3.9755	-0.00112	0.0001	900	0.27100	-	-	0.72900	0.86400	-	-	0.13600	-	-
8794	32	8.0838(3)	3.9766	0.00030	0.0001	1000	0.24700	-	-	0.75300	0.87600	-	-	0.12400	-	-
8796	32	8.0840(3)	3.9769	0.00075	0.0001	200	0.23800	-	-	0.76200	0.88100	-	-	0.11900	-	-
8797	32	8.0848(3)	3.9780	0.00235	0.0001	400	0.21300	-	-	0.78700	0.89400	-	-	0.10600	-	-
8798	32	8.0847(2)	3.9779	0.00220	0.0001	450	0.21300	-	-	0.78700	0.89400	-	-	0.10600	-	-
8799	32	8.0848(3)	3.9780	0.00239	0.0001	400	0.21000	-	-	0.79000	0.89500	-	-	0.10500	-	-
8801	32	8.0850(1)	3.9783	0.00272	0.0001	500	0.20800	-	-	0.79200	0.89600	-	-	0.10400	-	-
8802	32	8.08149(1)	3.97315	-0.00249	0.0001	450	0.21000	-	-	0.79000	0.89500	-	-	0.10500	-	-
8803	32	8.07262(1)	3.96008	-0.00322	0.0001	550	0.21000	-	-	0.79000	0.89500	-	-	0.10500	-	-
8804	32	8.06652(2)	3.95111	-0.00213	0.0001	600	0.21000	-	-	0.79000	0.89500	-	-	0.10500	-	-
8805	32	8.05714(2)	3.93735	-0.00408	0.0001	650	0.21000	-	-	0.79000	0.89500	-	-	0.10500	-	-
8806	32	8.04100(2)	3.91373	-0.00112	0.0001	700	0.21000	-	-	0.79000	0.89500	-	-	0.10500	-	-
8807	32	8.02441(7)	3.88956	-0.00003	0.0001	800	0.21000	-	-	0.79000	0.89500	-	-	0.10500	-	-
8808	32	8.01530(5)	3.87633	-0.00452	0.0001	900	0.21000	-	-	0.79000	0.89500	-	-	0.10500	-	-
8809	32	8.00560(7)	3.86227	-0.00322	0.0001	1000	0.21000	-	-	0.79000	0.89500	-	-	0.10500	-	-
8811	32	7.98909(9)	3.83842	-0.00564	0.0001	200	0.21000	-	-	0.79000	0.89500	-	-	0.10500	-	-
8812	32	7.98193(7)	3.82811	-0.00162	0.0001	400	0.21000	-	-	0.79000	0.89500	-	-	0.10500	-	-
8813	32	7.97068(7)	3.81195	-0.00230	0.0001	450	0.21000	-	-	0.79000	0.89500	-	-	0.10500	-	-
8814	32	7.96121(8)	3.79838	-0.00084	0.0001	400	0.21000	-	-	0.79000	0.89500	-	-	0.10500	-	-
8816	32	7.94976(9)	3.78201	-0.00258	0.0001	500	0.21000	-	-	0.79000	0.89500	-	-	0.10500	-	-
8817	32	7.93731(9)	3.76427	-0.00190	0.0001	450	0.21000	-	-	0.79000	0.89500	-	-	0.10500	-	-
8818	32	7.92235(11)	3.74303	-0.00266	0.0001	550	0.21000	-	-	0.79000	0.89500	-	-	0.10500	-	-
8819	32	7.90729(11)	3.72172	-0.00167	0.0001	600	0.21000	-	-	0.79000	0.89500	-	-	0.10500	-	-
8820	32	7.89371(14)	3.70258	-0.00313	0.0001	650	0.21000	-	-	0.79000	0.89500	-	-	0.10500	-	-
8821	32	7.88263(20)	3.68701	-0.00038	0.0001	700	0.21000	-	-	0.79000	0.89500	-	-	0.10500	-	-

8822	32	7.86493(18)	3.66223	-0.00513	0.0001	800	0.21000	-	-	0.79000	0.89500	-	-	0.10500	-	-
8823	32	7.84685(27)	3.63703	-0.00328	0.0001	900	0.21000	-	-	0.79000	0.89500	-	-	0.10500	-	-
8824	32	7.82825(24)	3.61123	-0.00228	0.0001	1000	0.21000	-	-	0.79000	0.89500	-	-	0.10500	-	-
4961	28	7.79994(26)	3.57219	-0.00202	0.0001	25	0.21000	-	-	0.79000	0.89500	-	-	0.10500	-	-
4962	28	8.4469(1)	4.5368	0.00118	0.0001	25	-	-	-	1.00000	-	-	-	0.50000	-	0.50000
4963	28	8.4456(1)	4.5347	0.00182	0.0001	25	-	-	-	1.00000	-	-	-	0.50000	-	0.50000
4964	28	8.4474(1)	4.5376	0.00103	0.0001	25	-	-	-	1.00000	-	-	-	0.50000	-	0.50000
4965	28	8.4520(1)	4.5451	0.00085	0.0001	25	-	-	-	1.00000	-	-	-	0.50000	-	0.50000
4966	28	8.4578(1)	4.5544	0.00066	0.0001	25	-	-	-	1.00000	-	-	-	0.50000	-	0.50000
4969	28	8.4638(1)	4.5641	0.00050	0.0001	25	-	-	-	1.00000	-	-	-	0.50000	-	0.50000
4919	24	8.4698(1)	4.5738	-0.00013	0.0001	25	-	-	-	1.00000	-	-	-	0.50000	-	0.50000
4920	24	8.4757(1)	4.5834	-0.00021	0.0001	25	-	-	-	1.00000	-	-	-	0.50000	-	0.50000
4921	24	8.4816(1)	4.5930	0.00061	0.0001	25	-	-	-	1.00000	-	-	-	0.50000	-	0.50000
4922	24	8.4877(1)	4.6029	-0.00116	0.0001	25	-	-	-	1.00000	-	-	-	0.50000	-	0.50000
4923	24	8.4941(1)	4.6133	-0.00111	0.0001	25	-	-	-	1.00000	-	-	-	0.50000	-	0.50000
2477	3	8.5008(1)	4.6242	-0.00059	0.0001	25	-	-	-	1.00000	-	-	-	0.50000	-	0.50000
2478	3	8.5073(1)	4.6349	-0.00075	0.0001	25	-	-	-	1.00000	-	-	-	0.50000	-	0.50000
2479	3	8.5140(1)	4.6458	-0.00045	0.0001	25	-	-	-	1.00000	-	-	-	0.50000	-	0.50000
2480	3	8.5208(1)	4.6570	-0.00036	0.0001	25	-	-	-	1.00000	-	-	-	0.50000	-	0.50000
2481	3	8.5277(1)	4.6683	-0.00014	0.0001	25	-	-	-	1.00000	-	-	-	0.50000	-	0.50000
2482	3	8.5353(1)	4.6808	-0.00023	0.0001	25	-	-	-	1.00000	-	-	-	0.50000	-	0.50000
2483	3	8.5389(1)	4.6867	-0.00045	0.0001	25	-	-	-	1.00000	-	-	-	0.50000	-	0.50000
2484	3	8.4510(1)	4.5434	0.00642	0.0001	25	-	-	-	1.00000	-	-	-	0.50000	-	0.50000
2485	3	8.4561(1)	4.5517	-0.00492	0.0001	25	-	-	-	1.00000	-	-	-	0.50000	-	0.50000
2486	3	8.4872(1)	4.6021	-0.00197	0.0001	25	-	-	-	1.00000	-	-	-	0.50000	-	0.50000
2487	3	8.5154(1)	4.6481	-0.00323	0.0001	25	-	-	-	1.00000	-	-	-	0.50000	-	0.50000
2823	2	8.5224(1)	4.6596	-0.00239	0.0001	25	-	-	-	1.00000	-	-	-	0.50000	-	0.50000
2824	2	8.5287(1)	4.6699	-0.00307	0.0001	25	-	-	-	1.00000	-	-	-	0.50000	-	0.50000

2825	2	8.5367(1)	4.6831	-0.00135	0.0001	25	-	-	-	1.00000	-	-	-	0.50000	-	0.50000
2826	2	8.5442(1)	4.6954	-0.00068	0.0001	25	-	-	-	1.00000	-	-	-	0.50000	-	0.50000
2827	2	8.5519(1)	4.7081	0.00008	0.0001	25	-	-	-	1.00000	-	-	-	0.50000	-	0.50000
2828	2	8.5597(1)	4.7210	0.00057	0.0001	25	-	-	-	1.00000	-	-	-	0.50000	-	0.50000
2829	2	8.5674(1)	4.7338	0.00063	0.0001	25	-	-	-	1.00000	-	-	-	0.50000	-	0.50000
2830	2	8.5754(1)	4.7471	0.00151	0.0001	25	-	-	-	1.00000	-	-	-	0.50000	-	0.50000
2831	2	8.5814(1)	4.7570	0.00250	0.0001	25	-	-	-	1.00000	-	-	-	0.50000	-	0.50000
2832	2	8.5820(1)	4.7580	0.00082	0.0001	25	-	-	-	1.00000	-	-	-	0.50000	-	0.50000
2833	2	8.5807(1)	4.7559	0.00257	0.0001	25	-	-	-	1.00000	-	-	-	0.50000	-	0.50000
2834	2	8.5735(1)	4.7439	0.00097	0.0001	25	-	-	-	1.00000	-	-	-	0.50000	-	0.50000
2835	2	8.5661(1)	4.7316	0.00123	0.0001	25	-	-	-	1.00000	-	-	-	0.50000	-	0.50000
2836	2	8.5586(1)	4.7192	0.00126	0.0001	25	-	-	-	1.00000	-	-	-	0.50000	-	0.50000
2837	2	8.5413(1)	4.6906	-0.00141	0.0001	25	-	-	-	1.00000	-	-	-	0.50000	-	0.50000
2838	2	8.5275(1)	4.6679	0.00041	0.0001	25	-	-	-	1.00000	-	-	-	0.50000	-	0.50000
2839	2	8.5199(1)	4.6555	-0.00132	0.0001	25	-	-	-	1.00000	-	-	-	0.50000	-	0.50000
2840	2	8.5110(1)	4.6409	-0.00150	0.0001	25	-	-	-	1.00000	-	-	-	0.50000	-	0.50000
2841	2	8.5075(1)	4.6352	-0.00042	0.0001	25	-	-	-	1.00000	-	-	-	0.50000	-	0.50000
2842	2	8.5011(1)	4.6247	-0.00058	0.0001	25	-	-	-	1.00000	-	-	-	0.50000	-	0.50000
2843	2	8.4947(1)	4.6143	-0.00092	0.0001	25	-	-	-	1.00000	-	-	-	0.50000	-	0.50000
2844	2	8.4886(1)	4.6044	-0.00094	0.0001	25	-	-	-	1.00000	-	-	-	0.50000	-	0.50000
2845	2	8.4828(1)	4.5949	-0.00049	0.0001	25	-	-	-	1.00000	-	-	-	0.50000	-	0.50000
2846	2	8.4769(1)	4.5853	-0.00036	0.0001	25	-	-	-	1.00000	-	-	-	0.50000	-	0.50000
2847	2	8.4716(1)	4.5768	0.00058	0.0001	25	-	-	-	1.00000	-	-	-	0.50000	-	0.50000
2933	29	8.4661(1)	4.5678	0.00089	0.0001	25	-	-	-	1.00000	-	-	-	0.50000	-	0.50000
2934	29	8.4612(1)	4.5599	0.00189	0.6	25	-	-	-	1.00000	-	-	-	0.50000	-	0.50000
2935	29	8.4569(1)	4.5530	0.00232	1.1	25	-	-	-	1.00000	-	-	-	0.50000	-	0.50000
2936	29	8.4545(1)	4.5491	0.00265	1.7	25	-	-	-	1.00000	-	-	-	0.50000	-	0.50000
2937	29	8.3771(2)	4.4253	0.00406	3.1	25	-	-	1.00000	-	-	0.50000	0.50000	-	-	-

2938	29	8.3686(2)	4.4118	0.00406	4.5	25	-	-	1.00000	-	-	0.50000	0.50000	-	-	-
2939	29	8.3585(2)	4.3959	0.00220	5	25	-	-	1.00000	-	-	0.50000	0.50000	-	-	-
2940	29	8.3515(3)	4.3848	0.00277	5.9	25	-	-	1.00000	-	-	0.50000	0.50000	-	-	-
2941	29	8.3453(1)	4.3751	0.00464	7.2	25	-	-	1.00000	-	-	0.50000	0.50000	-	-	-
2942	29	8.3856(1)	4.4388	0.00143	8.1	25	-	-	1.00000	-	-	0.50000	0.50000	-	-	-
2943	29	8.3747(3)	4.4215	0.00237	9.1	25	-	-	1.00000	-	-	0.50000	0.50000	-	-	-
2944	29	8.3601(1)	4.3984	0.00247	10.1	25	-	-	1.00000	-	-	0.50000	0.50000	-	-	-
2945	29	8.3861(11)	4.4396	0.00271	11.1	25	-	-	1.00000	-	-	0.50000	0.50000	-	-	-
2946	29	8.3821(8)	4.4332	0.00256	12.4	25	-	-	1.00000	-	-	0.50000	0.50000	-	-	-
2947	29	8.3805(5)	4.4307	0.00286	13.9	25	-	-	1.00000	-	-	0.50000	0.50000	-	-	-
2948	29	8.3793(3)	4.4288	0.00262	15.6	25	-	-	1.00000	-	-	0.50000	0.50000	-	-	-
2949	29	8.3755(6)	4.4228	0.00223	17	25	-	-	1.00000	-	-	0.50000	0.50000	-	-	-
2950	29	8.3725(5)	4.4180	0.00354	18.5	25	-	-	1.00000	-	-	0.50000	0.50000	-	-	-
2951	29	8.3709(7)	4.4155	0.00378	20.2	25	-	-	1.00000	-	-	0.50000	0.50000	-	-	-
2952	29	8.3683(6)	4.4114	0.00336	22.6	25	-	-	1.00000	-	-	0.50000	0.50000	-	-	-
2953	29	8.3675(2)	4.4101	0.00301	25.1	25	-	-	1.00000	-	-	0.50000	0.50000	-	-	-
2954	29	8.3660(6)	4.4077	0.00247	29	25	-	-	1.00000	-	-	0.50000	0.50000	-	-	-
3080	41	8.3647(6)	4.4057	0.00316	0.0001	90	-	-	1.00000	-	-	0.50000	0.50000	-	-	-
3081	41	8.3640(6)	4.4046	0.00387	0.0001	70	-	-	1.00000	-	-	0.50000	0.50000	-	-	-
3082	41	8.3633(8)	4.4035	0.00390	0.0001	97	-	-	1.00000	-	-	0.50000	0.50000	-	-	-
3083	41	8.3607(11)	4.3994	0.00365	0.0001	152	-	-	1.00000	-	-	0.50000	0.50000	-	-	-
3084	41	8.3555(2)	4.3912	0.00240	0.0001	220	-	-	1.00000	-	-	0.50000	0.50000	-	-	-
3085	41	8.3530(6)	4.3872	0.00381	0.0001	289	-	-	1.00000	-	-	0.50000	0.50000	-	-	-
3086	41	8.3496(5)	4.3819	0.00353	0.0001	360	-	-	1.00000	-	-	0.50000	0.50000	-	-	-
3087	41	8.3383(3)	4.3641	0.00208	0.0001	425	-	-	1.00000	-	-	0.50000	0.50000	-	-	-
3088	41	8.3879(3)	4.4424	0.00461	0.0001	483	-	-	1.00000	-	-	0.50000	0.50000	-	-	-
3089	41	8.3877(3)	4.4421	0.00261	0.0001	559	-	-	1.00000	-	-	0.50000	0.50000	-	-	-
3090	41	8.3976(6)	4.4579	0.00303	0.0001	625	-	-	1.00000	-	-	0.50000	0.50000	-	-	-

3091	41	8.3978(5)	4.4582	0.00286	0.0001	690	-	-	1.00000	-	-	0.50000	0.50000	-	-	-
3092	41	8.3932(2)	4.4509	-0.00372	0.0001	756	-	-	1.00000	-	-	0.50000	0.50000	-	-	-
3093	41	8.3691(2)	4.4126	-0.00230	0.0001	820	-	-	1.00000	-	-	0.50000	0.50000	-	-	-
3094	41	8.3489(2)	4.3808	-0.00420	0.0001	885	-	-	1.00000	-	-	0.50000	0.50000	-	-	-
3095	41	8.3490(2)	4.3809	-0.00249	0.0001	949	-	-	1.00000	-	-	0.50000	0.50000	-	-	-
3096	41	8.3111(2)	4.3215	-0.00569	0.0001	1020	-	-	1.00000	-	-	0.50000	0.50000	-	-	-
3097	41	8.2859(2)	4.2823	-0.00806	0.0001	1054	-	-	1.00000	-	-	0.50000	0.50000	-	-	-
3098	41	8.2660(2)	4.2515	-0.00997	0.0001	100	-	-	1.00000	-	-	0.50000	0.50000	-	-	-
3099	41	8.2587(2)	4.2403	-0.01034	0.0001	240	-	-	1.00000	-	-	0.50000	0.50000	-	-	-
3100	41	8.2562(2)	4.2364	-0.01108	0.0001	559	-	-	1.00000	-	-	0.50000	0.50000	-	-	-
3101	41	8.2421(12)	4.2148	-0.00962	0.0001	850	-	-	1.00000	-	-	0.50000	0.50000	-	-	-
3102	41	8.0930(3)	3.9902	0.00461	0.0001	912	0.12505	0.07614	-	0.79881	0.93728	0.00065	0.00090	0.06081	0.00010	0.00025
3103	41	8.3017(5)	4.3069	0.00430	0.0001	975	-	0.51017	0.00440	0.48543	0.27737	0.00780	0.09134	0.00235	0.61334	0.00780
3104	41	8.1104(5)	4.0159	-0.00224	0.0001	1039	0.12242	0.22345	-	0.65412	0.90659	0.00160	0.02910	0.05911	0.00325	0.00035
3105	41	8.1081(5)	4.0125	-0.00421	0.0001	1103	0.12145	0.22261	0.00110	0.65484	0.91038	-	0.02661	0.06082	0.00155	0.00065
3106	41	8.1122(4)	4.0186	-0.00068	0.0001	1167	0.12321	0.22591	-	0.65088	0.90363	0.00123	0.02881	0.06064	0.00495	0.00075
3107	41	8.1104(4)	4.0159	-0.00220	0.0001	1232	0.12244	0.22328	-	0.65429	0.90664	0.00165	0.02905	0.05906	0.00325	0.00035
3108	41	8.1099(3)	4.0152	-0.00318	0.0001	1297	0.12344	0.22448	-	0.65208	0.90609	0.00135	0.02930	0.05966	0.00325	0.00035
3109	41	8.1106(4)	4.0162	-0.00221	0.0001	1359	0.19862	0.22609	-	0.57529	0.86816	0.00155	0.02870	0.09800	0.00325	0.00035
3110	41	8.1100(3)	4.0154	-0.00298	0.0001	1403	0.24110	0.22038	0.00060	0.53792	0.84685	0.00490	0.02840	0.11625	0.00325	0.00035
3111	41	8.1096(4)	4.0148	-0.00325	0.0001	1416	0.24422	0.21800	-	0.53778	0.84545	0.00505	0.02860	0.11730	0.00325	0.00035
3112	41	8.1108(4)	4.0165	-0.00027	0.0001	1397	0.12220	0.21963	-	0.65817	0.90735	0.00032	0.02385	0.06133	0.00635	0.00080
3113	41	8.1113(3)	4.0173	0.00000	0.0001	1346	0.12011	0.21943	0.00890	0.65156	0.90790	-	0.01970	0.06525	0.00635	0.00080
3114	41	8.1089(4)	4.0137	-0.00414	0.0001	1283	0.22802	0.21843	-	0.55355	0.85309	0.00263	0.02520	0.11193	0.00635	0.00080
3115	41	8.1094(3)	4.0145	-0.00397	0.0001	1219	0.20638	0.22482	0.00400	0.56480	0.86389	-	0.02325	0.10571	0.00635	0.00080
3116	41	8.1097(3)	4.0149	-0.00305	0.0001	1081	0.19270	0.22199	0.00650	0.57881	0.87115	-	0.02150	0.10020	0.00635	0.00080
3117	41	8.1113(4)	4.0173	-0.00010	0.0001	944	0.12701	0.22146	0.00040	0.65113	0.90395	-	0.02450	0.06440	0.00635	0.00080
3118	41	8.1105(3)	4.0161	-0.00290	0.0001	882	0.15970	0.22801	0.00620	0.60609	0.88684	-	0.02270	0.08335	0.00635	0.00075

3119	41	8.1097(4)	4.0149	-0.00338	0.0001	797	0.16863	0.22535	-	0.60602	0.88305	0.00089	0.02525	0.08371	0.00635	0.00075
3120	41	8.1111(3)	4.0170	-0.00173	0.0001	756	0.16268	0.22475	0.00420	0.60836	0.88466	-	0.02410	0.08410	0.00635	0.00080
3121	41	8.1143(3)	4.0217	0.00020	0.0001	693	0.12240	0.23386	-	0.64374	0.90065	0.00357	0.02770	0.05808	0.00950	0.00050
3122	41	8.1138(3)	4.0210	-0.00111	0.0001	630	0.13189	0.24089	0.00120	0.62603	0.89569	-	0.02760	0.06680	0.00950	0.00040
3123	41	8.1151(3)	4.0229	0.00080	0.0001	567	0.11460	0.21024	0.03360	0.64156	0.90405	0.01607	0.01155	0.05843	0.00950	0.00040
3124	41	8.1081(5)	4.0125	-0.00419	0.0001	503	0.12115	0.22251	0.00190	0.65444	0.91058	-	0.02611	0.06111	0.00155	0.00065
3125	41	8.1122(4)	4.0186	-0.00066	0.0001	439	0.12321	0.22591	-	0.65088	0.90340	0.00123	0.02880	0.06087	0.00495	0.00075
3126	41	8.1136(3)	4.0207	-0.00051	0.0001	375	0.11910	0.23924	0.00110	0.64056	0.90385	-	0.02470	0.06120	0.00905	0.00120
3127	41	8.1121(4)	4.0185	-0.00334	0.0001	312	0.24210	0.20512	0.02640	0.52638	0.84026	0.01849	0.01465	0.11670	0.00900	0.00090
3128	41	8.1107(4)	4.0164	-0.00502	0.0001	250	0.26280	0.22919	-	0.50801	0.83090	0.00570	0.02675	0.12665	0.00900	0.00100
3129	41	8.1072(1)	4.0112	0.00379	0.0001	198	0.11600	0.06400	0.04600	0.77400	0.89400	0.00650	0.02450	0.07450	-	0.00050
3130	41	8.1057(1)	4.0090	0.00175	0.0001	168	0.11300	0.06100	0.04500	0.78100	0.89550	0.00700	0.02550	0.07150	-	0.00050
c	8	8.1104(4)	4.0159	-0.00244	0.0001	25	0.12200	0.22351	-	0.65449	0.90650	0.00150	0.02900	0.05900	0.00350	0.00050
c	8	8.1003(3)	4.0010	0.00930	0.0001	25	0.11266	0.00301	0.00997	0.87436	0.90595	-	0.03352	0.06053	-	-
c	8	8.0855(2)	3.9791	0.00301	0.0001	25	0.23500	-	-	0.76500	0.88200	-	-	0.11800	-	-
c	8	8.0844(1)	3.9774	0.00039	0.0001	25	0.27200	-	-	0.72800	0.86350	-	-	0.13550	0.00100	-
c	8	8.0770(1)	3.9665	0.00050	0.0001	25	0.27200	-	-	0.72800	0.86350	-	-	0.13550	0.00100	-
c	11	8.0688(1)	3.9545	0.00053	0.0001	25	0.27200	-	-	0.72800	0.86350	-	-	0.13550	0.00100	-
c	11	8.0621(1)	3.9446	0.00066	0.0001	25	0.27200	-	-	0.72800	0.86350	-	-	0.13550	0.00100	-
c	11	8.0509(1)	3.9282	0.00042	0.0001	25	0.27200	-	-	0.72800	0.86350	-	-	0.13550	0.00100	-
c	11	8.0440(2)	3.9181	0.00043	0.0001	25	0.27200	-	-	0.72800	0.86350	-	-	0.13550	0.00100	-
c	11	8.0296(3)	3.8971	-0.00003	0.0001	25	0.27200	-	-	0.72800	0.86350	-	-	0.13550	0.00100	-
c	11	8.0221(1)	3.8862	-0.00036	0.0001	25	0.27200	-	-	0.72800	0.86350	-	-	0.13550	0.00100	-
c	11	8.0074(1)	3.8649	-0.00098	0.0001	25	0.27200	-	-	0.72800	0.86350	-	-	0.13550	0.00100	-
c	11	8.0001(1)	3.8543	-0.00119	0.0001	25	0.27200	-	-	0.72800	0.86350	-	-	0.13550	0.00100	-
c	11	7.9955(1)	3.8477	-0.00144	0.0001	25	0.27200	-	-	0.72800	0.86350	-	-	0.13550	0.00100	-
c	11	7.9926(1)	3.8435	-0.00112	0.0001	25	0.27200	-	-	0.72800	0.86350	-	-	0.13550	0.00100	-
c	11	7.9912(1)	3.8415	-0.00119	0.0001	25	0.27200	-	-	0.72800	0.86350	-	-	0.13550	0.00100	-

c	11	7.9905(1)	3.8405	-0.00135	0.0001	25	0.27200	-	-	0.72800	0.86350	-	-	0.13550	0.00100	-
c	11	8.0891(1)	3.9844	0.00940	0.0001	25	0.14515	-	-	0.85485	0.92650	-	-	0.07250	0.00100	-
c	11	8.0817(1)	3.9735	0.00950	0.0001	25	0.14515	-	-	0.85485	0.92650	-	-	0.07250	0.00100	-
c	11	8.0737(2)	3.9617	0.00981	0.0001	25	0.14515	-	-	0.85485	0.92650	-	-	0.07250	0.00100	-
c	11	8.0670(1)	3.9518	0.00993	0.0001	25	0.14515	-	-	0.85485	0.92650	-	-	0.07250	0.00100	-
c	11	8.0557(1)	3.9352	0.00953	0.0001	25	0.14515	-	-	0.85485	0.92650	-	-	0.07250	0.00100	-
c	11	8.0485(2)	3.9247	0.00908	0.0001	25	0.14515	-	-	0.85485	0.92650	-	-	0.07250	0.00100	-
c	11	8.0345(1)	3.9042	0.00919	0.0001	25	0.14515	-	-	0.85485	0.92650	-	-	0.07250	0.00100	-
c	11	8.0272(1)	3.8936	0.00912	0.0001	25	0.14515	-	-	0.85485	0.92650	-	-	0.07250	0.00100	-
c	11	8.0124(1)	3.8721	0.00833	0.0001	25	0.14515	-	-	0.85485	0.92650	-	-	0.07250	0.00100	-
c	11	8.0053(1)	3.8618	0.00841	0.0001	25	0.14515	-	-	0.85485	0.92650	-	-	0.07250	0.00100	-
c	43	8.0006(1)	3.8550	0.00800	0.0001	25	0.14515	-	-	0.85485	0.92650	-	-	0.07250	0.00100	-
c	43	7.9977(1)	3.8508	0.00831	0.0001	25	0.14515	-	-	0.85485	0.92650	-	-	0.07250	0.00100	-
c	43	7.9960(1)	3.8484	0.00781	0.0001	25	0.14515	-	-	0.85485	0.92650	-	-	0.07250	0.00100	-
c	43	7.9958(1)	3.8481	0.00837	0.0001	25	0.14515	-	-	0.85485	0.92650	-	-	0.07250	0.00100	-
c	30	8.39389(5)	4.45196	-0.00380	0.0001	25	-	-	0.80200	0.19800	-	-	0.59900	0.40100	-	-
c	30	8.39230(5)	4.44943	-0.00348	0.11	25	-	-	0.80200	0.19800	-	-	0.59900	0.40100	-	-
c	30	8.38596(6)	4.43935	-0.00406	0.48	25	-	-	0.80200	0.19800	-	-	0.59900	0.40100	-	-
c	30	8.37649(9)	4.42433	-0.00077	1.21	25	-	-	0.80200	0.19800	-	-	0.59900	0.40100	-	-
c	30	8.3676(1)	4.4103	-0.00020	1.81	25	-	-	0.80200	0.19800	-	-	0.59900	0.40100	-	-
c	30	8.3586(2)	4.3960	0.00152	2.48	25	-	-	0.80200	0.19800	-	-	0.59900	0.40100	-	-
c	30	8.3540(2)	4.3888	0.00772	3.06	25	-	-	0.80200	0.19800	-	-	0.59900	0.40100	-	-
c	30	8.3466(2)	4.3771	0.00337	3.38	25	-	-	0.80200	0.19800	-	-	0.59900	0.40100	-	-
c	30	8.3324(1)	4.3548	0.00114	4.28	25	-	-	0.80200	0.19800	-	-	0.59900	0.40100	-	-
c	30	8.32381(9)	4.34138	0.00369	5.02	25	-	-	0.80200	0.19800	-	-	0.59900	0.40100	-	-
c	30	8.31178(6)	4.32258	0.00753	6.1	25	-	-	0.80200	0.19800	-	-	0.59900	0.40100	-	-
c	30	8.29759(7)	4.30048	0.00664	7.15	25	-	-	0.80200	0.19800	-	-	0.59900	0.40100	-	-
c	30	8.28469(8)	4.28045	0.00595	8.14	25	-	-	0.80200	0.19800	-	-	0.59900	0.40100	-	-

c	30	8.27321(8)	4.26268	0.00337	8.94	25	-	-	0.80200	0.19800	-	-	0.59900	0.40100	-	-
c	30	8.25608(9)	4.23626	0.00281	10.35	25	-	-	0.80200	0.19800	-	-	0.59900	0.40100	-	-
c	30	8.2477(1)	4.2234	0.00360	11.12	25	-	-	0.80200	0.19800	-	-	0.59900	0.40100	-	-
c	30	8.2409(1)	4.2129	0.00961	12.07	25	-	-	0.80200	0.19800	-	-	0.59900	0.40100	-	-
c	30	8.2218(1)	4.1837	0.00582	13.59	25	-	-	0.80200	0.19800	-	-	0.59900	0.40100	-	-
c	30	8.1885(1)	4.1331	0.00996	17.09	25	-	-	0.80200	0.19800	-	-	0.59900	0.40100	-	-
c	30	8.1693(1)	4.1041	0.00601	18.8	25	-	-	0.80200	0.19800	-	-	0.59900	0.40100	-	-
c	30	8.1659(1)	4.0990	0.01057	19.48	25	-	-	0.80200	0.19800	-	-	0.59900	0.40100	-	-
c	30	8.1611(1)	4.0917	0.01065	20	25	-	-	0.80200	0.19800	-	-	0.59900	0.40100	-	-
c	30	8.1532(1)	4.0799	0.00847	20.7	25	-	-	0.80200	0.19800	-	-	0.59900	0.40100	-	-
c	30	8.1236(2)	4.0356	0.00956	24.13	25	-	-	0.80200	0.19800	-	-	0.59900	0.40100	-	-
c	30	8.1143(3)	4.0217	0.01343	25.54	25	-	-	0.80200	0.19800	-	-	0.59900	0.40100	-	-
c	30	8.0961(4)	3.9947	0.01056	27.53	25	-	-	0.80200	0.19800	-	-	0.59900	0.40100	-	-
c	30	8.0815(4)	3.9732	0.01289	29.58	25	-	-	0.80200	0.19800	-	-	0.59900	0.40100	-	-
c	30	8.0598(4)	3.9412	0.00998	32.18	25	-	-	0.80200	0.19800	-	-	0.59900	0.40100	-	-
c	30	8.0467(4)	3.9221	0.01440	34.39	25	-	-	0.80200	0.19800	-	-	0.59900	0.40100	-	-
c	30	8.39389(5)	4.45196	-0.00380	0.0001	25	-	-	0.80200	0.19800	-	-	0.59900	0.40100	-	-
c	30	8.40154(7)	4.46414	-0.00064	0.0001	100	-	-	0.80819	0.19181	-	-	0.59550	0.40450	-	-
c	30	8.41250(7)	4.48163	0.00046	0.0001	200	-	-	0.79600	0.20400	-	-	0.60200	0.39800	-	-
c	30	8.42373(7)	4.49960	0.00335	0.0001	300	-	-	0.79200	0.20800	-	-	0.60400	0.39600	-	-
c	30	8.43323(7)	4.51484	0.00259	0.0001	400	-	-	0.78400	0.21600	-	-	0.60800	0.39200	-	-
c	30	8.44207(7)	4.52906	0.00479	0.0001	502	-	-	0.81000	0.19000	-	-	0.59500	0.40500	-	-
c	30	8.45200(7)	4.54506	0.00431	0.0001	600	-	-	0.80200	0.19800	-	-	0.59900	0.40100	-	-
c	30	8.45600(7)	4.55151	0.00538	0.0001	650	-	-	0.82100	0.17900	-	-	0.58950	0.41050	-	-
c	30	8.46280(7)	4.56250	0.00577	0.0001	700	-	-	0.80300	0.19700	-	-	0.59850	0.40150	-	-
c	30	8.46690(7)	4.56914	0.00321	0.0001	750	-	-	0.79600	0.20400	-	-	0.60200	0.39800	-	-
c	30	8.47260(7)	4.57837	0.00010	0.0001	800	-	-	0.76700	0.23300	-	-	0.61650	0.38350	-	-
c	30	8.47880(7)	4.58843	0.00004	0.0001	850	-	-	0.75500	0.24500	-	-	0.62250	0.37750	-	-

c	30	8.48400(6)	4.59688	-0.00218	0.0001	900	-	-	0.74000	0.26000	-	-	0.63000	0.37000	-	-
c	30	8.48960(8)	4.60599	-0.00083	0.0001	950	-	-	0.74700	0.25300	-	-	0.62650	0.37350	-	-
c	30	8.49630(7)	4.61690	-0.00249	0.0001	1000	-	-	0.72000	0.28000	-	-	0.64000	0.36000	-	-
c	30	8.50190(9)	4.62604	-0.00138	0.0001	1050	-	-	0.72700	0.27300	-	-	0.63650	0.36350	-	-
c	30	8.50749(6)	4.63517	-0.00551	0.0001	1100	-	-	0.69700	0.30300	-	-	0.65150	0.34850	-	-
c	30	8.52131(11)	4.65779	-0.00201	0.0001	1200	-	-	0.69400	0.30600	-	-	0.65300	0.34700	-	-
d	7	8.1872(5)	4.1311	-0.00627	0.0001	25	0.26810	0.07072	0.00588	0.65530	0.48640	0.03076	0.00528	0.10624	0.37133	-
d	7	8.1812(5)	4.1220	-0.02441	0.0001	25	0.27387	0.09722	0.00903	0.61988	0.46824	0.03978	0.00688	0.10167	0.38343	-
d	7	8.1770(40)	4.1157	-0.01458	0.0001	25	0.29287	0.07010	0.00597	0.63106	0.49408	0.03269	0.00491	0.11673	0.35158	-
d	7	8.1830(20)	4.1248	-0.02016	0.0001	25	0.26415	0.14970	0.01167	0.57448	0.49076	0.05406	0.00745	0.08384	0.36389	-
d	7	8.1735(3)	4.1104	-0.01053	0.0001	25	0.31274	0.07954	0.01432	0.59339	0.51548	0.03976	0.01055	0.12377	0.31044	-
d	7	8.1755(4)	4.1134	-0.00662	0.0001	25	0.32046	0.05988	0.00768	0.61197	0.50658	0.03113	0.00607	0.13294	0.32328	-
d	7	8.1750(4)	4.1127	-0.00400	0.0001	25	0.33488	0.07108	0.01209	0.58195	0.51370	0.03778	0.00870	0.13571	0.30412	-
d	7	8.1711(4)	4.1068	-0.00730	0.0001	25	0.34254	0.04930	0.01280	0.59536	0.51137	0.02823	0.00987	0.14944	0.30109	-
d	7	8.1914(7)	4.1375	-0.00516	0.0001	25	0.30254	0.12168	0.01562	0.56016	0.47466	0.05210	0.00984	0.10698	0.35642	-
d	7	8.2786(5)	4.2710	-0.01728	0.0001	25	0.12962	0.24322	-	0.62716	0.17431	0.03054	-	0.03427	0.76088	-
d	7	8.2725(4)	4.2616	-0.00588	0.0001	25	0.15411	0.15392	-	0.69197	0.20477	0.02692	-	0.05014	0.71817	-
d	7	8.2801(5)	4.2733	-0.01873	0.0001	25	0.11828	0.35017	0.00863	0.52293	0.19206	0.03771	0.00347	0.02574	0.74102	-
d	7	8.2640(4)	4.2485	-0.03072	0.0001	25	0.15072	0.21862	-	0.63066	0.18623	0.03271	-	0.04265	0.73841	-
d	7	8.2657(4)	4.2511	-0.00508	0.0001	25	0.17748	0.13841	0.00457	0.67954	0.22516	0.02913	0.00324	0.06190	0.68058	-
d	7	8.2694(4)	4.2568	-0.00781	0.0001	25	0.16373	0.21688	0.00366	0.61573	0.22173	0.03688	0.00204	0.04681	0.69254	-
d	7	8.2556(5)	4.2355	-0.01242	0.0001	25	0.19403	0.15974	0.01226	0.63397	0.24767	0.03674	0.00767	0.06641	0.64152	-
d	7	8.2615(3)	4.2446	-0.00542	0.0001	25	0.19605	0.13201	0.00520	0.66674	0.23319	0.03059	0.00350	0.07003	0.66269	-
d	7	8.2595(2)	4.2415	-0.00829	0.0001	25	0.18999	0.20642	0.00472	0.59887	0.24953	0.04153	0.00257	0.05583	0.65054	-
d	7	8.2534(4)	4.2321	-0.01284	0.0001	25	0.20984	0.15452	0.00868	0.62696	0.24660	0.03729	0.00518	0.07197	0.63896	-
d	7	8.2512(4)	4.2288	-0.01213	0.0001	25	0.21996	0.10697	0.00211	0.67097	0.24198	0.02813	0.00143	0.08290	0.64556	-
d	7	8.2507(4)	4.2280	-0.01048	0.0001	25	0.21113	0.18775	0.01704	0.58407	0.27319	0.04589	0.00939	0.06820	0.60333	-
d	7	8.3012(5)	4.3061	-0.01578	0.0001	25	0.09506	0.27900	-	0.62594	0.10293	0.02357	-	0.02396	0.84954	-

d	7	8.2927(4)	4.2929	-0.00549	0.0001	25	0.12253	0.17306	-	0.70441	0.13769	0.02241	-	0.03885	0.80105	-
d	7	8.3025(4)	4.3081	-0.00330	0.0001	25	0.10532	0.30827	-	0.58641	0.13269	0.02822	-	0.02444	0.81465	-
d	7	8.2910(3)	4.2902	-0.01332	0.0001	25	0.12404	0.23234	0.00370	0.63992	0.13498	0.02812	0.00184	0.03575	0.79930	-
d	7	8.2847(5)	4.2805	-0.00657	0.0001	25	0.14523	0.15214	0.00279	0.69984	0.15715	0.02435	0.00182	0.04966	0.76702	-
d	7	8.2923(5)	4.2923	-0.00262	0.0001	25	0.13131	0.23277	0.01300	0.62292	0.15990	0.03240	0.00679	0.03976	0.76115	-
d	7	8.3045(4)	4.3112	-0.00554	0.0001	25	0.11556	0.23764	0.00912	0.63768	0.10583	0.02696	0.00405	0.03538	0.82778	-
d	7	8.2991(3)	4.3028	-0.00471	0.0001	25	0.12885	0.17151	0.00424	0.69540	0.11251	0.02276	0.00227	0.04378	0.81867	-
d	7	8.3082(2)	4.3170	0.00085	0.0001	25	0.11518	0.24860	0.01562	0.62059	0.11234	0.02939	0.00693	0.03601	0.81532	-
d	7	8.2890(4)	4.2871	-0.00772	0.0001	25	0.15382	0.15575	0.00390	0.68653	0.13410	0.02498	0.00213	0.05388	0.78491	-
d	7	8.2936(4)	4.2943	-0.00915	0.0001	25	0.14088	0.21766	0.00747	0.63399	0.12792	0.03013	0.00343	0.04404	0.79448	-
d	7	8.2980(4)	4.3011	-0.00333	0.0001	25	0.13731	0.24787	0.01700	0.59782	0.13580	0.03470	0.00745	0.04246	0.77959	-
d	17/12 [e]	8.2854(15)	4.2816	-0.00744	0.0001	25	0.13934	-	-	0.86066	0.13002	0.00000	-	0.06967	0.80031	-
d	17/12 [e]	8.2880(13)	4.2856	-0.00687	0.0001	25	0.13488	-	-	0.86512	0.12263	0.00000	-	0.06744	0.80993	-
d	17/12 [e]	8.2881(8)	4.2857	0.00007	0.0001	25	0.15390	-	-	0.84610	0.13349	0.00000	-	0.07695	0.78956	-
d	17/12 [e]	8.2861(9)	4.2826	-0.00390	0.0001	25	0.15274	-	-	0.84726	0.13167	0.00000	-	0.07637	0.79197	-
d	17/12 [e]	8.2745(9)	4.2647	0.00005	0.0001	25	0.19175	-	-	0.80825	0.17402	0.00000	-	0.09587	0.73011	-
d	17/12 [e]	8.2729(10)	4.2622	-0.00824	0.0001	25	0.18419	-	-	0.81581	0.16187	0.00000	-	0.09210	0.74603	-
d	17/12 [e]	8.2719(8)	4.2607	-0.00321	0.0001	25	0.20280	-	-	0.79720	0.17199	0.00000	-	0.10140	0.72661	-
d	17/12 [e]	8.2986(5)	4.3021	0.00910	0.0001	25	0.13424	-	-	0.86576	0.12158	0.00000	-	0.06712	0.81130	-
d	17/12 [e]	8.2906(8)	4.2896	0.00598	0.0001	25	0.15661	-	-	0.84339	0.13776	0.00000	-	0.07831	0.78393	-
d	17/12 [e]	8.2924(12)	4.2924	-0.00030	0.0001	25	0.14425	-	-	0.85575	0.11870	0.00000	-	0.07212	0.80918	-
d	17/12 [e]	8.2857(12)	4.2820	0.01028	0.0001	25	0.18248	-	-	0.81752	0.15916	-	-	0.09124	0.74960	-
d	17/12 [e]	8.2879(13)	4.2854	-0.00246	0.0001	25	0.16015	-	-	0.83985	0.12558	-	-	0.08007	0.79435	-

Note: Reported cation site occupancy reported after projection into the model component space (see text)

[a] Experiments not listed in the AMCSD

[b] Experiments not listed in AMCSD; full structural refinements not reported

[c] References not included in the AMCSD

[d] Powder XRD/EMPA studies. Site occupancy determined with MELTS ordering model (Sack and Ghiorso 1991a, b)

[e] Compositional data from ref. 17; cell parameter from ref. 12

Supplement 3. Appendix

DATA ISSUES: ADJUSTMENTS AND EXCLUSIONS

High-*T*, room-*P* measurements

We allowed α to vary for four of the independent end members; there are no high-*T* data for $FeCr_2O_4$ or $MgCr_2O_4$. It was important for us to use both data from quenched samples and high-*T* in situ data in order to isolate the separate effects of ordering and thermal expansion, particularly above the blocking temperature where ordering state reaches equilibrium on the timescale of an XRD measurement.

Systematic residuals with temperature seen in early calibrations turned out to be the result of a discrepancy between the in situ high-temperature study of Harrison et al. (1998), which defines α for $FeAl_2O_4$, and the other room-*T* data for $FeAl_2O_4$ (Fig. A1a; all appendix figures are located in Supplementary Material 6; captions are located at the end of this appendix). The dependence of s_1 on *T* in the study of Harrison et al. is quite similar to that of Larsson et al. (1994) (Fig. A1b). So, while the Harrison et al. data could be made consistent with other data for $FeAl_2O_4$ either by adjusting their volume or by adjusting their site occupancy, the simplest fix is to adjust all the Harrison et al. volumes by a fixed amount. The value of α for hercynite is quite insensitive to this adjustment to the Harrison et al. data. As the ordering state of most hercynites is close to that of ideal normal spinel but most of the high-*T* data in the calibration data set are for dependent end members that tend toward inverse ordering states (i.e., $MgFe_2O_4$ and Mg_2TiO_4), the inconsistency has a detrimental effect on other calibrated values of V^o and α. We made the size of the volume adjustment a dependent parameter in the calibration so that the

chosen quantity gave the best-resolved values for V^o, α, and the coefficient for the variation with s_1; unless otherwise stated the Harrison et al. data are shown adjusted by +0.0173 J/bar/mol. Figure A2 shows that the resulting model fits all the Harrison et al. data well except the room-T data point that motivated this correction in the first place. Thus a closer fit for the Harrison et al. data might be achieved by using, for example, a multiplication factor rather than a fixed offset to the volume, but a reasonable value of α (i.e., consistent with the Harrison et al. study) is retrieved either way. We are required to make a compromise among the data sets in order to develop a better predictive volume model for spinel and emphasize that the choice of a fixed volume adjustment in no way reflects on the quality of the Harrison et al. measurements. Shifting all of the other room-T data for $FeAl_2O_4$ would result in violations of more constraints than making a slight adjustment to the high-T data. Note that, when lattice parameter and temperature error estimates reported by Harrison et al. are propagated, the resulting uncertainty in volume residual is approximately ±0.006 J/bar/mol (assuming the uncertainty in $s_1(T)$ is similar to the difference between Harrison et al. and Larsson et al.); also model residuals for the raw Harrison et al. data, without the adjustment, are well within the ±0.02 J/bar/mol range we consider as acceptable.

While performing the high-T fitting, we also discovered opposing trends between in situ high-T (Antao et al. 2005a) and annealed and quenched sample measurements (O'Neill et al. 1992) for $MgFe_2O_4$. Comparing the Mg^{2+} ordering variable (s_0) for the two studies (see Fig. 10), the slope of the equilibrium relationship between s_0 and T seems well determined. O'Neill et al. appear to have annealed their samples for a sufficiently

long time and quenched them rapidly enough to lock in ordering states down to 450 °C. There is, however, an offset of about 0.05 in s_0 at equal temperature between the two studies. One cannot attribute this to quench effects in the O'Neill et al. study because the quenched samples preserve an ordering state corresponding to a temperature 100 °C *higher* than their annealing temperature (when the equilibrium $s_0(T)$ is defined from the in situ data of Antao et al.). Rather, we suspect the discrepancy is due to differences in experimental methods for determining the ordering state. To isolate the effects of ordering and thermal expansion in $MgFe_2O_4$ using these two data sets we needed to adjust the measurements from one of the studies to account for the systematic offset between them. Even when the data were brought into agreement in this way they appeared to require a *T*-dependent thermal expansion term. Conversely, no offset exists between the O'Neill et al. data and the Levy et al. (2004) high-*T* measurements, and using data from the latter instead of Antao et al. yields a smooth thermal expansion trend that can be well fit with a constant value of α (Figs. A3a, b). We therefore adopted the study of Levy et al. (2004) to define the high-*T* volume of $MgFe_2O_4$, and excluded the study of Antao et al. (2005a). The Antao et al. (2005a) data show systematic differences in s_0 when compared to the MELTS ordering model (Fig. 10), which are reflected in the model residuals for volume. However, volume residuals for the whole Antao et al. (2005a) data set still fall within or very close to the ±0.02 J/bar/mol range.

High-*P*, room-*T* measurements

We initially fixed K_{oT} and K' for all five independent end members (see Table 4): K_{oT} to values estimated from ultrasonic studies and K' to 4. In this case the high-P $MgAl_2O_4$ data of Levy et al. (2003) displayed a concave-up trend in volume residuals versus pressure. This was eliminated by adopting the Levy et al. K_{oT} and K' for the $MgAl_2O_4$ end member. Using a similar argument, we tentatively set K_{oT} and K' for the Fe_3O_4 end member to the values from Nakagiri et al. (1986); we also set $K' = 5.5$ for Fe_2TiO_4. Finally, holding K_{oT} fixed for each end member and K' fixed for $MgAl_2O_4$, Fe_3O_4, and Fe_2TiO_4, optimizing the remaining values of K' suggests that $K' = 5.5$ is the most reasonable and best fitting value for $FeAl_2O_4$ (*N.B.*, $FeAl_2O_4 + MgFe_2O_4 = Fe_3O_4 + MgAl_2O_4$). We excluded the Fe_3O_4 data of Finger et al. (1986) and the $MgFe_2O_4$ data of Antao et al. (2005b) during this process; while the measured V/V_o ratios are consistent with those from other studies, the absolute volumes are systematically lower by ~0.03 J/bar/mol and ~0.05 J/bar/mol respectively. Residuals for $MgFe_2O_4$ do show a systematic increase with P and we investigated the effect of various P-dependent terms on the overall fit. However, as the largest discrepancy for $MgFe_2O_4$ at high P (~0.014 J/bar/mol) is well within our final cutoff of 0.02 J/bar/mol, P-dependent terms in the model were eventually rejected. The equation of state of a natural Cr-rich spinel was measured up to 26.8 GPa and 628 K by Fan et al. (2008). We used their data to constrain K' for $FeCr_2O_4$, with the optimum value being $K' = 6.5$.

The in situ high-P, room-T powder X-ray diffraction study by Haavik et al. (2000) measured the cell parameter of Fe_3O_4 up to much higher pressures than the high-P,

single-crystal experiments of Gatta et al. (2007), Nakagiri et al. (1986), and Reichmann and Jacobsen (2004). The Haavik et al. data agree with the other studies at low pressure, but begin to deviate above ~5 GPa (Fig. A4). Additionally, the calculated K_{oT} of Haavik et al. for Fe_3O_4 is significantly larger than that of the single-crystal X-ray diffraction studies, and of previous ultrasonic results (e.g., Doraiswami 1947 and Bhagavantam 1955). Haavik et al. used N_2 as the pressure medium in their diamond anvil cell experiments, and acknowledge that N_2 transitions to a solid phase at ~2.3 GPa and ambient temperature. This suggests that their experiments suffered from non-hydrostatic conditions with increasing pressure. We consider the perturbation that would be applied to the model by fitting the Haavik et al. data to be unacceptably large.

Measurements at high-*P*, *T*

Upon fitting the high-*P, T* experiments, we exposed two additional complications within the data. The in situ neutron diffraction experiments at very high-*T* and moderate-*P* by Méducin et al. (2004) are the only simultaneous high-*P, T* measurements of end-member $MgAl_2O_4$. These measurements seem to be discrepant with other studies of this composition, especially at elevated conditions (Finger et al. 1986; Levy et al. 2003; Nestola et al. 2007). Likewise, random and possibly systematic errors in the study of Antao et al. (2005b) for $MgFe_2O_4$ render the data unusable for the volume calibration, although the observed variation in volume as a function of *P* and *T* is largely captured by the final model.

The results of Méducin et al. (2004) produce model fits that are markedly different from the other data for the $MgAl_2O_4$ end member (Figs. A5a, b). As this is the only simultaneous high-*P, T* study, it is difficult to understand why the observed behavior differs so much from other in situ experiments performed on this composition (Finger et al. 1986; Levy et al. 2003; Nestola et al. 2007). Gradients in pressure and/or temperature in the Paris-Edinburgh (PE) cell employed in the experiments are a possibility and the authors do attribute the larger errors on the structural parameters at elevated conditions to limitations of the PE cell, e.g., smaller sample volume and lower signal-to-noise ratio. However, the observed trends in ordering state and lattice parameter are relatively smooth, suggesting that the combined effect of elevated *P* and *T* on ordering and volume in spinel does indeed deviate from that when high-*P* or high-*T* conditions are applied separately. In order to model volumes for these and the other $MgAl_2O_4$ data used in calibration, we would need to invoke a large cross-term, involving pressure, temperature, or likely both. Unfortunately, there are not yet enough data at simultaneous high-*P*, *T* conditions to calibrate such a term and the large deviation caused by fitting the Méducin et al. study would result in an overall less useful model for the parameter space of interest for peridotite calculations or activity-composition model calibrations. Final model volume residuals for the Méducin et al. data increase gently with *P* and *T*, from negligible at ambient conditions to just over the 0.02 J/bar/mol cut off at the most elevated conditions. The exception is the data points gathered at 0.4 GPa, which differ by ~0.04 J/bar/mol from the trend defined by the other data (Fig. A5b). This observation leads us to speculate that these two data points may be discrepant (perhaps because the

MgO pressure marker used in the experiments is less suited to lower pressure conditions) rather than the dataset as a whole.

The only other data for simultaneous high-*P* and high-*T* conditions come from the experiments of Antao et al. (2005b) for pure $MgFe_2O_4$. As noted in the previous section, absolute volumes measured in this study are ~0.05 J/bar/mol lower than would be expected from comparison with the other data for this composition at ambient and elevated conditions (O'Neill et al. 1992; Antao et al. 2005a; Levy et al. 2004). As with the Méducin et al. (2004) study previously mentioned, this may be an effect of combined high-*P* and high-*T* conditions but there are insufficient data to resolve any model parameters. Due to the complexity of the in situ high-*P*, *T* experiments, associated uncertainties must be significantly larger than for measurements at ambient, high-*T*, or high-*P* conditions. Antao et al (2005b) do not really quantify these errors and, given the difficulty in estimating measurement errors in general, we have no choice but to exclude the study from the calibration dataset. It appears that the data that Antao et al. (2005b) collected during heating are more reliable than those collected during cooling. Volume residuals for these data show a slight increase with increasing *P*, similar to that observed for the Levy et al. (2004) study, and a very slight decrease with increasing *T*. These variations are superimposed on a more or less constant negative misfit so that the typical residual, $V_{obs} - V_{model}$, is ~ –0.05 J/bar/mol. As the variation in volume with either *P* or *T* is well described, despite the offset, the updated MELTS ordering model (Sack and Ghiorso 1991a, b; this work) successfully predicts the ordering states for most of the data (Fig. 10).

CALIBRATION STRATEGY NOTES

Because different kinds of data with different and poorly known errors are used, we adopted a sequential multistep fitting procedure to avoid serious correlation between standard state and mixing parameters. We first fit the volume of all pure spinel end members (including dependent ones) as functions of P and T. Then taking that model as a starting point, we next fit all the room-P and room-T data for spinel solid solutions. In the first stage calibration, we used a nonlinear least squares algorithm and simultaneously fit end-member data for ambient, high-T, and high-P conditions. We used the three ordering-composition cross-terms described in the text. Two of the dependent end members ($MgCr_2O_4$ and $MgFe_2O_4$) show a measurable volume of reaction when formed from the appropriate independent end members. Therefore, for example, the excess volume at $MgCr_2O_4$ (where X_{sp} =1, X_{hc} = –1, and X_{ch} = 1) must include a non-zero contribution $W_{sp\text{-}ch} - W_{hc\text{-}ch} - W_{sp\text{-}hc}$. Foreshadowing calibration of the intermediate composition data, we chose to fix $W_{sp\text{-}hc}$ to zero and fit the quantities $W_{sp\text{-}ch} - W_{hc\text{-}ch}$ and $W_{mt\text{-}hc} - W_{mt\text{-}sp}$ using the end-member data.

The s_0-dependent and s_1-dependent parameters were fit using end-member data only. However, the modeled ordering effects agree well with volume measurements along the $MgAl_2O_4$-$FeAl_2O_4$ join (e.g., the data of Andreozzi and Lucchesi (2002), which are plotted in Fig. A1a as green squares) and validate the $W_{sp\text{-}hc}$ = 0 condition imposed during the first stage calibration. As the $MgAl_2O_4$-$FeAl_2O_4$ join is common to each of the Cr^{3+}-, Fe^{3+}-, and Ti^{4+}-bearing spinel subsystems this simple result was also convenient. It allowed us to identify those excess parameters that best describe each subsystem

separately; these parameters were then fit jointly to the whole solution data set. Our approach is perhaps best illustrated by the $MgAl_2O_4$-$FeAl_2O_4$-$MgFe_2O_4$-Fe_3O_4 reciprocal square in Fig. 7a where model and data are shown with ideal and ordering contributions subtracted. The convex volume surface in this case requires two regular solution parameters: $W_{\text{mt-sp}}$ and $W_{\text{mt-hc}}$ (Fig. A6). The slope (which is proportional to $W_{\text{mt-sp}} - W_{\text{mt-hc}}$) and intercept of the ordering adjusted volume variation along the $MgFe_2O_4$-Fe_3O_4 join are defined by data for the implicit end member $MgFe_2O_4$. The quantity $W_{\text{mt-sp}} + W_{\text{mt-hc}}$ (and hence $W_{\text{mt-hc}}$) is constrained in the second stage calibration using solution data: for example, the $MgAl_2O_4$-$MgFe_2O_4$ binary (Nakatsuka et al. 2004) requires an additional excess volume of ~0.03 J/bar/mol at $X_{\text{mt}} = 0.5$.

Data coverage in the $MgAl_2O_4$-$FeAl_2O_4$-$MgFe_2O_4$-Fe_3O_4 reciprocal square is uneven. The data from Mattioli et al. (1987) ($MgAl_2O_4$-Fe_3O_4), Golla-Schindler et al. (2005) ($FeAl_2O_4$-Fe_3O_4) and Zhao et al. (1998) ($MgFe_2O_4$-Fe_3O_4) were not included in the calibration as the site occupancy, in particular the ordering state of Fe^{3+}, was not determined. Calibrated data are concentrated along the $MgAl_2O_4$-$FeAl_2O_4$ and $MgAl_2O_4$-$MgFe_2O_4$ binaries but forward modeling, with s_0, s_1, and s_2 calculated using the MELTS ordering model of Sack and Ghiorso (1991a, b), shows that the volume model matches data on the other joins as well. Zhao et al. (1998) did not anneal the natural spinels they studied but their data agree with the volume model as long as equilibration temperatures were at least 300 °C. In the absence of other data, we conclude that there is no evidence for excess volumes along the $MgFe_2O_4$-Fe_3O_4 join, other than those due to ordering, and

no requirement for symmetric or asymmetric interaction parameters in addition to $W_{sp\text{-}mt}$ and $W_{hc\text{-}mt}$.

$W_{sp\text{-}ch}$ and $W_{hc\text{-}ch}$ were fit in a similar way to $W_{mt\text{-}sp}$ and $W_{mt\text{-}hc}$, allowing non-ideal interactions between Cr-free and Cr-bearing end members while preserving the more or less linear variation in volume along the $FeCr_2O_4$-$MgCr_2O_4$ join (Fig. 6b). In detail there is a slight negative deviation along this join (Lenaz et al. 2004); binary and ternary spinels in the subsystem also show ample evidence for asymmetric ordering-adjusted excess volumes (e.g., Brey et al. 1999). The best fit was obtained by simply allowing the asymmetry along the $MgAl_2O_4$-$FeCr_2O_4$ binary with a term of the form: $dW_{sp\text{-}ch} X_{sp} X_{ch} (X_{sp} - X_{ch})$. Along the $FeCr_2O_4$-$MgCr_2O_4$ binary, $X_{ch} = 1$ and X_{sp} varies between 0 and 1; therefore a positive value of $dW_{sp\text{-}ch}$ implies a negative volume of mixing between $FeCr_2O_4$ and $MgCr_2O_4$, as is observed. When all data were weighted equally, the value of $dW_{sp\text{-}ch}$ obtained by the least squares algorithm was skewed toward fitting the more $MgAl_2O_4$-rich part of the $MgAl_2O_4$-$FeAl_2O_4$-$MgCr_2O_4$-$FeCr_2O_4$ reciprocal square, where data are more densely clustered (refer to Fig. 6b), so that the predicted excess volume along the $FeCr_2O_4$-$MgCr_2O_4$ join was overly negative. This problem was solved by applying a weighting factor of 2 to the data of Doroshev et al. (1997), Brey et al. (1999), and Girnis et al. (2003); that is to say, those calibration data that required the MELTS ordering model were assigned a relative standard error twice that of other calibration data. We experimented with weighting factors between 1.5 and 3: the resulting models were very similar and all gave a visually good fit along the $FeCr_2O_4$-$MgCr_2O_4$ binary. Chi squared (χ^2) measures of the quality of fit are increased by this choice, but we

consider the resulting model to be better in the sense that it may be more safely extrapolated to high pressures (e.g., in forward MELTS calculations).

Unlike $MgFe_2O_4$ and $MgCr_2O_4$, the data indicate little or no volume of reaction for formation of cubic Mg_2TiO_4 from the independent end members (i.e., $Mg_2TiO_4 + 2FeAl_2O_4 = Fe_2TiO_4 + 2MgAl_2O_4$) which implies that $W_{sp\text{-}uv} \approx W_{hc\text{-}uv}$. During the calibration we set both parameters to zero as there was no evidence to suggest otherwise. In particular, we were unable to locate any data near the $MgAl_2O_4$-Fe_2TiO_4 join itself and, likewise, no data for compositions between Mg_2TiO_4 and Fe_2TiO_4. When the MELTS ordering model (Sack and Ghiorso 1991a, b) is used with the data of Muan et al. (1972) the volume residuals are approximately linear when plotted against X_{uv}. Along the $FeAl_2O_4$-Fe_2TiO_4 join the curvature of the volume variation is reproduced closely, but there are significant differences in the measured volume of end member Fe_2TiO_4. Measurements along the $MgAl_2O_4$-Mg_2TiO_4 join are noisier but once again suggest that, within error, the excess volume can be accounted for by ordering effects alone.

Once the Cr-bearing, Fe^{3+}-bearing, and Ti-bearing spinel volumes were calibrated, we used the available data to investigate the remaining excess volumes of mixing between the three subsystems. Along the Fe_3O_4-Fe_2TiO_4 binary the proportion of Fe_2TiO_4 controls the value of s_2. Wechsler et al. (1984) did not characterize the Fe^{3+} site occupancy for their samples so initially we assumed that $s_2 = 0$ (Akimoto 1954). In this case, model residuals for the Wechsler et al. data set show an asymmetric variation with X_{uv}, seemingly requiring excess volume of mixing terms like those in the current MELTS spinel volume model (Ghiorso 1990; Ghiorso and Sack 1991). However, if s_2 is instead

calculated using the MELTS ordering model (Sack and Ghiorso 1991a, b), the volume contribution due to ordering is sufficient such that no excess volume terms, symmetric or asymmetric, are required (see Fig. 8). Inclusion of a $W_{\text{ch-mt}}$ term does improve the overall fit noticeably because many of the natural chromian spinels in the dataset contain significant amounts of Fe^{3+} (Lenaz and Princivalle 2005; Lenaz et al. 2007). Lattice parameters for compositions along this binary are available (Robbins et al. 1971; Woodland et al. 2009), however site occupancies were not determined, so we used these data for comparison only. We fit the excess volume on this join with a single symmetric term; the asymmetry in excess volume is described by the s_2-dependent term (see Fig. 9).

Finally, we reexamined the high-*P* and high-*T* datasets to see if any *P* or *T*-dependent compositional terms were justified. Some high-*P* and high-*T* data were not directly calibrated by the model either because the sample used was only nominally pure (e.g., the natural $MgAl_2O_4$ crystals used in Carbonin et al. 2002, Finger et al. 1986, and Nestola et al. 2007 all contained small amounts of ZnO) or because they measured the in situ volumes of spinel solid solutions and hence were excluded from both stages of the fitting process (e.g., Martinago et al. 2003; Martinago et al. 2006). The 2nd stage model fits all these data well, without the need to appeal to additional parameters.

REFERENCES

Akimoto S (1954) Thermo-magnetic study of ferromagnetic minerals contained in igneous rocks. J Geomagn Geoelectr 6:1–14

Andreozzi GB, Lucchesi S (2002) Intersite distribution of Fe^{2+} and Mg in the spinel (sensu stricto)-hercynite series by single-crystal X-ray diffraction. Am Mineral 87:1113–1120

Andreozzi GB, Princivalle F (2002) Kinetics of cation ordering in synthetic $MgAl_2O_4$ spinel. Am Mineral 87:838–844

Andreozzi GB, Princivalle F, Skogby H, Della Giusta A (2000) Cation ordering and structural variations with temperature in $MgAl_2O_4$ spinel: An X-ray single-crystal study. Am Mineral 85:1164–1171

Andreozzi GB, Lucchesi S, Skogby H, Della Giusta A (2001) Compositional dependence of cation distribution in some synthetic (Mg, Zn)(Al, Fe^{3+})$_2O_4$ spinels. Eur J Mineral 13:391–402

Antao SM, Hassan I, Parise JB (2005a) Cation ordering in magnesioferrite, $MgFe_2O_4$, to 982 ºC using in situ synchrotron X-ray powder diffraction. Am Mineral 90:219–228

Antao SM, Hassan I, Crichton WA, Parise JB (2005b) Effects of high pressure and high temperature on cation ordering in magnesioferrite, $MgFe_2O_4$, using in situ synchrotron X-ray powder diffraction up to 1430 K and 6 GPa. Am Mineral 90:1500–1505

Asimow PD, Dixon JE, Langmuir CH (2004) A hydrous melting and fractionation model for mid-ocean ridge basalts: Application to the Mid-Atlantic Ridge near the Azores. Geochem Geophys Geosyst 5. doi:10.1029/2003GC000568

Barnes SJ, Roeder PL (2001) The range of spinel compositions in terrestrial mafic and ultramafic rocks. J Petrol 42:2279–2302

Berman RG (1988) Internally-consistent thermodynamic data for minerals in the system Na_2O-K_2O-CaO-MgO-FeO-Fe_2O_3-Al_2O_3-SiO_2-TiO_2-H_2O-CO_2. J Petrol 89:168–183

Berman RG, Koziol AM (1991) Ternary excess properties of grossular-pyrope-almandine garnet and their influence in geothermobarometry. Am Mineral 76:1223–1231

Bhagavantam S (1955) Elastic properties of single crystals and polycrystalline aggregates. Proc Math Sci 41:72–90

Bosi, F Hålenius U, Andreozzi GB, Skogby H, Lucchesi S (2007) Structural refinement and crystal chemistry of Mn-doped spinel: A case for tetrahedrally coordinated Mn^{3+} in an oxygen-based structure. Am Mineral 92:27–33

Bosi, F Hålenius U, Skogby H (2009) Crystal chemistry of the magnetite-ulvöspinel series. Am Mineral 94:181–189

Bragg W (1915) The structure of magnetite and the spinels. Nature 95:561

Brey GP, Doroshev AM, Girnis AV, Turkin AI (1999) Garnet-spinel-olivine-orthopyroxene equilibria in the FeO-MgO-Al_2O_3-SiO_2-Cr_2O_3 system: I. Composition and molar volumes of minerals. Eur J Mineral 11:599–617

Buddington AF, Lindsley DH (1964) Iron-titanium oxide minerals and synthetic equivalents. J Petrol 5:310–357

Callen HB, Harrison SE, Kriessman CJ (1956) Cation distributions in ferrospinels. Theoretical. Phys Rev 103:851–856

Carbonin S, Russo U, Della Giusta A (1996) Cation distribution in some natural spinels from X-ray diffraction and Mössbauer spectroscopy. Mineral Mag 60:355–368

Carbonin S, Martignago F, Menegazzo G, Dal Negro A (2002) X-ray single-crystal study of spinels: in situ heating. Phys Chem Miner 29:503–514

Carraro A (2003) Crystal chemistry of Cr-spinels from a suite of spinel peridotite mantle xenoliths from the Predazzo Area (Dolomites, Northern Italy). Eur J Mineral 15:681–688

Connolly JAD (2009) The geodynamic equation of state: What and how. Geochem Geophys Geosys 10. doi:10.1029/2009GC002540

Della Giusta A, Carbonin S, Ottonello G (1996) Temperature-dependent disorder in a natural Mg-Al-Fe^{2+}-Fe^{3+}-spinel. Mineral Mag 60:603–616

Dick HJB, Bullen T (1984) Chromian spinel as a petrogenetic indicator in abyssal and alpine-type peridotites and spatially associated lavas. Contrib Mineral Petrol 86:54–76.

Doraiswami MS (1947) Elastic constants of magnetite, pyrite and chromite. Proc Math Sci 25:413–416.

Doroshev AM, Brey GP, Girnis AV, Turkin AI, Kogarko LN (1997) Pyrope-knorringite garnets in the Earth's mantle: Experiments in the MgO-Al_2O_3-SiO_2-Cr_2O_3 system. Russ Geol Geophys 38:559–586

Downs RT, Hall-Wallace M (2003) The American Mineralogist crystal structure database. Am Mineral 88:247–250

Dunitz J, Orgel L (1957) Electronic properties of transition-metal oxides-II: Cation distribution amongst octahedral and tetrahedral sites: J Phys Chem Solids 3:318–323

Efron B (1982) The jackknife, the bootstrap, and other resampling plans. Soc Ind Appl Math, Philadelphia

Fan D, Zhou W, Liu C, Liu Y, Jiang X, Wan F, Liu J, Li X, Xie H (2008) Thermal equation of state of natural chromium spinel up to 26.8 GPa and 628 K. J Mater Sci 43:5546–5550

Finger LW, Hazen RM, Hofmeister AM (1986) High-pressure crystal chemistry of spinel ($MgAl_2O_4$) and magnetite (Fe_3O_4): Comparisons with silicate spinels. Phys Chem Miner 13:215–220

Fleet ME (1981) The structure of magnetite. Acta Crystallogr B37:917–920

Fleet ME (1984) The structure of magnetite: Two annealed natural magnetites, $Fe_{3.005}O_4$ and $Fe_{2.96}Mg_{0.04}O_4$. Acta Crystallogr C40:1491–1493

Gatta G, Kantor I, Boffa Ballaran T, Dubrovinsky L, McCammon C (2007) Effect of non-hydrostatic conditions on the elastic behaviour of magnetite: an in situ single-crystal X-ray diffraction study. Phys Chem Miner 34:627–635

Ghiorso MS (1990) Thermodynamic properties of hematite-ilmenite-geikielite solid solutions. Contrib Mineral Petrol 104:645–667

Ghiorso MS (2004a) An equation of state for silicate melts. I. Formulation of a general model. Am J Sci 304:637–678

Ghiorso MS (2004b) An equation of state for silicate melts. III. Analysis of stoichiometric liquids at elevated pressure: Shock compression data, molecular dynamics simulations, and mineral fusion curves. Am J Sci 304:752–810

Ghiorso MS (2004c) An equation of state for silicate melts. IV. Calibration of a multicomponent mixing model to 40 GPa. Am J Sci 304:811–838

Ghiorso MS, Evans BW (2008) Thermodynamics of rhombohedral oxide solid solutions and a revision of the Fe-Ti two-oxide geothermometer and oxygen-barometer. Am J Sci 308:957–1039

Ghiorso MS, Kress VC (2004) An equation of state for silicate melts. II. Calibration of volumetric properties at 10^5 Pa. Am J Sci 304:679–751

Ghiorso MS, Sack RO (1991) Fe-Ti oxide geothermometry: Thermodynamic formulation and the estimation of intensive variables in silicic magmas. Contrib Mineral Petrol 108:485–510

Ghiorso MS, Sack RO (1995) Chemical mass transfer in magmatic processes IV. A revised and internally consistent thermodynamic model for the interpolation and extrapolation of liquid-solid equilibria in magmatic systems at elevated temperatures and pressures. Contrib Mineral Petrol 119:197–212

Ghiorso MS, Hirschmann MM, Reiners PW, Kress III VC (2002) The pMELTS: A revision of MELTS for improved calculation of phase relations and major element partitioning related to partial melting of the mantle to 3 GPa. Geochem Geophys Geosyst 3. doi:10.1029/2001GC000217

Ghiorso MS, Hirschmann MM, Grove TL (2007) xMELTS: A thermodynamic model for the estimation of magmatic phase relations over the pressure range 0-30 GPa and at temperatures up to 2500 °C. Eos Trans Am Geophys Union 88(52), Fall Meet Suppl Abstr V31C-0608

Girnis A, Brey G, Doroshev A, Turkin A, Simon N (2003) The system MgO-Al_2O_3-Cr_2O_3 revisited: reanalysis of Doroshev et al.'s (1997) experiments and new experiments. Eur J Mineral 15:953–964

Golla-Schindler U, O'Neill HStC, Putnis A (2005) Direct observation of spinodal decomposition in the magnetite-hercynite system by susceptibility measurements and transmission electron microscopy. Am Mineral 90:1278–1283

Haavik C, Stølen S, Fjellvåg H, Hanfland M, Häusermann D (2000) Equation of state of magnetite and its high-pressure modification: Thermodynamics of the Fe-O system at high pressure. Am Mineral 85:514–523

Haggerty S (1971) Compositional variations in lunar spinels. Nature Phys Sci 233:156–160

Hamecher EA, Antoshechkina PM, Ghiorso MS, Asimow PD (2009) Thermodynamic calibration of Cr-Al exchange equilibria for garnet and spinel. Eos Trans Am Geophys Union 90(52), Fall Meet Suppl Abstr V31D-2056

Harrison RJ, Redfern SAT, O'Neill HStC (1998) The temperature dependence of the cation distribution in synthetic hercynite ($FeAl_{\sim 2}O_{\sim 4}$) from in-situ neutron structure refinements. Am Mineral 83:1092–1099

Hazen RM, Navrotsky A (1996) Effects of pressure on order-disorder reactions. Am Mineral 81:1021–1035

Hill RJ (1984) X-ray powder diffraction profile refinement of synthetic hercynite. Am Mineral 69:937–942

Hirschmann MM, Ghiorso MS, Davis FA, Gordon SM, Mukherjee S, Grove TL, Krawczynski M, Medard E, Till CB (2008) Library of Experimental Phase Relations (LEPR): A database and Web portal for experimental magmatic phase equilibria data. Geochem Geophys Geosyst 9. doi:10.1029/2007GC001894

Holland TJB, Powell R (1990) An enlarged and updated internally consistent thermodynamic dataset with uncertainties and correlations: the system K_2O–Na_2O–CaO–MgO–MnO–FeO–Fe_2O_3–Al_2O_3–TiO_2–SiO_2–C–H_2–O_2. J Metamorph Geol 8:89–124

Holland TJB, Powell R (1998) An internally consistent thermodynamic data set for phases of petrological interest. J Metamorph Geol 16:309–343

Holland TJB, Powell R (2011) An improved and extended internally consistent thermodynamic dataset for phases of petrological interest, involving a new equation of state for solids. J Metamorph Geol 29:333–383

Irifune T, Ohtani E, Kumazawa M (1982) Stability field of knorringite $Mg_3Cr_2Si_3O_{12}$ at high pressure and its implication to the occurrence of Cr-rich pyrope in the upper mantle. Phys Earth Planet Inter 27:263–272

Ishii M, Nakahira M, Yamanaka T (1972) Infrared absorption spectra and cation distributions in $(Mn,Fe)_3O_4$. Solid State Commun 11:209–212

Ishii M, Hiraishi J, Yamanaka T (1982) Structure and lattice vibrations of Mg-Al spinel solid solution. Phys Chem Miner 8:64–68

Kessel R, Beckett JR, Stolper EM (2003) Experimental determination of the activity of chromite in multicomponent spinels. Geochim Cosmochim Acta 67:3033–3044

Klemme S (2004) The influence of Cr on the garnet–spinel transition in the Earth's mantle: Experiments in the system $MgO–Cr_2O_3–SiO_2$ and thermodynamic modelling. Lithos 77:639–646

Klemme S, Ivanic TJ, Connolly JAD, Harte B (2009) Thermodynamic modelling of Cr-bearing garnets with implications for diamond inclusions and peridotite xenoliths. Lithos 112:986–991

Larsson L, O'Neill HStC, Annersten H (1994) Crystal chemistry of synthetic hercynite ($FeAl_2O_4$) from XRD structural refinements and Mössbauer spectroscopy. Eur J Mineral 6:39–51

Lavina B, Koneva A, Della Giusta A (2003) Cation distribution and cooling rates of Cr-substituted Mg-Al spinel from the Olkhon metamorphic complex, Russia. Eur J Mineral 15:435–441

Lavina B, Princivalle F, Della Giusta A (2005) Controlled time-temperature oxidation reaction in a synthetic Mg-hercynite. Phys Chem Miner 32:83–88

Lavina B, Cesare B, Alvarez-Valero AM, Uchida H, Downs RT, Koneva A, Dera P (2009) Closure temperatures of intracrystalline ordering in anatectic and metamorphic hercynite, $Fe^{2+}Al_2O_4$. Am Mineral 94:657–665

Lenaz D, Princivalle F (2005) The crystal chemistry of detrital chromian spinel from the southeastern Alps and outer Dinarides: The discrimination of supplies from areas of similar tectonic setting? Can Mineral 43:1305–1314

Lenaz D, Skogby H, Princivalle F, Hålenius U (2004) Structural changes and valence states in the $MgCr_2O_4$-$FeCr_2O_4$ solid solution series. Phys Chem Miner 31:633–642

Lenaz D, Braidotti R, Princivalle F, Garuti G, Zaccarini F (2007) Crystal chemistry and structural refinement of chromites from different chromitite layers and xenoliths of the Bushveld Complex. Eur J Mineral 19:599–609

Lenaz D, Logvinova AM, Princivalle F, Sobolev NV (2009) Structural parameters of chromite included in diamond and kimberlites from Siberia: A new tool for discriminating ultramafic source. Am Mineral 94:1067–1070

Levy D, Artioli G (1998) Thermal expansion of chromites and zinc spinels. Mater Sci Forum 278–281:390–395

Levy D, Pavese A, Hanfland M (2003) Synthetic $MgAl_2O_4$ (spinel) at high-pressure conditions (0.0001-30 GPa): A synchrotron X-ray powder diffraction study. Am Mineral 88:93–98

Levy D, Diella V, Dapiaggi M, Sani A, Gemmi M, Pavese A (2004) Equation of state, structural behaviour and phase diagram of synthetic $MgFe_2O_4$, as a function of pressure and temperature. Phys Chem Miner 31:122–129

Lindsley DH (1965) Iron-titanium oxides. Carnegie Inst Year B 64:144–148

Lucchesi S, Amoriello M, Della Giusta A (1998) Crystal chemistry of spinels from xenoliths of the Alban Hills volcanic region. Eur J Mineral 10:473–482

Martignago F, Dal Negro A, Carbonin S (2003) How Cr^{3+} and Fe^{3+} affect Mg–Al order–disorder transformation at high temperature in natural spinels. Phys Chem Miner 30:401–408

Martignago F, Andreozzi G, Dal Negro A (2006) Thermodynamics and kinetics of cation ordering in natural and synthetic $Mg(Al,Fe^{3+})_2O_4$ spinels from in situ high-temperature X-ray diffraction. Am Mineral 91:306–312

Mattioli GS, Wood BJ, Carmichael ISE (1987) Ternary-spinel volumes in the system $MgAl_2O_4$-Fe_3O_4- $\gamma Fe_{8/3}O_4$: Implications for the effect of *P* on intrinsic fo_2 measurements of mantle-xenolith spinels. Am Mineral 72:468–480

Méducin F, Redfern SAT, Le Godec Y, Stone HJ, Tucker MG, Dove MT, Marshall WG (2004) Study of cation order-disorder in $MgAl_2O_4$ spinel by in situ neutron diffraction up to 1600 K and 3.2 GPa. Am Mineral 89:981–986

Menegazzo G, Carbonin S (1998) Oxidation mechanisms in Al-Mg-Fe spinels. A second stage: α-Fe_2O_3 exsolution. Phys Chem Miner 25:541–547

Millard RL, Peterson RC, Hunter BK (1995) Study of the cubic to tetragonal transition in Mg_2TiO_4 and Zn_2TiO_4 spinels by ^{17}O MAS NMR and Rietveld refinement of X-ray diffraction data. Am Mineral 80:885–896

Muan A, Hauck J, Löfall T (1972) Equilibrium studies with a bearing on lunar rocks. In: Proceedings of the Third Lunar Science Conference (Suppl 3). Geochim Cosmochim Acta 1:185–196

Nakagiri N, Manghnani MH, Ming LC, Kimura S (1986) Crystal structure of magnetite under pressure. Phys Chem Miner 13:238–244

Nakatsuka A, Ueno H, Nakayama N, Mizota T, Maekawa H (2004) Single-crystal X-ray diffraction study of cation distribution in $MgAl_2O_4$–$MgFe_2O_4$ spinel solid solution. Phys Chem Miner 31:278–287

Nell J, Wood BJ (1989) Thermodynamic properties in a multicomponent solid solution involving cation disorder: Fe_3O_4-$MgFe_2O_4$-$FeAl_2O_4$-$MgAl_2O_4$ spinels. Am Mineral 74:1000–1015

Nestola F, Ballaran T, Balic-Zunic T, Princivalle F, Secco L, Dal Negro A (2007) Comparative compressibility and structural behavior of spinel $MgAl_2O_4$ at high pressures: The independency on the degree of cation order. Am Mineral 92:1838–1843

Oka Y, Steinke P, Chatterjee ND (1984) Thermodynamic mixing properties of $Mg(Al,Cr)_2O_4$ spinel crystalline solution at high temperatures and pressures. Contrib Mineral Petrol 87:196–204

O'Neill HStC, Dollase WA (1994) Crystal structures and cation distributions in simple spinels from powder XRD structural refinements: $MgCr_2O_4$, $ZnCr_2O_4$, Fe_3O_4, and the temperature dependence of the cation distribution in $ZnAl_2O_4$. Phys Chem Miner 20:541–555

O'Neill HStC, Navrotsky A (1983) Simple spinels: Crystallographic parameters, cation radii, lattice energies, and cation distribution. Am Mineral 68:181–194

O'Neill HStC, Navrotsky A (1984) Cations distributions and thermodynamic properties of binary spinel solid solutions. Am Mineral 69:733–753

O'Neill HStC, Annersten H, Virgo D (1992) The temperature dependence of the cation distribution in magnesioferrite ($MgFe_2O_4$) from powder XRD structural refinements and Mössbauer spectroscopy. Am Mineral 77:725–740

O'Neill HStC, Redfern S, Kesson S, Short S (2003) An in situ neutron diffraction study of cation disordering in synthetic qandilite Mg_2TiO_4 at high temperatures. Am Mineral 88:860–865

Pascal ML, Fonteilles M, Boudouma O, Principe C (2011) Qandilite from Vesuvius skarn ejecta: Conditions of formation and miscibility gap in the ternary spinel-qandilite-magnesioferrite. Can Mineral 49:459–485

Passerini L (1930) Richerche sugli spinelli. II. I composti. $CuAl_2O_4$, $MgAl_2O_4$, $MgFe_2O_4$, $ZnAl_2O_4$, $ZnCr_2O_4$, $ZnFe_2O_4$, $MnFe_2O_4$. Gazz Chim Ital 60:389–399

Peterson RC, Lager GA, Hitterman RL (1991) A time-of-flight neutron powder diffraction study of $MgAl_2O_4$ at temperatures up to 1273 K. Am Mineral 76:1455–1458

Powell R, Holland TJB (1985) An internally consistent thermodynamic dataset with uncertainties and correlations: 1. Methods and a worked example. J Metamorph Geol 3:327–342

Powell R, Holland TJB, Worley B (1998) Calculating phase diagrams involving solid solutions via non-linear equations, with examples using THERMOCALC. J Metamorph Geol 16:577–588

Princivalle F, Della Giusta A, De Min A, Piccirillo E (1999) Crystal chemistry and significance of cation ordering in Mg-Al rich spinels from high-grade hornfels (Predazzo-Monzoni, NE Italy). Mineral Mag 63:257–262

Princivalle F, Martignago F, Del Negro A (2006) Kinetics of cation ordering in natural $Mg(Al,Cr^{3+})_2O_4$ spinels. Am Mineral 91:313–318

Redfern SAT, Harrison RJ, O'Neill HStC, Wood DRR (1999) Thermodynamics and kinetics of cation ordering in $MgAl_2O_4$ spinel up to 1600 ºC from in situ neutron diffraction. Am Mineral 84:299–310

Reichmann HJ, Jacobsen SD (2004) High-pressure elasticity of a natural magnetite crystal. Am Mineral 89:1061–1066

Robbins M, Wertheim GK, Sherwood RC, Buchanan DNE (1971) Magnetic properties and site distributions in the system $FeCr_2O_4 – Fe_3O_4$ ($Fe^{2+}Cr_{2-x}Fe_x^{3+}O_4$). J Phys Chem Solids 32:717–729

Robie RA, Hemingway BS, Fisher JR (1979) Thermodynamic properties of minerals and related substances at 298.15 K and 1 bar (1e5 Pa) pressures and at higher temperatures. U. S. Geol Surv Bull 1452:1–456

Sack RO (1982) Spinels as petrogenetic indicators: Activity-composition relations at low pressures. Contrib Mineral Petrol 79:169–186

Sack RO, Ghiorso MS (1991a) An internally consistent model for the thermodynamic properties of Fe-Mg-titanomagnetite-aluminate spinels. Contrib Mineral Petrol 106:474–505

Sack RO, Ghiorso MS (1991b) Chromian spinels as petrogenetic indicators: Thermodynamics and petrological applications. Am Mineral 76:827–847

Sack RO, Ghiorso MS (1994a) Thermodynamics of multi component pyroxenes: II. Phase relations in the quadrilateral. Contrib Mineral Petrol 116:287–300

Sack RO, Ghiorso MS (1994b) Thermodynamics of multicomponent pyroxenes: III. Calibration of $Fe^{2+}(Mg)_{-1}$, $TiAl_2(MgSi_2)_{-1}$, $TiFe_2^{3+}(MgSi_2)_{-1}$, $AlFe^{3+}(MgSi)_{-1}$, $NaAl(CaMg)_{-1}$, $Al_2(MgSi)_{-1}$ and $Ca(Mg)_{-1}$ exchange reactions between pyroxenes and silicate melts. Contrib Mineral Petrol 118:271–296

Schwarz G (1978) Estimating the dimension of a model. Ann Stat 6:461–464

Sedler IK, Feenstra A, Peters T (1994) An X-ray powder diffraction study of synthetic $(Fe,Mn)_2TiO_4$ spinel. Eur J Mineral 6:873–885

Smith PM, Asimow PD (2005) Adiabat_1ph: A new public front-end to the MELTS, pMELTS, and pHMELTS models. Geochem Geophys Geosyst 6. doi:10.1029/2004GC000816

Stout M, Bayliss P (1980) Crystal structure of two ferrian ulvöspinels from British Columbia. Can Mineral 18:339–341

Taberna PL, Mitra S, Poizot P, Simon P, Tarascon JM (2006) High rate capabilities Fe_3O_4-based Cu nano-architectured electrodes for lithium-ion battery applications. Nature Mater 5:567–573

Tabira Y, Withers RL (1999) Cation ordering in $NiAl_2O_4$ spinel by a 111 systematic row CBED technique. Phys Chem Miner 27:112–118

Verwey E, Heilmann E (1947) Physical properties and cation arrangement of oxides with spinel structures I. Cation arrangement in spinels. J Chem Phys 15:174–180

Waerenborgh JC, Figueiredo MO, Cabral JMP, Pereira LCJ (1994) Powder XRD structure refinements and ^{57}Fe Mössbauer effect study of synthetic $Zn_{1-x}Fe_xAl_2O_4$ ($0<x\leq1$) spinels annealed at different temperatures. Phys Chem Miner 21:460–468

Wang H, Simmons G (1972) Elasticity of some mantle crystal structures 1. Pleonaste and hercynite spinel. J Geophys Res 77:4379–4392

Wechsler BA, Von Dreele RB (1989) Structure refinements of Mg_2TiO_4, $MgTiO_3$ and $MgTi_2O_5$ by time-of-flight neutron powder diffraction. Acta Crystallogr B45:542–549

Wechsler BA, Lindsley D, Prewitt C (1984) Crystal structure and cation distribution in titanomagnetites ($Fe_{3-x}Ti_xO_4$). Am Mineral 69:754–770

Woodland AB, Bauer M, Ballaran TB, Hanrahan M (2009) Crystal chemistry of $Fe_3^{2+}Cr_2Si_3O_{12}$ – $Fe_3^{2+}Fe_2^{3+}Si_3O_{12}$ garnet solid solutions and related spinels. Am Mineral 94:359–366

Workman RK, Hart SR (2005) Major and trace element composition of the depleted MORB mantle (DMM). Earth Planet Sci Lett 231:53–72

Yamanaka T, Shimazu H, Ota K (2001) Electric conductivity of Fe_2SiO_4-Fe_3O_4 spinel solid solutions. Phys Chem Miner 28:110–118

Yang Z, Xia GG, Li XH, Stevenson JW (2007) $(Mn,Co)_3O_4$ spinel coatings on ferritic stainless steels for SOFC interconnect applications. Int J Hydrogen Energy 32:3648–3654

Zhao Y, Zhang Y, Bi C, Guo L (1998) The discovery of magnesioferrite from Au(Fe, Cu) magnesian skarn deposits and study of the magnesioferrite-magnesiomagnetite series. Acta Geol Sin 74:382–391

FIGURE CAPTIONS

Fig. A1 a Data along the $MgAl_2O_4$ – $FeAl_2O_4$ binary. Measured volume vs. s_1. All data were measured at room-*P*. Circles denote pure $FeAl_2O_4$, diamonds are pure $MgAl_2O_4$, and squares lie on the join between the end members. Grey diamonds are pure $MgAl_2O_4$ from various studies in the dataset, measured at room-*P*, *T*; grey squares are binary compositions from various sources; other colors correspond to specific studies called out in the legend. The Harrison et al. (1998) data were measured at high-*T*, in situ; the raw data are plotted, i.e., before adding the volume correction we determined is needed to bring this study into agreement with the rest of the data. Larsson et al. (1994) samples were annealed at a series of temperatures; all others were measured at room-*T*; **b** Order variable s_1 vs. temperature for pure $FeAl_2O_4$ data of Harrison et al. (in situ *T*) and Larsson et al. (annealing *T*). The solid line is calculated using the MELTS ordering model for pure $FeAl_2O_4$. Colors are the same as in **a**.

Fig. A2 Measured volume vs. temperature for the Harrison et al. (1998) (adjusted) and Larsson et al. (1994) data sets (symbols are the same as Fig. A1). The temperature plotted is the in situ *T*, i.e., the Larsson et al. data all plot at 25 °C. Crosses are the modeled volumes for these data. Gray contours show modeled volume for pure $FeAl_2O_4$ at constant values of s_1, printed beneath each line.

Fig. A3 a Measured volume vs. temperature for the Levy et al. (2004) (diamonds) and O'Neill et al. (1992) (squares) datasets. The temperature plotted is the in situ *T*, i.e., the

O'Neill et al. data all plot at 25 °C. Crosses are the modeled volumes for these data. Gray contours show modeled volume for pure $MgFe_2O_4$ at constant values of s_0, printed beneath each line; **b** Measured and modeled volumes as a function of s_0 for the O'Neill et al. data set (symbols are the same as **a**) showing excellent agreement in the slope of the two trends.

Fig. A4 Volume vs. pressure for pure Fe_3O_4 measured at high-*P* in situ. Black line shows model volume at room-*T* for pure Fe_3O_4.

Fig. A5 a Volume vs. pressure for pure $MgAl_2O_4$ measured at high-*P* in situ. The data of Méducin et al. (2004) were measured at simultaneous high-*P*, *T* conditions. Black line shows model volume at room-*T* for pure $MgAl_2O_4$; **b** Equilibrium data from Méducin et al. (red diamonds) connected with tie lines to modeled volumes (open diamonds), which lie on lines of model volume at constant *T*, where the temperatures shown are the temperatures at which the measurements were made.

Fig. A6 Excess model volume in the $MgAl_2O_4$-$MgFe_2O_4$-Fe_3O_4-$FeAl_2O_4$ reciprocal square. Compare with Fig. 7a.

Supplement 4. Unconstrained standard deviation of fit parameters

	$1\sigma^*$	
V^o_{sp}	0.0010	(J/bar/mol)
V^o_{ch}	1.1	
V^o_{uv}	0.0072	
V^o_{mt}	0.00061	
V^o_{hc}	0.0018	
$W_{hc\text{-}ch}$	1.4	
$W_{ch\text{-}mt}$	0.92	
$W_{sp\text{-}ch}$	2.5	
$dW_{sp\text{-}ch}$	1.9	
$W_{mt\text{-}hc}$	0.17	
$W_{mt\text{-}sp}$	0.17	
W_{s0}	0.011	
W_{s1}	0.0052	
W_{s2}	0.016	
α_{sp}	1.4×10^{-7}	(K^{-1})
α_{uv}	4.0×10^{-7}	
α_{mt}	4.7×10^{-7}	
α_{hc}	1.8×10^{-7}	

*Bootstrap estimation of s.d. for each parameter, varying all other fit parameters

Supplement 5. Correlation matrix

	$W_{hc\text{-}ch}$	$W_{ch\text{-}mt}$	$W_{sp\text{-}ch}$	$W_{mt\text{-}hc}$	$W_{mt\text{-}sp}$	$dW_{sp\text{-}ch}$	W_{s0}	W_{s1}	W_{s2}	V^{o}_{ch}	V^{o}_{hc}	V^{o}_{mt}	V^{o}_{sp}	V^{o}_{uv}	α_{hc}	α_{mt}	α_{sp}	α_{uv}
$W_{hc\text{-}ch}$	1.000000	0.681128	0.999204	-0.142064	-0.142152	-0.998338	0.000293	0.001864	-0.004929	-0.995713	0.002072	0.000969	0.005313	-0.000843	-0.000828	0.008894	-0.006624	0.005691
$W_{ch\text{-}mt}$	0.681128	1.000000	0.706088	-0.209011	-0.209431	-0.673564	-0.006219	0.005461	-0.006690	-0.737388	0.006082	0.001929	-0.001385	-0.005982	-0.002212	0.012528	-0.002529	0.000233
$W_{sp\text{-}ch}$	0.999204	0.706088	1.000000	-0.141474	-0.141562	-0.997329	0.000125	0.001507	-0.005023	-0.998608	0.001853	0.001042	0.004028	-0.000812	-0.001203	0.009003	-0.005996	0.004968
$W_{mt\text{-}hc}$	-0.142064	-0.209011	-0.141474	1.000000	0.997770	0.132552	-0.038691	0.038024	0.062472	0.140418	0.034498	0.001181	-0.009634	-0.038440	-0.000141	-0.025189	-0.000336	0.006521
$W_{mt\text{-}sp}$	-0.142152	-0.209431	-0.141562	0.997770	1.000000	0.132413	0.015804	-0.012616	0.008086	0.140414	-0.013168	-0.001296	0.004717	0.015404	-0.001064	-0.007038	-0.001784	-0.000736
$dW_{sp\text{-}ch}$	-0.998338	-0.673564	-0.997329	0.132552	0.132413	1.000000	-0.003829	0.002309	0.006394	0.993561	0.001833	-0.001092	-0.004068	-0.002853	0.001354	-0.008267	0.005549	-0.004335
W_{s0}	0.000293	-0.006219	0.000125	-0.038691	0.015804	-0.003829	1.000000	-0.921771	-0.352496	-0.001628	-0.877785	0.013443	0.287766	0.979551	0.002269	0.011201	-0.053375	-0.103861
W_{s1}	0.001864	0.005461	0.001507	0.038024	-0.012616	0.002309	-0.921771	1.000000	0.316223	0.000467	0.957363	-0.008815	0.091576	-0.932750	-0.012192	0.028469	-0.069653	0.155578
W_{s2}	-0.004929	-0.006690	-0.005023	0.062472	0.008086	0.006394	-0.352496	0.316223	1.000000	0.005776	0.312230	-0.019166	-0.126589	-0.336569	-0.036115	-0.552354	0.025122	0.005455
V^{o}_{ch}	-0.995713	-0.737388	-0.998608	0.140418	0.140414	0.993561	-0.001628	0.000467	0.005776	1.000000	0.000005	-0.001169	-0.003115	-0.000813	0.001336	-0.009354	0.005493	-0.004227
V^{o}_{hc}	0.002072	0.006082	0.001853	0.034498	-0.013168	0.001833	-0.877785	0.957363	0.312230	0.000005	1.000000	-0.012332	0.092235	-0.846647	-0.220755	-0.060582	-0.047895	-0.020523
V^{o}_{mt}	0.000969	0.001929	0.001042	0.001181	-0.001296	-0.001092	0.013443	-0.008815	-0.019166	-0.001169	-0.012332	1.000000	0.013508	0.009486	0.002501	0.006797	-0.002753	0.004579
V^{o}_{sp}	0.005313	-0.001385	0.004028	-0.009634	0.004717	-0.004068	0.287766	0.091576	-0.126589	-0.003115	0.092235	0.013508	1.000000	0.187638	-0.006207	0.144395	-0.454325	0.212560
V^{o}_{uv}	-0.000843	-0.005982	-0.000812	-0.038440	0.015404	-0.002853	0.979551	-0.932750	-0.336569	-0.000813	-0.846647	0.009486	0.187638	1.000000	-0.097614	-0.052469	0.025006	-0.243304
α_{hc}	-0.000828	-0.002212	-0.001203	-0.000141	-0.001064	0.001354	0.002269	-0.012192	-0.036115	0.001336	-0.220755	0.002501	-0.006207	-0.097614	1.000000	0.384253	-0.053184	0.774644
α_{mt}	0.008894	0.012528	0.009003	-0.025189	-0.007038	-0.008267	0.011201	0.028469	-0.552354	-0.009354	-0.060582	0.006797	0.144395	-0.052469	0.384253	1.000000	-0.269828	0.435996
α_{sp}	-0.006624	-0.002529	-0.005996	-0.000336	-0.001784	0.005549	-0.053375	-0.069653	0.025122	0.005493	-0.047895	-0.002753	-0.454325	0.025006	-0.053184	-0.269828	1.000000	-0.586005
α_{uv}	0.005691	0.000233	0.004968	0.006521	-0.000736	-0.004335	-0.103861	0.155578	0.005455	-0.004227	-0.020523	0.004579	0.212560	-0.243304	0.774644	0.435996	-0.586005	1.000000

Supplement 6. Appendix Figures

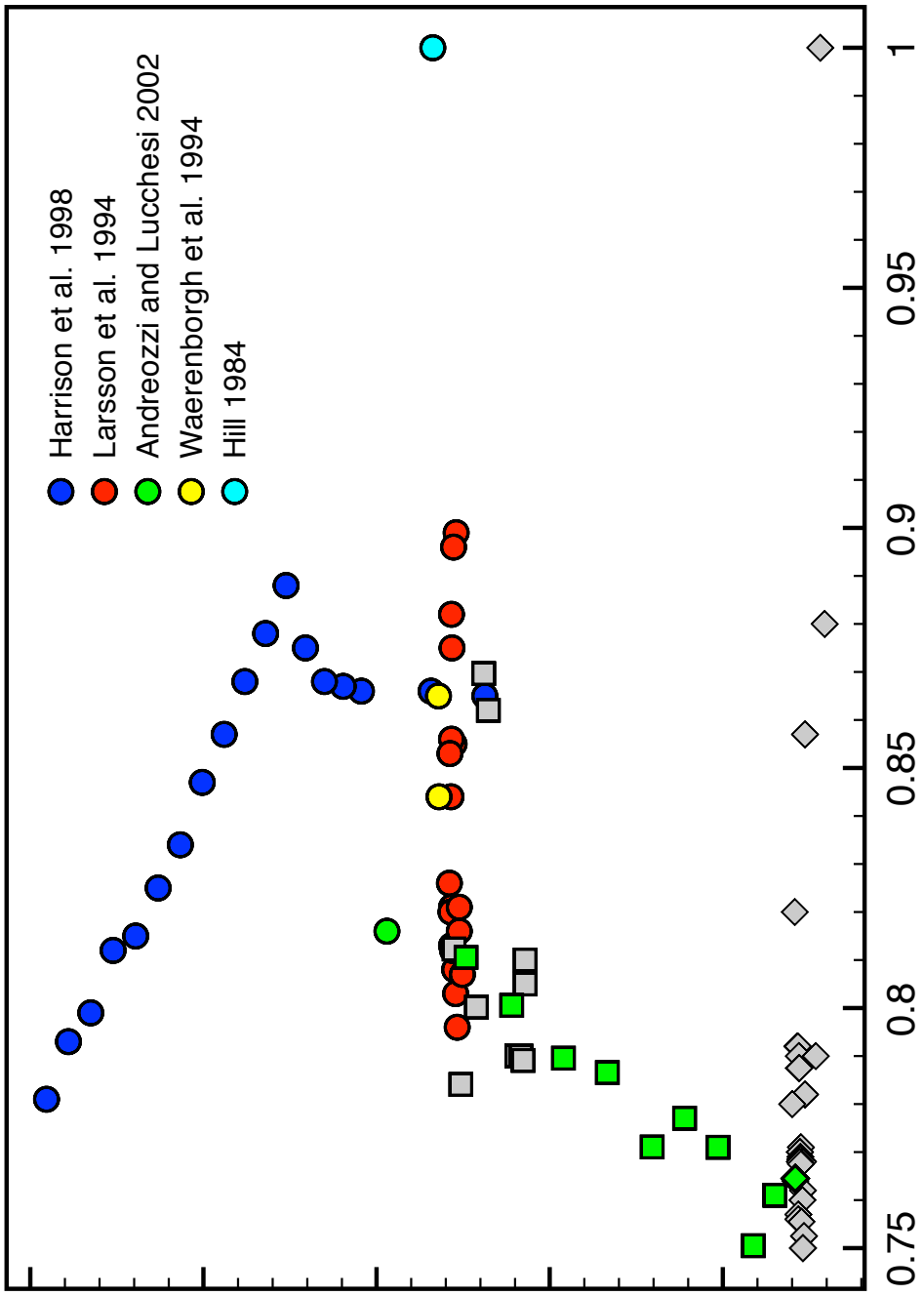

Fig. A1a

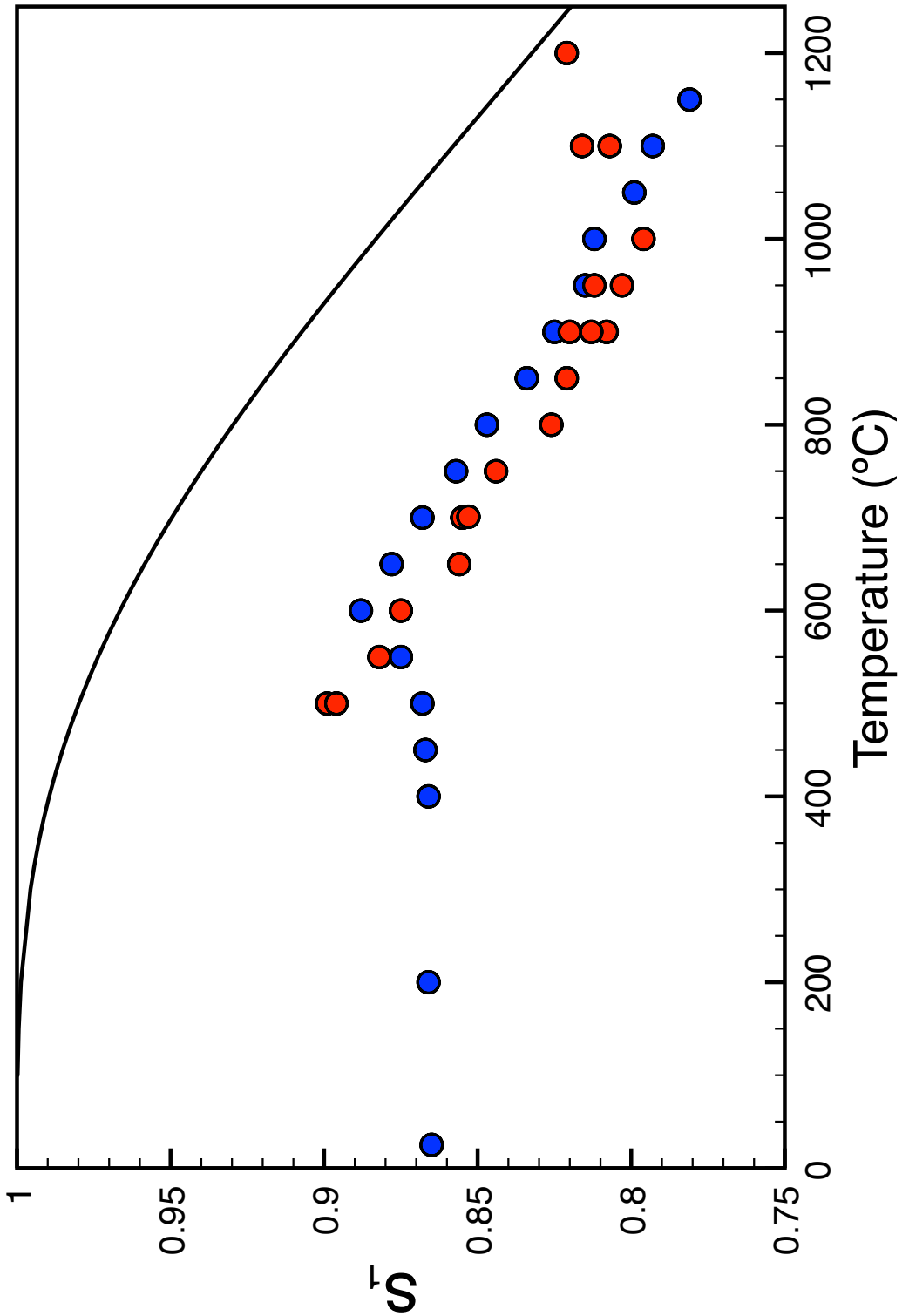

Fig. A1b

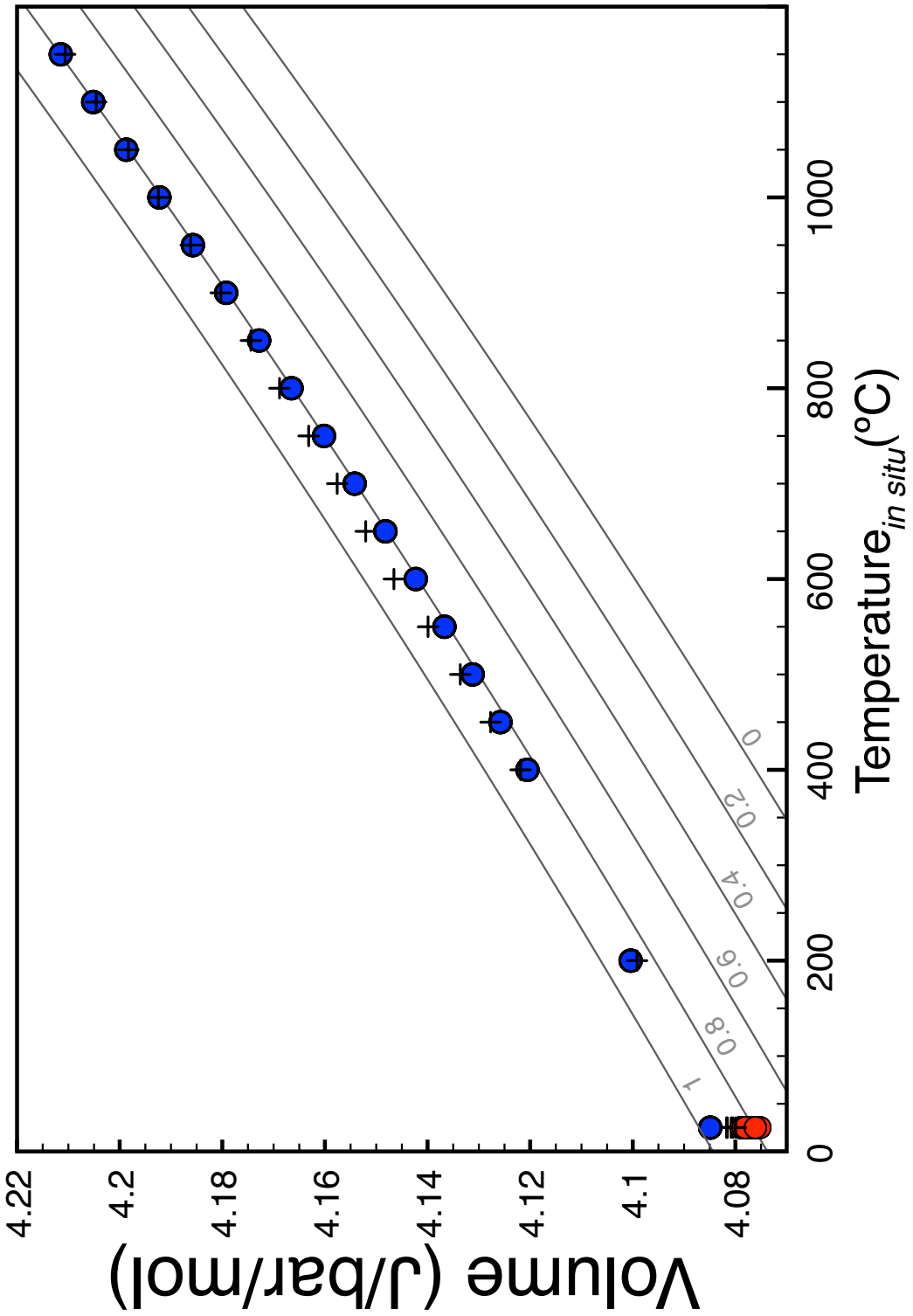
Volume (J/bar/mol)
4.22
4.2
4.18
4.16
4.14
4.12
4.1
4.08
0
200
400
600
800
1000
Temperature$_{in\ situ}$(°C)
1
0.8
0.6
0.4
0.2
0

Fig. A2

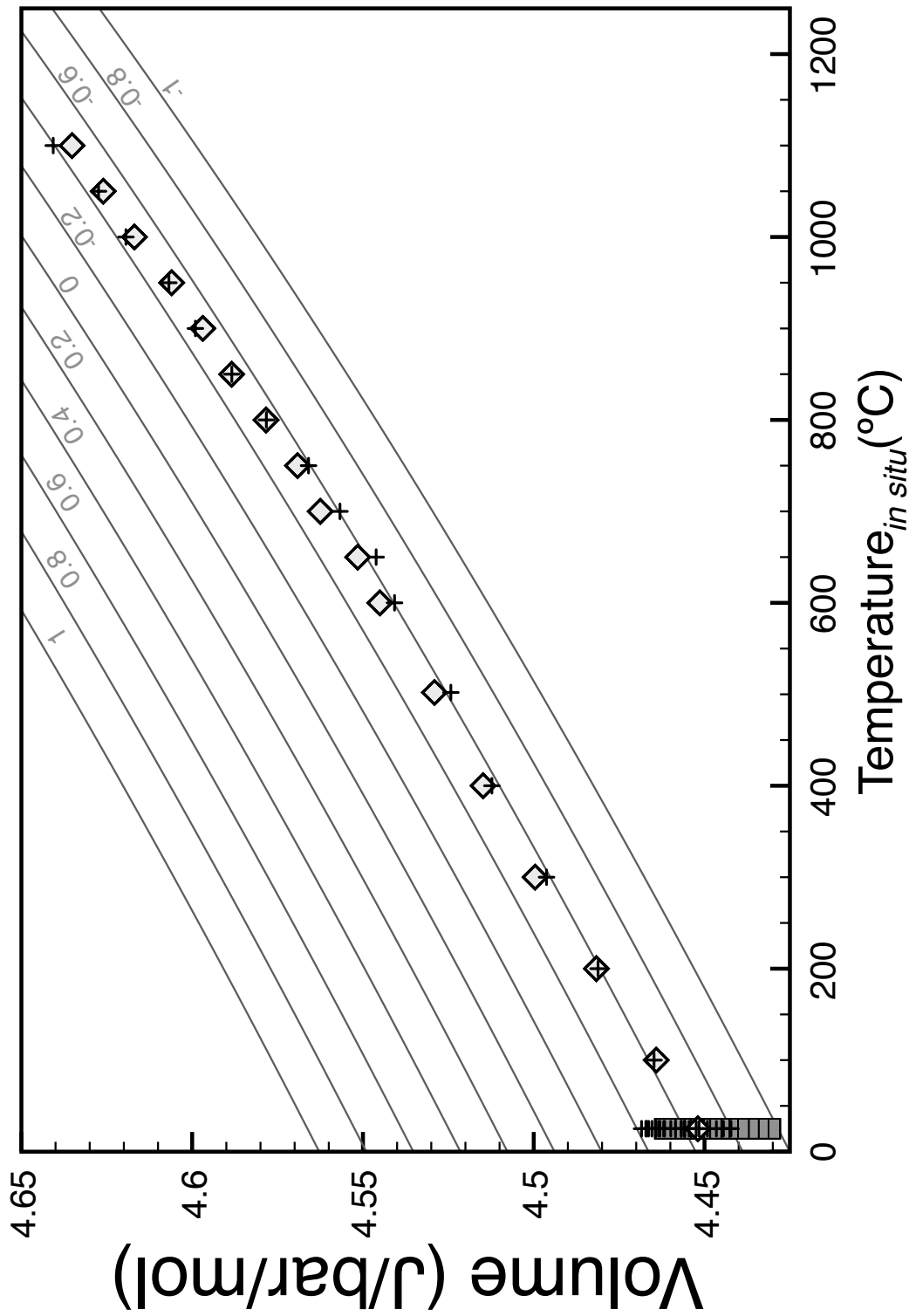
Volume (J/bar/mol)
4.65
4.6
4.55
4.5
4.45
0
200
400
600
800
1000
1200
Temperature$_{in\ situ}$(°C)
1
0.8
0.6
0.4
0.2
0
-0.2
-0.4
-0.6
-0.8
-1

Fig. A3a

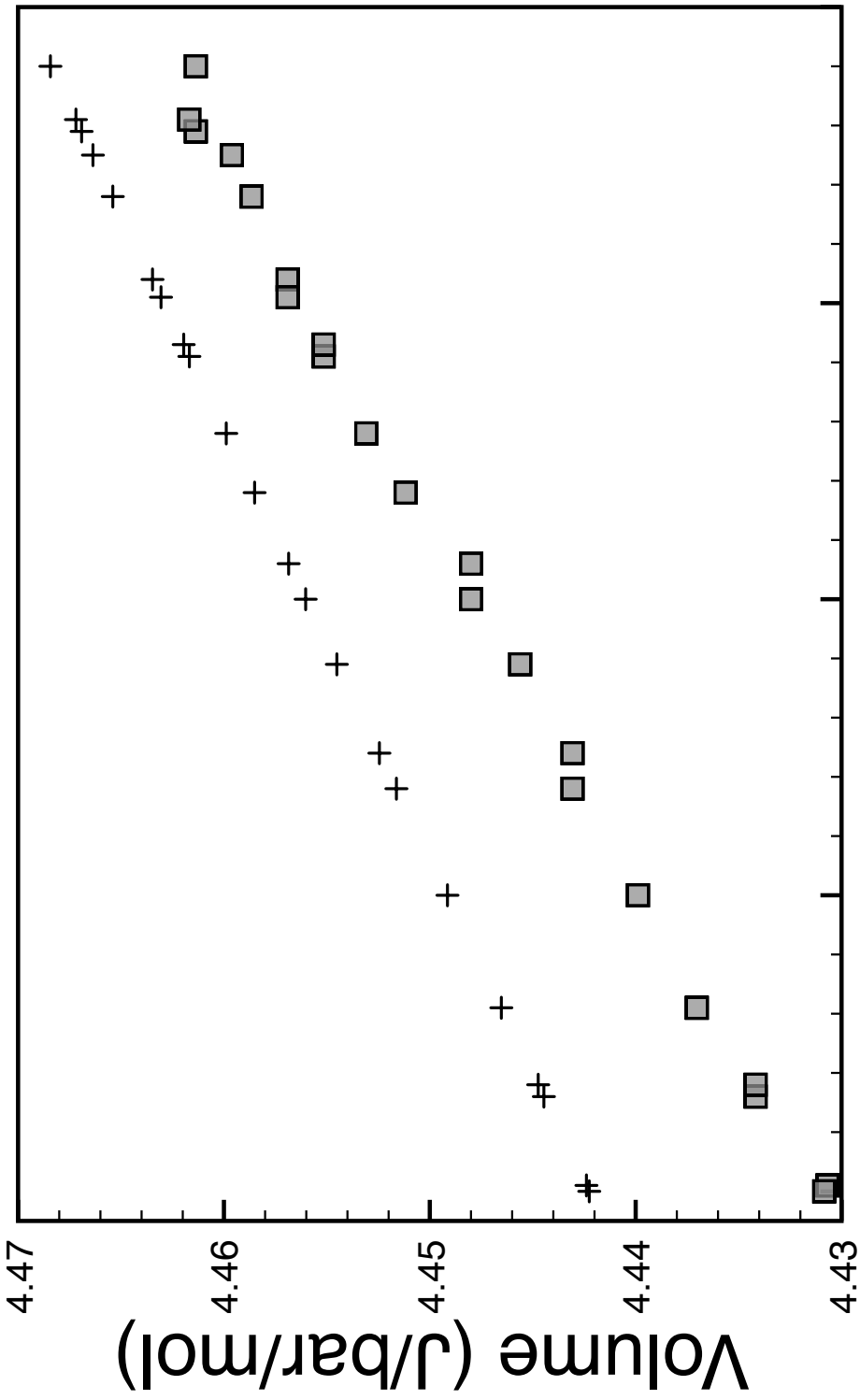

Fig. A3b

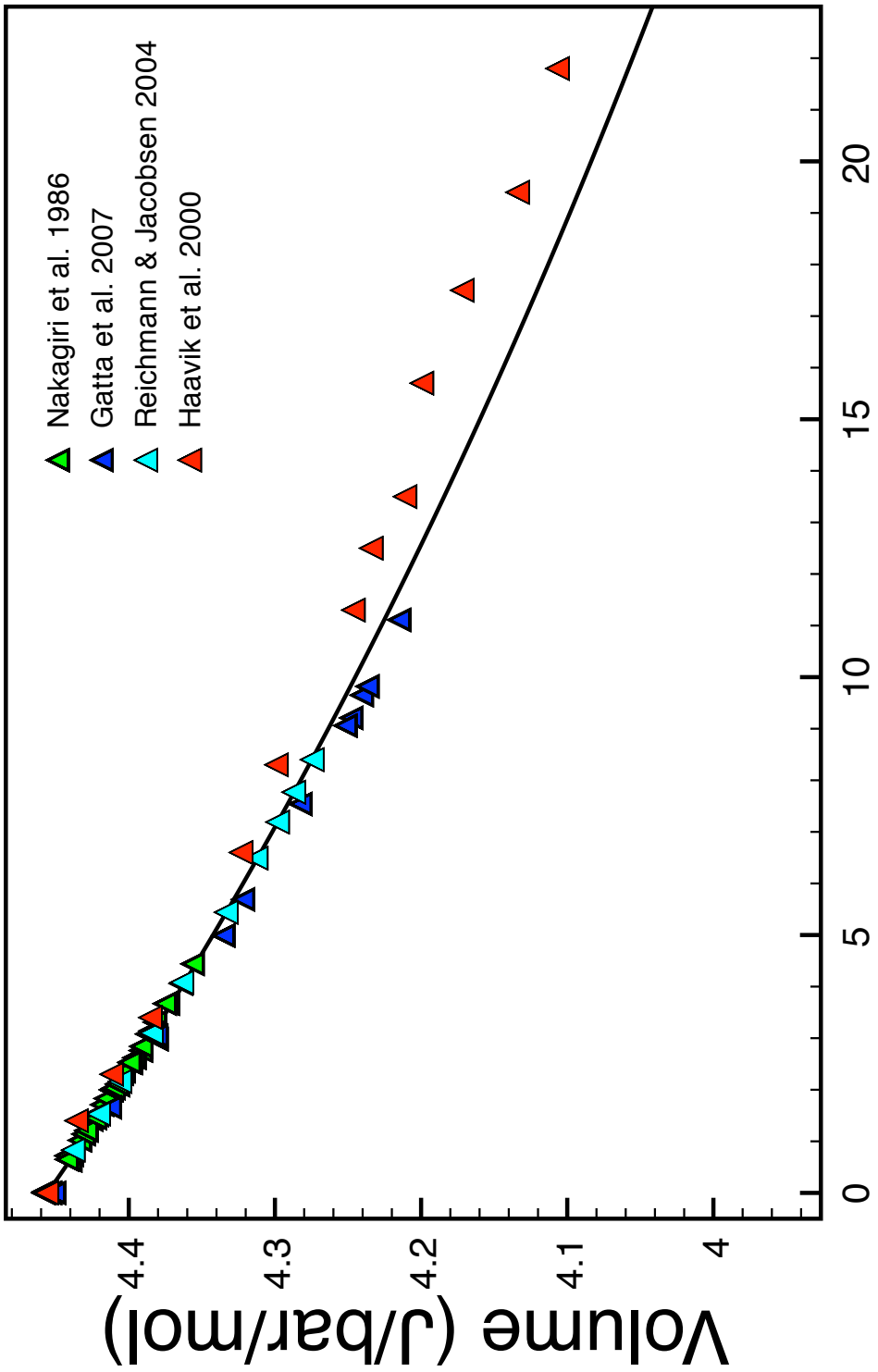
Nakagiri et al. 1986
Gatta et al. 2007
Reichmann & Jacobsen 2004
Haavik et al. 2000
Volume (J/bar/mol)
4
4.1
4.2
4.3
4.4
0
5
10
15
20
Pressure (GPa)

Fig. A4

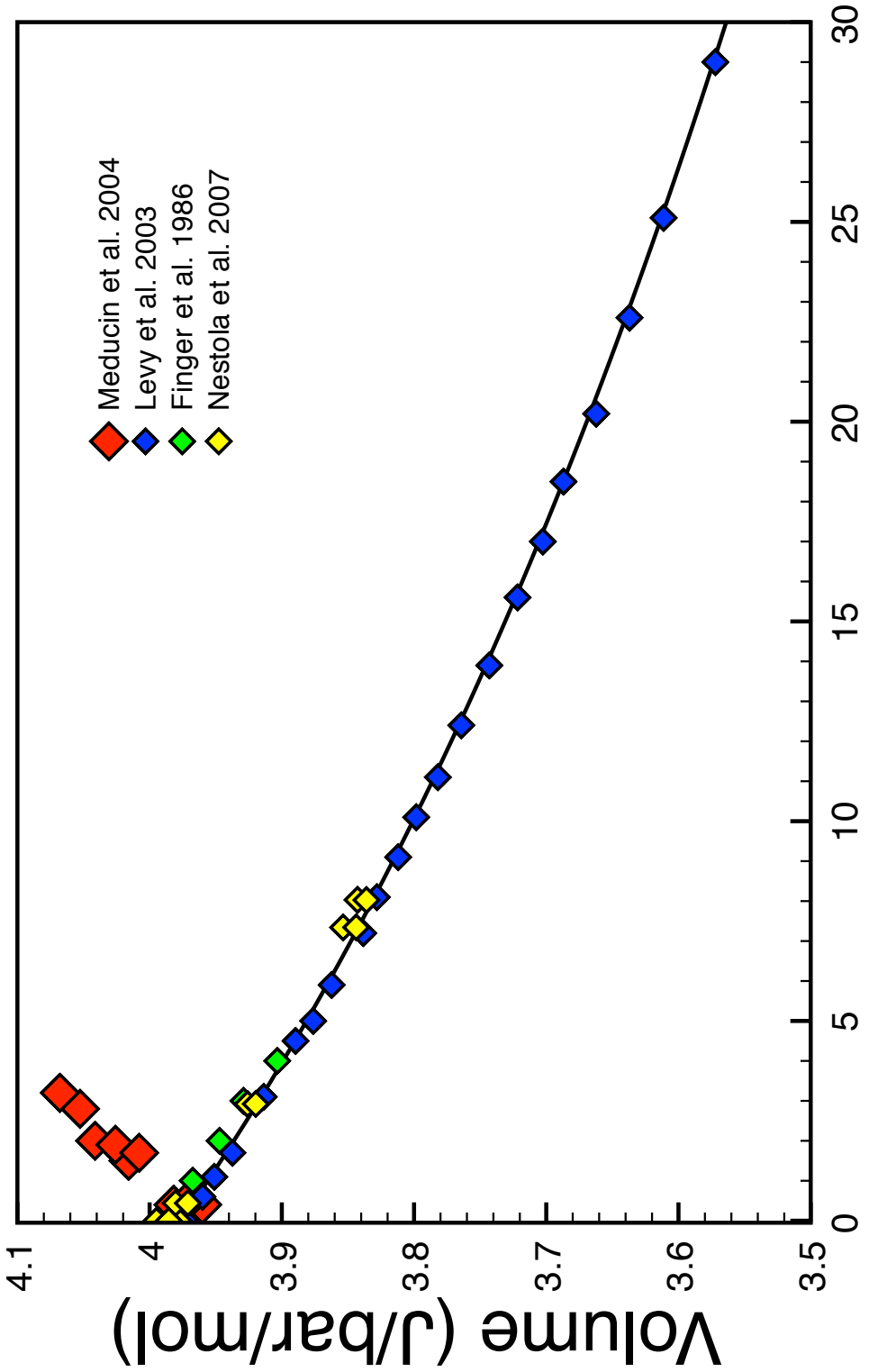
Meducin et al. 2004
Levy et al. 2003
Finger et al. 1986
Nestola et al. 2007
Volume (J/bar/mol)
Pressure (GPa)
4.1
4
3.9
3.8
3.7
3.6
3.5
0
5
10
15
20
25
30

Fig. A5a

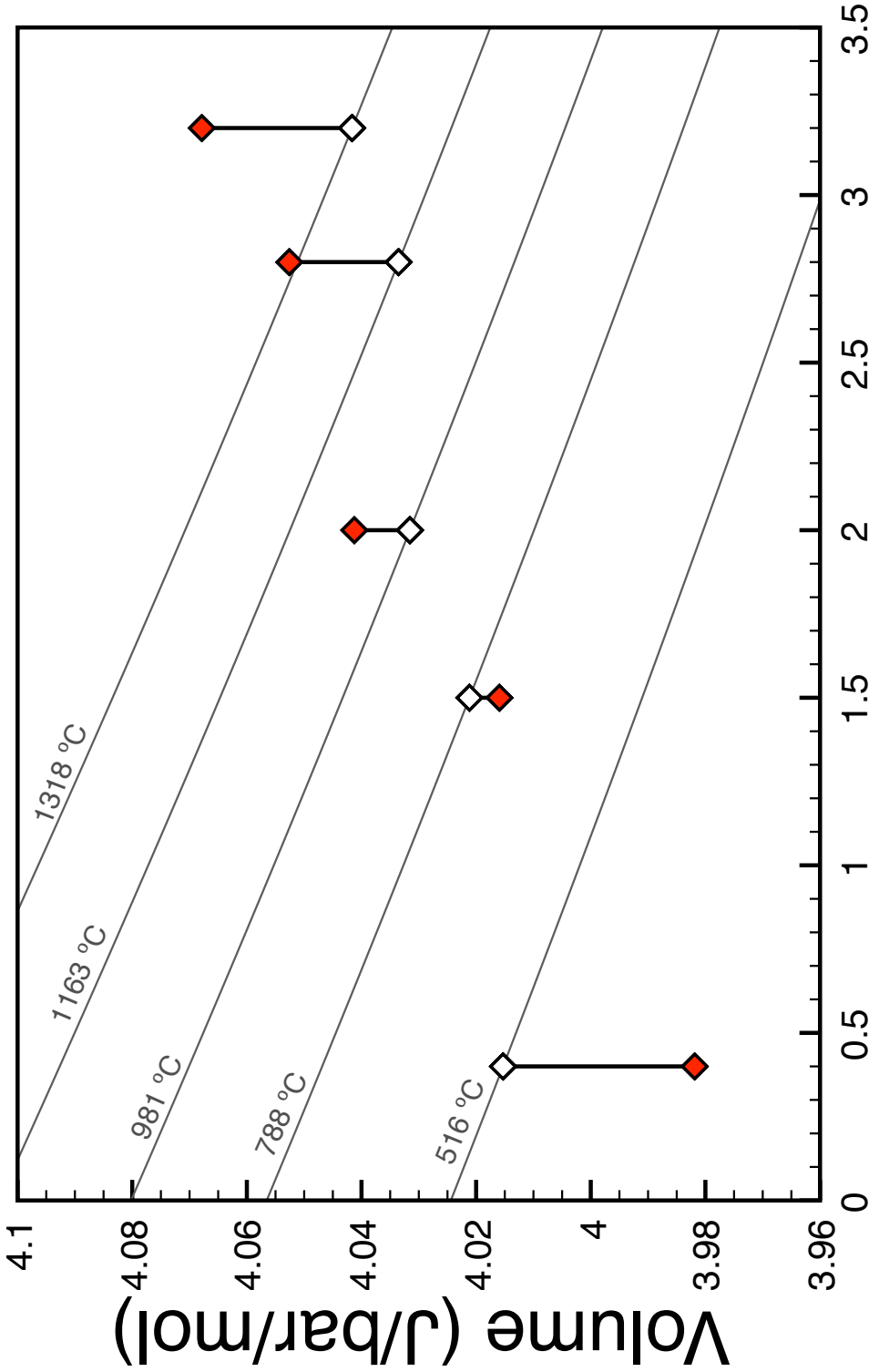
Volume (J/bar/mol)
4.1
4.08
4.06
4.04
4.02
4
3.98
3.96
0
0.5
1
1.5
2
2.5
3
3.5
Pressure (GPa)
1318 °C
1163 °C
981 °C
788 °C
516 °C

Fig. A5b

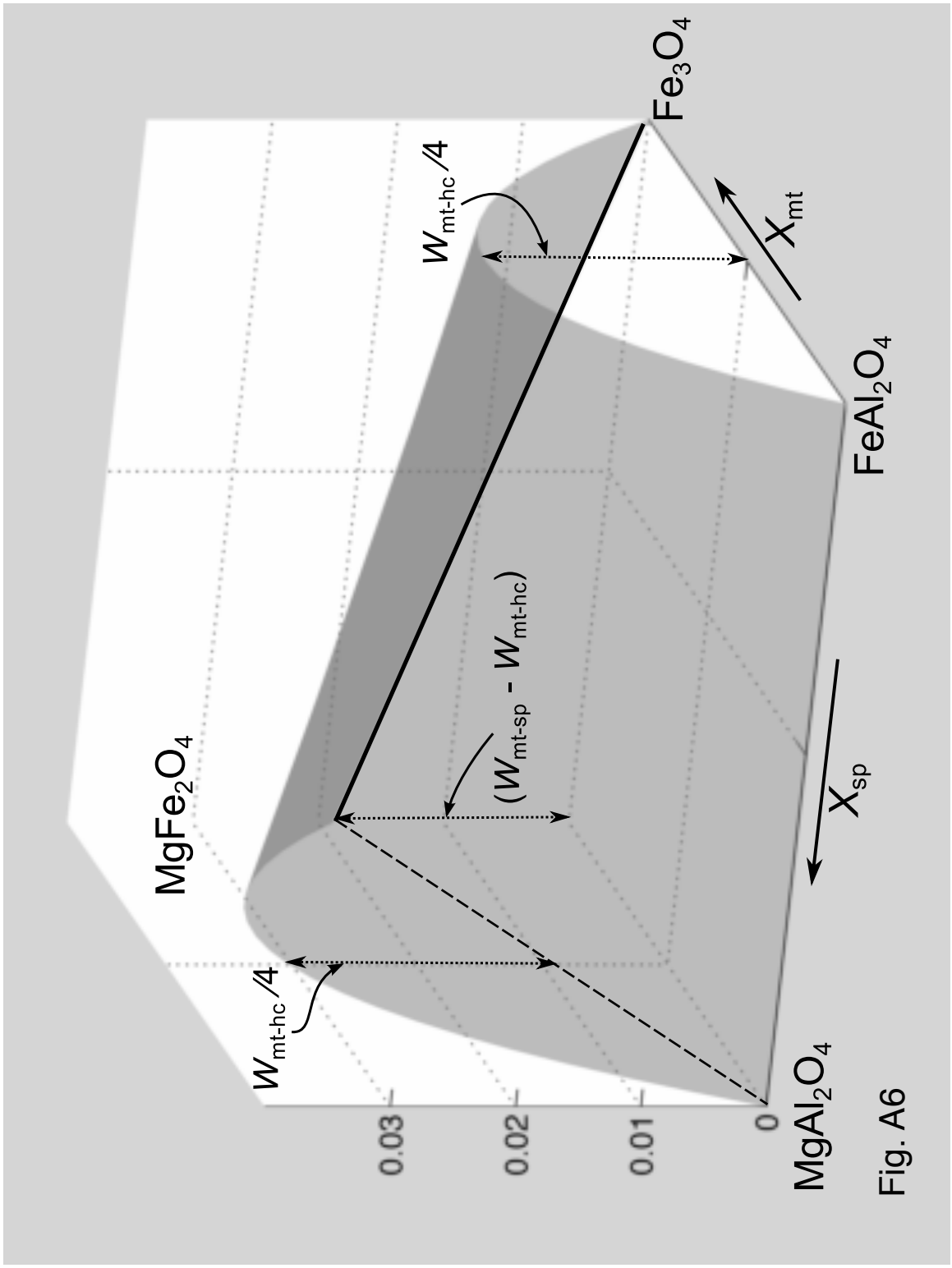
Fe_3O_4
$FeAl_2O_4$
$MgFe_2O_4$
$MgAl_2O_4$
$W_{mt\text{-}hc}/4$
$W_{mt\text{-}hc}/4$
$(W_{mt\text{-}sp} - W_{mt\text{-}hc})$
X_{mt}
X_{sp}
0.03
0.02
0.01
0

Fig. A6

Chapter 2

THE MOLAR VOLUME OF CUBIC GARNETS IN THE SYSTEM SiO_2-Al_2O_3-TiO_2-Fe_2O_3-Cr_2O_3-FeO-MnO-MgO-CaO-Na_2O

Emily A. Hamecher

Paula M. Antoshechkina

Mark S. Ghiorso

Paul D. Asimow

This chapter to be submitted to Contributions to Mineralogy and Petrology

ABSTRACT

We define and calibrate a new model of molar volume as a function of pressure, temperature, and composition for cubic garnets (space group *Ia*3*d*) in the oxide system listed in the title. We use 766 X-ray diffraction measurements performed on garnets at ambient and in situ high-*P*, *T* conditions to calibrate end-member equations of state and an excess volume model for this system. Optimal values of the bulk modulus and its pressure derivative are obtained by analyzing published compression and/or ultrasonic data for the end members for which such studies exist; for other end members, density functional theory results and systematics in cation radii are used. For any cubic garnet in this chemical system, the model molar volume is obtained by adding excess volume terms to a linear combination of nine independent end-member volumes. In the first step of our least squares fitting procedure we calculate volumes of the explicit end members as a function of *P* and *T* using the Vinet equation of state, with the Mie-Grüneisen-Debye thermal pressure formalism to model thermal expansion. For each dependent end member for which there are data, we calculate the volume of reaction for formation of the phase from the independent end members, ΔV. We then fit the binary and mixed composition data, using singular value analysis to ensure that the calibrated combinations of excess parameters obey the ΔV constraints from the first step. The preferred model has 19 excess volume parameters and fits nearly all experiments to within 0.06 J/bar/mol, or approximately 0.5% in volume. The implications our model has for the density of the lithospheric mantle are explored.

INTRODUCTION

Garnet-group minerals are important constituents of upper mantle and high-grade metamorphic crustal rocks. Garnets can accommodate a wide variety of cations, and form extensive solid solutions between end members. Garnets are also stable over a wide pressure range. These qualities, along with their abundance in the Earth's upper mantle, make them excellent indicators of the *P*- and *T*-conditions of crystallization. Because of this, the properties of garnets have been studied exhaustively (see Geiger 2008 for a recent review). However, there remains vast disagreement between different measurements of molar volume of the various garnet end members and their solid solutions.

Garnets have the general formula $X_3Y_2Z_3O_{12}$. Cations denoted by X are coordinated by eight nearest-neighbor oxygen atoms (dodecahedral coordination). The Y cations are octahedrally coordinated (six), and the Z cations are tetrahedrally coordinated (four) by oxygen. In cubic garnets (*Ia*3*d*), all sites of a given coordination are symmetrically equivalent, and the structure can be described as chains of octahedrally coordinated cations linked by non-sharing dodecahedral and tetrahedral polyhedra (Deer et al. 1997). Garnet is a critical phase that controls major and trace element partitioning at pressures above ~3 GPa during partial melting of the upper mantle. Any useful thermodynamic model of mantle phase equilibria must include a treatment of garnet that affords accurate prediction of garnet stability with respect to spinel, pyroxene, and melt.

Molar volume is an important thermodynamic quantity at high pressures, both when using garnets to infer petrogenetic information from high-pressure rocks and particularly when using garnets from high-pressure experiments to define chemical

potentials in coexisting phases. A model of garnet volumes with the necessary accuracy needs to account not only for equations of state of pure end members, but also to take into account considerable deviation from ideal mixing of compositions along some binary joins. Generally, studies are restricted to subsystems of garnets, e.g., along a solid solution binary. While limiting the system of interest usually allows one to recover the data used in calibration, discrepancies that exist between various end-member and solid solution data sets and currently available models are inadequate for modeling of volumes over the full compositional range of garnets formed in the Earth's upper mantle. This is especially true for pressures above ~15 GPa, where majoritic garnet becomes a major constituent of the mantle phase assemblage. It is necessary to devise a comprehensive model applicable to the entire chemical system of the upper mantle.

In this work, we present a model of molar volumes of stoichiometric garnets containing the oxide components SiO_2-Al_2O_3-TiO_2-Fe_2O_3-Cr_2O_3-FeO-MnO-MgO-CaO-Na_2O. Our model system contains nine independent end members. The end-member compositions, designations, and abbreviations used in this paper are given in Table 1. Our primary motivation in this work is to develop a comprehensive garnet molar volume model for use in calibration of activity-composition models of garnet and pyroxene solid solutions. The thermodynamic models, along with a new silicate liquid equation of state (Ghiorso 2004a, 2004b, 2004c; Ghiorso and Kress 2004) and a new model of molar volume for spinel (Hamecher et al. 2013), will be incorporated into the next generation MELTS (Ghiorso and Sack 1995; Ghiorso et al. 2002; Asimow et al. 2004) model, xMELTS (Ghiorso et al. 2007). The new solid solution models will include some minor

components, including Ti, Na, and Cr. The new garnet and spinel molar volume models will enable coupled recalibration of the garnet and pyroxene thermodynamic models.

In this chapter, we first discuss previous determinations of garnet end-member properties and previous models of garnet molar volume, with attention to the ranges of compositions they cover and inconsistencies among data and models. We then present the X-ray diffraction data used in our calibration, and the formulation of our model in terms of the components in Table 1. The calibration strategy we used to estimate the parameters of the model and assess goodness of fit to the data is outlined. Finally, we compare the final model to some models from the literature and present a test of the effect of our new volume models on density of mantle rocks extracted from three different thermodynamic models.

PREVIOUS WORK ON GARNET VOLUME

A considerable amount of work has been done in deriving the physical properties of end-member garnets, mostly among the aluminosilicate garnets. Comparatively fewer studies have examined garnets containing Cr, Ti, Na, or a majoritic component. However, even in the heavily sampled regions of garnet composition space, the various published determinations of standard state properties for end members are inconsistent with one another. Considering not only end-member properties but also mixing in solid solutions, numerous models for the molar volume of garnet solutions have been proposed, but most are restricted to single compositional binaries, and there are many discrepancies among the models that do exist. In this section we discuss previous determinations of end-

member volumetric properties and examples of previous volume of mixing models for garnets.

Of the end-member garnets, the aluminosilicate garnets (grossular, pyrope, almandine, and spessartine) and their solid solutions have received by far the most attention. There have been numerous determinations of the cell parameter, *a*, for these garnets over the past 50+ years, but still uncertainty persists regarding their correct values (e.g., Abrahams and Geller 1958; Boyd and England 1959; Gibbs and Smith 1965; Novak and Gibbs 1971; Geiger et al. 1992; Geiger and Armbruster 1997). Thermal expansion for the aluminosilicate garnets and their solid solutions have been determined by Skinner (1956), Meagher (1975), Geiger et al. (1992), Pavese et al. (1995), Artioli et al. (1997), Thieblot et al. (1998), and Rodehorst et al. (2002).

The bulk moduli (K_{oT}) for the aluminosilicate garnets have been determined by ultrasonic, Brillouin spectroscopic, and static compression X-ray diffraction methods. There is much disagreement between values determined by the different methods (e.g., Takahashi and Liu 1970; Weaver et al. 1976; Bonczar et al. 1977; Babuska et al. 1978; Sato et al. 1978; Levien et al. 1979; Leitner et al. 1980; Bass 1989; Webb 1989; Leger et al. 1990; Olijnyk et al. 1991; Hazen et al. 1994; Zhang et al. 1998; 1999). We discuss our strategy to constrain the bulk moduli, and their pressure derivatives, in the Model Calibration section below.

There is much less data, if any, available for the rest of our chosen independent set of end members. There are published lattice parameters for garnets synthesized along the pyrope-knorringite binary (Ringwood 1977). Information about the compressibility of uvarovite is reported in Bass (1986) and Leger et al. (1990). Data for Fe^{3+}-bearing garnets

are available from Bass (1986), Hazen and Finger (1989), Armbruster and Geiger (1993), Woodland and O'Neill (1993), Woodland and Ross (1994), Zhang et al. (1999), Jiang et al. (2004), Pavese et al. (2001), and Woodland et al. (2009). Ringwood and Major (1971) synthesized and measured the lattice parameters of some high-pressure Ti- and Na-bearing garnets, as well as a synthetic sample of cubic majorite. Armbruster et al. (1998) determined cell parameters for natural Ti-bearing andradites. Properties of cubic majorite garnets are given in Bass and Kanzaki (1990), Yeganeh-Haeri et al. (1990), Pacalo et al. (1992), Hazen et al. (1994), and Wang et al. (1998).

The current molar volume model for garnets in MELTS and pMELTS is applicable only in the ternary grossular-pyrope-almandine system. The model adopts the Berman (1990) symmetric excess volume model along the grossular-pyrope join and asymmetric model for the grossular-almandine and pyrope-almandine binaries. Terms involving spessartine are not included in the current MELTS models. Geiger (2000) also models the Ca-Mg-Fe-Mn aluminosilicate system. Pyrope-almandine is modeled with ideal volume of mixing, and all other binaries are modeled with slightly positive, symmetric excess volume parameters. Bosenick et al. (2001; see table 1) fit experimental data along all six binaries in this garnet subsystem with positive symmetric volume mixing terms. However, there is little agreement in the literature on the excess volume along the grossular-pyrope join (e.g., Newton et al. 1977; Haselton and Newton 1980; Wood 1988; Koziol and Newton 1989; Berman 1990; Berman and Aranovich 1996; Du 2012). Bosenick et al. (2001) fit experimental data on this binary with a symmetric excess volume term, though the original authors (Ganguly et al. 1993; Bosenick and Geiger 1997) fit their respective data with asymmetric terms. Figure 1 shows the various models

that have been proposed for the grossular-pyrope binary. The asymmetric models agree in the sense that the larger excess volumes exist at the grossular-rich end of the binary, but the magnitudes of the excess volume models are quite different. Du (2012) suggests that the large variability in shape and magnitude of excess volume at room temperature along the grossular-pyrope join could be due to differences in the way in which the samples were synthesized (e.g., piston cylinder versus multi-anvil).

Ungaretti et al. (1995) model excess volume of ternary grossular-pyrope-almandine garnets, using data along the grossular-pyrope (discussed in previous paragraph), grossular-almandine (Cressey et al. 1978; Perkins 1979; Geiger et al. 1987; Koziol 1990), and almandine-pyrope (Armbruster et al. 1992; Geiger and Feenstra 1997) binary joins. Mukhopadhyay et al. (1997) also modeled mixing properties in the Ca-Mg-Fe^{2+} ternary using the data of Newton et al. (1977), Wood (1988), Ganguly et al. (1993), Hackler and Wood (1989), and Koziol (1990), but excluded the data of Cressey et al. (1978), based on the observation by Berman (1990), who also modeled this ternary system, that the other data show no evidence for negative volume of mixing along the grossular-almandine join. Other binary models exist for grossular-almandine (Berman 1990; Geiger et al. 1989), pyrope-almandine (Berman 1990), spessartine-grossular (Rodehorst et al. 2002), spessartine-almandine (Geiger and Feenstra 1997), almandine-skiagite, and andradite-skiagite (Woodland and Ross 1994).

DATA SOURCES

The sources of garnet volume data used in model calibration are given in Supplementary Material 1. The American Mineralogist Crystal Structure Database (AMCSD) (Downs

and Hall-Wallace 2003) provides a collection of published X-ray diffraction refinements of cell volume and site occupancy; we fit all included garnets with *Ia*3*d* space group symmetry in the system SiO_2-Al_2O_3-TiO_2-Fe_2O_3-Cr_2O_3-FeO-MnO-MgO-CaO-Na_2O. Additionally, we culled volume determinations for applicable garnet compositions from the literature. Other garnets in the AMCSD and other sources—e.g., hydrogarnets, tetragonal garnets, garnets with cations other than Si in the tetrahedral site—were excluded.

Our final model is calibrated using a total of 766 experiments. The compositional and *P*-*T* coverage of the data is summarized in Table 2. Experimental conditions, observed cell parameters, and composition are given in Supplementary Material 2. The majority of the solid solution data is clustered in the grossular-pyrope-almandine ternary system.

To limit the data used to fit the model to those garnets that are most applicable to the upper mantle, we developed a set of exclusion criteria. All garnets that contained vacancies were excluded. We rejected experiments that contained greater than 5% occupancy by Mn^{3+} and greater than 0.5% occupancy of Sc^{3+} on any crystallographic site. In order that the composition of all calibrated garnets conform to the stoichiometry of the chosen model end members, within a reasonable tolerance, we filtered out any site occupancy data with reported site totals differing from unity by more than ±0.01 and any data with total cation charge greater than +24.08 or less than +23.92 per formula unit.

One downside to the chosen data set is lack of reliable error estimates for observed volume and composition, which makes it difficult to weight the calibration data in any meaningful way. While many of the unit cell determinations do include error

bounds, there is no way to estimate errors in site occupancy, particularly since many of the garnet compositions reported this way are assumed to have ideal stoichiometry. Only a subset of the compositions determined by electron microprobe analysis includes errors. Given that it was impossible to come up with an automated strategy for assigning errors, we used unweighted nonlinear least squares, where all data were assigned the same nominal error.

MODEL FORMULATION

For fitting molar volume data to our model, the data must first be recast in a consistent manner into the representation of composition we adopted. The compositions of the data are reported in one of two ways: (a) cation mole fraction on each of the crystallographic sites or (b) weight percent of the oxides. For site occupancy data, we first transformed the molar cation proportions into the following set of linearly independent variables:

$$r_0 = {}^{[6]}\mathrm{Al} - {}^{[8]}\mathrm{Ca} - {}^{[8]}\mathrm{Fe}^{2+} - \left(\frac{2}{3}\right){}^{[6]}\mathrm{Fe}^{2+} - {}^{[8]}\mathrm{Mn} - \left(\frac{2}{3}\right){}^{[6]}\mathrm{Mn} \quad (1)$$

$$r_1 = {}^{[8]}\mathrm{Fe}^{2+} + \left(\frac{2}{3}\right){}^{[6]}\mathrm{Fe}^{2+} \quad (2)$$

$$r_2 = {}^{[6]}\mathrm{Cr} \quad (3)$$

$$r_3 = 2\,{}^{[6]}\mathrm{Si} - 3\,{}^{[8]}\mathrm{Na} \quad (4)$$

$$r_4 = {}^{[6]}\mathrm{Fe}^{3+} \quad (5)$$

$$r_5 = \left(\frac{3}{2}\right){}^{[8]}\mathrm{Na} \quad (6)$$

$$r_6 = 2\,{}^{[6]}\mathrm{Ti} \quad (7)$$

$$r_7 = {}^{[8]}\mathrm{Mn} + \left(\frac{2}{3}\right){}^{[6]}\mathrm{Mn}\ , \tag{8}$$

where superscript [8] indicates the dodecahedrally coordinated cation and [6] indicates the octahedrally coordinated cation. Then, we obtained the set of end-member component molar proportions by:

$$X_{\mathrm{grs}} = 1 - r_0 - r_1 - r_2 - r_3 - r_4 - r_5 - r_6 - r_7 \tag{9}$$

$$X_{\mathrm{pyr}} = r_0 \tag{10}$$

$$X_{\mathrm{alm}} = r_1 \tag{11}$$

$$X_{\mathrm{knr}} = r_2 \tag{12}$$

$$X_{\mathrm{maj}} = r_3 \tag{13}$$

$$X_{\mathrm{kho}} = r_4 \tag{14}$$

$$X_{\mathrm{nag}} = r_5 \tag{15}$$

$$X_{\mathrm{mmr}} = r_6 \tag{16}$$

$$X_{\mathrm{sps}} = r_7\ . \tag{17}$$

For compositional data reported in oxide weight percent, we first calculated the number of moles of cations per formula unit, then calculated moles of end-member components (given here by *m*):

$$m_{\mathrm{grs}} = \frac{\text{mols Ca}}{3} \tag{18}$$

$$m_{\mathrm{pyr}} = \frac{\text{mols Al}}{2} - \frac{\text{mols Ca}}{3} - \frac{\text{mols Fe}^{2+}}{3} - \frac{\text{mols Mn}}{3} \tag{19}$$

$$m_{\mathrm{alm}} = \frac{\text{mols Fe}^{2+}}{3} \tag{20}$$

$$m_{\mathrm{knr}} = \frac{\text{mols Cr}}{2} \tag{21}$$

$$m_{\mathrm{maj}} = \frac{\text{mols Mg}}{4} - 3\frac{\text{mols Fe}^{3+}}{8} - \text{mols Ti} - 3\frac{\text{mols Cr}}{8} - \frac{\text{mols Na}}{8} - 3\frac{\text{mols Al}}{8} + \frac{\text{mols Ca}}{4} + \frac{\text{mols Fe}^{2+}}{4} + \frac{\text{mols Mn}}{4} \tag{22}$$

$$m_{\mathrm{kho}} = \frac{\text{mols Fe}^{3+}}{2} \tag{23}$$

$$m_{\mathrm{nag}} = \frac{\text{mols Na}}{2} \tag{24}$$

$$m_{\mathrm{mmr}} = \text{mols Ti} \tag{25}$$

$$m_{\mathrm{sps}} = \frac{\text{mols Mn}}{3} \tag{26}$$

.

Once the moles of components have been calculated, it is then trivial to compute the set of end-member component molar proportions.

The general expression for the molar volume of a crystalline solid is $V = V_{\mathrm{ideal}} + V_{\mathrm{excess}}$, where excess volume of mixing is determined by an appropriate mixing model. The expression for V_{ideal} as a function of pressure, temperature, and composition is

$$V_{\mathrm{ideal}} = \sum_i X_i V_i(P, T) \tag{27}$$

,

where i = [grs, pyr, alm, knr, maj, kho, nag, mmr, sps]. $V_i(P, T)$ is found by using Newton's method to search along the Vinet equation of state, plus a term to account for thermal pressure:

$$P = 3K_{\mathrm{oT},i}\left(\frac{V_i}{V_{\mathrm{o},i}}\right)^{-2/3}\left[1-\left(\frac{V_i}{V_{\mathrm{o},i}}\right)^{1/3}\right]\exp\left\{\frac{3}{2}\left(K_i'-1\right)\left[1-\left(\frac{V_i}{V_{\mathrm{o},i}}\right)^{1/3}\right]\right\} + P_{thermal} \tag{28}$$

,

where V_o is molar volume at reference pressure P_o = 1 bar and reference temperature T_o = 298.15 K, K_{oT} is the isothermal bulk modulus, and K' is the pressure derivative of the bulk modulus. In our spinel molar volume model (Hamecher et al. 2013) we used a thermal pressure term with a constant coefficient of thermal expansion, α, $P_{thermal} = \alpha_i K_{oT,i}(T - T_o)$. However, during model calibration of in situ high-T garnet volume data, it became clear that this formalism is not sufficient to explain the thermal expansion of the garnets in our system (Fig. 2). Instead, we adopt the Mie-Grüneisen-Debye thermal pressure formalism (Luo et al. 2003):

$$P_{thermal} = \frac{\gamma_i C_{vm,i}}{V_i}\left[TD\left(\frac{\theta}{T}\right) - T_o D\left(\frac{\theta_{o,i}}{T_o}\right)\right], \tag{29}$$

where

$$D(x) = \frac{3}{x^3}\int_0^x \frac{y^3 dy}{e^y - 1}, \tag{30}$$

$$\theta = \theta_o \exp\left[-\int_{V_o}^{V} \frac{\gamma}{v} dv\right], \tag{31}$$

and γ is the T-independent Grüneisen parameter, C_{vm} is the high-temperature limit of isochoric specific heat (close to the Dulong-Petit value of $3nR$), θ_o is the reference Debye temperature, and $D(x)$ is the Debye function. A common expression for γ is

$$\frac{\gamma}{\gamma_o} = \left(\frac{V}{V_o}\right)^q, \tag{32}$$

where q is the logarithmic volume dependence of γ and γ_o is the Grüneisen parameter at the reference volume. The conversion between isochoric specific heat and isobaric specific heat (and, thus, thermal expansion) is given by

$$\frac{C_p}{C_V} = 1 + \alpha\gamma T \quad (33)$$

,

where α is the coefficient of thermal expansion, $\frac{1}{V}\frac{\partial V}{\partial T}\Big|_P$. We used the approximation of Masyukov and Dmitriev (2007) to compute the Debye function, which returns the same values as numerical integration, but significantly reduces computing time. Values and sources of the standard state end-member properties (V_o, K_{oT}, K', γ_o, C_{vm}, θ_o, q) used in the volume model calibration are discussed in the following section.

During model calibration, we considered excess volume terms of the symmetric regular solution form $W_{ij}X_iX_j$ and asymmetric regular solution form $W_{ij}X_iX_j + dW_{ij}X_iX_j(X_i - X_j)$. We considered the possibility of allowing terms to depend on P and T as a way to encode non-ideal mixing of compressibility or thermal expansion, but ultimately determined that such P- and T-dependent parameters were not justified by the data. Calibration and significance of excess volume parameters are discussed below.

MODEL CALIBRATION

Because of the different types of data and chemical complexity of our system, the volume model calibration required a multi-step approach. First, we needed to determine the standard state end-member properties discussed in the previous section for each of our independent end members. Since data do not exist for all of our chosen end members, different methods were used to determine these properties based on the information available. The first step of our global fitting routine fits all end-member data, at ambient and high-P or -T conditions, while also obtaining constraints from dependent end

members for fitting the excess volume. We then moved on to calibrating the mixing properties for the binary joins between both the independent end members and the three dependent end members for which there are data (andradite, uvarovite, and skiagite). In this section, we first discuss the determinations of the standard state properties for the end members, and then discuss our strategy for calibrating the excess volume model.

End-member standard state properties

K_{oT} and K'

Because there is so much disagreement in the literature with regards to the bulk modulus (e.g., between static compression and ultrasonic studies), we needed to come up with a way to use the high-*P* data to constrain K_{oT} and *K*' for the independent end members. In some cases, we had to use dependent end-member data to constrain the behavior of the independent end members, due to the availability, or lack thereof, of data for some compositions, e.g., we needed to use andradite data to constrain the khoharite end-member properties. For the end members that have in situ high-*P* data (i.e., grossular, pyrope, almandine, spessartine, and dependent end member andradite), we normalized each XRD study to its own reported V_o. This eliminates interlaboratory calibration differences and small specimen composition differences, focuses as well as possible on the actual thermal expansion and compression, and should be most comparable to ultrasonic or other elasticity measurements. We then performed a least squares minimization to determine the optimal values of the bulk modulus and its pressure derivative for these compositions. Values of K_{oT} and *K*' are given in Table 3.

Zhang et al. (1998; 1999) performed in situ high-*P* XRD on single crystals of all five of the high-*P* compositions listed above. We also included the high-*P* data of Olijnyk et al. (1991) and Pavese et al. (2001) in fitting K_{oT} and *K*' for grossular. Our value for the bulk modulus of grossular, K_{oT} = 168.0 GPa, agrees well with previous ultrasonic (Babuska et al. 1978) and Brillouin spectroscopy (Bass 1989) single crystal measurements. The fit value of *K*' = 6.1 also compares well with determinations by Olijnyk et al. (1991) and Pavese et al. (2001).

We used the compression data of Levien et al. (1979) in addition to Zhang et al. (1998) to fit K_{oT} and *K*' of pyrope. There have been several studies on pyrope (see table 4 in Zhang et al. 1998). Previously determined values for K_{oT} vary from 168.2 to 190 GPa with *K*' values from 1.8 to 5.45. Our fit of the high-*P* diffraction data yielded K_{oT} = 168.3 GPa and *K*' = 4.8. Almandine and spessartine K_{oT} and *K*' were fit over the data of Zhang et al. (1999). Our K_{oT} and *K*' values for almandine compare well with theirs, and our chosen values for spessartine are consistent with their values given without constraining the value of *K*' (Zhang et al. 1999; table 3).

There are no high-*P* data for khoharite, so we used the compression data of Zhang et al. (1999) and Pavese et al. (2001) for andradite to constrain K_{oT} and *K*' for the ferric iron end member. We ended up adopting the Pavese et al. (2001) andradite value for the bulk modulus of khoharite, K_{oT} = 158.5 GPa, and then adjusted *K*' down to a best fitting value of 4.7, which allowed us to better fit both the Zhang et al. (1999) and the Pavese et al. (2001) data. These values also agree well with the density functional theory (DFT) results of Milman et al. (2001) for khoharite. They calculated that K_{oT} = 163 GPa and *K*' = 4.4 for khoharite.

Similarly, high-*P* data for knorringite does not exist, so we used data for another Cr-bearing garnet end member, uvarovite. Bass (1986) measured the elastic properties of a single crystal of synthetic uvarovite using Brillouin spectroscopy. Leger et al. (1990) used the Bass (1986) value for the bulk modulus, $K_{oT} = 162$ to fit $K' = 4.7$ with the Birch-Murnaghan equation of state. We have adopted these values for the knorringite end member. Our chosen values fall between calculated values reported by Ottonello et al. (1996) and Milman et al. (2001).

There is no high-*P* data on pure samples of the three remaining independent end members—cubic majorite, Na-garnet, and Mg-Mg-morimotoite. For majorite we used the values recommended by Saxena (1996) and Fabrichnaya et al. (2004). Hazen et al. (1994) determined K_{oT} of a synthetic garnet with the formula $(Na_{1.88}Mg_{0.12})(Mg_{0.06}Si_{1.94})Si_3O_{12}$ to be 191.5 GPa, assuming $K' = 4$; we have adopted these values for the Na-garnet end member. We performed a DFT calculation of the Ti-bearing end member, Mg-Mg-morimotoite. DFT calculations were also performed for grossular, pyrope, and majorite. To account for the systematic errors that typically occur in volume and bulk modulus estimates from DFT calculations with the LDA functional, we took the ratios of our preferred bulk moduli (from Table 3) to the DFT-determined bulk moduli for grossular, pyrope, and majorite. We then refined the estimate of K_{oT} for Mg-Mg-morimotoite by scaling the DFT result by the average of the ratios for the other three end members. Comparing the DFT results for grossular, pyrope, and majorite with independent estimates suggests that K_{oT} is overestimated by the DFT calculation (and V_o slightly underestimated). K_{oT} is plotted as a function of R_x/R_y, where R_x is the ionic radius of the x-site cation and R_y is the ionic radius of the y-site cation, for each end member in Fig. 3.

Systematic trends in K_{oT} versus cation size are evident among Ca-rich garnets (grs, uvr, and), Al-rich garnets (alm, sps, grs), and Mg-rich garnets (pyr, knr, kho, maj, mmr).

Thermal pressure parameters (θ_o, γ_o, C_{vm}, q)

In order to calibrate the parameters for the Mie-Grüneisen-Debye thermal pressure term, we again were forced to appeal to different methods depending on the data available for the end members. After some trial-and-error, we set $q = 1.5$ for all end members, which is within the typical range of values reported for garnets (Stixrude and Lithgow-Bertelloni 2005). We then turned to fitting the three remaining parameters—θ_o, γ_o, and C_{vm}. Our preferred set of parameters are given in Table 3.

Skinner (1956) measured thermal expansion for four of our chosen independent end members: grossular, pyrope, almandine, and spessartine. We used these along with additional high-T data for grossular (Thieblot et al. 1998; Rodehorst et al. 2002), pyrope (Meagher 1975; Pavese et al. 1995), almandine (Geiger et al. 1992), and spessartine (Rodehorst et al. 2002) to tune the θ_o, γ_o, and C_{vm} parameters. We found that while volume, V, and heat capacity, C_p, both depend on θ_o, γ_o, and C_{vm}, γ_o is better constrained by fitting V, but θ_o and C_{vm} are better constrained by fitting C_p. We iterated between fitting γ_o to the thermal expansion data, then fitting θ_o and C_{vm} to the C_p expression of Berman (1988) over the relevant temperature range, until we converged on a best-fitting set of parameters for each of these end members.

To calibrate the parameters for khoharite, we again had to look to andradite data, as there are no high-T data for the independent Fe^{3+}-bearing end member. We performed the same type of iterations as above using high-T andradite volume data of Skinner

(1956) and the C_p expression from Ottonello et al. (1996); Berman (1988) does not include andradite. We iteratively fit both the C_p and α expressions of Ottonello et al. (1996) for khoharite, which yielded a similar set of parameters as the andradite fit. Ottonello et al. (1996) also gives values for C_p and α for knorringite and uvarovite, and fitting over both expressions gives similar values of parameters for the Cr-bearing end members as well. For majorite, we set $C_{vm} = 3nR$ and $\theta_o = 980$ K, then used systematics to estimate the values for Mg-Mg-morimotoite (Figs. 4 and 5). We set the values of θ_o and C_{vm} for Na-garnet equal to those of majorite and γ_o to unity, for convenience, as there is no data available to constrain the parameters for that end member.

V_o

For end members with good constraints on V_o from the data set (i.e., grossular, pyrope, almandine, knorringite (via uvarovite), and spessartine), we allowed standard state volumes to vary during the first step of our global least squares fitting routine, discussed below. Khoharite was also fit during that step using an intermediate Fe^{3+}-bearing composition to constrain the value; details are given in the next section. Majorite was fixed to the value given by Fabrichnaya et al. (2004), Na-garnet was fixed to the value determined by Hazen et al. (1994) for a Na-bearing garnet with the formula $(Na_{1.88}Mg_{0.12})(Mg_{0.06}Si_{1.94})Si_3O_{12}$, and Mg-Mg-morimotoite was fixed to a value determined by our DFT calculation, refined in the same way as K_{oT} for this end member, as described above. Values of V_o are given in Table 3 and shown plotted in Fig. 6. Novak and Gibbs (1971) noted the same variations of V_o with cation radii shown for the "ugrandite" and "pyralspite" garnet series.

Volume model calibration

End members

Our computational scheme for model calibration using our full data set is detailed in Hamecher et al. (2013). During the first step of least squares fitting we allowed the end-member V_o to adjust for the five end members listed in the previous section. For each dependent end member for which there are data (andradite, uvarovite, and skiagite), we calculated the volume of reaction for formation of the phase from the independent end members, ΔV (e.g., $\Delta V_{and} = V_{grs} - V_{pyr} + V_{kho}$), to be used as constraints as described below. There is only one data point in the database for dependent end member calderite, $Mn_3Fe_2Si_3O_{12}$ (Nishizawa et al. 1977). We set $\Delta V_{calderite}$ to zero (N.B., $\Delta V_{calderite} = V_{kho} + V_{sps} - V_{pyr}$), which helped constrain V_o of khoharite and improved the fit of the end-member andradite data.

Excess volume

We fit the binary and mixed composition data using the method of singular value analysis (SVA) of Lawson and Hanson (1974) to solve the least squares problem. Briefly, we use the ΔV constraints from the first step to constrain which combinations of excess parameters, i.e., the Ws and dWs, can be varied without affecting the constrained values. The Ws are assembled into a matrix and an eigenvector-eigenvalue decomposition is performed on the matrix. The eigenvalues with non-zero values correspond to the set of constrained values. Eigenvectors associated with zero eigenvalues define the linear combination of Ws that are orthogonal to the constraint set. We can vary this set of linear

combinations without affecting the constrained values. Detailed descriptions of solving least squares problems with eigenvector-eigenvalue decomposition and SVA can be found in Lawson and Hanson (1974) and Press et al. (2007).

The SVA yields a starting set of parameters to vary. We then used a combination of the Bayesian information criteria (BIC) (Schwarz 1978; Hamecher et al. 2013), analysis of the reduced χ^2 statistic, and visual inspection of excess volume data and models along binary joins to reduce our number of parameters to a minimum set (Table 4). Data and models along select binary joins are shown in Fig. 7.

In the final model, each of the nine explicit end members has a pure component equation of state described by seven parameters: V_o, K_{oT}, K', θ_o, γ_o, C_{vm}, q (Table 3). The additional parameters of the preferred final model include symmetric excess terms ($W_{ij}X_iX_j$) along nine compositional binaries and asymmetric terms ($W_{ij}X_iX_j + dW_{ij}X_iX_j(X_i - X_j)$) along five binaries. The values of the excess volume parameters are given in Table 4. This model fits virtually all of the data to within 0.06 J/bar/mol, or better than 0.5% in volume (Fig. 8), with a few exceptions for data points and/or studies that were excluded from the calibration. The mean of the absolute values of the residuals for calibrated data is 0.0113 J/bar/mol and the root mean squared error is 0.0156 J/bar/mol. It is difficult to obtain a more quantitative evaluation of goodness-of-fit given uncertain knowledge of errors on the different types of data used as inputs to the model, and because of our multi-step approach to fitting the data.

We have completed a preliminary bootstrap estimation (Efron 1982) to attempt to derive confidence bounds on the derived parameters. Uncertainty bounds on each fitted parameter and a correlation matrix for the parameter set derived from 3000 bootstrap

iterations are given in Supplementary Material 3 and 4. All the excess volume parameters and non-fixed V_o values were varied, except for khoharite V_o which was constrained by ΔV for calderite as described above. Many of the compositional excess parameters are strongly correlated, as expected. This observation highlights that the calibrated parameters should be used in the context of the full model derivation and that they may not be optimal descriptions of subsystems if ideal and excess terms are separated. As noted above, the calibration data vary in coverage and quality and full estimates of uncertainties are sparse, which means confidence bounds calculated using random sampling are unrealistically wide. We obtained a more conservative confidence bound for each parameter, again using the bootstrapping technique but holding all other parameters at their optimal values; these uncertainties are reported in Table 4.

DISCUSSION

Model comparison

Figure 9 shows excess volume along the grossular-pyrope join for the various models shown in Fig. 1, our proposed model, and the calibration data along this join; the ideal end-member contributions to the volume have been subtracted from other models and data. As noted above, there is a very large scatter in the data along this binary, especially at the pyrope-rich end, where excess volumes range from approximately -0.03 to +0.025 J/bar/mol. Similar to other models, our model fits this binary with an asymmetric term skewed towards grossular, but with much smaller magnitude. The difference between our model and the others is partly a matter of the data selected to calibrate each model, but is also due to the fact that we are simultaneously fitting the pyrope-knorringite and

grossular-uvarovite binaries (Figs. 7d, e). The total lack of agreement of the numerous studies for the grossular-pyrope binary suggest that there is much more work to be done to understand the effect that Ca-Mg ordering has on molar volume in garnets (Du 2012).

Figure 10 shows excess volume along the grossular-almandine join for the calibration data, the models of Geiger et al. (1989) and Berman (1990), and our proposed model. Our model fit is in general agreement with the Berman (1990) model. There is quite a bit of scatter in the data on this join, as well, with excess volumes ranging from approximately -0.013 to +0.049 J/bar/mol. The Geiger et al. (1989) model is based only on the data of Geiger et al. (1987), whereas the Berman (1990) model also used the data of Koziol (1990). Our model uses both of these data sets in addition to the data of Cressey et al. (1978), and agrees fairly well even with the inclusion of that data.

Rodehorst et al. (2002) modeled the molar volume of the grossular-spessartine binary at room-T and fit a symmetric excess volume parameter W^V = 0.08(4) J/bar/mol, essentially the same value that we obtain, $W_{\text{grs-sps}}$ = 0.0811 J/bar/mol (Fig. 7a). Rodehorst et al. (2004) repeated the fitting at temperatures of 290 and 30 K and extracted the mixing parameters W^V = 0.058(9) J/bar/mol and W^V = 0.10(1) J/bar/mol, respectively. They observe that the apparent asymmetry of mixing in the data that occurs with change in temperature does not appear to be systematic, and that more study is required to establish whether excess volume along the grossular-spessartine join is dependent on temperature or not.

Berman (1990) models the pyrope-almandine join with a very small asymmetric term slightly skewed towards the almandine-rich end. Geiger et al. (1989) and Geiger and

Feenstra (1997) treat this join as ideal. Our model also adopts ideal molar volume along the pyrope-almandine join as the data do not suggest excess volume of mixing. Geiger and Feenstra (1997) model the almandine-spessartine binary with a symmetric excess volume term W^V = 0.024(5) J/bar/mol; this join is treated as ideal in our model.

Enthalpy of formation and standard state entropy of knorringite

As discussed in Hamecher et al. (2013), we would like to examine the effect that our new garnet and spinel volume models have on the enthalpy of formation (H^o) and standard state entropy (S^o) of our model Cr-bearing garnet, knorringite. Klemme (2004) presented experimental reversals for the garnet-spinel transition reaction $MgCr_2O_4 + 4\ MgSiO_3 = Mg_3Cr_2Si_3O_{12} + Mg_2SiO_4$. H^o and S^o of knorringite were extracted using the experimental brackets from that study, and then again by Klemme et al. (2009). Klemme's (2004) values were designed to be consistent with the thermodynamic dataset of Holland and Powell (1990), whereas Klemme et al. (2009) used a later version (Holland and Powell 1998). When Hamecher et al. (2009) repeated the exercise using the provisional xMELTS thermodynamic dataset (based on Berman (1988), but updated to use the Vinet equation of state) the recovered standard-state entropy of $Mg_3Cr_2Si_3O_{12}$ was significantly lower than the values given by Klemme and co-workers. We tested the effect of our newly calibrated garnet and spinel (Hamecher et al. 2013) models, and obtained $H^o = -5672$kJ/mol and S^o = 322.1 J/mol/K, compared with $H^o = -5542$ kJ/mol and S^o = 376.7 J/mol/K from Klemme (2004) and $H^o = -5276$ kJ/mol and S^o = 357.9 J/mol/K from Klemme et al. (2009).

Much, though perhaps not all, of the difference between our fitted value of S^o and that of Klemme (2004) and Klemme et al. (2009) can be attributed to the choice of V_o for knorringite. Klemme (2004) claims to use V_o for knorringite from Irifune et al. (1982). However, the Perple_X (Connolly 1990; Connolly and Petrini 2002) data files available on the web (http://www.perplex.ethz.ch/) and Klemme et al. (2009) use V_o of pyrope from Holland and Powell (1998) for knorringite standard state molar volume. We tested fitting H^o and S^o using both Holland and Powell (1990) and Holland and Powell (1998) based code, using the V_o of pyrope (11.318 J/bar/mol) and the volume expressions from Perple_X in each case, and retrieved values for S^o close to those given in Klemme (2004) and Klemme et al. (2009), respectively. Our tests suggest that the S^o we obtain for knorringite with the xMELTS model is not that dissimilar to what Perple_X using Holland and Powell (1998) would give had the V_o value for knorringite been comparable to that of Irifune et al. (1982) (V_o = 11.738 J/bar/mol) or of this study (V_o = 11.7412 J/bar/mol).

Comparison of model densities

As a test, we compared garnet densities retrieved with our proposed model to densities from other models, to see what effect, if any, our new model has on densities of upper mantle rocks. First, we compared grossular-pyrope-almandine garnet densities with those calculated with the current garnet model in pMELTS (Ghiorso et al. 2002). Calculations with pMELTS are performed in the pressure range of 0 to 3 GPa, applicable to oceanic lithosphere and asthenospheric melts. Second, we compared densities with the model of Klemme et al. (2009), which is applicable to deep continental lithosphere (pressures from

3 to 6 GPa). Finally, we compare model densities with those of the global mantle model of Stixrude and Lithgow-Bertelloni (2011) (calculated for pressures from 0 to 30 GPa).

We used pMELTS to calculate a near-fractional decompression melting path using the DMM composition of Workman and Hart (2005) with 150 ppm H_2O with total entropy of 256 J/K, which corresponds to a potential temperature of 1344 ºC and a solidus of 3.3 GPa. This path and source generates 6 km of oceanic crust, on the slightly low-temperature end of normal ridges. As noted above, pMELTS is currently calibrated only for grossular-pyrope-almandine garnets. To compare the pMELTS residual density to the new model using the proposed garnet model and the spinel model of Hamecher et al. (2013), we calculated the garnet and spinel densities using the new models, and then recomputed the bulk density using the masses and volumes of the model olivine and pyroxenes (Fig. 11a). The difference in density between the models is ~1 kg/m^3 relative to a change in bulk density of ~100 kg/m^3 along the melting path. One reason for this small difference is that there is very little difference in the volume models for grossular-pyrope-almandine garnets; the molar volume of garnets in this compositional system is well constrained by the current model used by pMELTS. Additionally, there is not much garnet in the residue, and the modal abundance of garnet decreases rapidly with decompression melting.

Although the difference in density between the pMELTS model and our proposed model is small, this analysis provides us with the opportunity to consider the implications for compositional buoyancy of peridotites. The density determined above is a combination of compositional buoyancy, thermal expansion, and compression, and

applies along the sub-ridge melting path. To understand the behavior of the peridotites later in the lithosphere, or during subduction, we need to isolate purely compositional buoyancy. We took the series of evolving residual bulk compositions and recomputed all their phase assemblages and properties during progressive depletion at constant *P* and *T*: 3.5 GPa and 1400 ºC for the garnet stability field and 1.5 GPa and 1200 ºC for the spinel stability field. Results for the two models are shown in Fig. 11b and 11c in terms of absolute density and compositional buoyancy (i.e., density minus density of the unmelted source) versus extent of melting. There is not significant difference between the two models, which is not surprising as the grossular-pyrope-almandine volumes are already well constrained in pMELTS. The density difference between fertile source and the most-depleted harzburgite is ~50 kg/m^3 at 3.5 GPa, but only ~20 kg/m^3 at 1.5 GPa, where the fertile composition is not crystallizing garnet. The reduced ability to form modal garnet due to Al extraction in depleted peridotites has a large effect on compositional buoyancy (compare Figs. 11b and 11c). Hence, the magnitude of compositional buoyancy in the garnet stability field is more than twice as large as in the spinel stability field.

Figure 12 shows a calculation using the Cr-bearing harzburgite bulk composition B47 of Klemme et al. (2009). We used the mineral mode and composition output from the Klemme et al. model (Klemme, personal communication) to recalculate garnet and spinel densities with our models, and recombined with the other mineral modes and compositions, as described in the pMELTS example. Our retrieved bulk density ends up being between 40 to 80 kg/m^3 lower than the Klemme model. This could be in large part due to the difference in thermodynamic properties being used for knorringite between the

two models, as discussed in the previous section. The predicted difference is large enough to be quite significant to our understanding of Cr-rich lithosphere, e.g., diamond-bearing kimberlites.

We repeated this exercise for three additional compositions from Stixrude and Lithgow-Bertelloni (2012; figure 6) using the model output of the HeFESTo code (Stixrude and Lithgow-Bertelloni 2011; Stixrude, personal communication). Figure 13 shows the Stixrude and Lithgow-Bertelloni model for a basalt/eclogite bulk composition and the model with density recomputed using our garnet volume model. We also performed the calculation for harzburgite and pyrolite mantle compositions. Figure 14a shows the difference in density of the basalt and harzburgite compositions for the two models; Fig. 14b shows the difference in density between the basalt and pyrolite compositions. It is interesting to note that the largest difference between the models is at ~20 GPa, in the mantle transition zone where the majorite garnet field begins to grow (e.g., see figure 17 in Stixrude and Lithgow-Bertelloni 2011). This is likely due to the differences in our majorite end-member properties.

Basalt has the greatest abundance of garnet of the three compositions. The largest difference between the models is for the basalt composition at ~20 GPa, where the amount of majorite being crystallized is increasing. The maximum difference in density between the models (~20 kg/m^3) is small compared to the bulk density of peridotite (~4000 kg/m^3), but the density difference between the different rock types needs to be considered for compositional buoyancy. Compositional buoyancy of eclogite relative to pyrolite is thought to be driving force for slab pull and plate tectonics. The basaltic part of slabs in our model is less dense, so the model predicts smaller negative compositional

buoyancy for eclogite in the transition zone where garnets are majoritic. These differences in model results have consequences for the overall buoyancy of slabs and the tendency of different parts of slabs to separate (e.g., eclogite descending to the lower mantle and harzburgite remaining in the upper mantle). Results from convection models will depend to a large extent on the differences in compositional buoyancy in the chosen density models.

Conclusions

Regardless of the fact that garnets have been studied in depth for well over 50 years, disagreement about the end-member and excess volumetric properties of garnets persists. In fact, the most heavily investigated regions of garnet compositions space have the largest scatter in data. More work is needed to understand the volume effects of Ca-Mg ordering in grossular-pyrope garnets. It is our hope that more high-quality volume data will become available for both the aluminosilicate garnets and garnets with substantial cubic majorite component, as well as for samples measured at in situ high-P, -T conditions.

Acknowledgements

Many gracious thanks to Lars Stixrude and Carolina Lithgow-Bertelloni, and to Stephan Klemme and Jamie Connolly for providing us with their respective model outputs. This work was supported by the Division of Geological and Planetary Sciences, California Institute of Technology.

REFERENCES

Abrahams SC, Geller S (1958) Refinement of the structure of a grossularite garnet. Acta Crystallogr 11:437–441. doi:10.1107/S0365110X5800116X

Armbruster T, Geiger CA (1993) Andradite crystal chemistry, dynamic X-site disorder and structural strain in silicate garnets. Eur J Mineral 5:59–71

Armbruster T, Geiger CA, Lager GA (1992) Single-crystal X-ray structure study of synthetic pyrope almandine garnets at 100 and 293 K. Am Mineral 77:512–521

Armbruster T, Birrer J, Libowitzky E, Beran A (1998) Crystal chemistry of Ti-bearing andradites. Eur J Mineral 10:907–921

Artioli G, Pavese A, Stahl K, McMullan RK (1997) Single-crystal neutron-diffraction study of pyrope in the temperature range 30–1173 K. Can Mineral 35:1009–1019

Asimow PD, Dixon JE, Langmuir CH (2004) A hydrous melting and fractionation model for mid-ocean ridge basalts: Application to the Mid-Atlantic Ridge near the Azores. Geochem Geophys Geosyst 5. doi:10.1029/2003GC000568

Babuska V, Fiala J, Kumazawa M, Ohno I, Sumino Y (1978) Elastic properties of garnet solid-solution series. Phys Earth Planet Inter 16:157–176

Bass JD (1986) Elasticity of uvarovite and andradite garnets. J Geophys Res 91:7505–7516

Bass JD (1989) Elasticity of grossular and spessartite garnets by Brillouin spectroscopy. J Geophys Res 94:7621–7628

Bass J, Kanzaki M (1990) Elasticity of a majorite‐pyrope solid solution. Geophys Res Lett 17:1989–1992

Berman RG (1988) Internally-consistent thermodynamic data for minerals in the system Na_2O-K_2O-CaO-MgO-FeO-Fe_2O_3-Al_2O_3-SiO_2-TiO_2-H_2O-CO_2. J Petrol 89:168–183

Berman RG (1990) Mixing properties of Ca-Mg-Fe-Mn garnets. Am Mineral 75:328–344

Berman RG, Aranovich LY (1996) Optimized standard state and solution properties of minerals. I. Model calibration for olivine, orthopyroxene, cordierite, garnet, and ilmenite in the system FeO-MgO-CaO-Al_2O_3-TiO_2-SiO_2. Contrib Mineral Petrol 126:1–24

Bonczar L, Graham E, Wang H (1977) The pressure and temperature dependence of the elastic constants of pyrope garnet. J Geophys Res 82:2529–2534

Bosenick A, Geiger CA (1997) Powder X ray diffraction study of synthetic pyrope-grossular garnets between 20 and 295 K. J Geophys Res 102:22649–22657

Bosenick A, Dove MT, Heine V, Geiger CA (2001) Scaling of thermodynamic mixing properties in garnet solid solutions. Phys Chem Miner 28:177–187

Boyd FR, England JL (1959) Pyrope. Carnegie Inst Year B 58:83–87

Connolly JAD (1990) Multivariable phase diagrams; an algorithm based on generalized thermodynamics. Am J Sci 290:666–718

Connolly JAD, Petrini K (2002) An automated strategy for calculation of phase diagram sections and retrieval of rock properties as a function of physical conditions. J Metamorph Geol 20:697–708

Cressey G, Schmid R, Wood BJ (1978) Thermodynamic properties of almandine-grossular garnet solid solutions. Contrib Mineral Petrol:397–404

Deer WA, Howie RA, Zussman J (1997) Rock-forming Minerals: Volume 1A: Orthosilicates. The Geological Society, London

Downs RT, Hall-Wallace M (2003) The American Mineralogist crystal structure database. Am Mineral 88:247–250

Du W (2012) Excess volume and exsolution in pyrope-grossular garnet. Dissertation, Columbia University

Efron B (1982) The jackknife, the bootstrap, and other resampling plans. Soc Ind Appl Math, Philadelphia

Fabrichnaya O, Saxena SK, Richet P, Westrum EF (2004) Thermodynamic data, models and phase diagrams in multicomponent systems. Springer, New York

Ganguly J, Cheng W, O'Neill HStC (1993) Syntheses, volume, and structural changes of garnets in the pyrope-grossular join: Implications for stability and mixing properties. Am Mineral 78:583–593

Geiger CA (2000) Volumes of mixing in aluminosilicate garnets: Solid solution and strain behavior. Am Mineral 85:893–897

Geiger CA (2008) Silicate garnet: A micro to macroscopic (re)view. Am Mineral 93:360–372. doi:10.2138/am.2008.2588

Geiger CA, Armbruster T (1997) $Mn_3Al_2Si_3O_{12}$ spessartine and $Ca_3Al_2Si_3O_{12}$ grossular garnet: Structural dynamic and thermodynamic properties. Am Mineral 82:740–747

Geiger CA, Feenstra A (1997) Molar volumes of mixing of almandine-pyrope and almandine-spessartine garnets and the crystal chemistry and thermodynamic-mixing properties of the aluminosilicate garnets. Am Mineral 82:571–581

Geiger CA, Newton RC, Kleppa OJ (1987) Enthalpy of mixing of synthetic almandine-grossular and almandine-pyrope garnets from high-temperature solution calorimetry. Geochim Cosmochim Acta 51:1755–1763

Geiger CA, Winkler B, Langer K (1989) Infrared spectra of synthetic almandine-grossular and almandine-pyrope garnet solid solutions: evidence for equivalent site behaviour. Mineral Mag 53:231–237

Geiger CA, Merwin L, Sebald A (1992) Structural investigation of pyrope garnet using temperature-dependent FTIR and ^{29}Si and ^{27}Al MAS NMR spectroscopy. Am Mineral 77:713–717

Ghiorso MS (2004a) An equation of state for silicate melts. I. Formulation of a general model. Am J Sci 304:637–678

Ghiorso MS (2004b) An equation of state for silicate melts. III. Analysis of stoichiometric liquids at elevated pressure: Shock compression data, molecular dynamics simulations, and mineral fusion curves. Am J Sci 304:752–810

Ghiorso MS (2004c) An equation of state for silicate melts. IV. Calibration of a multicomponent mixing model to 40 GPa. Am J Sci 304:811–838

Ghiorso MS, Kress VC (2004) An equation of state for silicate melts. II. Calibration of volumetric properties at 10^5 Pa. Am J Sci 304:679–751

Ghiorso MS, Sack RO (1995) Chemical mass transfer in magmatic processes IV. A revised and internally consistent thermodynamic model for the interpolation and extrapolation of liquid-solid equilibria in magmatic systems at elevated temperatures and pressures. Contrib Mineral Petrol 119:197–212

Ghiorso MS, Hirschmann MM, Reiners PW, Kress III VC (2002) The pMELTS: A revision of MELTS for improved calculation of phase relations and major element partitioning related to partial melting of the mantle to 3 GPa. Geochem Geophys Geosyst 3. doi:10.1029/2001GC000217

Ghiorso MS, Hirschmann MM, Grove TL (2007) xMELTS: A thermodynamic model for the estimation of magmatic phase relations over the pressure range 0–30 GPa and at temperatures up to 2500 °C. Eos Trans Am Geophys Union 88(52), Fall Meet Suppl Abstr V31C-0608

Gibbs GV, Smith JV (1965) Refinement of the crystal structure of synthetic pyrope. Am Mineral 50:2023–2039

Hackler RT, Wood BJ (1989) Experimental determination of Fe and Mg exchange between garnet and olivine and estimation of Fe-Mg mixing properties in garnet. Am Mineral 74:994–999

Hamecher EA, Antoshechkina PM, Ghiorso MS, Asimow PD (2009) Thermodynamic calibration of Cr-Al exchange equilibria for garnet and spinel. Eos Trans Am Geophys Union 90(52), Fall Meet Suppl Abstr V31D-2056

Hamecher EA, Antoshechkina PM, Ghiorso MS, Asimow PD (2013) The molar volume of FeO–MgO–Fe_2O_3–Cr_2O_3–Al_2O_3–TiO_2 spinels. Contrib Mineral Petrol 165:25-43. doi:10.1007/s00410-012-0790-0

Haselton HT, Newton RC (1980) Thermodynamics of pyrope-grossular garnets and their stabilities at high temperatures and high pressures. J Geophys Res 85:6973–6982

Hazen RM, Finger LW (1989) High-pressure crystal chemistry of andradite and pyrope: Revised procedures for high-pressure diffraction experiments. Am Mineral 74:352–359

Hazen RM, Downs RT, Conrad PG, Finger LW, Gasparik T (1994) Comparative compressibilities of majorite-type garnets. Phys Chem Miner 21:344–349

Holland TJB, Powell R (1990) An enlarged and updated internally consistent thermodynamic dataset with uncertainties and correlations: the system K_2O–Na_2O–CaO–MgO–MnO–FeO–Fe_2O_3–Al_2O_3–TiO_2–SiO_2–C–H_2–O_2. J Metamorph Geol 8:89–124

Holland TJB, Powell R (1998) An internally consistent thermodynamic data set for phases of petrological interest. J Metamorph Geol 16:309–343

Irifune T, Ohtani E, Kumazawa M (1982) Stability field of knorringite $Mg_3Cr_2Si_3O_{12}$ at high pressure and its implication to the occurrence of Cr-rich pyrope in the upper mantle. Phys Earth Planet Inter 27:263–272

Jiang F, Speziale S, Shieh SR, Duffy TS (2004) Single-crystal elasticity of andradite garnet to 11 GPa. J Phys: Condens Matter 16:S1041–S1052. doi:10.1088/0953-8984/16/14/014

Klemme S (2004) The influence of Cr on the garnet–spinel transition in the Earth's mantle: Experiments in the system MgO–Cr_2O_3–SiO_2 and thermodynamic modelling. Lithos 77:639–646

Klemme S, Ivanic TJ, Connolly JAD, Harte B (2009) Thermodynamic modelling of Cr-bearing garnets with implications for diamond inclusions and peridotite xenoliths. Lithos 112:986–991

Koziol AM (1990) Activity-composition relationships of binary Ca-Fe and Ca-Mn garnets determined by reversed, displaced equilibrium experiments. Am Mineral 75:319–327

Koziol AM, Newton RC (1989) Grossular activity-composition relationships in ternary garnets determined by reversed displaced-equilibrium experiments. Contrib Mineral Petrol 103:423–433

Lawson CL, Hanson RJ (1974) Solving least squares problems. Prentice-Hall, New Jersey

Leger JM, Redon AM, Chateau C (1990) Compressions of synthetic pyrope, spessartine and uvarovite garnets up to 25 GPa. Phys Chem Miner 17:161-167

Leitner BJ, Weidner DJ, Liebermann RC (1980) Elasticity of single crystal pyrope and implications for garnet solid solution series. Phys Earth Planet Inter 22:111–121

Levien L, Prewitt CT, Weidner DJ (1979) Compression of pyrope. Am Mineral 64:805–808

Luo S-N, Ahrens TJ, Asimow PD (2003) Polymorphism, superheating, and amorphization of silica upon shock wave loading and release. J Geophys Res 108:2421. doi:10.1029/2002JB002317

Masyukov NA, Dmitriev AV (2007) Approximation formulas in the Debye theory of the low-temperature specific heat of solids. Bull Russ Acad Sci: Phys 71:1076–1078. doi:10.3103/S1062873807080060

Meagher EP (1975) The crystal structures of pyrope and grossularite at elevated temperatures. Am Mineral 60:218–228

Milman V, Akhmatskaya EV, Nobes RH, Winkler B, Pickard CJ, White JA (2001) Systematic ab initio study of the compressibility of silicate garnets. Acta Crystallogr Sect B 57:163–177. doi:10.1107/S0108768100018188

Mukhopadhyay B, Holdaway MJ, Koziol AM (1997) A statistical model of thermodynamic mixing properties of Ca-Mg-Fe^{2+} garnets. Am Mineral 82:165–181

Newton RC, Charlu TV, Kleppa OJ (1977) Thermochemistry of high pressure garnets and clinopyroxenes in the system CaO-MgO-Al_2O_3-SiO_2. Geochim Cosmochim Acta 41:369–377

Nishizawa H, Shimada M, Matsuoka K, Koizumi M (1977) Infrared and Mössbauer spectra of synthetic garnets $A_3Fe_2Si_3O_{12}$(A:Mn,Cd,Ca). Bull Chem Soc Jpn 50:3186–3188

Novak GA, Gibbs GV (1971) The crystal chemistry of the silicate garnets. Am Mineral 56:791–825

Olijnyk H, Paris E, Geiger CA, Lager GA (1991) Compressional study of katoite [$Ca_3Al_2(O_4H_4)_3$] and grossular garnet. J Geophys Res 96:14313–14318

Ottonello G, Bokreta M, Sciuto PF (1996) Parameterization of energy and interactions in garnets: End-member properties. Am Mineral 81:429–447

Pacalo REG, Weidner DJ, Gasparik T (1992) Elastic properties of sodium-rich majorite garnet. Geophys Res Lett 19:1895–1898

Pavese A, Artioli G, Prencipe M (1995) X-ray single-crystal diffraction study of pyrope in the temperature range 30-973 K. Am Mineral 80:457–464

Pavese A, Levy D, Pischedda V (2001) Elastic properties of andradite and grossular, by synchrotron X-ray diffraction at high pressure conditions. Eur J Mineral 13:929–937. doi:10.1127/0935-1221/2001/0013/0929

Perkins III D (1979) Application of new thermodynamic data to mineral equilibria. Dissertation, University of Michigan

Press WH, Teukolsky SA, Vetterling WT, Flannery BP (2007) Numerical recipes: The art of scientific computing, 3rd edn. Cambridge University Press, Cambridge

Ringwood AE (1977) Synthesis of pyrope-knorringite solid solution series. Earth Planet Sci Lett 36:443–448

Ringwood AE, Major A (1971) Synthesis of majorite and other high pressure garnets and perovskites. Earth Planet Sci Lett 12:411–418

Rodehorst U, Geiger CA, Armbruster T (2002) The crystal structures of grossular and spessartine between 100 and 600 K and the crystal chemistry of grossular-spessartine solid solutions. Am Mineral 87:542–549

Rodehorst U, Carpenter MA, Ballaran TB, Geiger CA (2004) Local structural heterogeneity, mixing behaviour and saturation effects in the grossular-spessartine solid solution. Phys Chem Miner 31:387–404. doi:10.1007/s00269-004-0410-2

Sato Y, Akaogi M, Akimoto S (1978) Hydrostatic compression of the synthetic garnets pyrope and almandine. J Geophys Res 83:335–338

Saxena SK (1996) Earth mineralogical model: Gibbs free energy minimization computation in the system MgO-FeO-SiO_2. Geochim Cosmochim Acta 60:2379–2395

Schwarz G (1978) Estimating the dimension of a model. Ann Stat 6:461–464

Skinner BJ (1956) Physical properties of end-members of the garnet group. Am Mineral 41:428–436

Shannon RD (1976) Revised effective ionic radii and systematic studies of interatomic distances in halides and chalcogenides. Acta Crystallogr Sect A 32:751-767

Stixrude L, Lithgow-Bertelloni C (2005) Thermodynamics of mantle minerals — I. Physical properties. Geophys J Int 162:610–632

Stixrude L, Lithgow-Bertelloni C (2011) Thermodynamics of mantle minerals — II. Phase equilibria. Geophys J Int 184:1180–1213. doi:10.1111/j.1365-246X.2010.04890.x

Stixrude L, Lithgow-Bertelloni C (2012) Geophysics of chemical heterogeneity in the mantle. Annu Rev Earth Planet Sci 40:569–595. doi:10.1146/annurev.earth.36.031207.124244

Takahashi T, Liu L (1970) Compression of ferromagnesian garnets and the effect of solid solutions on the bulk modulus. J Geophys Res 75:5757–5766

Thieblot L, Roux J, Richet P (1998) High-temperature thermal expansion and decomposition of garnets. Eur J Mineral 10:7–15

Ungaretti L, Leona M, Merli M, Oberti R (1995) Non-ideal solid-solution in garnet; crystal-structure evidence and modelling. Eur J Mineral 7:1299–1312

Wang Y, Weidner DJ, Zhang J, Gwanrnesia GD, Liebermann RC (1998) Thermal equation of state of garnets along the pyrope-majorite join. Phys Earth Planet Inter 105:59–71

Weaver JS, Takahashi T, Bass J (1976) Isothermal compression of grossular garnets to 250 kbar and the effect of calcium on the bulk modulus. J Geophys Res 81:2475–2482

Webb SL (1989) The elasticity of the upper mantle orthosilicates olivine and garnet to 3 GPa. Phys Chem Miner 16:684–692

Wood BJ (1988) Activity measurements and excess entropy-volume relationships for pyrope-grossular garnets. J Geol 96:721–729

Woodland AB, O'Neill HStC (1993) Synthesis and stability of $Fe^{2+}_3Fe^{3+}_2Si_3O_{12}$ garnet and phase relations with $Fe_3Al_2Si_3O_{12}$-$Fe^{2+}_3Fe^{3+}_2Si_3O_{12}$ solutions. Am Mineral 78:1002–1015

Woodland AB, Ross II CR (1994) A crystallographic and Mössbauer spectroscopy study of $Fe_3^{2+}Al_2Si_3O_{12}$-$Fe_3^{2+}Fe_2^{3+}Si_3O_{12}$ (almandine-"skiagite") and $Ca_3Fe_2^{3+}Si_3O_{12}$-$Fe_3^{2+}Fe_2^{3+}Si_3O_{12}$ (andradite -"skiagite") garnet solid solutions. Phys Chem Miner 21:117–132

Woodland AB, Bauer M, Ballaran TB, Hanrahan M (2009) Crystal chemistry of $Fe_3^{2+}Cr_2Si_3O_{12}$-$Fe_3^{2+}Fe_2^{3+}Si_3O_{12}$ garnet solid solutions and related spinels. Am Mineral 94:359–366

Workman RK, Hart SR (2005) Major and trace element composition of the depleted MORB mantle (DMM). Earth Planet Sci Lett 231:53–72

Yeganeh-Haeri A, Weidner DJ, Ito E (1990) Elastic properties of the pyrope‐majorite solid solution series. Geophys Res Lett 17:2453–2456

Zhang L, Ahsbahs H, Kutoglu A (1998) Hydrostatic compression and crystal structure of pyrope to 33 GPa. Phys Chem Miner 25:301–307

Zhang L, Ahsbahs H, Kutoglu A, Geiger CA (1999) Single-crystal hydrostatic compression of synthetic pyrope, almandine, spessartine, grossular and andradite garnets at high pressures. Phys Chem Miner 27:52–58

Table 1. Model components

Name	Symbol	Formula
Independent end members		
Grossular	grs	$Ca_3Al_2Si_3O_{12}$
Pyrope	pyr	$Mg_3Al_2Si_3O_{12}$
Almandine	alm	$Fe_3Al_2Si_3O_{12}$
Knorringite	knr	$Mg_3Cr_2Si_3O_{12}$
Majorite	maj	$Mg_3(MgSi)Si_3O_{12}$
Khoharite	kho	$Mg_3Fe_2Si_3O_{12}$
Na-garnet	nag	$(Na_2Mg)Si_2Si_3O_{12}$
Mg-Mg-morimotoite	mmr	$Mg_3(TiMg)Si_3O_{12}$
Spessartine	sps	$Mn_3Al_2Si_3O_{12}$
Dependent end members (for which there are data)		
Andradite	and	$Ca_3Fe_2Si_3O_{12}$
Uvarovite	uvr	$Ca_3Cr_2Si_3O_{12}$
Skiagite	ski	$Fe_3Fe_2Si_3O_{12}$

Table 2. Summary table of data coverage in composition, *P*, and *T*

Composition	Total Experiments	Ambient-*P*, *T*	High-*P*	*P* Range (GPa)	High-*T*	*T* Range (ºC)
End members						
grs	63	21	15	2.3 - 11.8	27	57 - 1140
pyr	98	33	43	2.27 - 33.38	22	56 - 758
alm	53	21	18	2.3 - 21.3	14	50 - 581
knr	3	3	0	-	0	-
sps	40	11	12	2.3 - 14.6	17	68 - 702
and	35	9	13	2.3 - 14	13	59 - 690
uvr	4	4	0	-	0	-
ski	5	5	0	-	0	-
Binaries						
grs-pyr	41	41	0	-	0	-
grs-alm	26	26	0	-	0	-
grs-sps	9	9	0	-	0	-
grs-and	1	1	0	-	0	-
grs-uvr	11	11	0	-	0	-
grs-nct	1	1	0	-	0	-
grs-csg	1	1	0	-	0	-
pyr-alm	11	11	0	-	0	-
pyr-maj	94	13	81*	1.241 - 10.253	81*	33 - 890
pyr-knr	9	9	0	-	0	-
alm-sps	28	28	0	-	0	-

alm-ski	42	42	0	-	0	-
knr-maj	1	1	0	-	0	-
maj-nag	9	1	8	0.39 - 4.72	0	-
and-uvr	12	12	0	-	0	-
and-ski	38	38	0	-	0	-
ski-fcg	8	8	0	-	0	-
Ternary						
grs-pyr-alm	30	22	8	0.39 - 4.72	0	-
Multi-component	93	60	4	5.8 - 19	29	80 - 1225
Total	766					

* Measured at simultaneous high-*P, -T*

Table 3. Optimized standard state end-member properties

	V_o (J/bar/mol)	a (Å)	ρ (kg/m^3)	K_{oT} (GPa)	K'	γ_o	q	C_{vm} (J/K/mol)	θ_o (K)
$Ca_3Al_2Si_3O_{12}$	12.5275	11.8504	3596	168.0	6.1	1.038	1.5	502.2	960
$Mg_3Al_2Si_3O_{12}$	11.3207	11.4570	3561	168.3	4.8	1.055	1.5	503.0	959.7
$Fe_3Al_2Si_3O_{12}$	11.5308	11.5274	4317	188.2	3.9	1.065	1.5	507.6	889.5
$Mg_3Cr_2Si_3O_{12}$	11.7412	11.5971	3860	162.0	4.7	1.084	1.5	506.9	946.7
$Mg_3(MgSi)Si_3O_{12}$	11.4000	11.4837	3522	154.2	4.0	1.08	1.5	498.87	980
$Mg_3Fe_2Si_3O_{12}$	11.9596	11.6686	3853	158.5	4.7	1.081	1.5	510.2	928.4
$(Na_2Mg)Si_2Si_3O_{12}$	11.1831	11.4104	3601	191.5	4.0	1	1.5	498.87	980
$Mg_3(TiMg)Si_3O_{12}$	11.8150	11.6214	3566	148.9	4.5	1.08	1.5	502	970
$Mn_3Al_2Si_3O_{12}$	11.7953	11.6149	4197	184.5	5.1	1.267	1.5	492.4	900.9

Table 4. Model parameters

		$1\sigma^{*}$	
$W_{grs\text{-}pyr}$	0.0487	0.0246	(J/bar/mol)
$W_{grs\text{-}alm}$	0.1073	0.0893	
$W_{grs\text{-}knr}$	0.1205	0.0493	
$W_{grs\text{-}maj}$	-0.3035	3.4454	
$W_{grs\text{-}nag}$	0.1054	1.5421	
$W_{grs\text{-}mmr}$	0.1079	0.2851	
$W_{grs\text{-}sps}$	0.0811	0.2768	
$W_{pyr\text{-}knr}$	0.0641	0.0396	
$W_{pyr\text{-}maj}$	0.0596	0.0000	
$W_{pyr\text{-}kho}$	-0.4093	0.0000	
$W_{pyr\text{-}mmr}$	-0.2585	1.9250	
$W_{alm\text{-}kho}$	-0.1764	0.0161	
$W_{knr\text{-}kho}$	-0.1355	0.2020	
$W_{kho\text{-}sps}$	-0.1369	11.8864	
$dW_{grs\text{-}pyr}$	-0.0234	0.0130	
$dW_{grs\text{-}alm}$	-0.0511	0.2782	
$dW_{grs\text{-}nag}$	-0.1456	21.7412	
$dW_{pyr\text{-}knr}$	-0.0453	0.0220	
$dW_{pyr\text{-}kho}$	0.1362	0.0100	

*Bootstrap estimation of s.d. for each parameter, holding all other parameters at optimal values

FIGURE CAPTIONS

Fig. 1 Various published models of excess volume along the grossular-pyrope binary. Models shown: Wood (1988) (red); Berman (1990) (magenta); Ganguly et al. (1993) (green); Bosenick and Geiger (1997) (blue); Bosenick et al. (2001) (cyan).

Fig. 2 High-*T*, room-*P* data of Skinner (1956) for almandine (upper) and spessartine (lower) plotted as residuals in pressure versus temperature. Black squares show the fit when using the constant α thermal pressure term; blue filled circles show the data fit with the Mie-Grüneisen-Debye thermal pressure formalism.

Fig. 3 Preferred values of K_{oT} versus R_x/R_y for end members, where R_x is the ionic radius of the x-site cation and R_y is the ionic radius of the y-site cation. Effective ionic radii from Shannon (1976). Dashed arrows show trends of increasing cation radius among Ca-rich, Mg-rich, and Al-rich end members. Colors highlight systematic relationships for Ca-rich and Mg-rich garnet K_{oT} with y-site cation radii: Al (red), Cr (green), Fe^{3+} (blue), Mg (gray).

Fig. 4 Debye temperature (θ_o) versus R_x/R_y for end members. Colors have same meaning as in Fig. 3. Dashed arrows show systematic relationship for garnets with Mg of Ca on the x-site.

Fig. 5 C_{vm} versus R_x/R_y for end members. Colors have same meaning as in Fig. 3.

Fig. 6 V_o versus R_x/R_y for end members. Dashed arrows show clear systematic relationships between V_o and cation radius for the "pyralspite" (pyrope-almandine-spessartine) and "ugrandite" (uvarovite-grossular-andradite) garnet series, which was also observed by Novak and Gibbs (1971).

Fig. 7 Excess volume models (black curves) and excess volume of calibration data (gray filled circles) along the **a** grossular-spessartine; **b** andradite-uvarovite; **c** pyrope-knorringite; **d** uvarovite-grossular binaries.

Fig. 8 Model residuals versus measured volume.

Fig. 9 Excess volume model along the grossular-pyrope binary from this work (black curve) plotted with models shown in Fig. 1 (muted colors correspond to colors in Fig. 1). Excess volume of calibration data plotted as gray filled circles.

Fig. 10 Excess volume models along the grossular-almandine binary from this work (solid curve), Geiger et al. (1989) (dotted curve), and Berman (1990) (dashed curve). Excess volume of calibration data plotted as gray filled circles.

Fig. 11 a Left-hand axis shows bulk density versus pressure for the DMM bulk composition of Workman and Hart (2005) calculated with current pMELTS model (black

dashed curve) and recalculated with garnet density from this work and spinel density from Hamecher et al. (2013) (solid black line). Right-hand axis shows the difference in bulk density between the two models (red dashed curve); **b** Bulk density and compositional buoyancy versus extent of melt depletion in the spinel stability field (1.5 GPa and 1200 ºC); **c** Bulk density and compositional buoyancy versus extent of melt depletion in the garnet stability field (3.5 GPa and 1400 ºC).

Fig. 12 Left-hand axis shows bulk density versus pressure for the B47 bulk composition of Klemme et al. (2009) for the Klemme et al. (2009) model (black dashed curve) and recalculated with garnet density from this work and spinel density from Hamecher et al. (2013) (solid black line). Right-hand axis shows the difference in bulk density between the two models (red dashed curve).

Fig. 13 Left-hand axis shows bulk density versus pressure for the basalt bulk composition used by Stixrude and Lithgow-Bertelloni (2012; figure 6) for their model computed with HeFESTo (Stixrude and Lithgow-Bertelloni 2011) (black dashed curve) and recalculated with garnet density from this work (solid black line). Right-hand axis shows the difference in bulk density between the two models (red dashed curve).

Fig. 14 a Left-hand axis shows the difference in bulk density difference between the basalt and harzburgite compositions used by Stixrude and Lithgow-Bertelloni (2012; figure 6) versus pressure for their model computed with HeFESTo (Stixrude and Lithgow-Bertelloni 2011) (black dashed curve) and recalculated with garnet density from

this work (solid black line). Right-hand axis shows the difference between the two models (red dashed curve); **b** Left-hand axis shows the difference in bulk density difference between the basalt and pyrolite compositions used by Stixrude and Lithgow-Bertelloni (2012; figure 6) versus pressure for their model computed with HeFESTo (Stixrude and Lithgow-Bertelloni 2011) (black dashed curve) and recalculated with garnet density from this work and spinel density from Hamecher et al. (2013) (solid black line). Right-hand axis shows the difference between the two models (red dashed curve).

FIGURES

Fig. 1

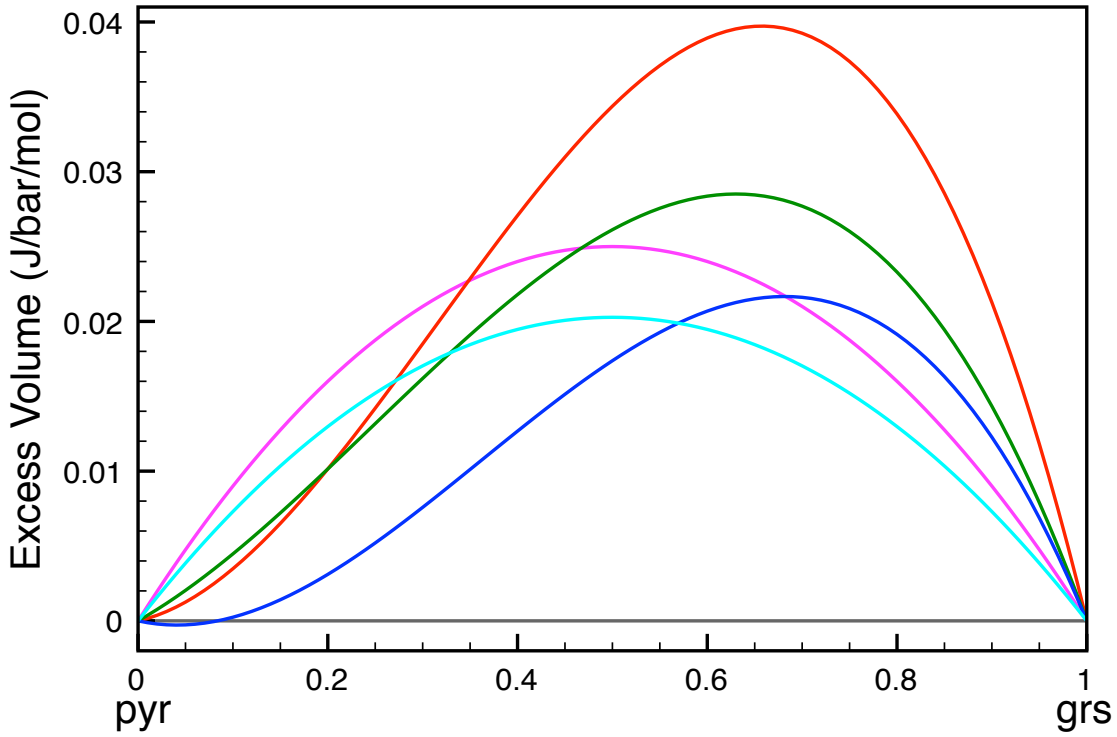

Fig. 2

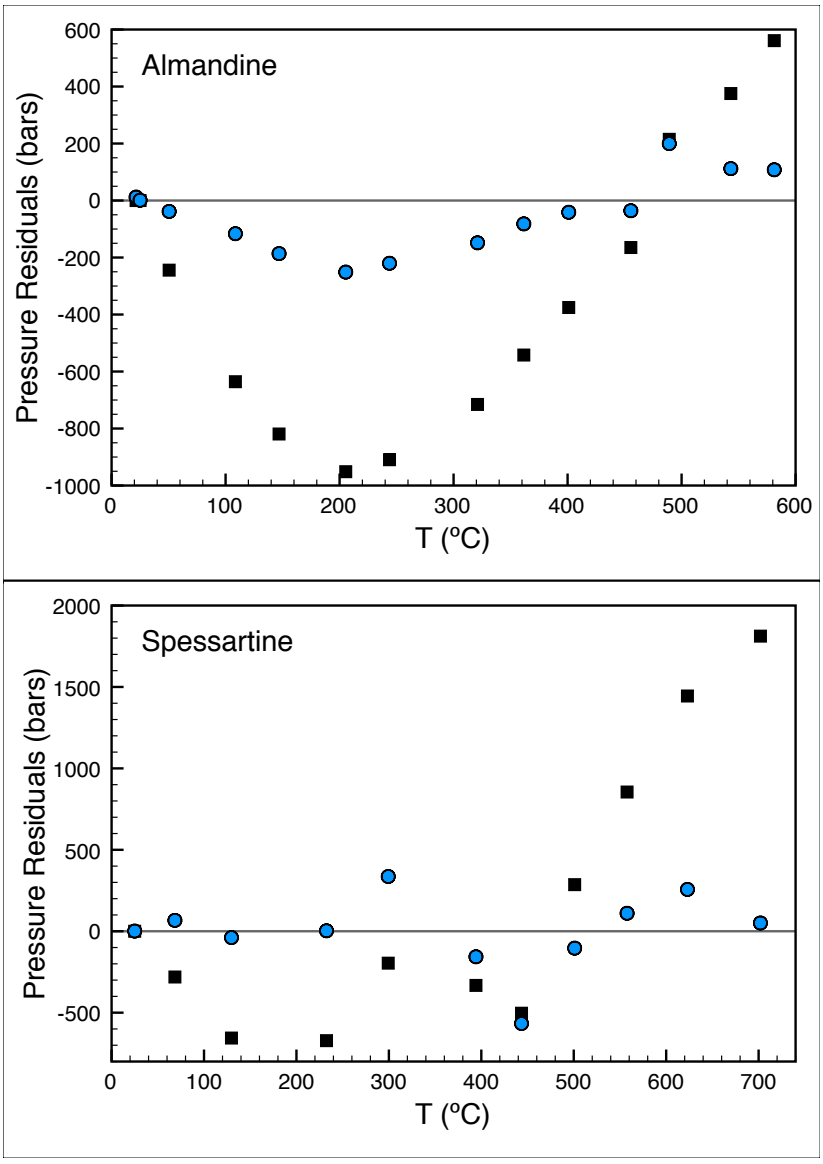
Almandine
Pressure Residuals (bars)
T (ºC)
Spessartine
Pressure Residuals (bars)
T (ºC)

Fig. 3

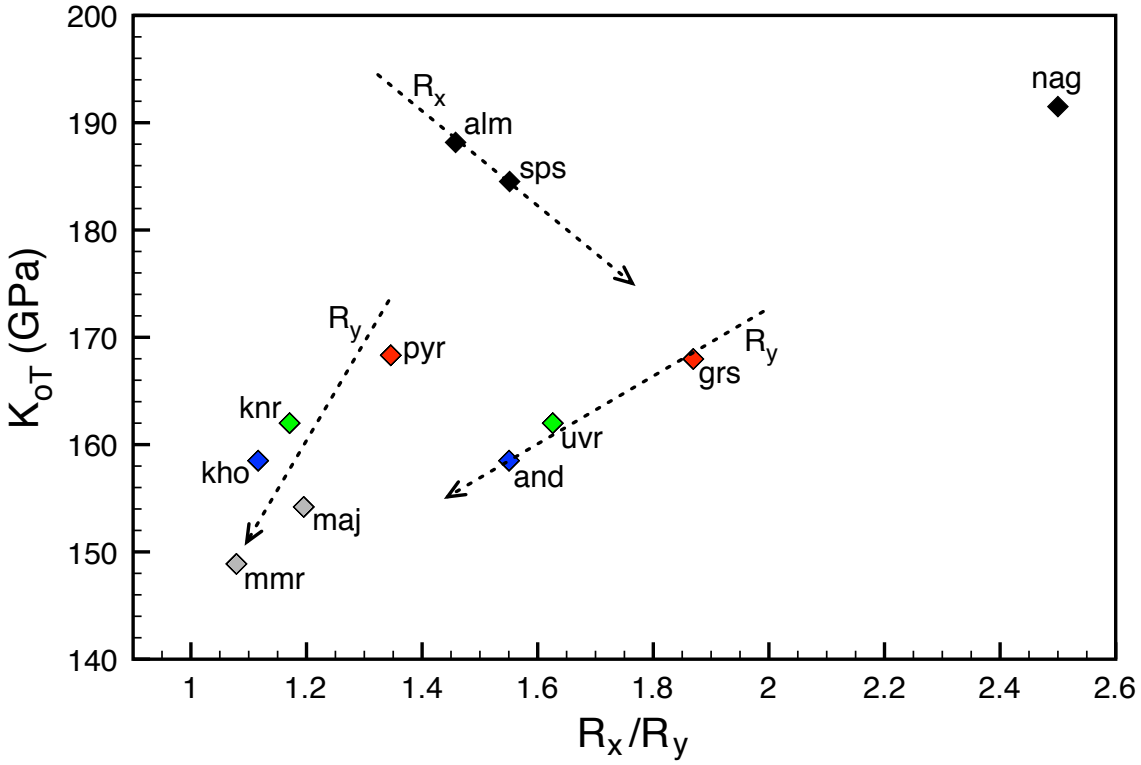
200
190
180
170
160
150
140
K_{oT} (GPa)
1
1.2
1.4
1.6
1.8
2
2.2
2.4
2.6
R_x/R_y
R_x
alm
sps
nag
R_y
pyr
knr
kho
maj
mmr
R_y
grs
uvr
and

Fig. 4

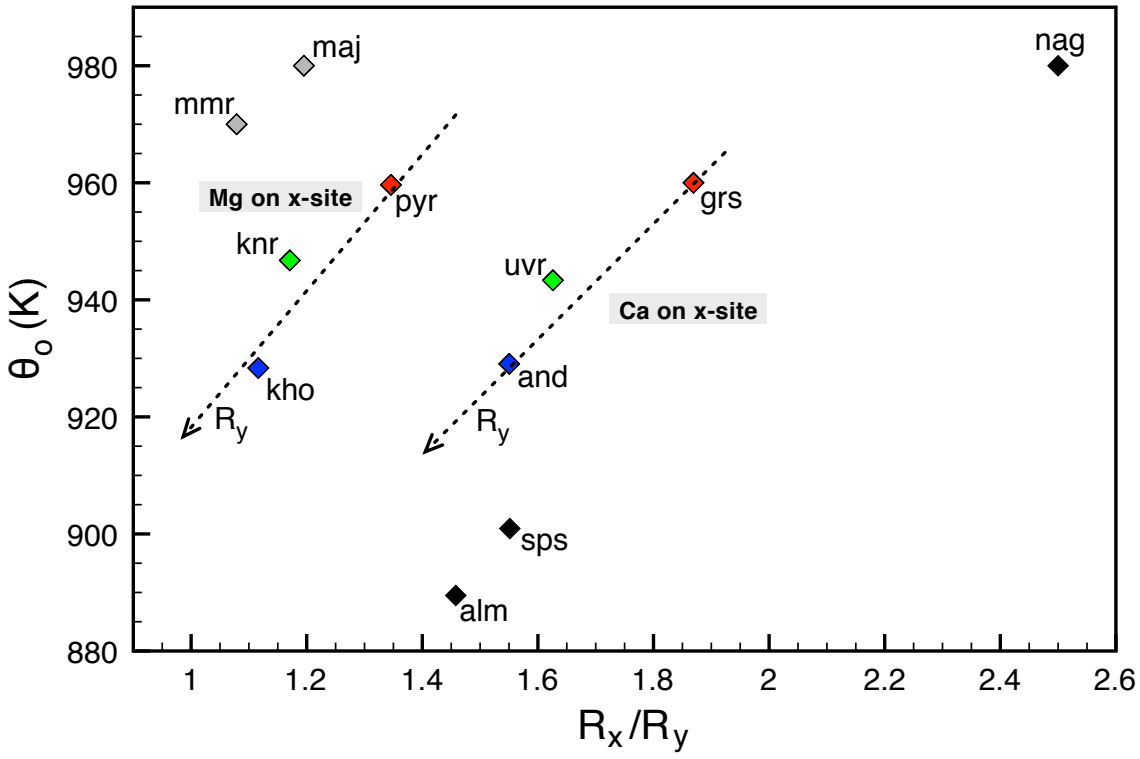
980
960
940
920
900
880
θ_o (K)
1
1.2
1.4
1.6
1.8
2
2.2
2.4
2.6
R_x/R_y
maj
nag
mmr
Mg on x-site
pyr
grs
knr
uvr
Ca on x-site
kho
and
R_y
R_y
sps
alm

Fig. 5

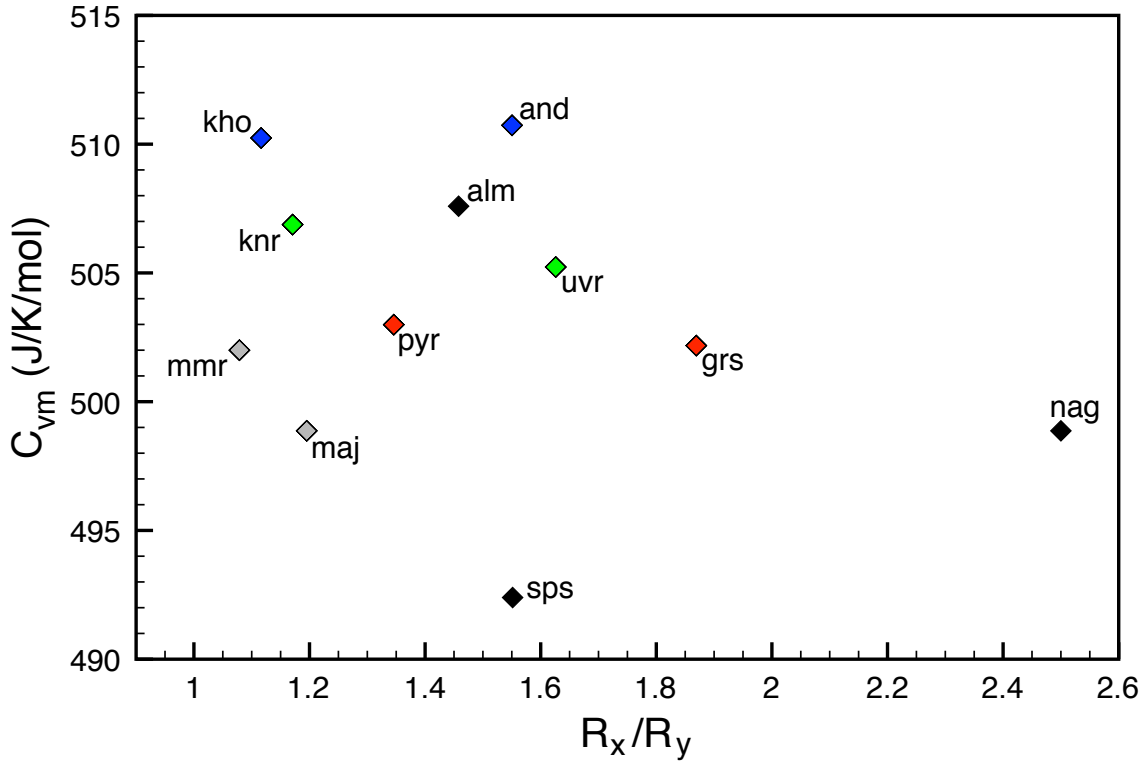
515
510
505
500
495
490
C_{vm} (J/K/mol)
1
1.2
1.4
1.6
1.8
2
2.2
2.4
2.6
R_x/R_y
kho
and
alm
knr
uvr
pyr
mmr
grs
nag
maj
sps

Fig. 6

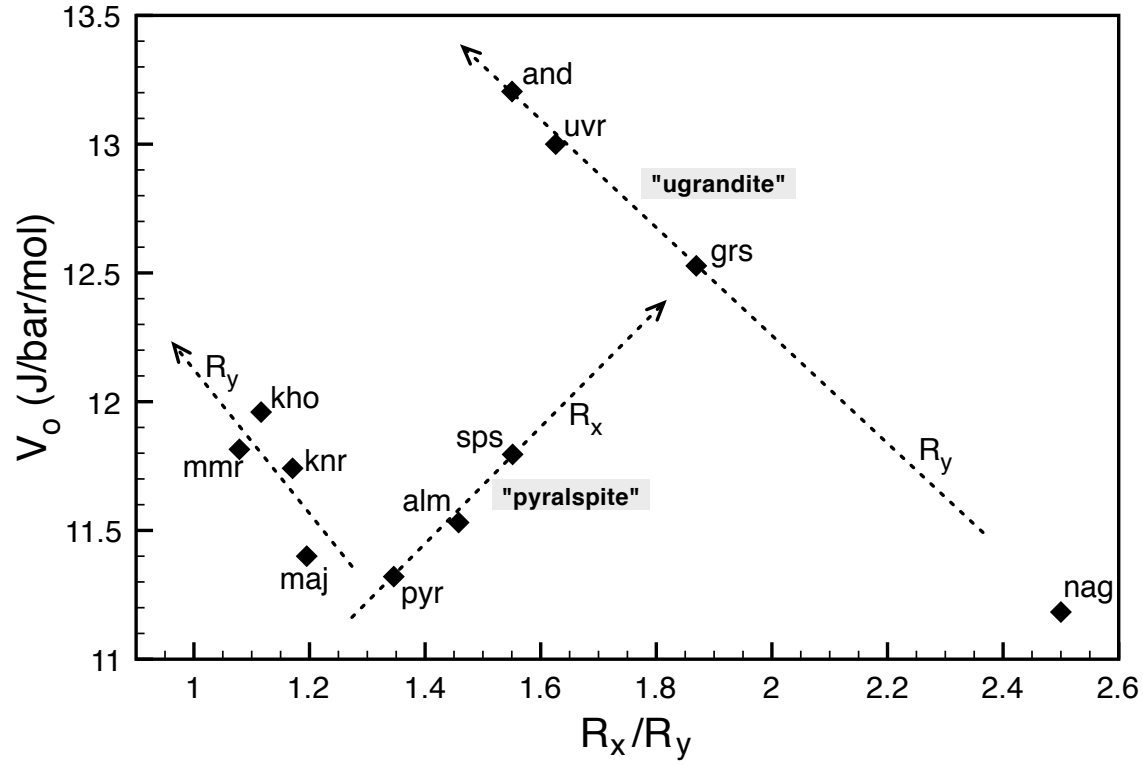
13.5
13
12.5
12
11.5
11
V_o (J/bar/mol)
1
1.2
1.4
1.6
1.8
2
2.2
2.4
2.6
R_x/R_y
and
uvr
"ugrandite"
grs
R_y
kho
mmr
knr
sps
R_x
R_y
alm
"pyralspite"
maj
pyr
nag

Fig. 7

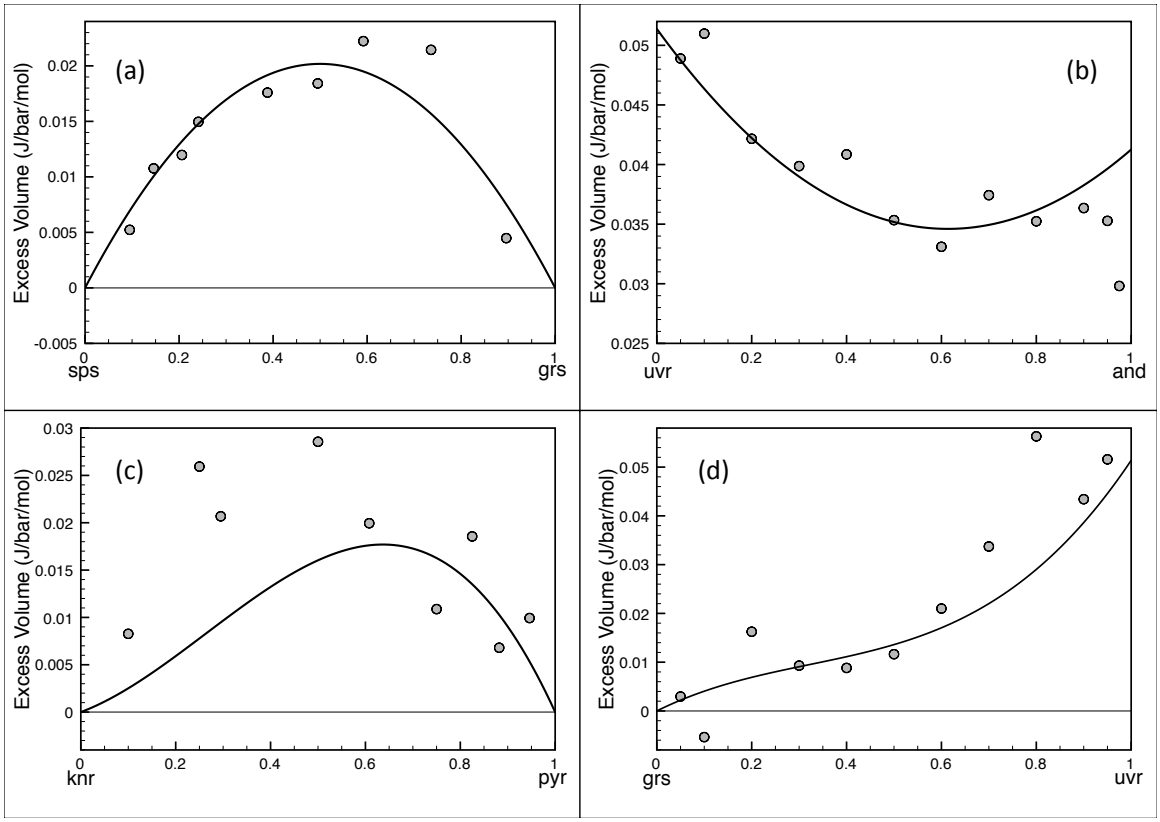
(a)
Excess Volume (J/bar/mol)
0.02
0.015
0.01
0.005
0
-0.005
0
0.2
0.4
0.6
0.8
1
sps
grs
(b)
Excess Volume (J/bar/mol)
0.05
0.045
0.04
0.035
0.03
0.025
uvr
and
(c)
Excess Volume (J/bar/mol)
0.03
0.025
0.02
0.015
0.01
0.005
knr
pyr
(d)
Excess Volume (J/bar/mol)
grs
uvr

Fig. 8

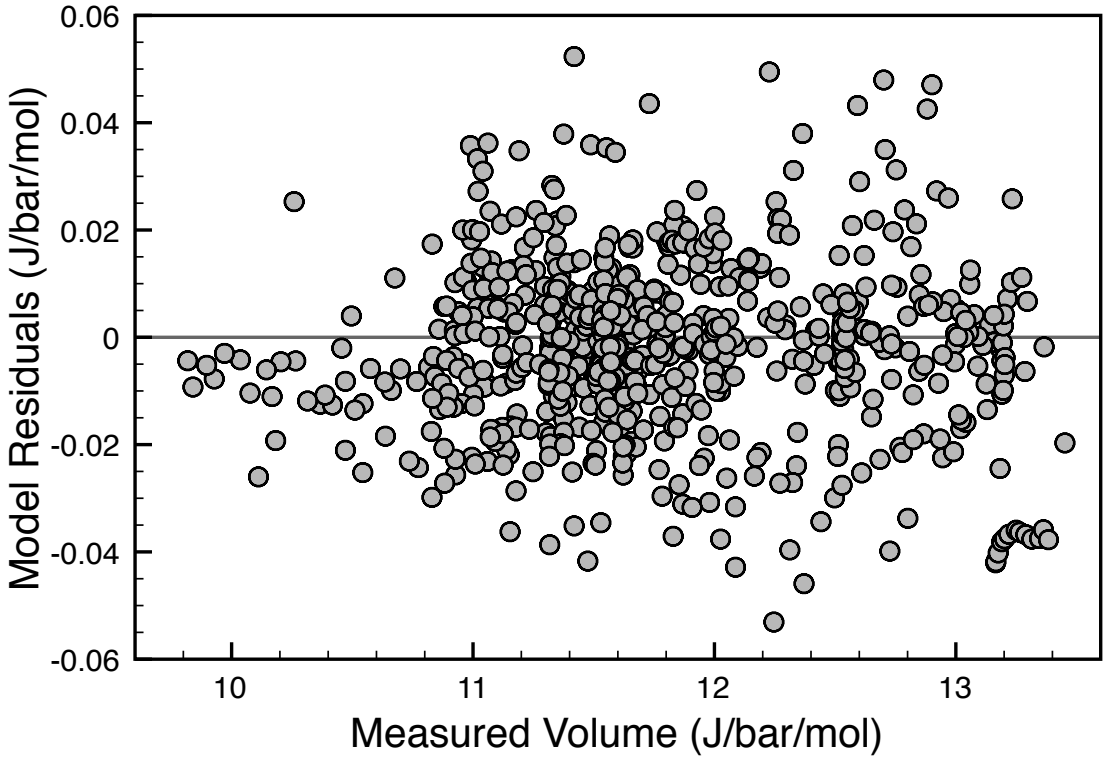
0.06
0.04
0.02
0
-0.02
-0.04
-0.06
Model Residuals (J/bar/mol)
10
11
12
13
Measured Volume (J/bar/mol)

Fig. 9

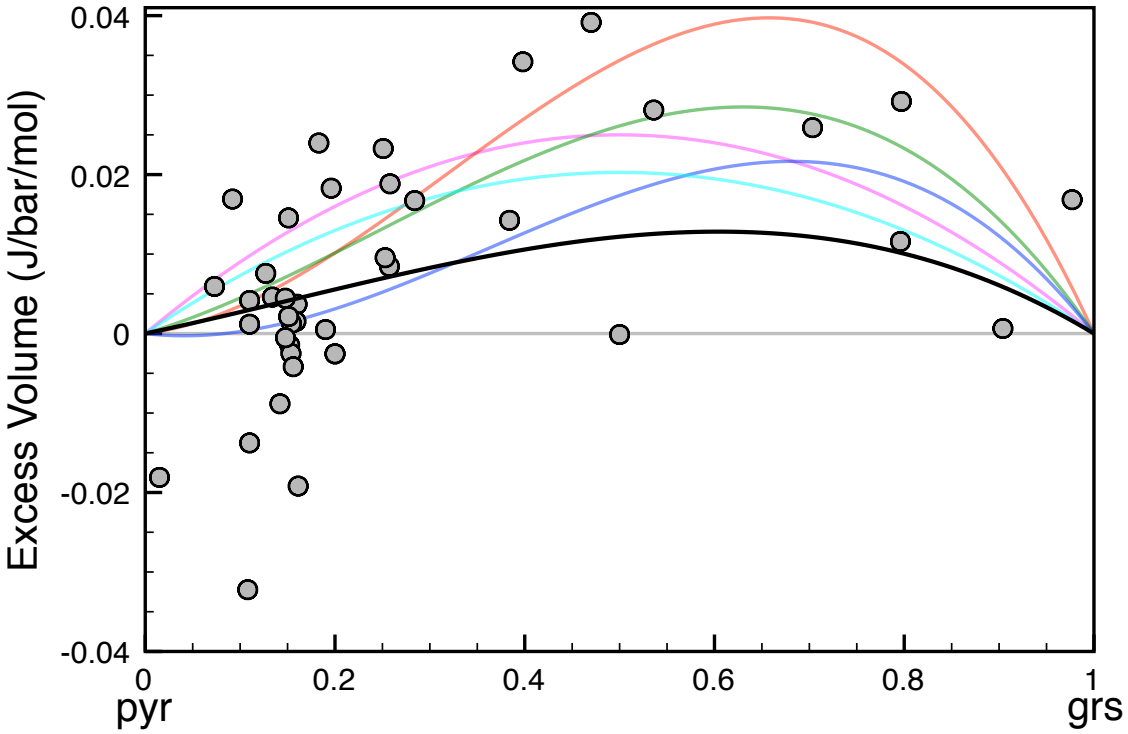
0.04
0.02
0
-0.02
-0.04
Excess Volume (J/bar/mol)
0
0.2
0.4
0.6
0.8
1
pyr
grs

Fig. 10

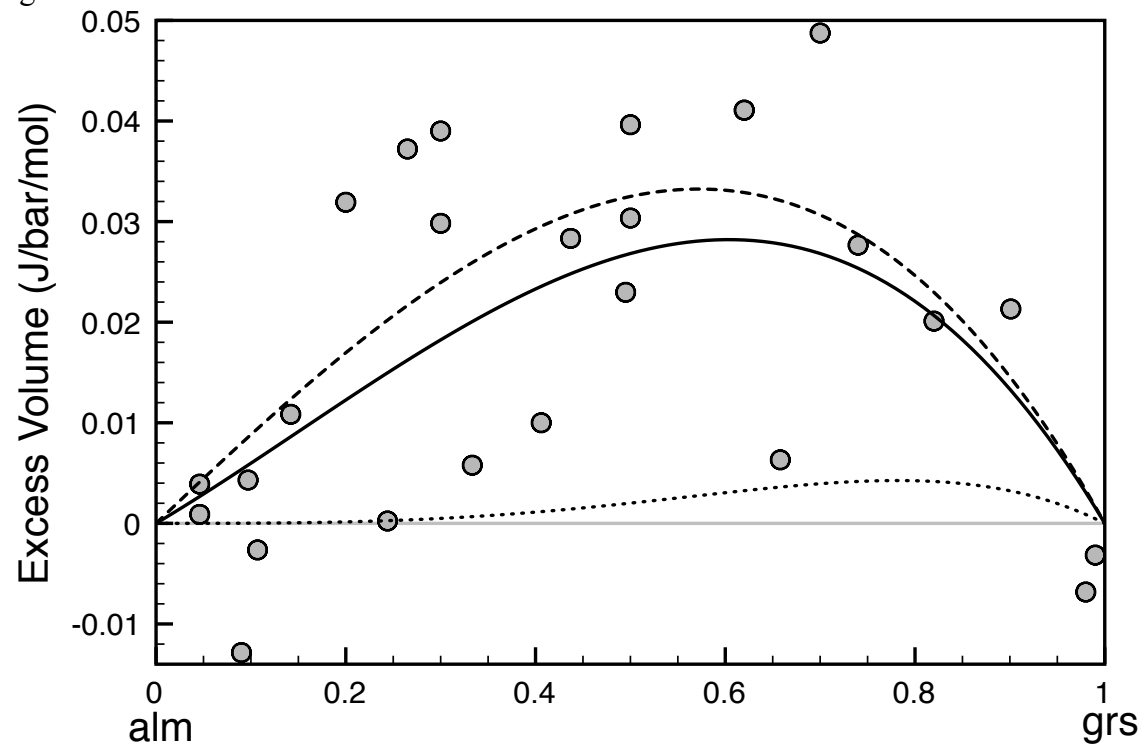
0.05
0.04
0.03
0.02
0.01
0
-0.01
Excess Volume (J/bar/mol)
0
0.2
0.4
0.6
0.8
1
alm
grs

Fig. 11

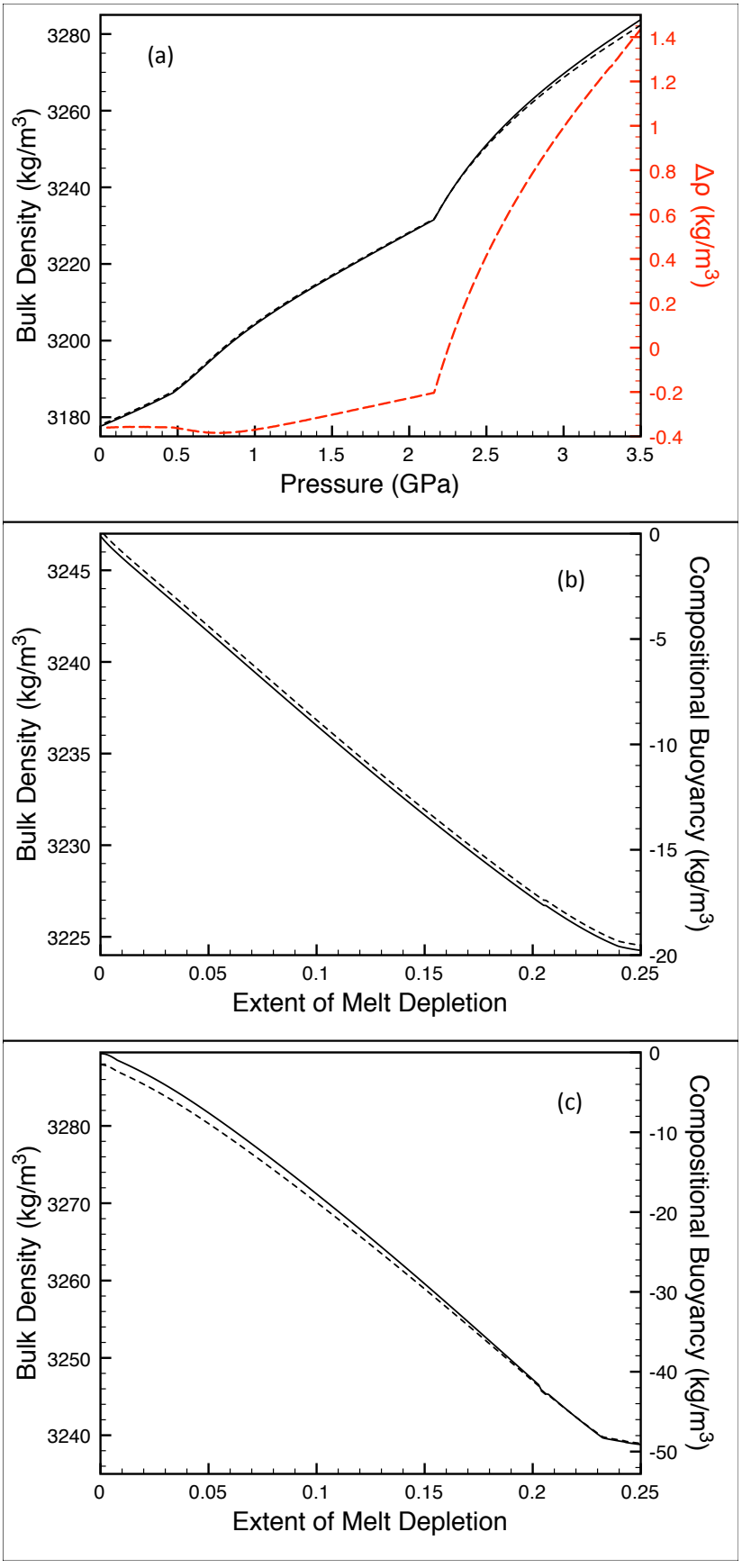
(a)
Bulk Density (kg/m3)
Δρ (kg/m3)
Pressure (GPa)
(b)
Bulk Density (kg/m3)
Compositional Buoyancy (kg/m3)
Extent of Melt Depletion
(c)
Bulk Density (kg/m3)
Compositional Buoyancy (kg/m3)
Extent of Melt Depletion

Fig. 12

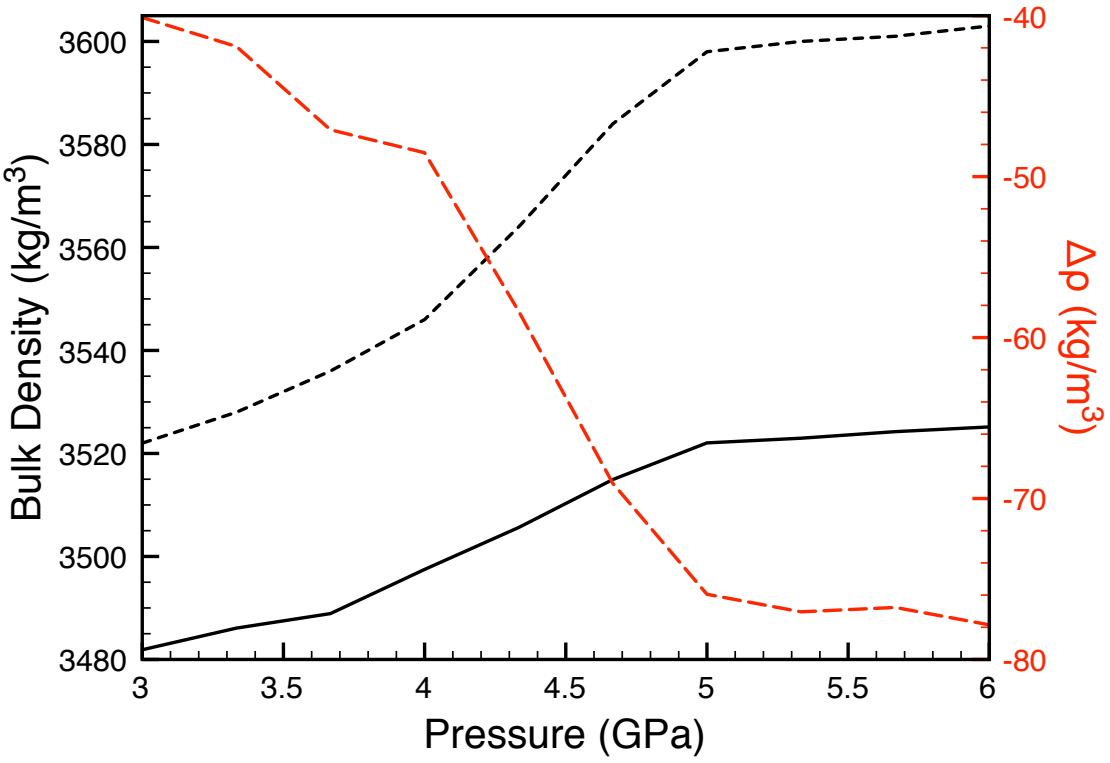
Bulk Density (kg/m3)
Δρ (kg/m3)
Pressure (GPa)
3600
3580
3560
3540
3520
3500
3480
-40
-50
-60
-70
-80
3
3.5
4
4.5
5
5.5
6

Fig. 13

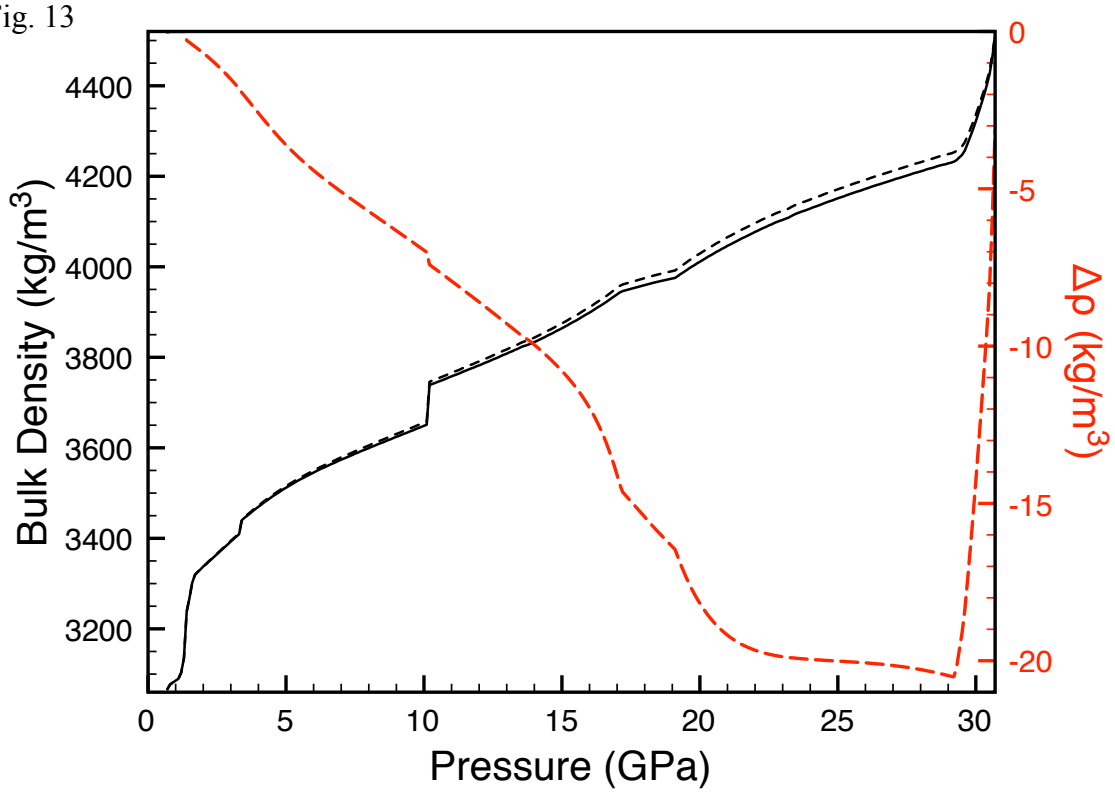
Bulk Density (kg/m3)
Δρ (kg/m3)
Pressure (GPa)
4400
4200
4000
3800
3600
3400
3200
0
-5
-10
-15
-20
0
5
10
15
20
25
30

Fig. 14

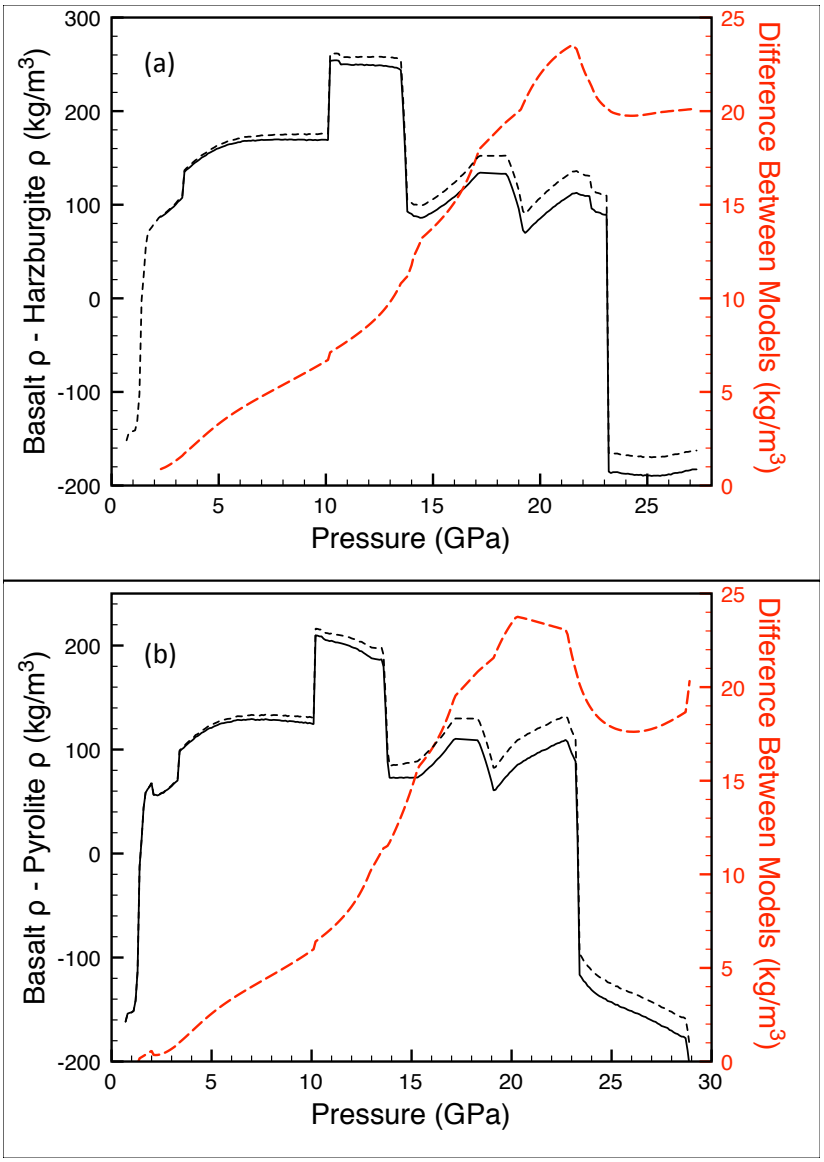
(a)
Basalt ρ - Harzburgite ρ (kg/m3)
Difference Between Models (kg/m3)
Pressure (GPa)
(b)
Basalt ρ - Pyrolite ρ (kg/m3)
Difference Between Models (kg/m3)
Pressure (GPa)

Supplement 1. Data sources used in model calibration*

(1) Akaogi M, Akimoto S (1977) Pyroxene-garnet solid-solution equilibria in the systems $Mg_4Si_4O_{12}$-$Mg_3Al_2Si_3O_{12}$ and $Fe_4Si_4O_{12}$-$Fe_3Al_2Si_3O_{12}$ at high pressures and temperatures. Phys Earth Planet Inter 15:90–106

(2) Andrut M, Wildner M (2002) The crystal chemistry of birefringent natural uvarovites. Part III. Application of the superposition model of crystal fields with a characterization of synthetic cubic uvarovite. Phys Chem Miner 29:595–608

(3) Anovitz LM, Essene EJ, Metz GW, Bohlen SR, Westrum Jr EF, Hemingway BS (1993) Heat capacity and phase equilibria of almandine, $Fe_3Al_2Si_3O_{12}$. Geochim Cosmochim Acta 57:4191–4204

(4) Armbruster T, Geiger CA (1993) Andradite crystal chemistry, dynamic X-site disorder and structural strain in silicate garnets. Eur J Mineral 5:59–71

(5) Armbruster T, Geiger CA, Lager GA (1992) Single-crystal X-ray structure study of synthetic pyrope almandine garnets at 100 and 293 K. Am Mineral 77:512–521

(6) Armbruster T, Birrer J, Libowitzky E, Beran A (1998) Crystal chemistry of Ti-bearing andradites. Eur J Mineral 10:907–921

(7) Bass JD (1986) Elasticity of uvarovite and andradite garnets. J Geophys Res 91:7505–7516

(8) Bass JD (1989) Elasticity of grossular and spessartite garnets by Brillouin spectroscopy. J Geophys Res 94:7621–7628

(9) Bobrov AV, Litvin YA, Bindi L, Dymshits AM (2008) Phase relations and formation of sodium-rich majoritic garnet in the system $Mg_3Al_2Si_3O_{12}$–$Na_2MgSi_5O_{12}$ at 7.0 and 8.5 GPa. Contrib Mineral Petrol 156:243–257

(10) Bohlen SR, Wall VJ, Boettcher AL (1983) Experimental investigation and application of garnet granulite equilibria. Contrib Mineral Petrol 83:52–61

(11) Bosenick A, Geiger CA (1997) Powder X ray diffraction study of synthetic pyrope-grossular garnets between 20 and 295 K. J Geophys Res 102:22649–22657

(12) Bosenick A, Geiger CA, Philips BL (1999) Local Ca-Mg distribution of Mg-rich pyrope-grossular garnets synthesized at different temperatures revealed by 29 Si MAS NMR spectroscopy. Am Mineral 84:1422–1432

* Number in parentheses corresponds to Reference # in Supplement 2

(13) Boyd FR, England JL (1959) Pyrope. Carnegie Inst Year B 58:83–87

(14) Cressey G, Schmid R, Wood BJ (1978) Thermodynamic properties of almandine-grossular garnet solid solutions. Contrib Mineral Petrol:397–404

(15) Fursenko BA (1981) Synthesis of new high pressure garnets: $Mn_3Cr_2Si_3O_{12}$ and $Fe_3Cr_2Si_3O_{12}$. Bull Mineral 104:418–422

(16) Ganguly J, Kennedy GC (1974) The energetics of natural garnet solid solution. Contrib Mineral Petrol 48:137–148

(17) Ganguly J, Cheng W, O'Neill HStC (1993) Syntheses, volume, and structural changes of garnets in the pyrope-grossular join: Implications for stability and mixing properties. Am Mineral 78:583–593

(18) Geiger CA, Armbruster T (1997) $Mn_3Al_2Si_3O_{12}$ spessartine and $Ca_3Al_2Si_3O_{12}$ grossular garnet: Structural dynamic and thermodynamic properties. Am Mineral 82:740–747

(19) Geiger CA, Feenstra A (1997) Molar volumes of mixing of almandine-pyrope and almandine-spessartine garnets and the crystal chemistry and thermodynamic-mixing properties of the aluminosilicate garnets. Am Mineral 82:571–581

(20) Geiger CA, Newton RC, Kleppa OJ (1987) Enthalpy of mixing of synthetic almandine-grossular and almandine-pyrope garnets from high-temperature solution calorimetry. Geochim Cosmochim Acta 51:1755–1763

(21) Geiger CA, Langer K, Bell DR, Rossman GR, Winkler B (1991) The hydroxide component in synthetic pyrope. Am Mineral 76:49–59

(22) Geiger CA, Merwin L, Sebald A (1992) Structural investigation of pyrope garnet using temperature-dependent FTIR and ^{29}Si and ^{27}Al MAS NMR spectroscopy. Am Mineral 77:713–717

(23) Gibbs GV, Smith JV (1965) Refinement of the crystal structure of synthetic pyrope. Am Mineral 50:2023–2039

(24) Haselton Jr HT, Westrum Jr EF (1980) Low-temperature heat capacities of synthetic pyrope, grossular, and pyrope60grossular40. Geochim Cosmochim Acta 44:701–709

(25) Hazen RM, Finger LW (1978) Crystal structures and compressibilities of pyrope and grossular to 60 kbar. Am Mineral 63:297–303

(26) Hazen RM, Downs RT, Conrad PG, Finger LW, Gasparik T (1994) Comparative compressibilities of majorite-type garnets. Phys Chem Miner 21:344–349

(27) Heinemann S, Sharp TG, Seifert F, Rubie DC (1997) The cubic-tetragonal phase transition in the system majorite ($Mg_4Si_4O_{12}$)-pyrope ($Mg_3Al_2Si_3O_{12}$), and garnet symmetry in the Earth's transition zone. Phys Chem Miner 24:206–221

(28) Hensen BJ, Schmid R, Wood BJ (1975) Activity-composition relationships for pyrope-grossular garnet. Contrib Mineral Petrol 51:161–166

(29) Hsu LC (1968) Selected phase relationships in the system Al-Mn-Fe-Si-O-H: A model for garnet equilibria. J Petrol 9:40–83

(30) Huckenholz HG (1975) Uvarovite stability in the $CaSiO_3$-Cr_2O_3 join up to 10 kbar. Neues Jahrb Mineral Monatshefte 1975:337–360

(31) Huckenholz HG, Knittel D (1975) Uvarovite: Stability of uvarovite-grossularite solid solution at low pressure. Contrib Mineral Petrol 49:211–232

(32) Huckenholz HG, Knittel D (1976) Uvarovite: Stability of uvarovite-andradite solid solutions at low pressure. Contrib Mineral Petrol 56:61–76

(33) Irifune T, Hariya Y (1983) Phase relationships in the system $Mg_3Al_2Si_3O_{12}$-$Mg_3Cr_2Si_3O_{12}$ at high pressure and some mineralogical properties of synthetic garnet solid solutions. Mineral J 11:269–281

(34) Irifune T, Ohtani E, Kumazawa M (1982) Stability field of knorringite $Mg_3Cr_2Si_3O_{12}$ at high pressure and its implication to the occurrence of Cr-rich pyrope in the upper mantle. Phys Earth Planet Inter 27:263–272

(35) Isaak DG, Graham EK (1976) The elastic properties of an almandine-spessartine garnet and elasticity in the garnet solid solution series. J Geophys Res 81:2483–2489

(36) Jiang F, Speziale S, Duffy TS (2004a) Single-crystal elasticity of grossular- and almandine-rich garnets to 11 GPa by Brillouin scattering. J Geophys Res 109:B10210. doi:10.1029/2004JB003081

(37) Jiang F, Speziale S, Shieh SR, Duffy TS (2004b) Single-crystal elasticity of andradite garnet to 11 GPa. J Phys: Condens Matter 16:S1041–S1052. doi:10.1088/0953-8984/16/14/014

(38) Juhin A, Morin G, Elkaim E, Frost DJ, Fialin M, Juillot F, Calas G (2010) Structure refinement of a synthetic knorringite, $Mg_3(Cr_{0.8}Mg_{0.1}Si_{0.1})_2(SiO_4)_3$. Am Mineral 95:59–63

(39) Karpinskaya TB, Ostrovskiy IA, Yevstigneyeva TL (1983) Synthetic pure iron garnet skiagite. Int Geol Rev 25:1129–1130

(40) Kavner A (2007) Garnet yield strength at high pressures and implications for upper mantle and transition zone rheology. J Geophys Res 112:B12207. doi:10.1029/2007JB004931

(41) Koziol AM (1990) Activity-composition relationships of binary Ca-Fe and Ca-Mn garnets determined by reversed, displaced equilibrium experiments. Am Mineral 75:319–327

(42) Koziol AM, Newton RC (1989) Grossular activity-composition relationships in ternary garnets determined by reversed displaced-equilibrium experiments. Contrib Mineral Petrol 103:423–433

(43) Krupka KM, Robie RA, Hemingway BS (1979) High-temperature heat capacities of corundum, periclase, anorthite, $CaAl_2Si_2O_8$ glass, muscovite, pyrophyllite, $KAlSi_3O_8$ glass, grossular, and $NaAlSi_3O_8$ glass. Am Mineral 64:86–101

(44) Leitner BJ, Weidner DJ, Liebermann RC (1980) Elasticity of single crystal pyrope and implications for garnet solid solution series. Phys Earth Planet Inter 22:111–121

(45) Levien L, Prewitt CT, Weidner DJ (1979) Compression of pyrope. Am Mineral 64:805–808

(46) Meagher EP (1975) The crystal structures of pyrope and grossularite at elevated temperatures. Am Mineral 60:218–228

(47) Merli M, Ungaretti L, Oberti R (2000) Leverage analysis and structure refinement of minerals. Am Mineral 85:532–542

(48) Nakatsuka A, Yoshiasa A, Yamanaka T, Ohtaka O, Katsura T, Ito E (1999) Symmetry change of majorite solid solution in the system $Mg_3Al_2Si_3O_{12}$-$MgSiO_3$. Am Mineral 84:1135–1143

(49) Newton RC, Charlu TV, Kleppa OJ (1977) Thermochemistry of high pressure garnets and clinopyroxenes in the system CaO-MgO-Al_2O_3-SiO_2. Geochim Cosmochim Acta 41:369–377

(50) Nishizawa H, Shimada M, Matsuoka K, Koizumi M (1977) Infrared and Mössbauer spectra of synthetic garnets $A_3Fe_2Si_3O_{12}$(A:Mn,Cd,Ca). Bull Chem Soc Jpn 50:3186–3188

(51) Novak GA, Gibbs GV (1971) The crystal chemistry of the silicate garnets. Am Mineral 56:791–825

(52) O'Neill B, Bass JD, Smyth JR, Vaughan MT (1989) Elasticity of a grossular-pyrope-almandine garnet. J Geophys Res 94:17819–17824

(53) O'Neill B, Bass JD, Rossman GR, Geiger CA, Langer K (1991) Elastic properties of pyrope. Phys Chem Miner 17:617–621

(54) Olijnyk H, Paris E, Geiger CA, Lager GA (1991) Compressional study of katoite [$Ca_3Al_2(O_4H_4)_3$] and grossular garnet. J Geophys Res 96:14313–14318

(55) Pacalo REG, Weidner DJ, Gasparik T (1992) Elastic properties of sodium-rich majorite garnet. Geophys Res Lett 19:1895–1898

(56) Parise JB, Wang Y, Gwanmesia GD, Zhang J, Sinelnikov Y, Chmielowski J, Weidner DJ, Liebermann RC (1996) The symmetry of garnets on the pyrope ($Mg_3Al_2Si_3O_{12}$)-majorite ($MgSiO_3$) join. Geophys Res Lett 23:3799–3802

(57) Pavese A, Artioli G, Prencipe M (1995) X-ray single-crystal diffraction study of pyrope in the temperature range 30-973 K. Am Mineral 80:457–464

(58) Quartieri S, Chaboy J, Merli M, Oberti R, Ungaretti L (1995) Local structural environment of calcium in garnets: a combined structure-refinement and XANES investigation. Phys Chem Miner 22:159–169

(59) Quartieri S, Oberti R, Boiocchi M, Dalconi MC, Boscherini F, Safonova O, Woodland AB (2006) Site preference and local geometry of Sc in garnets: Part II. The crystal-chemistry of octahedral Sc in the andradite-$Ca_3Sc_2Si_3O_{12}$ join. Am Mineral 91:1240–1248

(60) Rakai RJ (1975) Crystal structure of spessartine and andradite at elevated temperatures. Dissertation, University of British Columbia

(61) Resende JALC, Fernandes NG (2005) X-ray powder refinement of a natural garnet from Diamantina, Minas Gerais, Brazil. Acta Crystallogr Sect E: Struct Rep Online 61:i265–i267

(62) Ringwood AE (1977) Synthesis of pyrope-knorringite solid solution series. Earth Planet Sci Lett 36:443–448

(63) Ringwood AE, Major A (1971) Synthesis of majorite and other high pressure garnets and perovskites. Earth Planet Sci Lett 12:411–418

(64) Rodehorst U, Geiger CA, Armbruster T (2002) The crystal structures of grossular and spessartine between 100 and 600 K and the crystal chemistry of grossular-spessartine solid solutions. Am Mineral 87:542–549

(65) Schreyer W, Seifert F (1969) High-pressure phases in the system MgO-Al_2O_3-SiO_2-H_2O. Am J Sci 267-A:407–443

(66) Shtukenberg AG, Punin YO, Frank-Kamenetskaya OV, Kovalev OG, Sokolov PB (2001) On the origin of anomalous birefringence in grandite garnets. Mineral Mag 65:445–459

(67) Sinogeikin SV, Bass JD, O'Neill B, Gasparik T (1997) Elasticity of tetragonal end-member majorite and solid solutions in the system $Mg_4Si_4O_{12}$-$Mg_3Al_2Si_3O_{12}$. Phys Chem Miner 24:115–121

(68) Skinner BJ (1956) Physical properties of end-members of the garnet group. Am Mineral 41:428–436

(69) Soga N (1967) Elastic constants of garnet under pressure and temperature. J Geophys Res 72:4227–4234

(70) Takahashi T, Liu L (1970) Compression of ferromagnesian garnets and the effect of solid solutions on the bulk modulus. J Geophys Res 75:5757–5766

(71) Taran MN, Langer K, Abs-Wurmbach I, Frost DJ, Platonov AN (2004) Local relaxation around $^{[6]}Cr^{3+}$ in synthetic pyrope-knorringite garnets, $^{[8]}Mg_3{}^{[6]}(Al_{1-X}Cr_X{}^{3+})_2{}^{[4]}Si_3O_{12}$, from electronic absorption spectra. Phys Chem Miner 31:650–657

(72) Thieblot L, Roux J, Richet P (1998) High-temperature thermal expansion and decomposition of garnets. Eur J Mineral 10:7–15

(73) Wang Y, Weidner DJ, Zhang J, Gwanrnesia GD, Liebermann RC (1998) Thermal equation of state of garnets along the pyrope-majorite join. Phys Earth Planet Inter 105:59–71

(74) Wood BJ (1988) Activity measurements and excess entropy-volume relationships for pyrope-grossular garnets. J Geol 96:721–729

(75) Woodland AB, O'Neill HStC (1993) Synthesis and stability of $Fe^{2+}{}_3Fe^{3+}{}_2Si_3O_{12}$ garnet and phase relations with $Fe_3Al_2Si_3O_{12}$-$Fe^{2+}{}_3Fe^{3+}{}_2Si_3O_{12}$ solutions. Am Mineral 78:1002–1015

(76) Woodland AB, O'Neill HStC (1995) Phase relations between $Ca_3Fe_2{}^{3+}Si_3O_{12}$-$Fe_3{}^{2+}Fe_2{}^{3+}Si_3O_{12}$ garnet and $CaFeSi_2O_6$-$Fe_2Si_2O_6$ pyroxene solid solutions. Contrib Mineral Petrol 121:87–98

(77) Woodland AB, Ross II CR (1994) A crystallographic and Mössbauer spectroscopy study of $Fe_3{}^{2+}Al_2Si_3O_{12}$-$Fe_3{}^{2+}Fe_2{}^{3+}Si_3O_{12}$ (almandine-"skiagite") and $Ca_3Fe_2{}^{3+}Si_3O_{12}$-$Fe_3{}^{2+}Fe_2{}^{3+}Si_3O_{12}$ (andradite -"skiagite") garnet solid solutions. Phys Chem Miner 21:117–132

(78) Woodland AB, Bauer M, Ballaran TB, Hanrahan M (2009) Crystal chemistry of $Fe_3^{2+}Cr_2Si_3O_{12}$-$Fe_3^{2+}Fe_2^{3+}Si_3O_{12}$ garnet solid solutions and related spinels. Am Mineral 94:359–366

(79) Yagi T, Akaogi M, Shimomura O, Tamai H, Akimoto S (1987) High pressure and high temperature equations of state of majorite. In: Manghnani MH, Syono Y (eds) High-pressure research in mineral physics, Geophys Monogr 39, AGU, Washington DC, pp 141-147

(80) Zhang L, Ahsbahs H, Kutoglu A (1998) Hydrostatic compression and crystal structure of pyrope to 33 GPa. Phys Chem Miner 25:301–307

(81) Zhang L, Ahsbahs H, Kutoglu A, Geiger CA (1999) Single-crystal hydrostatic compression of synthetic pyrope, almandine, spessartine, grossular and andradite garnets at high pressures. Phys Chem Miner 27:52–58

Supplement 2. Data used in model calibration

Reference # (see Supplement 1)	AMCSD ID[a]	*a* (Å)	*V* (J/bar/mol)	*V residuals* (J/bar/mol)	*P* (GPa)	*T* (°C)	cations per formula unit									
							Si	Ti	Al	Fe^{3+}	Cr	Fe^{2+}	Mn	Mg	Ca	Na
1	-	11.457(1)	11.321	0.00000	0.0001	25	3.000	0.000	2.000	0.000	0.000	0.000	0.000	3.000	0.000	0.000
1	-	11.526(1)	11.526	-0.00434	0.0001	25	3.000	0.000	2.000	0.000	0.000	3.000	0.000	0.000	0.000	0.000
1	-	11.461(1)	11.333	-0.01086	0.0001	25	3.177	0.000	1.646	0.000	0.000	0.000	0.000	3.177	0.000	0.000
1	-	11.459(1)	11.327	-0.00245	0.0001	25	3.062	0.000	1.876	0.000	0.000	0.000	0.000	3.062	0.000	0.000
1	-	11.536(1)	11.557	0.00483	0.0001	25	3.152	0.000	1.696	0.000	0.000	3.152	0.000	0.000	0.000	0.000
2	8734	11.997(1)	12.999	0.00071	0.0001	20	3.000	0.000	0.000	0.000	2.000	0.000	0.000	0.000	3.000	0.000
3	-	11.521(1)	11.511	-0.02113	0.0001	25	3.001	0.000	1.993	0.000	0.000	3.009	0.000	0.000	0.000	0.000
4	6471	12.063(1)	13.214	0.00718	0.0001	20	3.000	0.000	0.000	2.000	0.000	0.000	0.000	0.000	3.000	0.000
4	6472	12.068(1)	13.230	0.01024	0.0001	77	3.000	0.000	0.000	2.000	0.000	0.000	0.000	0.000	3.000	0.000
4	6473	12.081(1)	13.273	0.01117	0.0001	227	3.000	0.000	0.000	2.000	0.000	0.000	0.000	0.000	3.000	0.000
4	6474	11.476(1)	11.377	0.00755	0.0001	227	3.000	0.000	2.000	0.000	0.000	0.000	0.000	3.000	0.000	0.000
5	1468	11.516(2)	11.497	0.00867	0.0001	20	3.000	0.000	2.000	0.000	0.000	2.400	0.000	0.600	0.000	0.000
5	1469	11.525(1)	11.523	-0.00639	0.0001	20	3.000	0.000	2.000	0.000	0.000	3.000	0.000	0.000	0.000	0.000
5	1465	11.452(1)	11.306	-0.01383	0.0001	20	3.000	0.000	2.000	0.000	0.000	0.000	0.000	3.000	0.000	0.000
5	1466	11.473(2)	11.368	0.00645	0.0001	20	3.000	0.000	2.000	0.000	0.000	0.600	0.000	2.400	0.000	0.000
5	1467	11.485(2)	11.404	0.00013	0.0001	20	3.000	0.000	2.000	0.000	0.000	1.200	0.000	1.800	0.000	0.000
6	6759	11.764(1)	12.255	0.02529	0.0001	20	2.982	0.014	1.702	0.272	0.000	0.729	0.690	0.006	1.587	0.000
7	-	12.054(2)	13.184	0.00103	0.0001	25	3.000	0.000	0.080	1.920	0.000	0.000	0.000	0.009	2.991	0.000
7	-	11.997	12.998	-0.00132	0.0001	25	3.000	0.000	0.000	0.000	2.000	0.000	0.000	0.000	3.000	0.000
8	-	11.848(7)	12.520	-0.01100	0.0001	25	3.000	0.000	1.984	0.016	0.000	0.000	0.006	0.000	2.994	0.000
8	-	11.617(3)	11.802	0.01798	0.0001	25	3.000	0.000	2.000	0.000	0.000	0.150	2.844	0.000	0.006	0.000
9	-	11.456(1)	11.318	-0.03867	0.0001	25	3.164	0.000	1.790	0.000	0.000	0.000	0.000	2.860	0.000	0.198
10	-	11.639(1)	11.869	-0.01428	0.0001	25	3.000	0.000	2.000	0.000	0.000	2.000	0.000	0.000	1.000	0.000

11	-	11.4553(3)	11.3157	-0.00444	0.0001	22	3.000	0.000	2.000	0.000	0.000	0.000	0.000	3.000	0.000	0.000
11	-	11.4992(4)	11.4463	-0.00294	0.0001	22	2.985	0.000	1.972	0.000	0.000	0.002	0.000	2.757	0.311	0.000
11	-	11.5578(4)	11.6222	-0.02567	0.0001	22	3.057	0.000	1.968	0.000	0.000	0.002	0.000	2.152	0.780	0.000
11	-	11.6670(5)	11.9547	0.00405	0.0001	22	3.026	0.000	1.977	0.000	0.000	0.001	0.000	1.455	1.526	0.000
11	-	11.7665(4)	12.2632	0.02214	0.0001	22	3.022	0.000	1.989	0.000	0.000	0.001	0.000	0.730	2.241	0.000
11	-	11.8163(5)	12.4195	0.00136	0.0001	22	2.996	0.000	1.976	0.000	0.000	0.001	0.000	0.294	2.749	0.000
11	-	11.8510(5)	12.5293	0.00236	0.0001	22	3.000	0.000	2.000	0.000	0.000	0.000	0.000	0.000	3.000	0.000
12	-	11.5223(10)	11.5154	-0.00247	0.0001	25	2.980	0.000	1.995	0.000	0.000	0.002	0.000	2.563	0.482	0.000
12	-	11.5195(11)	11.5070	-0.00293	0.0001	25	2.989	0.000	2.025	0.000	0.000	0.001	0.000	2.522	0.462	0.000
12	-	11.5191(5)	11.5058	-0.00178	0.0001	25	2.970	0.000	2.014	0.000	0.000	0.001	0.000	2.579	0.458	0.000
12	-	11.5185(5)	11.5040	-0.00540	0.0001	25	2.995	0.000	1.991	0.000	0.000	0.001	0.000	2.562	0.459	0.000
12	-	11.5187(6)	11.5046	-0.00650	0.0001	25	2.996	0.000	1.990	0.000	0.000	0.001	0.000	2.559	0.463	0.000
12	-	11.5169(4)	11.4992	-0.00434	0.0001	25	2.982	0.000	2.006	0.000	0.000	0.001	0.000	2.579	0.447	0.000
12	-	11.5191(5)	11.5058	-0.00835	0.0001	25	2.988	0.000	1.994	0.000	0.000	0.001	0.000	2.562	0.472	0.000
12	-	11.5186(4)	11.5043	0.00048	0.0001	25	3.003	0.000	1.984	0.000	0.000	0.001	0.000	2.574	0.444	0.000
12	-	11.5163(6)	11.4974	-0.02348	0.0001	25	2.989	0.000	1.987	0.000	0.000	0.001	0.000	2.553	0.488	0.000
12	-	11.5120(7)	11.4845	-0.01268	0.0001	25	2.997	0.000	1.982	0.000	0.000	0.001	0.000	2.603	0.428	0.000
12	-	11.5579(15)	11.6225	-0.02221	0.0001	25	2.994	0.000	1.970	0.000	0.000	0.001	0.000	2.263	0.793	0.000
12	-	11.5662(6)	11.6475	0.01673	0.0001	25	2.974	0.000	2.009	0.000	0.000	0.001	0.000	2.277	0.761	0.000
12	-	11.5636(9)	11.6397	0.00122	0.0001	25	3.015	0.000	1.992	0.000	0.000	0.001	0.000	2.213	0.768	0.000
12	-	11.5622(6)	11.6354	0.00256	0.0001	25	2.989	0.000	2.009	0.000	0.000	0.001	0.000	2.246	0.761	0.000
13	-	11.456(2)	11.318	-0.00296	0.0001	25	3.000	0.000	2.000	0.000	0.000	0.000	0.000	3.000	0.000	0.000
14	-	11.526(1)	11.526	-0.00434	0.0001	25	3.000	0.000	2.000	0.000	0.000	3.000	0.000	0.000	0.000	0.000
14	-	11.553(1)	11.608	-0.01820	0.0001	25	3.000	0.000	2.000	0.000	0.000	2.730	0.000	0.000	0.270	0.000
14	-	11.604(1)	11.762	0.01966	0.0001	25	3.000	0.000	2.000	0.000	0.000	2.400	0.000	0.000	0.600	0.000
14	-	11.636(1)	11.860	0.01159	0.0001	25	3.000	0.000	2.000	0.000	0.000	2.100	0.000	0.000	0.900	0.000
14	-	11.639(1)	11.869	0.02076	0.0001	25	3.000	0.000	2.000	0.000	0.000	2.100	0.000	0.000	0.900	0.000

14	-	11.704(1)	12.069	0.01281	0.0001	25	3.000	0.000	2.000	0.000	0.000	1.500	0.000	0.000	1.500	0.000
14	-	11.701(1)	12.060	0.00353	0.0001	25	3.000	0.000	2.000	0.000	0.000	1.500	0.000	0.000	1.500	0.000
14	-	11.743(1)	12.190	0.01291	0.0001	25	3.000	0.000	2.000	0.000	0.000	1.140	0.000	0.000	1.860	0.000
14	-	11.743(1)	12.190	0.01291	0.0001	25	3.000	0.000	2.000	0.000	0.000	1.140	0.000	0.000	1.860	0.000
14	-	11.771(1)	12.277	0.02192	0.0001	25	3.000	0.000	2.000	0.000	0.000	0.900	0.000	0.000	2.100	0.000
14	-	11.800(1)	12.368	-0.00055	0.0001	25	3.000	0.000	2.000	0.000	0.000	0.540	0.000	0.000	2.460	0.000
14	-	11.842(1)	12.501	-0.00989	0.0001	25	3.000	0.000	2.000	0.000	0.000	0.060	0.000	0.000	2.940	0.000
14	-	11.849(1)	12.523	-0.00458	0.0001	25	3.000	0.000	2.000	0.000	0.000	0.000	0.000	0.000	3.000	0.000
15	-	11.766(2)	12.262	0.01937	0.0001	25	3.000	0.000	0.000	0.000	2.000	0.000	3.000	0.000	0.000	0.000
15	-	11.679(2)	11.992	0.01383	0.0001	25	3.000	0.000	0.000	0.000	2.000	3.000	0.000	0.000	0.000	0.000
16	-	11.462(3)	11.336	0.01483	0.0001	25	3.000	0.000	2.000	0.000	0.000	0.000	0.000	3.000	0.000	0.000
16	-	11.852(3)	12.532	0.00494	0.0001	25	3.000	0.000	2.000	0.000	0.000	0.000	0.000	0.000	3.000	0.000
16	-	11.657(2)	11.924	-0.01231	0.0001	25	3.000	0.000	2.000	0.000	0.000	0.000	0.000	1.500	1.500	0.000
17	1567	11.7445(3)	12.1945	0.01375	0.0001	20	3.000	0.000	2.000	0.000	0.000	0.000	0.000	0.888	2.106	0.000
17	1568	11.7817(3)	12.3108	0.01906	0.0001	20	3.000	0.000	2.000	0.000	0.000	0.000	0.000	0.609	2.391	0.000
17	1570	11.8515(2)	12.5309	0.00432	0.0001	20	3.000	0.000	2.000	0.000	0.000	0.000	0.000	0.000	3.000	0.000
17	1564	11.4566(2)	11.3195	-0.00020	0.0001	20	3.000	0.000	2.000	0.000	0.000	0.000	0.000	3.000	0.000	0.000
17	1565	11.5420(4)	11.5746	0.01285	0.0001	20	3.000	0.000	2.000	0.000	0.000	0.000	0.000	2.412	0.588	0.000
17	1566	11.5670(2)	11.6499	0.01168	0.0001	20	3.000	0.000	2.000	0.000	0.000	0.000	0.000	2.226	0.774	0.000
17	-	11.4883(2)	11.4137	0.00398	0.0001	20	3.000	0.000	2.000	0.000	0.000	0.000	0.000	2.781	0.219	0.000
17	-	11.5125(4)	11.4860	0.00092	0.0001	20	3.000	0.000	2.000	0.000	0.000	0.000	0.000	2.598	0.402	0.000
17	-	11.6156(4)	11.7974	0.00400	0.0001	20	3.000	0.000	2.000	0.000	0.000	0.000	0.000	1.848	1.152	0.000
17	-	11.6800(2)	11.9947	0.01558	0.0001	20	3.000	0.000	2.000	0.000	0.000	0.000	0.000	1.392	1.608	0.000
18	1924	11.847(1)	12.517	-0.00995	0.0001	20	3.000	0.000	2.000	0.000	0.000	0.000	0.000	0.000	3.000	0.000
18	1925	11.872(1)	12.596	0.00660	0.0001	277	3.000	0.000	2.000	0.000	0.000	0.000	0.000	0.000	3.000	0.000
18	1927	11.619(1)	11.808	0.01360	0.0001	20	3.000	0.000	2.000	0.000	0.000	0.000	3.000	0.000	0.000	0.000
19	-	11.5283(6)	11.5334	0.00256	0.0001	25	3.000	0.000	2.000	0.000	0.000	3.000	0.000	0.000	0.000	0.000

19	-	11.5270(7)	11.5295	-0.00134	0.0001	25	3.000	0.000	2.000	0.000	0.000	3.000	0.000	0.000	0.000	0.000
19	-	11.5369(12)	11.5592	0.00697	0.0001	25	3.000	0.000	2.000	0.000	0.000	2.757	0.243	0.000	0.000	0.000
19	-	11.5366(8)	11.5583	0.00105	0.0001	25	3.000	0.000	2.000	0.000	0.000	2.700	0.300	0.000	0.000	0.000
19	-	11.5389(5)	11.5652	-0.00499	0.0001	25	3.000	0.000	2.000	0.000	0.000	2.553	0.447	0.000	0.000	0.000
19	-	11.5405(4)	11.5700	0.00563	0.0001	25	3.000	0.000	2.000	0.000	0.000	2.619	0.381	0.000	0.000	0.000
19	-	11.5383(3)	11.5634	0.00087	0.0001	25	3.000	0.000	2.000	0.000	0.000	2.640	0.360	0.000	0.000	0.000
19	-	11.5523(3)	11.6056	0.00758	0.0001	25	3.000	0.000	2.000	0.000	0.000	2.238	0.762	0.000	0.000	0.000
19	-	11.5509(3)	11.6013	0.00415	0.0001	25	3.000	0.000	2.000	0.000	0.000	2.247	0.753	0.000	0.000	0.000
19	-	11.5504(2)	11.5998	0.00370	0.0001	25	3.000	0.000	2.000	0.000	0.000	2.259	0.741	0.000	0.000	0.000
19	-	11.5502(4)	11.5992	0.00204	0.0001	25	3.000	0.000	2.000	0.000	0.000	2.247	0.753	0.000	0.000	0.000
19	-	11.5745(3)	11.6726	0.00453	0.0001	25	3.000	0.000	2.000	0.000	0.000	1.443	1.557	0.000	0.000	0.000
19	-	11.5736(2)	11.6699	0.00446	0.0001	25	3.000	0.000	2.000	0.000	0.000	1.473	1.527	0.000	0.000	0.000
19	-	11.5753(4)	11.6750	0.00828	0.0001	25	3.000	0.000	2.000	0.000	0.000	1.458	1.542	0.000	0.000	0.000
19	-	11.5757(2)	11.6762	0.00182	0.0001	25	3.000	0.000	2.000	0.000	0.000	1.371	1.629	0.000	0.000	0.000
19	-	11.5906(9)	11.7214	0.00307	0.0001	25	3.000	0.000	2.000	0.000	0.000	0.873	2.127	0.000	0.000	0.000
19	-	11.5918(2)	11.7250	0.00221	0.0001	25	3.000	0.000	2.000	0.000	0.000	0.822	2.178	0.000	0.000	0.000
19	-	11.6025(6)	11.7575	0.00827	0.0001	25	3.000	0.000	2.000	0.000	0.000	0.522	2.478	0.000	0.000	0.000
19	-	11.5967(3)	11.7399	0.00149	0.0001	25	3.000	0.000	2.000	0.000	0.000	0.645	2.355	0.000	0.000	0.000
19	-	11.6003(4)	11.7508	0.00898	0.0001	25	3.000	0.000	2.000	0.000	0.000	0.606	2.394	0.000	0.000	0.000
19	-	11.6102(5)	11.7809	0.00816	0.0001	25	3.000	0.000	2.000	0.000	0.000	0.255	2.745	0.000	0.000	0.000
19	-	11.6139(3)	11.7922	-0.00306	0.0001	25	3.000	0.000	2.000	0.000	0.000	0.000	3.000	0.000	0.000	0.000
19	-	11.6151(6)	11.7959	0.00060	0.0001	25	3.000	0.000	2.000	0.000	0.000	0.000	3.000	0.000	0.000	0.000
19	-	11.5291(3)	11.5358	-0.00206	0.0001	25	2.991	0.000	1.970	0.030	0.000	2.991	0.000	0.000	0.000	0.000
19	-	11.5227(2)	11.5166	-0.00182	0.0001	25	3.009	0.000	1.980	0.010	0.000	2.799	0.000	0.210	0.000	0.000
19	-	11.5170(2)	11.4995	-0.00761	0.0001	25	2.991	0.000	1.980	0.040	0.000	2.529	0.000	0.459	0.000	0.000
19	-	11.5105(2)	11.4800	-0.00212	0.0001	25	2.991	0.000	1.980	0.030	0.000	2.220	0.000	0.780	0.000	0.000
19	-	11.4925(3)	11.4263	-0.00916	0.0001	25	3.000	0.000	1.960	0.050	0.000	1.521	0.000	1.479	0.000	0.000

19	-	11.4830(2)	11.3980	-0.00583	0.0001	25	3.009	0.000	1.970	0.010	0.000	1.170	0.000	1.839	0.000	0.000
19	-	11.4737(2)	11.3703	-0.00449	0.0001	25	3.000	0.000	1.980	0.020	0.000	0.741	0.000	2.259	0.000	0.000
19	-	11.4612(2)	11.3332	-0.00711	0.0001	25	3.009	0.000	1.980	0.010	0.000	0.270	0.000	2.739	0.000	0.000
19	-	11.4555(3)	11.3163	-0.00444	0.0001	25	3.021	0.000	1.980	0.000	0.000	0.000	0.000	2.991	0.000	0.000
20	-	11.526(1)	11.526	-0.00434	0.0001	25	3.000	0.000	2.000	0.000	0.000	3.000	0.000	0.000	0.000	0.000
20	-	11.543(1)	11.578	-0.00178	0.0001	25	3.000	0.000	2.000	0.000	0.000	2.862	0.000	0.000	0.138	0.000
20	-	11.562(2)	11.635	-0.00906	0.0001	25	3.000	0.000	2.000	0.000	0.000	2.679	0.000	0.000	0.321	0.000
20	-	11.561(1)	11.632	-0.00149	0.0001	25	3.000	0.000	2.000	0.000	0.000	2.709	0.000	0.000	0.291	0.000
20	-	11.578(1)	11.683	0.00223	0.0001	25	3.000	0.000	2.000	0.000	0.000	2.574	0.000	0.000	0.426	0.000
20	-	11.627(2)	11.832	0.02099	0.0001	25	3.000	0.000	2.000	0.000	0.000	2.205	0.000	0.000	0.795	0.000
20	-	11.664(2)	11.945	-0.01356	0.0001	25	3.000	0.000	2.000	0.000	0.000	1.782	0.000	0.000	1.218	0.000
20	-	11.697(2)	12.047	-0.00372	0.0001	25	3.000	0.000	2.000	0.000	0.000	1.515	0.000	0.000	1.485	0.000
20	-	11.744(2)	12.193	-0.02146	0.0001	25	3.000	0.000	2.000	0.000	0.000	1.026	0.000	0.000	1.974	0.000
20	-	11.777(2)	12.296	0.00230	0.0001	25	3.000	0.000	2.000	0.000	0.000	0.780	0.000	0.000	2.220	0.000
20	-	11.826(1)	12.450	0.00809	0.0001	25	3.000	0.000	2.000	0.000	0.000	0.297	0.000	0.000	2.703	0.000
20	-	11.851(1)	12.529	0.00176	0.0001	25	3.000	0.000	2.000	0.000	0.000	0.000	0.000	0.000	3.000	0.000
20	-	11.525(1)	11.523	-0.00734	0.0001	25	3.000	0.000	2.000	0.000	0.000	3.000	0.000	0.000	0.000	0.000
20	-	11.521(1)	11.511	-0.00042	0.0001	25	3.000	0.000	2.000	0.000	0.000	2.730	0.000	0.270	0.000	0.000
20	-	11.515(1)	11.494	-0.00117	0.0001	25	3.000	0.000	2.000	0.000	0.000	2.484	0.000	0.516	0.000	0.000
20	-	11.508(1)	11.473	0.00079	0.0001	25	3.000	0.000	2.000	0.000	0.000	2.157	0.000	0.843	0.000	0.000
20	-	11.498(1)	11.443	-0.00052	0.0001	25	3.000	0.000	2.000	0.000	0.000	1.749	0.000	1.251	0.000	0.000
20	-	11.492(1)	11.425	0.00133	0.0001	25	3.000	0.000	2.000	0.000	0.000	1.467	0.000	1.533	0.000	0.000
20	-	11.480(1)	11.389	-0.01215	0.0001	25	3.000	0.000	2.000	0.000	0.000	1.149	0.000	1.851	0.000	0.000
20	-	11.472(1)	11.365	-0.00443	0.0001	25	3.000	0.000	2.000	0.000	0.000	0.699	0.000	2.301	0.000	0.000
20	-	11.462(1)	11.336	-0.00765	0.0001	25	3.000	0.000	2.000	0.000	0.000	0.321	0.000	2.679	0.000	0.000
20	-	11.454(1)	11.312	-0.00889	0.0001	25	3.000	0.000	2.000	0.000	0.000	0.000	0.000	3.000	0.000	0.000
21	-	11.458(1)	11.324	0.00297	0.0001	25	3.000	0.000	2.000	0.000	0.000	0.000	0.000	3.000	0.000	0.000

21	-	11.458(1)	11.324	0.00297	0.0001	25	3.000	0.000	2.000	0.000	0.000	0.000	0.000	3.000	0.000	0.000
21	-	11.457(1)	11.321	0.00000	0.0001	25	3.000	0.000	2.000	0.000	0.000	0.000	0.000	3.000	0.000	0.000
21	-	11.457(1)	11.321	0.00000	0.0001	25	3.000	0.000	2.000	0.000	0.000	0.000	0.000	3.000	0.000	0.000
22	7690	11.525(1)	11.523	-0.00639	0.0001	20	3.000	0.000	2.000	0.000	0.000	3.000	0.000	0.000	0.000	0.000
22	7691	11.525(1)	11.523	-0.00639	0.0001	20	3.000	0.000	2.000	0.000	0.000	3.000	0.000	0.000	0.000	0.000
22	7692	11.538(1)	11.563	0.00529	0.0001	147	3.000	0.000	2.000	0.000	0.000	3.000	0.000	0.000	0.000	0.000
22	7693	11.546(1)	11.587	0.00968	0.0001	227	3.000	0.000	2.000	0.000	0.000	3.000	0.000	0.000	0.000	0.000
23	142	11.459	11.327	0.00691	0.0001	20	3.000	0.000	2.000	0.000	0.000	0.000	0.000	3.000	0.000	0.000
24	-	11.4540(5)	11.312	-0.00889	0.0001	25	3.000	0.000	2.000	0.000	0.000	0.000	0.000	3.000	0.000	0.000
24	-	11.8507(3)	12.528	0.00081	0.0001	25	3.000	0.000	2.000	0.000	0.000	0.000	0.000	0.000	3.000	0.000
24	-	11.628(1)	11.835	0.02366	0.0001	25	3.000	0.000	2.000	0.000	0.000	0.000	0.000	1.806	1.194	0.000
25	634	11.846(1)	12.513	-0.00471	0.0001	20	3.000	0.000	2.000	0.000	0.000	0.030	0.000	0.000	2.970	0.000
25	629	11.456(1)	11.318	-0.00198	0.0001	20	3.000	0.000	2.000	0.000	0.000	0.000	0.000	3.000	0.000	0.000
26	-	11.4101(11)	11.1823	-0.01429	0.0001	25	4.940	0.000	0.000	0.000	0.000	0.000	0.000	1.179	0.000	1.881
26	-	11.4015(8)	11.1570	-0.01654	0.39	25	4.940	0.000	0.000	0.000	0.000	0.000	0.000	1.179	0.000	1.881
26	-	11.3895(12)	11.1218	-0.01678	0.99	25	4.940	0.000	0.000	0.000	0.000	0.000	0.000	1.179	0.000	1.881
26	-	11.3769(8)	11.0849	-0.01753	1.62	25	4.940	0.000	0.000	0.000	0.000	0.000	0.000	1.179	0.000	1.881
26	-	11.3681(10)	11.0592	-0.00881	2.23	25	4.940	0.000	0.000	0.000	0.000	0.000	0.000	1.179	0.000	1.881
26	-	11.3643(12)	11.0481	-0.00928	2.42	25	4.940	0.000	0.000	0.000	0.000	0.000	0.000	1.179	0.000	1.881
26	-	11.3483(12)	11.0015	-0.01063	3.24	25	4.940	0.000	0.000	0.000	0.000	0.000	0.000	1.179	0.000	1.881
26	-	11.3317(11)	10.9533	-0.01235	4.1	25	4.940	0.000	0.000	0.000	0.000	0.000	0.000	1.179	0.000	1.881
26	-	11.3201(10)	10.9197	-0.01303	4.72	25	4.940	0.000	0.000	0.000	0.000	0.000	0.000	1.179	0.000	1.881
26	-	11.4715(17)	11.3637	0.01139	0.0001	25	3.000	0.000	2.000	0.000	0.000	0.099	0.000	2.841	0.060	0.000
26	-	11.4612(8)	11.3332	0.00684	0.39	25	3.000	0.000	2.000	0.000	0.000	0.099	0.000	2.841	0.060	0.000
26	-	11.4488(15)	11.2964	0.00949	0.99	25	3.000	0.000	2.000	0.000	0.000	0.099	0.000	2.841	0.060	0.000
26	-	11.4361(9)	11.2589	0.01247	1.62	25	3.000	0.000	2.000	0.000	0.000	0.099	0.000	2.841	0.060	0.000
26	-	11.4215(22)	11.2158	0.00786	2.23	25	3.000	0.000	2.000	0.000	0.000	0.099	0.000	2.841	0.060	0.000

26	-	11.4205(14)	11.2129	0.01674	2.42	25	3.000	0.000	2.000	0.000	0.000	0.099	0.000	2.841	0.060	0.000
26	-	11.4020(11)	11.1585	0.01258	3.24	25	3.000	0.000	2.000	0.000	0.000	0.099	0.000	2.841	0.060	0.000
26	-	11.3837(8)	11.1048	0.01029	4.1	25	3.000	0.000	2.000	0.000	0.000	0.099	0.000	2.841	0.060	0.000
26	-	11.3715(14)	11.0691	0.01083	4.72	25	3.000	0.000	2.000	0.000	0.000	0.099	0.000	2.841	0.060	0.000
27	-	11.4755(2)	11.3756	-0.01526	0.0001	25	3.741	0.000	0.518	0.000	0.000	0.000	0.000	3.741	0.000	0.000
27	-	11.4710(3)	11.3623	-0.01285	0.0001	25	3.498	0.000	1.004	0.000	0.000	0.000	0.000	3.498	0.000	0.000
27	-	11.4644(4)	11.3427	-0.00892	0.0001	25	3.249	0.000	1.502	0.000	0.000	0.000	0.000	3.249	0.000	0.000
27	-	11.4564(4)	11.3189	-0.00180	0.0001	25	3.000	0.000	2.000	0.000	0.000	0.000	0.000	3.000	0.000	0.000
28	-	11.502(5)	11.455	-0.00181	0.0001	25	3.000	0.000	2.000	0.000	0.000	0.000	0.000	2.670	0.330	0.000
28	-	11.497(5)	11.440	-0.01674	0.0001	25	3.000	0.000	2.000	0.000	0.000	0.000	0.000	2.670	0.330	0.000
28	-	11.534(5)	11.551	-0.00477	0.0001	25	3.000	0.000	2.000	0.000	0.000	0.000	0.000	2.430	0.570	0.000
28	-	11.503(5)	11.458	0.00118	0.0001	25	3.000	0.000	2.000	0.000	0.000	0.000	0.000	2.670	0.330	0.000
28	-	11.523(5)	11.517	-0.00072	0.0001	25	3.000	0.000	2.000	0.000	0.000	0.000	0.000	2.520	0.480	0.000
28	-	11.537(5)	11.560	-0.00810	0.0001	25	3.000	0.000	2.000	0.000	0.000	0.000	0.000	2.400	0.600	0.000
29	-	11.528	11.532	0.00166	0.0001	25	3.000	0.000	2.000	0.000	0.000	3.000	0.000	0.000	0.000	0.000
29	-	11.525	11.523	-0.00734	0.0001	25	3.000	0.000	2.000	0.000	0.000	3.000	0.000	0.000	0.000	0.000
29	-	11.542	11.575	-0.00916	0.0001	25	3.000	0.000	2.000	0.000	0.000	2.400	0.600	0.000	0.000	0.000
29	-	11.545	11.584	-0.00013	0.0001	25	3.000	0.000	2.000	0.000	0.000	2.400	0.600	0.000	0.000	0.000
29	-	11.558	11.623	-0.01384	0.0001	25	3.000	0.000	2.000	0.000	0.000	1.800	1.200	0.000	0.000	0.000
29	-	11.563	11.638	0.00125	0.0001	25	3.000	0.000	2.000	0.000	0.000	1.800	1.200	0.000	0.000	0.000
29	-	11.578	11.683	-0.00629	0.0001	25	3.000	0.000	2.000	0.000	0.000	1.200	1.800	0.000	0.000	0.000
29	-	11.577	11.680	-0.00932	0.0001	25	3.000	0.000	2.000	0.000	0.000	1.200	1.800	0.000	0.000	0.000
29	-	11.594	11.732	-0.01068	0.0001	25	3.000	0.000	2.000	0.000	0.000	0.600	2.400	0.000	0.000	0.000
29	-	11.594	11.732	-0.01068	0.0001	25	3.000	0.000	2.000	0.000	0.000	0.600	2.400	0.000	0.000	0.000
29	-	11.614	11.793	-0.00275	0.0001	25	3.000	0.000	2.000	0.000	0.000	0.000	3.000	0.000	0.000	0.000
29	-	11.612	11.786	-0.00884	0.0001	25	3.000	0.000	2.000	0.000	0.000	0.000	3.000	0.000	0.000	0.000
30	-	11.999(2)	13.005	0.00518	0.0001	25	3.000	0.000	0.000	0.000	2.000	0.000	0.000	0.000	3.000	0.000

31	-	11.996(2)	12.995	-0.00457	0.0001	25	3.000	0.000	0.000	0.000	2.000	0.000	0.000	0.000	3.000	0.000
31	-	11.991(2)	12.979	0.00702	0.0001	25	3.000	0.000	0.100	0.000	1.900	0.000	0.000	0.000	3.000	0.000
31	-	11.982(3)	12.949	0.00479	0.0001	25	3.000	0.000	0.200	0.000	1.800	0.000	0.000	0.000	3.000	0.000
31	-	11.973(3)	12.920	0.02729	0.0001	25	3.000	0.000	0.400	0.000	1.600	0.000	0.000	0.000	3.000	0.000
31	-	11.953(2)	12.856	0.01171	0.0001	25	3.000	0.000	0.600	0.000	1.400	0.000	0.000	0.000	3.000	0.000
31	-	11.936(2)	12.801	0.00395	0.0001	25	3.000	0.000	0.800	0.000	1.200	0.000	0.000	0.000	3.000	0.000
31	-	11.920(2)	12.749	-0.00197	0.0001	25	3.000	0.000	1.000	0.000	1.000	0.000	0.000	0.000	3.000	0.000
31	-	11.906(2)	12.705	-0.00231	0.0001	25	3.000	0.000	1.200	0.000	0.800	0.000	0.000	0.000	3.000	0.000
31	-	11.893(2)	12.663	0.00023	0.0001	25	3.000	0.000	1.400	0.000	0.600	0.000	0.000	0.000	3.000	0.000
31	-	11.882(2)	12.628	0.00935	0.0001	25	3.000	0.000	1.600	0.000	0.400	0.000	0.000	0.000	3.000	0.000
31	-	11.862(2)	12.564	-0.00941	0.0001	25	3.000	0.000	1.800	0.000	0.200	0.000	0.000	0.000	3.000	0.000
31	-	11.858(3)	12.551	0.00075	0.0001	25	3.000	0.000	1.900	0.000	0.100	0.000	0.000	0.000	3.000	0.000
31	-	11.850(2)	12.526	-0.00141	0.0001	25	3.000	0.000	2.000	0.000	0.000	0.000	0.000	0.000	3.000	0.000
32	-	12.059(3)	13.201	-0.00706	0.0001	25	3.000	0.000	0.000	2.000	0.000	0.000	0.000	0.000	3.000	0.000
32	-	12.056(4)	13.191	-0.01061	0.0001	25	3.000	0.000	0.000	1.950	0.050	0.000	0.000	0.000	3.000	0.000
32	-	12.056(2)	13.191	-0.00437	0.0001	25	3.000	0.000	0.000	1.900	0.100	0.000	0.000	0.000	3.000	0.000
32	-	12.053(3)	13.181	-0.00191	0.0001	25	3.000	0.000	0.000	1.800	0.200	0.000	0.000	0.000	3.000	0.000
32	-	12.046(2)	13.158	-0.00091	0.0001	25	3.000	0.000	0.000	1.600	0.400	0.000	0.000	0.000	3.000	0.000
32	-	12.040(2)	13.138	0.00249	0.0001	25	3.000	0.000	0.000	1.400	0.600	0.000	0.000	0.000	3.000	0.000
32	-	12.032(3)	13.112	-0.00151	0.0001	25	3.000	0.000	0.000	1.200	0.800	0.000	0.000	0.000	3.000	0.000
32	-	12.026(3)	13.093	0.00016	0.0001	25	3.000	0.000	0.000	1.000	1.000	0.000	0.000	0.000	3.000	0.000
32	-	12.021(3)	13.076	0.00422	0.0001	25	3.000	0.000	0.000	0.800	1.200	0.000	0.000	0.000	3.000	0.000
32	-	12.014(2)	13.053	0.00088	0.0001	25	3.000	0.000	0.000	0.600	1.400	0.000	0.000	0.000	3.000	0.000
32	-	12.008(2)	13.034	-0.00006	0.0001	25	3.000	0.000	0.000	0.400	1.600	0.000	0.000	0.000	3.000	0.000
32	-	12.004(4)	13.021	0.00463	0.0001	25	3.000	0.000	0.000	0.200	1.800	0.000	0.000	0.000	3.000	0.000
32	-	12.000(3)	13.008	0.00014	0.0001	25	3.000	0.000	0.000	0.100	1.900	0.000	0.000	0.000	3.000	0.000
33	-	11.468(1)	11.353	0.00459	0.0001	25	3.000	0.000	1.892	0.000	0.108	0.000	0.000	3.000	0.000	0.000

33	-	11.476(1)	11.377	-0.00348	0.0001	25	3.000	0.000	1.764	0.000	0.236	0.000	0.000	3.000	0.000	0.000
33	-	11.488(1)	11.413	0.00504	0.0001	25	3.000	0.000	1.650	0.000	0.350	0.000	0.000	3.000	0.000	0.000
33	-	11.496(1)	11.437	-0.00540	0.0001	25	3.000	0.000	1.500	0.000	0.500	0.000	0.000	3.000	0.000	0.000
33	-	11.519(1)	11.505	0.00233	0.0001	25	3.000	0.000	1.216	0.000	0.784	0.000	0.000	3.000	0.000	0.000
33	-	11.563(2)	11.638	0.01120	0.0001	25	3.000	0.000	0.590	0.000	1.410	0.000	0.000	3.000	0.000	0.000
34	-	11.596(1)	11.738	-0.00344	0.0001	25	3.000	0.000	0.000	0.000	2.000	0.000	0.000	3.000	0.000	0.000
35	-	11.572(1)	11.665	0.00047	0.0001	25	3.000	0.000	2.000	0.000	0.000	1.560	1.380	0.000	0.030	0.000
36	-	11.886	12.641	0.07335	0.0001	25	2.987	0.022	1.848	0.000	0.000	0.227	0.005	0.073	2.906	0.000
36	-	11.536	11.557	-0.00162	0.0001	25	2.972	0.001	2.012	0.000	0.000	2.207	0.093	0.586	0.151	0.000
37	-	12.0565	13.1924	-0.00102	0.0001	25	3.260	0.000	0.045	0.000	0.000	2.137	0.004	0.008	3.263	0.000
38	4999	11.5935(1)	11.7302	0.04356	0.0001	25	3.160	0.000	0.000	0.000	1.680	0.000	0.000	3.160	0.000	0.000
39	-	11.710(50)	12.087	-0.04286	0.0001	25	3.000	0.000	0.000	2.000	0.000	3.000	0.000	0.000	0.000	0.000
40	-	11.755(25)	12.227	0.04947	5.8	25	2.987	0.022	1.848	0.000	0.000	0.227	0.005	0.073	2.906	0.000
40	-	11.566(18)	11.647	-0.01444	15.7	25	2.987	0.022	1.848	0.000	0.000	0.227	0.005	0.073	2.906	0.000
40	-	11.527(6)	11.529	-0.03456	17.9	25	2.987	0.022	1.848	0.000	0.000	0.227	0.005	0.073	2.906	0.000
40	-	11.509(23)	11.476	-0.04171	19	25	2.987	0.022	1.848	0.000	0.000	0.227	0.005	0.073	2.906	0.000
41	-	11.753(3)	12.221	0.00365	0.0001	25	3.000	0.000	2.000	0.000	0.000	1.017	0.000	0.000	1.983	0.000
41	-	11.680(1)	11.995	0.00351	0.0001	25	3.000	0.000	2.000	0.000	0.000	1.689	0.000	0.000	1.311	0.000
41	-	11.608(1)	11.774	-0.01473	0.0001	25	3.000	0.000	2.000	0.000	0.000	2.268	0.000	0.000	0.732	0.000
41	-	11.544(2)	11.581	0.00123	0.0001	25	3.000	0.000	2.000	0.000	0.000	2.862	0.000	0.000	0.138	0.000
42	-	11.536(1)	11.557	-0.00200	0.0001	25	3.000	0.000	2.000	0.000	0.000	2.508	0.000	0.345	0.147	0.000
42	-	11.584(1)	11.701	-0.00336	0.0001	25	3.000	0.000	2.000	0.000	0.000	2.076	0.000	0.360	0.564	0.000
42	-	11.622(2)	11.817	-0.00232	0.0001	25	3.000	0.000	2.000	0.000	0.000	1.833	0.000	0.291	0.876	0.000
42	-	11.530(1)	11.538	0.00056	0.0001	25	3.000	0.000	2.000	0.000	0.000	2.304	0.000	0.564	0.132	0.000
42	-	11.549(3)	11.596	-0.00292	0.0001	25	3.000	0.000	2.000	0.000	0.000	2.154	0.000	0.546	0.300	0.000
42	-	11.619(3)	11.808	-0.00354	0.0001	25	3.000	0.000	2.000	0.000	0.000	1.704	0.000	0.417	0.879	0.000
42	-	11.653(2)	11.912	0.00258	0.0001	25	3.000	0.000	2.000	0.000	0.000	1.422	0.000	0.417	1.161	0.000

42	-	11.690(3)	12.026	-0.01003	0.0001	25	3.000	0.000	2.000	0.000	0.000	1.194	0.000	0.300	1.506	0.000
42	-	11.522(2)	11.514	-0.00730	0.0001	25	3.000	0.000	2.000	0.000	0.000	2.040	0.000	0.825	0.138	0.000
42	-	11.577(1)	11.680	-0.00510	0.0001	25	3.000	0.000	2.000	0.000	0.000	1.728	0.000	0.696	0.576	0.000
42	-	11.614(2)	11.793	-0.01932	0.0001	25	3.000	0.000	2.000	0.000	0.000	1.512	0.000	0.573	0.912	0.000
42	-	11.689(2)	12.022	0.00944	0.0001	25	3.000	0.000	2.000	0.000	0.000	1.110	0.000	0.423	1.467	0.000
42	-	11.511(3)	11.482	0.00195	0.0001	25	3.000	0.000	2.000	0.000	0.000	1.671	0.000	1.230	0.099	0.000
42	-	11.570(2)	11.659	-0.01374	0.0001	25	3.000	0.000	2.000	0.000	0.000	1.359	0.000	1.032	0.609	0.000
42	-	11.647(2)	11.893	-0.00242	0.0001	25	3.000	0.000	2.000	0.000	0.000	1.026	0.000	0.774	1.200	0.000
42	-	11.503(4)	11.458	-0.00946	0.0001	25	3.000	0.000	2.000	0.000	0.000	1.242	0.000	1.617	0.141	0.000
42	-	11.560(1)	11.629	-0.01185	0.0001	25	3.000	0.000	2.000	0.000	0.000	1.074	0.000	1.344	0.582	0.000
42	-	11.604(3)	11.762	-0.00131	0.0001	25	3.000	0.000	2.000	0.000	0.000	0.915	0.000	1.182	0.903	0.000
42	-	11.642(2)	11.878	0.01751	0.0001	25	3.000	0.000	2.000	0.000	0.000	0.795	0.000	1.047	1.158	0.000
43	-	11.850(2)	12.526	-0.00141	0.0001	25	3.000	0.000	2.000	0.000	0.000	0.000	0.000	0.000	3.000	0.000
43	-	11.853(2)	12.536	0.00811	0.0001	25	3.000	0.000	2.000	0.000	0.000	0.000	0.000	0.000	3.000	0.000
44	-	11.451	11.303	-0.01777	0.0001	25	3.000	0.000	2.000	0.000	0.000	0.000	0.000	3.000	0.000	0.000
45	-	11.456(2)	11.318	-0.00296	0.0001	25	3.000	0.000	2.000	0.000	0.000	0.000	0.000	3.000	0.000	0.000
45	-	11.408(2)	11.176	0.00239	2.27	25	3.000	0.000	2.000	0.000	0.000	0.000	0.000	3.000	0.000	0.000
45	-	11.392(1)	11.129	0.00472	3.07	25	3.000	0.000	2.000	0.000	0.000	0.000	0.000	3.000	0.000	0.000
45	-	11.382(1)	11.100	0.00562	3.57	25	3.000	0.000	2.000	0.000	0.000	0.000	0.000	3.000	0.000	0.000
45	-	11.367(1)	11.056	0.00623	4.32	25	3.000	0.000	2.000	0.000	0.000	0.000	0.000	3.000	0.000	0.000
45	-	11.354(1)	11.018	0.00547	4.96	25	3.000	0.000	2.000	0.000	0.000	0.000	0.000	3.000	0.000	0.000
46	450	11.846(2)	12.513	-0.02000	0.0001	25	3.000	0.000	1.950	0.050	0.000	0.000	0.039	0.000	2.961	0.000
46	451	11.880(2)	12.621	0.00030	0.0001	365	3.000	0.000	1.950	0.050	0.000	0.000	0.039	0.000	2.961	0.000
46	452	11.917(4)	12.740	0.01967	0.0001	675	3.000	0.000	1.950	0.050	0.000	0.000	0.039	0.000	2.961	0.000
46	446	11.456(2)	11.318	-0.00296	0.0001	25	3.000	0.000	2.000	0.000	0.000	0.000	0.000	3.000	0.000	0.000
46	447	11.490	11.419	0.01391	0.0001	350	3.000	0.000	2.000	0.000	0.000	0.000	0.000	3.000	0.000	0.000
46	448	11.507	11.470	0.00209	0.0001	550	3.000	0.000	2.000	0.000	0.000	0.000	0.000	3.000	0.000	0.000

46	449	11.530	11.538	0.00369	0.0001	750	3.000	0.000	2.000	0.000	0.000	0.000	0.000	3.000	0.000	0.000
47	2417	11.4573(9)	11.3216	0.00187	0.0001	20	3.000	0.000	2.000	0.000	0.000	0.000	0.000	3.000	0.000	0.000
48	2255	11.467(1)	11.349	0.02169	0.0001	25	3.050	0.000	1.900	0.000	0.000	0.000	0.000	3.050	0.000	0.000
48	2256	11.4755(9)	11.3756	0.03788	0.0001	25	3.130	0.000	1.740	0.000	0.000	0.000	0.000	3.130	0.000	0.000
48	2257	11.4915(8)	11.4233	0.07289	0.0001	25	3.238	0.000	1.524	0.000	0.000	0.000	0.000	3.238	0.000	0.000
49	-	11.457(1)	11.321	0.00000	0.0001	25	3.000	0.000	2.000	0.000	0.000	0.000	0.000	3.000	0.000	0.000
49	-	11.457(1)	11.321	0.00000	0.0001	25	3.000	0.000	2.000	0.000	0.000	0.000	0.000	3.000	0.000	0.000
49	-	11.490(1)	11.419	-0.03515	0.0001	25	3.000	0.000	2.000	0.000	0.000	0.000	0.000	2.676	0.324	0.000
49	-	11.539(1)	11.566	0.01891	0.0001	25	3.000	0.000	2.000	0.000	0.000	0.000	0.000	2.451	0.549	0.000
49	-	11.577(1)	11.680	0.00887	0.0001	25	3.000	0.000	2.000	0.000	0.000	0.000	0.000	2.148	0.852	0.000
49	-	11.658(1)	11.927	0.02736	0.0001	25	3.000	0.000	2.000	0.000	0.000	0.000	0.000	1.590	1.410	0.000
49	-	11.776(1)	12.293	0.00141	0.0001	25	3.000	0.000	2.000	0.000	0.000	0.000	0.000	0.612	2.388	0.000
49	-	11.814(1)	12.412	-0.00524	0.0001	25	3.000	0.000	2.000	0.000	0.000	0.000	0.000	0.288	2.712	0.000
49	-	11.849(1)	12.523	-0.00458	0.0001	25	3.000	0.000	2.000	0.000	0.000	0.000	0.000	0.000	3.000	0.000
50	-	12.060	13.204	-0.00377	0.0001	25	3.000	0.000	0.000	2.000	0.000	0.000	0.000	0.000	3.000	0.000
50	-	11.821	12.434	0.00018	0.0001	25	3.000	0.000	0.000	2.000	0.000	0.000	3.000	0.000	0.000	0.000
51	240	11.531(1)	11.541	-0.01584	0.0001	20	3.000	0.000	1.980	0.000	0.000	2.589	0.010	0.270	0.129	0.000
51	246	12.058(1)	13.197	0.00212	0.0001	20	3.000	0.000	0.010	1.990	0.000	0.000	0.010	0.020	2.970	0.000
51	242	11.690(1)	12.026	-0.03762	0.0001	20	3.000	0.010	1.990	0.000	0.000	0.759	0.810	0.090	1.341	0.000
51	243	11.845(1)	12.510	-0.02220	0.0001	20	3.000	0.000	1.950	0.050	0.000	0.000	0.039	0.000	2.961	0.000
51	238	11.459(1)	11.327	0.00691	0.0001	20	3.000	0.000	2.000	0.000	0.000	0.000	0.000	3.000	0.000	0.000
51	239	11.526(1)	11.526	0.00211	0.0001	20	3.000	0.000	1.340	0.090	0.570	0.270	0.009	2.631	0.090	0.000
51	241	11.612(1)	11.786	-0.00235	0.0001	20	3.000	0.000	1.990	0.010	0.000	0.339	2.580	0.000	0.081	0.000
51	244	11.988(1)	12.969	0.02596	0.0001	20	3.000	0.010	0.210	0.050	1.730	0.000	0.009	0.000	2.991	0.000
52	-	11.682(3)	12.001	0.02248	0.0001	25	3.000	0.009	1.982	0.009	0.000	0.702	0.018	0.828	1.452	0.000
53	-	11.490(3)	11.419	0.05233	0.0001	25	3.000	0.000	2.000	0.000	0.000	0.228	0.000	2.697	0.072	0.000
53	-	11.457(2)	11.321	-0.01848	0.0001	25	2.991	0.000	1.970	0.000	0.000	0.000	0.000	3.030	0.000	0.000

54	-	11.765(14)	12.258	-0.00628	3.8	25	3.000	0.000	2.000	0.000	0.000	0.000	0.000	0.000	3.000	0.000
54	-	11.702(4)	12.063	-0.01914	6.8	25	3.000	0.000	2.000	0.000	0.000	0.000	0.000	0.000	3.000	0.000
54	-	11.639(10)	11.869	-0.03111	10.1	25	3.000	0.000	2.000	0.000	0.000	0.000	0.000	0.000	3.000	0.000
54	-	11.668(7)	11.958	-0.02253	8.6	25	3.000	0.000	2.000	0.000	0.000	0.000	0.000	0.000	3.000	0.000
54	-	11.851(1)	12.529	0.00176	0.0001	25	3.000	0.000	2.000	0.000	0.000	0.000	0.000	0.000	3.000	0.000
55	-	11.4086(20)	11.1778	-0.01676	0.0001	25	4.940	0.000	0.000	0.000	0.000	0.000	0.000	1.179	0.000	1.869
56	-	11.468(1)	11.353	-0.01154	0.0001	25	3.380	0.000	1.240	0.000	0.000	0.000	0.000	3.380	0.000	0.000
56	-	11.4735(5)	11.3697	-0.00396	0.0001	25	3.480	0.000	1.040	0.000	0.000	0.000	0.000	3.480	0.000	0.000
56	-	11.4783(3)	11.3840	-0.00739	0.0001	25	3.750	0.000	0.500	0.000	0.000	0.000	0.000	3.750	0.000	0.000
57	1741	11.4544(2)	11.3130	-0.00810	0.0001	27	3.000	0.000	2.000	0.000	0.000	0.000	0.000	3.000	0.000	0.000
57	1742	11.5129(5)	11.4872	0.03588	0.0001	500	3.000	0.000	2.000	0.000	0.000	0.000	0.000	3.000	0.000	0.000
57	1743	11.5348(5)	11.5529	0.03534	0.0001	700	3.000	0.000	2.000	0.000	0.000	0.000	0.000	3.000	0.000	0.000
58	7901	11.533	11.547	0.00788	0.0001	20	3.000	0.010	1.990	0.000	0.010	1.590	0.039	1.119	0.240	0.000
58	7902	11.565	11.644	0.00240	0.0001	20	3.000	0.000	2.000	0.000	0.000	1.431	0.039	1.020	0.510	0.000
58	7903	11.571	11.662	0.01666	0.0001	20	3.000	0.010	1.980	0.000	0.000	1.560	0.039	0.921	0.510	0.000
58	7905	11.787	12.327	0.03110	0.0001	20	3.000	0.010	1.870	0.120	0.000	0.729	0.039	0.090	2.139	0.000
58	7906	11.967	12.901	0.04708	0.0001	20	3.000	0.120	1.000	0.760	0.000	0.189	0.039	0.000	2.889	0.000
58	7907	11.871	12.593	0.04321	0.0001	20	3.000	0.010	1.810	0.190	0.000	0.030	0.009	0.060	2.901	0.000
58	7904	11.663	11.942	0.00987	0.0001	20	3.000	0.000	1.990	0.010	0.000	0.459	0.009	1.140	1.389	0.000
59	4182	12.0578(2)	13.1967	-0.00990	0.0001	20	3.000	0.000	0.000	2.000	0.000	0.000	0.000	0.000	3.000	0.000
60	-	11.613(1)	11.789	-0.00039	0.0001	25	3.000	0.000	1.990	0.010	0.000	0.339	2.580	0.000	0.081	0.000
60	-	11.634(2)	11.854	-0.02749	0.0001	350	3.000	0.000	1.990	0.010	0.000	0.339	2.580	0.000	0.081	0.000
60	-	12.059(1)	13.201	0.00430	0.0001	25	3.000	0.000	0.010	1.990	0.000	0.000	0.010	0.020	2.970	0.000
60	-	12.088(2)	13.296	0.00670	0.0001	350	3.000	0.000	0.010	1.990	0.000	0.000	0.010	0.020	2.970	0.000
60	-	12.109(2)	13.366	-0.00178	0.0001	575	3.000	0.000	0.010	1.990	0.000	0.000	0.010	0.020	2.970	0.000
60	-	12.135(2)	13.452	-0.01969	0.0001	850	3.000	0.000	0.010	1.990	0.000	0.000	0.010	0.020	2.970	0.000
61	10465	11.922(1)	12.756	0.00933	0.0001	20	3.000	0.000	1.338	0.662	0.000	0.000	0.000	0.000	3.000	0.000

62	-	11.715(5)	12.103	0.01111	0.0001	25	4.000	0.000	1.000	0.000	0.000	0.000	0.000	0.000	2.001	0.999
62	-	11.542(2)	11.575	-0.00659	0.0001	25	5.000	0.000	0.000	0.000	0.000	0.000	0.000	0.000	0.999	2.001
62	-	11.943(2)	12.823	-0.01073	0.0001	25	3.000	1.000	1.000	0.000	0.000	0.000	0.000	0.000	2.001	0.999
62	-	11.9680(2)	12.9040	0.00664	0.0001	25	3.000	2.000	0.000	0.000	0.000	0.000	0.000	0.000	0.999	2.001
62	-	12.085(2)	13.286	-0.00638	0.0001	25	3.000	1.000	0.000	0.000	0.000	0.000	0.000	1.000	3.000	0.000
63	-	11.460(1)	11.330	0.00890	0.0001	25	3.000	0.000	2.000	0.000	0.000	0.000	0.000	3.000	0.000	0.000
63	-	11.537(2)	11.560	0.01252	0.0001	25	3.000	0.000	1.000	0.000	1.000	0.000	0.000	3.000	0.000	0.000
63	-	11.571(2)	11.662	0.01815	0.0001	25	3.000	0.000	0.500	0.000	1.500	0.000	0.000	3.000	0.000	0.000
63	-	11.586(2)	11.707	0.00576	0.0001	25	3.000	0.000	0.200	0.000	1.800	0.000	0.000	3.000	0.000	0.000
63	-	11.600(1)	11.750	0.00871	0.0001	25	3.000	0.000	0.000	0.000	2.000	0.000	0.000	3.000	0.000	0.000
64	2771	11.850(1)	12.526	-0.00141	0.0001	25	3.000	0.000	2.000	0.000	0.000	0.000	0.000	0.000	3.000	0.000
64	2772	11.853(1)	12.536	-0.00229	0.0001	75	3.000	0.000	2.000	0.000	0.000	0.000	0.000	0.000	3.000	0.000
64	2773	11.855(1)	12.542	-0.00748	0.0001	125	3.000	0.000	2.000	0.000	0.000	0.000	0.000	0.000	3.000	0.000
64	2774	11.860(1)	12.558	-0.00405	0.0001	175	3.000	0.000	2.000	0.000	0.000	0.000	0.000	0.000	3.000	0.000
64	2775	11.867(1)	12.580	0.00503	0.0001	225	3.000	0.000	2.000	0.000	0.000	0.000	0.000	0.000	3.000	0.000
64	2781	11.615(1)	11.796	0.00030	0.0001	25	3.000	0.000	2.000	0.000	0.000	0.000	3.000	0.000	0.000	0.000
64	2782	11.621(1)	11.814	0.00671	0.0001	75	3.000	0.000	2.000	0.000	0.000	0.000	3.000	0.000	0.000	0.000
64	2783	11.622(1)	11.817	-0.00330	0.0001	125	3.000	0.000	2.000	0.000	0.000	0.000	3.000	0.000	0.000	0.000
64	2784	11.624(1)	11.823	-0.01119	0.0001	175	3.000	0.000	2.000	0.000	0.000	0.000	3.000	0.000	0.000	0.000
64	2785	11.627(1)	11.832	-0.01678	0.0001	225	3.000	0.000	2.000	0.000	0.000	0.000	3.000	0.000	0.000	0.000
64	2786	11.632(1)	11.847	-0.01686	0.0001	275	3.000	0.000	2.000	0.000	0.000	0.000	3.000	0.000	0.000	0.000
64	2787	11.642(1)	11.878	-0.00216	0.0001	325	3.000	0.000	2.000	0.000	0.000	0.000	3.000	0.000	0.000	0.000
64	2788	11.646(1)	11.890	-0.00625	0.0001	375	3.000	0.000	2.000	0.000	0.000	0.000	3.000	0.000	0.000	0.000
64	-	11.6155(3)	11.7971	0.00182	0.0001	25	3.000	0.000	2.000	0.000	0.000	0.000	3.000	0.000	0.000	0.000
64	-	11.6394(5)	11.8701	-0.00175	0.0001	25	3.000	0.000	2.000	0.000	0.000	0.000	2.715	0.000	0.285	0.000
64	-	11.6534(4)	11.9129	0.00065	0.0001	25	3.000	0.000	2.000	0.000	0.000	0.000	2.562	0.000	0.438	0.000
64	-	11.6681(7)	11.9581	-0.00130	0.0001	25	3.000	0.000	2.000	0.000	0.000	0.000	2.382	0.000	0.618	0.000

64	-	11.6774(4)	11.9867	0.00012	0.0001	25	3.000	0.000	2.000	0.000	0.000	0.000	2.277	0.000	0.723	0.000
64	-	11.7131(5)	12.0970	-0.00167	0.0001	25	3.000	0.000	2.000	0.000	0.000	0.000	1.836	0.000	1.164	0.000
64	-	11.7386(9)	12.1761	-0.00186	0.0001	25	3.000	0.000	2.000	0.000	0.000	0.000	1.515	0.000	1.485	0.000
64	-	11.7626(3)	12.2510	0.00263	0.0001	25	3.000	0.000	2.000	0.000	0.000	0.000	1.224	0.000	1.776	0.000
64	-	11.7960(1)	12.3556	0.00568	0.0001	25	3.000	0.000	2.000	0.000	0.000	0.000	0.792	0.000	2.208	0.000
64	-	11.8278(7)	12.4558	-0.00308	0.0001	25	3.000	0.000	2.000	0.000	0.000	0.000	0.312	0.000	2.688	0.000
64	-	11.8502(4)	12.5267	-0.00077	0.0001	25	3.000	0.000	2.000	0.000	0.000	0.000	0.000	0.000	3.000	0.000
65	-	11.464(1)	11.341	0.02077	0.0001	25	3.000	0.000	2.000	0.000	0.000	0.000	0.000	3.000	0.000	0.000
66	-	11.915(2)	12.733	-0.00786	0.0001	25	3.031	0.008	1.244	0.719	0.000	0.000	0.011	0.000	2.967	0.000
66	-	11.926(2)	12.769	-0.02050	0.0001	25	2.935	0.027	1.196	0.717	0.000	0.000	0.015	0.000	3.194	0.000
66	-	11.889(2)	12.650	-0.01483	0.0001	25	2.910	0.009	1.567	0.459	0.000	0.000	0.070	0.000	3.055	0.000
66	-	11.961(2)	12.881	0.04255	0.0001	25	2.985	0.010	1.090	0.888	0.000	0.000	0.011	0.000	3.031	0.000
66	-	11.905(2)	12.701	0.04796	0.0001	25	3.016	0.030	1.440	0.554	0.000	0.000	0.040	0.000	2.875	0.000
67	-	11.4821(25)	11.3953	-0.00725	0.0001	25	3.790	0.000	0.400	0.000	0.000	0.000	0.000	3.810	0.000	0.000
68	-	11.8503(10)	12.5271	0.00070	0.0001	19	3.000	0.000	2.000	0.000	0.000	0.000	0.000	0.000	3.000	0.000
68	-	11.8504(10)	12.5274	0.00056	0.0001	21.4	3.000	0.000	2.000	0.000	0.000	0.000	0.000	0.000	3.000	0.000
68	-	11.8507(10)	12.5283	0.00081	0.0001	25	3.000	0.000	2.000	0.000	0.000	0.000	0.000	0.000	3.000	0.000
68	-	11.8529(10)	12.5353	0.00124	0.0001	57.2	3.000	0.000	2.000	0.000	0.000	0.000	0.000	0.000	3.000	0.000
68	-	11.8556(10)	12.5439	0.00168	0.0001	94.1	3.000	0.000	2.000	0.000	0.000	0.000	0.000	0.000	3.000	0.000
68	-	11.8566(10)	12.5470	0.00145	0.0001	108.8	3.000	0.000	2.000	0.000	0.000	0.000	0.000	0.000	3.000	0.000
68	-	11.8626(10)	12.5661	0.00150	0.0001	185.5	3.000	0.000	2.000	0.000	0.000	0.000	0.000	0.000	3.000	0.000
68	-	11.8705(10)	12.5912	0.00163	0.0001	277.7	3.000	0.000	2.000	0.000	0.000	0.000	0.000	0.000	3.000	0.000
68	-	11.8805(10)	12.6231	0.00137	0.0001	387.9	3.000	0.000	2.000	0.000	0.000	0.000	0.000	0.000	3.000	0.000
68	-	11.8807(10)	12.6237	0.00141	0.0001	389.9	3.000	0.000	2.000	0.000	0.000	0.000	0.000	0.000	3.000	0.000
68	-	11.8893(10)	12.6511	0.00113	0.0001	480.1	3.000	0.000	2.000	0.000	0.000	0.000	0.000	0.000	3.000	0.000
68	-	11.8996(10)	12.6841	-0.00091	0.0001	589.3	3.000	0.000	2.000	0.000	0.000	0.000	0.000	0.000	3.000	0.000
68	-	11.9123(10)	12.7247	0.00029	0.0001	707.7	3.000	0.000	2.000	0.000	0.000	0.000	0.000	0.000	3.000	0.000

68	-	12.0481(10)	13.1649	-0.04203	0.0001	21.4	3.000	0.000	0.000	2.000	0.000	0.000	0.000	0.000	3.000	0.000
68	-	12.0484(10)	13.1659	-0.04184	0.0001	25	3.000	0.000	0.000	2.000	0.000	0.000	0.000	0.000	3.000	0.000
68	-	12.0513(10)	13.1754	-0.04019	0.0001	59	3.000	0.000	0.000	2.000	0.000	0.000	0.000	0.000	3.000	0.000
68	-	12.0558(10)	13.1901	-0.03811	0.0001	109.1	3.000	0.000	0.000	2.000	0.000	0.000	0.000	0.000	3.000	0.000
68	-	12.0593(10)	13.2016	-0.03756	0.0001	149.3	3.000	0.000	0.000	2.000	0.000	0.000	0.000	0.000	3.000	0.000
68	-	12.0648(10)	13.2197	-0.03672	0.0001	208.9	3.000	0.000	0.000	2.000	0.000	0.000	0.000	0.000	3.000	0.000
68	-	12.0740(10)	13.2500	-0.03596	0.0001	304.2	3.000	0.000	0.000	2.000	0.000	0.000	0.000	0.000	3.000	0.000
68	-	12.0783(10)	13.2641	-0.03633	0.0001	349	3.000	0.000	0.000	2.000	0.000	0.000	0.000	0.000	3.000	0.000
68	-	12.0861(10)	13.2898	-0.03679	0.0001	427.1	3.000	0.000	0.000	2.000	0.000	0.000	0.000	0.000	3.000	0.000
68	-	12.0937(10)	13.3149	-0.03761	0.0001	501.8	3.000	0.000	0.000	2.000	0.000	0.000	0.000	0.000	3.000	0.000
68	-	12.1032(10)	13.3463	-0.03751	0.0001	589.2	3.000	0.000	0.000	2.000	0.000	0.000	0.000	0.000	3.000	0.000
68	-	12.1082(10)	13.3629	-0.03587	0.0001	629.9	3.000	0.000	0.000	2.000	0.000	0.000	0.000	0.000	3.000	0.000
68	-	12.1144(10)	13.3834	-0.03773	0.0001	690	3.000	0.000	0.000	2.000	0.000	0.000	0.000	0.000	3.000	0.000
68	-	11.5256(10)	11.5253	-0.00487	0.0001	21.5	3.000	0.000	2.000	0.000	0.000	3.000	0.000	0.000	0.000	0.000
68	-	11.5258(10)	11.5259	-0.00494	0.0001	25	3.000	0.000	2.000	0.000	0.000	3.000	0.000	0.000	0.000	0.000
68	-	11.5274(10)	11.5307	-0.00518	0.0001	50.5	3.000	0.000	2.000	0.000	0.000	3.000	0.000	0.000	0.000	0.000
68	-	11.5314(10)	11.5427	-0.00566	0.0001	108.6	3.000	0.000	2.000	0.000	0.000	3.000	0.000	0.000	0.000	0.000
68	-	11.5342(10)	11.5511	-0.00610	0.0001	146.9	3.000	0.000	2.000	0.000	0.000	3.000	0.000	0.000	0.000	0.000
68	-	11.5388(10)	11.5649	-0.00653	0.0001	205.4	3.000	0.000	2.000	0.000	0.000	3.000	0.000	0.000	0.000	0.000
68	-	11.5421(10)	11.5749	-0.00636	0.0001	243.8	3.000	0.000	2.000	0.000	0.000	3.000	0.000	0.000	0.000	0.000
68	-	11.5490(10)	11.5956	-0.00595	0.0001	321	3.000	0.000	2.000	0.000	0.000	3.000	0.000	0.000	0.000	0.000
68	-	11.5528(10)	11.6071	-0.00555	0.0001	361.6	3.000	0.000	2.000	0.000	0.000	3.000	0.000	0.000	0.000	0.000
68	-	11.5565(10)	11.6182	-0.00530	0.0001	401	3.000	0.000	2.000	0.000	0.000	3.000	0.000	0.000	0.000	0.000
68	-	11.5616(10)	11.6336	-0.00528	0.0001	455.5	3.000	0.000	2.000	0.000	0.000	3.000	0.000	0.000	0.000	0.000
68	-	11.5653(10)	11.6448	-0.00375	0.0001	489.2	3.000	0.000	2.000	0.000	0.000	3.000	0.000	0.000	0.000	0.000
68	-	11.5703(10)	11.6599	-0.00432	0.0001	543.2	3.000	0.000	2.000	0.000	0.000	3.000	0.000	0.000	0.000	0.000
68	-	11.5740(10)	11.6711	-0.00434	0.0001	581.3	3.000	0.000	2.000	0.000	0.000	3.000	0.000	0.000	0.000	0.000

68	-	11.6200(10)	11.8108	0.01693	0.0001	18.7	3.000	0.000	2.000	0.000	0.000	0.000	3.000	0.000	0.000	0.000
68	-	11.6203(10)	11.8117	0.01771	0.0001	19.3	3.000	0.000	2.000	0.000	0.000	0.000	3.000	0.000	0.000	0.000
68	-	11.6207(10)	11.8129	0.01767	0.0001	25	3.000	0.000	2.000	0.000	0.000	0.000	3.000	0.000	0.000	0.000
68	-	11.6242(10)	11.8236	0.01809	0.0001	68.5	3.000	0.000	2.000	0.000	0.000	0.000	3.000	0.000	0.000	0.000
68	-	11.6292(10)	11.8389	0.01740	0.0001	129.7	3.000	0.000	2.000	0.000	0.000	0.000	3.000	0.000	0.000	0.000
68	-	11.6390(10)	11.8688	0.01763	0.0001	232.5	3.000	0.000	2.000	0.000	0.000	0.000	3.000	0.000	0.000	0.000
68	-	11.6465(10)	11.8918	0.01984	0.0001	299.3	3.000	0.000	2.000	0.000	0.000	0.000	3.000	0.000	0.000	0.000
68	-	11.6555(10)	11.9194	0.01649	0.0001	394.2	3.000	0.000	2.000	0.000	0.000	0.000	3.000	0.000	0.000	0.000
68	-	11.6600(10)	11.9332	0.01365	0.0001	443.5	3.000	0.000	2.000	0.000	0.000	0.000	3.000	0.000	0.000	0.000
68	-	11.6675(10)	11.9562	0.01683	0.0001	501	3.000	0.000	2.000	0.000	0.000	0.000	3.000	0.000	0.000	0.000
68	-	11.6745(10)	11.9778	0.01835	0.0001	557.7	3.000	0.000	2.000	0.000	0.000	0.000	3.000	0.000	0.000	0.000
68	-	11.6825(10)	12.0024	0.01944	0.0001	623	3.000	0.000	2.000	0.000	0.000	0.000	3.000	0.000	0.000	0.000
68	-	11.6915(10)	12.0302	0.01801	0.0001	702	3.000	0.000	2.000	0.000	0.000	0.000	3.000	0.000	0.000	0.000
68	-	11.4578(10)	11.3231	0.00508	0.0001	11	3.000	0.000	2.000	0.000	0.000	0.000	0.000	3.000	0.000	0.000
68	-	11.4590(10)	11.3266	0.00593	0.0001	25	3.000	0.000	2.000	0.000	0.000	0.000	0.000	3.000	0.000	0.000
68	-	11.4592(10)	11.3272	0.00599	0.0001	27.7	3.000	0.000	2.000	0.000	0.000	0.000	0.000	3.000	0.000	0.000
68	-	11.4612(10)	11.3332	0.00606	0.0001	56	3.000	0.000	2.000	0.000	0.000	0.000	0.000	3.000	0.000	0.000
68	-	11.4642(10)	11.3421	0.00747	0.0001	89.6	3.000	0.000	2.000	0.000	0.000	0.000	0.000	3.000	0.000	0.000
68	-	11.4670(10)	11.3504	0.00803	0.0001	122.3	3.000	0.000	2.000	0.000	0.000	0.000	0.000	3.000	0.000	0.000
68	-	11.4697(10)	11.3584	0.00818	0.0001	153.9	3.000	0.000	2.000	0.000	0.000	0.000	0.000	3.000	0.000	0.000
68	-	11.4736(10)	11.3700	0.00893	0.0001	195.5	3.000	0.000	2.000	0.000	0.000	0.000	0.000	3.000	0.000	0.000
68	-	11.4780(10)	11.3831	0.00793	0.0001	247.1	3.000	0.000	2.000	0.000	0.000	0.000	0.000	3.000	0.000	0.000
68	-	11.4805(10)	11.3905	0.00879	0.0001	270.5	3.000	0.000	2.000	0.000	0.000	0.000	0.000	3.000	0.000	0.000
68	-	11.4822(10)	11.3956	0.00856	0.0001	289	3.000	0.000	2.000	0.000	0.000	0.000	0.000	3.000	0.000	0.000
68	-	11.4859(10)	11.4066	0.00818	0.0001	328.1	3.000	0.000	2.000	0.000	0.000	0.000	0.000	3.000	0.000	0.000
68	-	11.4924(10)	11.4260	0.00719	0.0001	395.9	3.000	0.000	2.000	0.000	0.000	0.000	0.000	3.000	0.000	0.000
68	-	11.4973(10)	11.4406	0.00788	0.0001	441	3.000	0.000	2.000	0.000	0.000	0.000	0.000	3.000	0.000	0.000

68	-	11.5050(10)	11.4636	0.00448	0.0001	524.2	3.000	0.000	2.000	0.000	0.000	0.000	0.000	3.000	0.000	0.000
68	-	11.5138(10)	11.4899	0.00698	0.0001	597.1	3.000	0.000	2.000	0.000	0.000	0.000	0.000	3.000	0.000	0.000
68	-	11.5163(10)	11.4974	0.00368	0.0001	629.5	3.000	0.000	2.000	0.000	0.000	0.000	0.000	3.000	0.000	0.000
68	-	11.5240(10)	11.5205	0.00343	0.0001	698.5	3.000	0.000	2.000	0.000	0.000	0.000	0.000	3.000	0.000	0.000
68	-	11.5305(10)	11.5400	0.00241	0.0001	758	3.000	0.000	2.000	0.000	0.000	0.000	0.000	3.000	0.000	0.000
69	-	11.531(2)	11.541	0.01487	0.0001	25	2.974	0.001	1.998	0.195	0.000	1.997	0.074	0.598	0.093	0.000
70	-	11.532(17)	11.544	0.01405	0.0001	23	3.000	0.000	2.000	0.000	0.000	3.000	0.000	0.000	0.000	0.000
70	-	11.523(17)	11.517	-0.00875	0.0001	23	2.974	0.001	1.998	0.195	0.000	1.997	0.074	0.598	0.093	0.000
70	-	11.521(17)	11.511	-0.00728	0.0001	23	3.048	0.017	1.839	0.078	0.008	0.911	0.016	1.789	0.266	0.000
70	-	11.454(17)	11.312	-0.00849	0.0001	23	3.000	0.000	2.000	0.000	0.000	0.000	0.000	3.000	0.000	0.000
71	-	11.5954(5)	11.7359	-0.00526	0.0001	25	3.000	0.000	0.000	0.000	2.000	0.000	0.000	3.000	0.000	0.000
72	-	11.8512(6)	12.5299	0.00279	0.0001	27	3.029	0.000	1.980	0.000	0.000	0.000	0.000	0.002	2.971	0.000
72	-	11.8642(24)	12.5712	0.02083	0.0001	132	3.029	0.000	1.980	0.000	0.000	0.000	0.000	0.002	2.971	0.000
72	-	11.8737(24)	12.6014	0.02901	0.0001	218	3.029	0.000	1.980	0.000	0.000	0.000	0.000	0.002	2.971	0.000
72	-	11.8796(13)	12.6202	0.01524	0.0001	334	3.029	0.000	1.980	0.000	0.000	0.000	0.000	0.002	2.971	0.000
72	-	11.8927(13)	12.6620	0.02182	0.0001	451	3.029	0.000	1.980	0.000	0.000	0.000	0.000	0.002	2.971	0.000
72	-	11.9069(24)	12.7074	0.03499	0.0001	553	3.029	0.000	1.980	0.000	0.000	0.000	0.000	0.002	2.971	0.000
72	-	11.9211(24)	12.7529	0.03121	0.0001	702	3.029	0.000	1.980	0.000	0.000	0.000	0.000	0.002	2.971	0.000
72	-	11.9318(13)	12.7873	0.02375	0.0001	823	3.029	0.000	1.980	0.000	0.000	0.000	0.000	0.002	2.971	0.000
72	-	11.9401(13)	12.8140	0.01689	0.0001	917	3.029	0.000	1.980	0.000	0.000	0.000	0.000	0.002	2.971	0.000
72	-	11.9472(13)	12.8369	0.02115	0.0001	968	3.029	0.000	1.980	0.000	0.000	0.000	0.000	0.002	2.971	0.000
72	-	11.9508(13)	12.8485	0.00789	0.0001	1035	3.029	0.000	1.980	0.000	0.000	0.000	0.000	0.002	2.971	0.000
72	-	11.9567(13)	12.8675	0.00576	0.0001	1091	3.029	0.000	1.980	0.000	0.000	0.000	0.000	0.002	2.971	0.000
72	-	11.9626(13)	12.8866	0.00601	0.0001	1140	3.029	0.000	1.980	0.000	0.000	0.000	0.000	0.002	2.971	0.000
72	-	11.4587(5)	11.3258	0.00052	0.0001	27	3.092	0.000	1.961	0.000	0.000	0.039	0.000	2.826	0.009	0.000
72	-	11.4667(23)	11.3495	0.01298	0.0001	80	3.092	0.000	1.961	0.000	0.000	0.039	0.000	2.826	0.009	0.000
72	-	11.4713(23)	11.3632	0.01012	0.0001	149	3.092	0.000	1.961	0.000	0.000	0.039	0.000	2.826	0.009	0.000

72	-	11.4736(13)	11.3700	-0.00060	0.0001	216	3.092	0.000	1.961	0.000	0.000	0.039	0.000	2.826	0.009	0.000
72	-	11.4839(13)	11.4006	-0.00079	0.0001	325	3.092	0.000	1.961	0.000	0.000	0.039	0.000	2.826	0.009	0.000
72	-	11.4977(13)	11.4418	0.00370	0.0001	446	3.092	0.000	1.961	0.000	0.000	0.039	0.000	2.826	0.009	0.000
72	-	11.5091(13)	11.4759	0.00336	0.0001	554	3.092	0.000	1.961	0.000	0.000	0.039	0.000	2.826	0.009	0.000
72	-	11.5240(13)	11.5205	-0.00644	0.0001	717	3.092	0.000	1.961	0.000	0.000	0.039	0.000	2.826	0.009	0.000
72	-	11.5332(13)	11.5481	-0.01395	0.0001	818	3.092	0.000	1.961	0.000	0.000	0.039	0.000	2.826	0.009	0.000
72	-	11.5469(13)	11.5893	-0.00744	0.0001	915	3.092	0.000	1.961	0.000	0.000	0.039	0.000	2.826	0.009	0.000
72	-	11.5504(13)	11.5998	-0.01442	0.0001	963	3.092	0.000	1.961	0.000	0.000	0.039	0.000	2.826	0.009	0.000
72	-	11.5595(13)	11.6273	-0.01107	0.0001	1028	3.092	0.000	1.961	0.000	0.000	0.039	0.000	2.826	0.009	0.000
72	-	11.5630(13)	11.6378	-0.02161	0.0001	1084	3.092	0.000	1.961	0.000	0.000	0.039	0.000	2.826	0.009	0.000
72	-	11.5698(13)	11.6584	-0.01940	0.0001	1132	3.092	0.000	1.961	0.000	0.000	0.039	0.000	2.826	0.009	0.000
72	-	11.5756(13)	11.6759	-0.02044	0.0001	1180	3.092	0.000	1.961	0.000	0.000	0.039	0.000	2.826	0.009	0.000
72	-	11.5893(69)	11.7174	0.00342	0.0001	1225	3.092	0.000	1.961	0.000	0.000	0.039	0.000	2.826	0.009	0.000
72	-	11.5326(4)	11.5463	-0.01156	0.0001	27	2.990	0.003	1.981	0.000	0.003	2.494	0.119	0.337	0.087	0.000
72	-	11.5407(12)	11.5706	-0.00819	0.0001	124	2.990	0.003	1.981	0.000	0.003	2.494	0.119	0.337	0.087	0.000
72	-	11.5511(12)	11.6020	-0.00138	0.0001	223	2.990	0.003	1.981	0.000	0.003	2.494	0.119	0.337	0.087	0.000
72	-	11.5603(23)	11.6297	-0.02003	0.0001	393	2.990	0.003	1.981	0.000	0.003	2.494	0.119	0.337	0.087	0.000
72	-	11.5741(23)	11.6714	-0.00825	0.0001	496	2.990	0.003	1.981	0.000	0.003	2.494	0.119	0.337	0.087	0.000
72	-	11.5856(35)	11.7062	-0.01727	0.0001	641	2.990	0.003	1.981	0.000	0.003	2.494	0.119	0.337	0.087	0.000
72	-	11.6018(35)	11.7554	-0.00509	0.0001	759	2.990	0.003	1.981	0.000	0.003	2.494	0.119	0.337	0.087	0.000
72	-	11.6168(23)	11.8010	0.00413	0.0001	872	2.990	0.003	1.981	0.000	0.003	2.494	0.119	0.337	0.087	0.000
72	-	11.6260(23)	11.8291	0.00648	0.0001	950	2.990	0.003	1.981	0.000	0.003	2.494	0.119	0.337	0.087	0.000
73	-	11.370(1)	11.065	0.00538	5.686	302	3.380	0.000	1.240	0.000	0.000	0.000	0.000	3.380	0.000	0.000
73	-	11.390(1)	11.123	-0.00391	5.439	505	3.380	0.000	1.240	0.000	0.000	0.000	0.000	3.380	0.000	0.000
73	-	11.413(1)	11.191	0.03476	5.406	602	3.380	0.000	1.240	0.000	0.000	0.000	0.000	3.380	0.000	0.000
73	-	11.419(2)	11.208	0.01341	5.217	696	3.380	0.000	1.240	0.000	0.000	0.000	0.000	3.380	0.000	0.000
73	-	11.405(1)	11.167	0.00627	4.898	503	3.380	0.000	1.240	0.000	0.000	0.000	0.000	3.380	0.000	0.000

73	-	11.398(1)	11.147	0.00468	4.757	400	3.380	0.000	1.240	0.000	0.000	0.000	0.000	3.380	0.000	0.000
73	-	11.390(1)	11.123	-0.00325	4.595	301	3.380	0.000	1.240	0.000	0.000	0.000	0.000	3.380	0.000	0.000
73	-	11.386(2)	11.112	0.00014	4.445	201	3.380	0.000	1.240	0.000	0.000	0.000	0.000	3.380	0.000	0.000
73	-	11.376(2)	11.082	-0.01733	4.277	101	3.380	0.000	1.240	0.000	0.000	0.000	0.000	3.380	0.000	0.000
73	-	11.373(2)	11.074	-0.01716	4.195	28	3.380	0.000	1.240	0.000	0.000	0.000	0.000	3.380	0.000	0.000
73	-	11.374(2)	11.076	0.01422	7.357	705	3.380	0.000	1.240	0.000	0.000	0.000	0.000	3.380	0.000	0.000
73	-	11.362(2)	11.041	0.01308	7.02	499	3.380	0.000	1.240	0.000	0.000	0.000	0.000	3.380	0.000	0.000
73	-	11.348(2)	11.001	0.00382	6.715	298	3.380	0.000	1.240	0.000	0.000	0.000	0.000	3.380	0.000	0.000
73	-	11.335(2)	10.963	-0.00492	6.258	28	3.380	0.000	1.240	0.000	0.000	0.000	0.000	3.380	0.000	0.000
73	-	11.344(2)	10.989	0.03573	8.297	500	3.380	0.000	1.240	0.000	0.000	0.000	0.000	3.380	0.000	0.000
73	-	11.354(1)	11.018	0.03327	8.614	698	3.380	0.000	1.240	0.000	0.000	0.000	0.000	3.380	0.000	0.000
73	-	11.369(2)	11.062	0.03620	8.78	890	3.380	0.000	1.240	0.000	0.000	0.000	0.000	3.380	0.000	0.000
73	-	11.362(2)	11.041	0.03096	8.628	799	3.380	0.000	1.240	0.000	0.000	0.000	0.000	3.380	0.000	0.000
73	-	11.355(2)	11.021	0.02722	8.471	700	3.380	0.000	1.240	0.000	0.000	0.000	0.000	3.380	0.000	0.000
73	-	11.346(2)	10.995	0.01816	8.321	599	3.380	0.000	1.240	0.000	0.000	0.000	0.000	3.380	0.000	0.000
73	-	11.338(1)	10.972	0.01056	8.155	498	3.380	0.000	1.240	0.000	0.000	0.000	0.000	3.380	0.000	0.000
73	-	11.334(2)	10.960	0.01076	7.947	400	3.380	0.000	1.240	0.000	0.000	0.000	0.000	3.380	0.000	0.000
73	-	11.327(1)	10.940	0.00477	7.789	300	3.380	0.000	1.240	0.000	0.000	0.000	0.000	3.380	0.000	0.000
73	-	11.320(2)	10.919	-0.00362	7.608	199	3.380	0.000	1.240	0.000	0.000	0.000	0.000	3.380	0.000	0.000
73	-	11.313(1)	10.899	-0.01062	7.278	29	3.380	0.000	1.240	0.000	0.000	0.000	0.000	3.380	0.000	0.000
73	-	11.472(1)	11.365	-0.00006	0.0001	27	3.380	0.000	1.240	0.000	0.000	0.000	0.000	3.380	0.000	0.000
73	-	11.470(1)	11.359	-0.00663	0.0001	30	3.380	0.000	1.240	0.000	0.000	0.000	0.000	3.380	0.000	0.000
73	-	11.284(1)	10.816	-0.00559	10.253	404	3.380	0.000	1.240	0.000	0.000	0.000	0.000	3.380	0.000	0.000
73	-	11.306(1)	10.879	0.00574	10.13	599	3.380	0.000	1.240	0.000	0.000	0.000	0.000	3.380	0.000	0.000
73	-	11.333(1)	10.957	0.02000	9.864	796	3.380	0.000	1.240	0.000	0.000	0.000	0.000	3.380	0.000	0.000
73	-	11.322(1)	10.925	0.01018	9.388	599	3.380	0.000	1.240	0.000	0.000	0.000	0.000	3.380	0.000	0.000
73	-	11.310(1)	10.891	0.00583	9.079	399	3.380	0.000	1.240	0.000	0.000	0.000	0.000	3.380	0.000	0.000

73	-	11.299(1)	10.859	0.00151	8.785	199	3.380	0.000	1.240	0.000	0.000	0.000	0.000	3.380	0.000	0.000
73	-	11.291(1)	10.836	-0.00358	8.567	34	3.380	0.000	1.240	0.000	0.000	0.000	0.000	3.380	0.000	0.000
73	-	11.293(1)	10.841	-0.00731	8.39	33	3.380	0.000	1.240	0.000	0.000	0.000	0.000	3.380	0.000	0.000
73	-	11.300(1)	10.862	-0.01347	7.911	33	3.380	0.000	1.240	0.000	0.000	0.000	0.000	3.380	0.000	0.000
73	-	11.347(1)	10.998	0.02007	9.194	802	3.380	0.000	1.240	0.000	0.000	0.000	0.000	3.380	0.000	0.000
73	-	11.334(1)	10.960	0.01124	8.809	601	3.380	0.000	1.240	0.000	0.000	0.000	0.000	3.380	0.000	0.000
73	-	11.321(1)	10.922	0.00129	8.439	400	3.380	0.000	1.240	0.000	0.000	0.000	0.000	3.380	0.000	0.000
73	-	11.310(1)	10.891	-0.00431	8.112	200	3.380	0.000	1.240	0.000	0.000	0.000	0.000	3.380	0.000	0.000
73	-	11.303(1)	10.870	-0.00862	7.845	34	3.380	0.000	1.240	0.000	0.000	0.000	0.000	3.380	0.000	0.000
73	-	11.357(1)	11.027	0.01971	8.688	800	3.380	0.000	1.240	0.000	0.000	0.000	0.000	3.380	0.000	0.000
73	-	11.345(1)	10.992	0.01381	8.305	601	3.380	0.000	1.240	0.000	0.000	0.000	0.000	3.380	0.000	0.000
73	-	11.332(1)	10.954	0.00404	7.931	400	3.380	0.000	1.240	0.000	0.000	0.000	0.000	3.380	0.000	0.000
73	-	11.322(1)	10.925	0.00030	7.575	199	3.380	0.000	1.240	0.000	0.000	0.000	0.000	3.380	0.000	0.000
73	-	11.313(1)	10.899	-0.01045	7.295	34	3.380	0.000	1.240	0.000	0.000	0.000	0.000	3.380	0.000	0.000
73	-	11.372(1)	11.071	0.02350	8.034	802	3.380	0.000	1.240	0.000	0.000	0.000	0.000	3.380	0.000	0.000
73	-	11.359(1)	11.033	0.01475	7.629	600	3.380	0.000	1.240	0.000	0.000	0.000	0.000	3.380	0.000	0.000
73	-	11.347(1)	10.998	0.00878	7.269	401	3.380	0.000	1.240	0.000	0.000	0.000	0.000	3.380	0.000	0.000
73	-	11.335(1)	10.963	0.00070	6.925	199	3.380	0.000	1.240	0.000	0.000	0.000	0.000	3.380	0.000	0.000
73	-	11.327(1)	10.940	-0.00579	6.663	34	3.380	0.000	1.240	0.000	0.000	0.000	0.000	3.380	0.000	0.000
73	-	11.388(1)	11.117	0.02110	7.231	801	3.380	0.000	1.240	0.000	0.000	0.000	0.000	3.380	0.000	0.000
73	-	11.375(1)	11.079	0.01208	6.814	600	3.380	0.000	1.240	0.000	0.000	0.000	0.000	3.380	0.000	0.000
73	-	11.363(1)	11.044	0.00911	6.483	399	3.380	0.000	1.240	0.000	0.000	0.000	0.000	3.380	0.000	0.000
73	-	11.351(1)	11.009	0.00115	6.142	200	3.380	0.000	1.240	0.000	0.000	0.000	0.000	3.380	0.000	0.000
73	-	11.342(1)	10.983	-0.00739	5.883	34	3.380	0.000	1.240	0.000	0.000	0.000	0.000	3.380	0.000	0.000
73	-	11.409(1)	11.179	0.02245	6.274	800	3.380	0.000	1.240	0.000	0.000	0.000	0.000	3.380	0.000	0.000
73	-	11.396(1)	11.141	0.01234	5.83	600	3.380	0.000	1.240	0.000	0.000	0.000	0.000	3.380	0.000	0.000
73	-	11.383(1)	11.103	0.00529	5.468	400	3.380	0.000	1.240	0.000	0.000	0.000	0.000	3.380	0.000	0.000

73	-	11.371(1)	11.068	0.00009	5.153	200	3.380	0.000	1.240	0.000	0.000	0.000	0.000	3.380	0.000	0.000
73	-	11.362(1)	11.041	-0.00615	4.922	34	3.380	0.000	1.240	0.000	0.000	0.000	0.000	3.380	0.000	0.000
73	-	11.437(1)	11.262	0.02365	5.037	801	3.380	0.000	1.240	0.000	0.000	0.000	0.000	3.380	0.000	0.000
73	-	11.423(1)	11.220	0.01169	4.587	600	3.380	0.000	1.240	0.000	0.000	0.000	0.000	3.380	0.000	0.000
73	-	11.409(1)	11.179	0.00274	4.221	400	3.380	0.000	1.240	0.000	0.000	0.000	0.000	3.380	0.000	0.000
73	-	11.395(1)	11.138	-0.00857	3.882	200	3.380	0.000	1.240	0.000	0.000	0.000	0.000	3.380	0.000	0.000
73	-	11.387(1)	11.114	-0.00907	3.681	34	3.380	0.000	1.240	0.000	0.000	0.000	0.000	3.380	0.000	0.000
73	-	11.459(1)	11.327	0.02831	4.141	800	3.380	0.000	1.240	0.000	0.000	0.000	0.000	3.380	0.000	0.000
73	-	11.407(1)	11.173	-0.00806	2.763	32	3.380	0.000	1.240	0.000	0.000	0.000	0.000	3.380	0.000	0.000
73	-	11.462(1)	11.336	0.02759	4.006	801	3.380	0.000	1.240	0.000	0.000	0.000	0.000	3.380	0.000	0.000
73	-	11.448(1)	11.294	0.02141	3.63	601	3.380	0.000	1.240	0.000	0.000	0.000	0.000	3.380	0.000	0.000
73	-	11.433(1)	11.250	0.01855	3.376	399	3.380	0.000	1.240	0.000	0.000	0.000	0.000	3.380	0.000	0.000
73	-	11.418(1)	11.205	-0.00161	2.93	198	3.380	0.000	1.240	0.000	0.000	0.000	0.000	3.380	0.000	0.000
73	-	11.409(1)	11.179	-0.00667	2.696	33	3.380	0.000	1.240	0.000	0.000	0.000	0.000	3.380	0.000	0.000
73	-	11.417(1)	11.203	-0.00562	2.345	32	3.380	0.000	1.240	0.000	0.000	0.000	0.000	3.380	0.000	0.000
73	-	11.479(1)	11.386	0.02273	3.225	803	3.380	0.000	1.240	0.000	0.000	0.000	0.000	3.380	0.000	0.000
73	-	11.465(1)	11.344	0.01714	2.825	599	3.380	0.000	1.240	0.000	0.000	0.000	0.000	3.380	0.000	0.000
73	-	11.449(1)	11.297	0.00609	2.49	400	3.380	0.000	1.240	0.000	0.000	0.000	0.000	3.380	0.000	0.000
73	-	11.435(1)	11.256	0.00423	2.265	200	3.380	0.000	1.240	0.000	0.000	0.000	0.000	3.380	0.000	0.000
73	-	11.424(1)	11.223	-0.00470	2.046	33	3.380	0.000	1.240	0.000	0.000	0.000	0.000	3.380	0.000	0.000
73	-	11.480(1)	11.389	0.01383	2.149	600	3.380	0.000	1.240	0.000	0.000	0.000	0.000	3.380	0.000	0.000
73	-	11.467(1)	11.350	0.00893	1.753	399	3.380	0.000	1.240	0.000	0.000	0.000	0.000	3.380	0.000	0.000
73	-	11.453(1)	11.309	0.00249	1.45	200	3.380	0.000	1.240	0.000	0.000	0.000	0.000	3.380	0.000	0.000
73	-	11.442(1)	11.276	-0.00503	1.241	33	3.380	0.000	1.240	0.000	0.000	0.000	0.000	3.380	0.000	0.000
74	-	11.459(1)	11.327	0.00593	0.0001	25	3.000	0.000	2.000	0.000	0.000	0.000	0.000	3.000	0.000	0.000
74	-	11.500	11.449	0.01445	0.0001	25	3.000	0.000	2.000	0.000	0.000	0.000	0.000	2.724	0.276	0.000
74	-	11.511	11.482	0.00410	0.0001	25	3.000	0.000	2.000	0.000	0.000	0.000	0.000	2.619	0.381	0.000

74	-	11.523	11.517	0.01040	0.0001	25	3.000	0.000	2.000	0.000	0.000	0.000	0.000	2.547	0.453	0.000
74	-	11.537	11.560	-0.00810	0.0001	25	3.000	0.000	2.000	0.000	0.000	0.000	0.000	2.400	0.600	0.000
74	-	11.847	12.517	0.01524	0.0001	25	3.000	0.000	2.000	0.000	0.000	0.000	0.000	0.069	2.931	0.000
74	-	11.851	12.529	0.00176	0.0001	25	3.000	0.000	2.000	0.000	0.000	0.000	0.000	0.000	3.000	0.000
75	-	11.5310(2)	11.5415	0.01067	0.0001	25	3.000	0.000	2.000	0.000	0.000	3.000	0.000	0.000	0.000	0.000
75	-	11.5292(7)	11.5361	0.00527	0.0001	25	3.000	0.000	2.000	0.000	0.000	3.000	0.000	0.000	0.000	0.000
75	-	11.5333(2)	11.5484	0.00817	0.0001	25	3.000	0.000	1.960	0.040	0.000	3.000	0.000	0.000	0.000	0.000
75	-	11.5380(2)	11.5625	-0.01304	0.0001	25	3.000	0.000	1.820	0.180	0.000	3.000	0.000	0.000	0.000	0.000
75	-	11.5494(2)	11.5968	0.00508	0.0001	25	3.000	0.000	1.760	0.240	0.000	3.000	0.000	0.000	0.000	0.000
75	-	11.5495(2)	11.5971	0.00538	0.0001	25	3.000	0.000	1.760	0.240	0.000	3.000	0.000	0.000	0.000	0.000
75	-	11.5594(2)	11.6270	0.00704	0.0001	25	3.000	0.000	1.660	0.340	0.000	3.000	0.000	0.000	0.000	0.000
75	-	11.5426(5)	11.5764	-0.00454	0.0001	25	3.000	0.000	1.800	0.200	0.000	3.000	0.000	0.000	0.000	0.000
75	-	11.5336(5)	11.5493	0.00424	0.0001	25	3.000	0.000	1.940	0.060	0.000	3.000	0.000	0.000	0.000	0.000
75	-	11.5522(6)	11.6053	0.00800	0.0001	25	3.000	0.000	1.740	0.260	0.000	3.000	0.000	0.000	0.000	0.000
75	-	11.5477(7)	11.5917	0.00542	0.0001	25	3.000	0.000	1.780	0.220	0.000	3.000	0.000	0.000	0.000	0.000
75	-	11.5501(2)	11.5989	0.00719	0.0001	25	3.000	0.000	1.760	0.240	0.000	3.000	0.000	0.000	0.000	0.000
75	-	11.5507(10)	11.6007	0.00348	0.0001	25	3.000	0.000	1.740	0.260	0.000	3.000	0.000	0.000	0.000	0.000
75	-	11.5430(4)	11.5776	0.00199	0.0001	25	3.000	0.000	1.820	0.180	0.000	3.000	0.000	0.000	0.000	0.000
75	-	11.5489(2)	11.5953	-0.00195	0.0001	25	3.000	0.000	1.740	0.260	0.000	3.000	0.000	0.000	0.000	0.000
75	-	11.5647(5)	11.6430	0.01723	0.0001	25	3.000	0.000	1.640	0.360	0.000	3.000	0.000	0.000	0.000	0.000
75	-	11.6123(8)	11.7873	-0.00303	0.0001	25	3.000	0.000	1.120	0.880	0.000	3.000	0.000	0.000	0.000	0.000
75	-	11.6615(4)	11.9378	-0.02391	0.0001	25	3.000	0.000	0.600	1.400	0.000	3.000	0.000	0.000	0.000	0.000
75	-	11.6841(7)	12.0073	-0.01001	0.0001	25	3.000	0.000	0.420	1.580	0.000	3.000	0.000	0.000	0.000	0.000
75	-	11.6735(4)	11.9747	-0.01833	0.0001	25	3.000	0.000	0.500	1.500	0.000	3.000	0.000	0.000	0.000	0.000
75	-	11.6818(3)	12.0002	0.00108	0.0001	25	3.000	0.000	0.480	1.520	0.000	3.000	0.000	0.000	0.000	0.000
75	-	11.6840(4)	12.0070	0.00176	0.0001	25	3.000	0.000	0.460	1.540	0.000	3.000	0.000	0.000	0.000	0.000
75	-	11.7286(10)	12.1451	0.01483	0.0001	25	3.000	0.000	0.000	2.000	0.000	3.000	0.000	0.000	0.000	0.000

75	-	11.7273(4)	12.1410	0.01079	0.0001	25	3.000	0.000	0.000	2.000	0.000	3.000	0.000	0.000	0.000	0.000
75	-	11.726(20)	12.1370	0.00676	0.0001	25	3.000	0.000	0.000	2.000	0.000	3.000	0.000	0.000	0.000	0.000
75	-	11.7254(4)	12.1351	0.01433	0.0001	25	3.000	0.000	0.040	1.960	0.000	3.000	0.000	0.000	0.000	0.000
75	-	11.5510(1)	11.6016	0.00438	0.0001	25	3.000	0.000	1.740	0.260	0.000	3.000	0.000	0.000	0.000	0.000
75	-	11.5909(2)	11.7223	0.00405	0.0001	25	3.000	0.000	1.340	0.660	0.000	3.000	0.000	0.000	0.000	0.000
75	-	11.6430(12)	11.8811	-0.00917	0.0001	25	3.000	0.000	0.820	1.180	0.000	3.000	0.000	0.000	0.000	0.000
76	-	12.0102(6)	13.0410	0.00316	0.0001	25	3.000	0.000	0.000	2.000	0.000	0.540	0.000	0.000	2.460	0.000
76	-	12.0040(5)	13.0208	-0.01703	0.0001	25	3.000	0.000	0.000	2.000	0.000	0.540	0.000	0.000	2.460	0.000
76	-	12.0104(4)	13.0417	-0.01586	0.0001	25	3.000	0.000	0.000	2.000	0.000	0.480	0.000	0.000	2.520	0.000
76	-	12.0153(6)	13.0576	0.00992	0.0001	25	3.000	0.000	0.000	2.000	0.000	0.510	0.000	0.000	2.490	0.000
76	-	11.8559(8)	12.5448	-0.00011	0.0001	25	3.000	0.000	0.000	2.000	0.000	1.920	0.000	0.000	1.080	0.000
76	-	11.8363(3)	12.4827	0.00608	0.0001	25	3.000	0.000	0.000	2.000	0.000	2.100	0.000	0.000	0.900	0.000
76	-	11.7856(6)	12.3230	-0.00410	0.0001	25	3.000	0.000	0.000	2.000	0.000	2.490	0.000	0.000	0.510	0.000
76	-	11.8681(17)	12.5836	-0.00654	0.0001	25	3.000	0.000	0.000	2.000	0.000	1.800	0.000	0.000	1.200	0.000
76	-	11.7990(9)	12.3651	0.03799	0.0001	25	3.000	0.000	0.000	2.000	0.000	2.490	0.000	0.000	0.510	0.000
77	7859	11.5546(4)	11.6125	0.00401	0.0001	25	3.000	0.000	1.700	0.300	0.000	3.000	0.000	0.000	0.000	0.000
77	7861	11.7663(2)	12.2625	0.00490	0.0001	25	3.000	0.000	0.000	2.000	0.000	2.670	0.000	0.000	0.330	0.000
77	7862	11.8002(5)	12.3688	-0.00442	0.0001	25	3.000	0.000	0.000	2.000	0.000	2.370	0.000	0.000	0.630	0.000
77	7863	11.8568(7)	12.5477	0.00274	0.0001	25	3.000	0.000	0.000	2.000	0.000	1.920	0.000	0.000	1.080	0.000
77	7860	11.7076(7)	12.0799	-0.00010	0.0001	25	3.000	0.000	0.200	1.800	0.000	3.000	0.000	0.000	0.000	0.000
77	7864	11.9150(4)	12.7334	0.00972	0.0001	25	3.000	0.000	0.000	2.000	0.000	1.440	0.000	0.000	1.560	0.000
77	7865	11.9503(8)	12.8469	-0.00635	0.0001	25	3.000	0.000	0.000	2.000	0.000	1.080	0.000	0.000	1.920	0.000
77	-	12.0690(5)	13.2335	0.02581	0.0001	25	3.000	0.000	0.000	2.000	0.000	0.000	0.000	0.000	3.000	0.000
77	-	12.0596(2)	13.2026	-0.00509	0.0001	25	3.000	0.000	0.000	2.000	0.000	0.000	0.000	0.000	3.000	0.000
77	-	12.0457(15)	13.1570	0.00406	0.0001	25	3.000	0.000	0.000	2.000	0.000	0.180	0.000	0.000	2.820	0.000
77	-	12.0375(1)	13.1302	-0.01348	0.0001	25	3.000	0.000	0.000	2.000	0.000	0.210	0.000	0.000	2.790	0.000
77	-	12.0361(7)	13.1256	-0.00870	0.0001	25	3.000	0.000	0.000	2.000	0.000	0.240	0.000	0.000	2.760	0.000

77	-	12.0255(8)	13.0909	-0.00537	0.0001	25	3.000	0.000	0.000	2.000	0.000	0.360	0.000	0.000	2.640	0.000
77	-	12.0161(7)	13.0603	0.01253	0.0001	25	3.000	0.000	0.000	2.000	0.000	0.510	0.000	0.000	2.490	0.000
77	-	12.0045(6)	13.0225	-0.01540	0.0001	25	3.000	0.000	0.000	2.000	0.000	0.540	0.000	0.000	2.460	0.000
77	-	11.9807(7)	12.9452	-0.02246	0.0001	25	3.000	0.000	0.000	2.000	0.000	0.750	0.000	0.000	2.250	0.000
77	-	11.9803(6)	12.9439	-0.00330	0.0001	25	3.000	0.000	0.000	2.000	0.000	0.810	0.000	0.000	2.190	0.000
77	-	11.9755(1)	12.9283	-0.00857	0.0001	25	3.000	0.000	0.000	2.000	0.000	0.840	0.000	0.000	2.160	0.000
77	-	11.9565(7)	12.8669	-0.01799	0.0001	25	3.000	0.000	0.000	2.000	0.000	0.990	0.000	0.000	2.010	0.000
77	-	11.9572(5)	12.8691	-0.00522	0.0001	25	3.000	0.000	0.000	2.000	0.000	1.020	0.000	0.000	1.980	0.000
77	-	11.9382(3)	12.8079	-0.00264	0.0001	25	3.000	0.000	0.000	2.000	0.000	1.200	0.000	0.000	1.800	0.000
77	-	11.9290(9)	12.7783	-0.02148	0.0001	25	3.000	0.000	0.000	2.000	0.000	1.230	0.000	0.000	1.770	0.000
77	-	11.9150(7)	12.7334	-0.00125	0.0001	25	3.000	0.000	0.000	2.000	0.000	1.410	0.000	0.000	1.590	0.000
77	-	11.8911(6)	12.6569	-0.01154	0.0001	25	3.000	0.000	0.000	2.000	0.000	1.590	0.000	0.000	1.410	0.000
77	-	11.8880(5)	12.6470	0.00082	0.0001	25	3.000	0.000	0.000	2.000	0.000	1.650	0.000	0.000	1.350	0.000
77	-	11.8612(6)	12.5617	0.00539	0.0001	25	3.000	0.000	0.000	2.000	0.000	1.890	0.000	0.000	1.110	0.000
77	-	11.8580(5)	12.5515	0.00655	0.0001	25	3.000	0.000	0.000	2.000	0.000	1.920	0.000	0.000	1.080	0.000
77	-	11.8541(7)	12.5391	-0.00583	0.0001	25	3.000	0.000	0.000	2.000	0.000	1.920	0.000	0.000	1.080	0.000
77	-	11.8546(4)	12.5407	-0.00424	0.0001	25	3.000	0.000	0.000	2.000	0.000	1.920	0.000	0.000	1.080	0.000
77	-	11.8204(6)	12.4325	0.00167	0.0001	25	3.000	0.000	0.000	2.000	0.000	2.220	0.000	0.000	0.780	0.000
77	-	11.8025(6)	12.3761	-0.00872	0.0001	25	3.000	0.000	0.000	2.000	0.000	2.340	0.000	0.000	0.660	0.000
77	-	11.7923(9)	12.3440	-0.01771	0.0001	25	3.000	0.000	0.000	2.000	0.000	2.400	0.000	0.000	0.600	0.000
77	-	11.7683(7)	12.2688	0.01116	0.0001	25	3.000	0.000	0.000	2.000	0.000	2.670	0.000	0.000	0.330	0.000
77	-	11.5285(2)	11.5340	0.00316	0.0001	25	3.000	0.000	2.000	0.000	0.000	3.000	0.000	0.000	0.000	0.000
77	-	11.5285(2)	11.5340	0.00316	0.0001	25	3.000	0.000	2.000	0.000	0.000	3.000	0.000	0.000	0.000	0.000
77	-	11.5299(5)	11.5382	-0.00205	0.0001	25	3.000	0.000	1.960	0.040	0.000	3.000	0.000	0.000	0.000	0.000
77	-	11.5312(8)	11.5421	0.00186	0.0001	25	3.000	0.000	1.960	0.040	0.000	3.000	0.000	0.000	0.000	0.000
77	-	11.5405(2)	11.5700	0.00493	0.0001	25	3.000	0.000	1.860	0.140	0.000	3.000	0.000	0.000	0.000	0.000
77	-	11.5400(6)	11.5685	-0.00177	0.0001	25	3.000	0.000	1.840	0.160	0.000	3.000	0.000	0.000	0.000	0.000

77	-	11.5390(9)	11.5655	-0.00478	0.0001	25	3.000	0.000	1.840	0.160	0.000	3.000	0.000	0.000	0.000	0.000
77	-	11.5408(3)	11.5709	-0.00462	0.0001	25	3.000	0.000	1.820	0.180	0.000	3.000	0.000	0.000	0.000	0.000
77	-	11.5571(5)	11.6200	-0.02344	0.0001	25	3.000	0.000	1.580	0.420	0.000	3.000	0.000	0.000	0.000	0.000
77	-	11.5837(7)	11.7005	0.00139	0.0001	25	3.000	0.000	1.400	0.600	0.000	3.000	0.000	0.000	0.000	0.000
77	-	11.5777(7)	11.6823	-0.01045	0.0001	25	3.000	0.000	1.420	0.580	0.000	3.000	0.000	0.000	0.000	0.000
77	-	11.6034(7)	11.7603	0.00295	0.0001	25	3.000	0.000	1.220	0.780	0.000	3.000	0.000	0.000	0.000	0.000
77	-	11.6061(9)	11.7685	-0.00202	0.0001	25	3.000	0.000	1.180	0.820	0.000	3.000	0.000	0.000	0.000	0.000
77	-	11.6273(3)	11.8331	0.00271	0.0001	25	3.000	0.000	1.000	1.000	0.000	3.000	0.000	0.000	0.000	0.000
77	-	11.6283(7)	11.8361	-0.00758	0.0001	25	3.000	0.000	0.960	1.040	0.000	3.000	0.000	0.000	0.000	0.000
77	-	11.6841(7)	12.0073	-0.01001	0.0001	25	3.000	0.000	0.420	1.580	0.000	3.000	0.000	0.000	0.000	0.000
77	-	11.6903(7)	12.0265	-0.00864	0.0001	25	3.000	0.000	0.360	1.640	0.000	3.000	0.000	0.000	0.000	0.000
77	-	11.7270(6)	12.1401	0.01454	0.0001	25	3.000	0.000	0.020	1.980	0.000	3.000	0.000	0.000	0.000	0.000
77	-	11.7272(7)	12.1407	0.01048	0.0001	25	3.000	0.000	0.000	2.000	0.000	3.000	0.000	0.000	0.000	0.000
78	-	11.6749(1)	11.9790	-0.00318	0.0001	25	3.000	0.000	0.000	0.080	1.920	3.000	0.000	0.000	0.000	0.000
78	-	11.6770(3)	11.9855	-0.00240	0.0001	25	3.000	0.000	0.000	0.180	1.820	3.000	0.000	0.000	0.000	0.000
78	-	11.6813(3)	11.9987	-0.00625	0.0001	25	3.000	0.000	0.000	0.460	1.540	3.000	0.000	0.000	0.000	0.000
78	-	11.6806(1)	11.9966	-0.00841	0.0001	25	3.000	0.000	0.000	0.460	1.540	3.000	0.000	0.000	0.000	0.000
78	-	11.6901(2)	12.0258	0.00204	0.0001	25	3.000	0.000	0.000	0.740	1.260	3.000	0.000	0.000	0.000	0.000
78	-	11.6972(3)	12.0478	-0.00127	0.0001	25	3.000	0.000	0.000	1.080	0.920	3.000	0.000	0.000	0.000	0.000
78	-	11.7002(1)	12.0570	0.00956	0.0001	25	3.000	0.000	0.000	1.060	0.940	3.000	0.000	0.000	0.000	0.000
78	-	11.7082(2)	12.0818	-0.00725	0.0001	25	3.000	0.000	0.000	1.560	0.440	3.000	0.000	0.000	0.000	0.000
79	-	11.455(3)	11.315	-0.00592	0.0001	25	3.000	0.000	2.000	0.000	0.000	0.000	0.000	3.000	0.000	0.000
79	-	11.474(3)	11.371	-0.01004	0.0001	25	3.580	0.000	0.840	0.000	0.000	0.000	0.000	3.580	0.000	0.000
79	-	11.533(4)	11.547	0.01668	0.0001	25	3.000	0.000	2.000	0.000	0.000	3.000	0.000	0.000	0.000	0.000
79	-	11.547(4)	11.590	0.03448	0.0001	25	3.180	0.000	1.640	0.000	0.000	3.180	0.000	0.000	0.000	0.000
80	8138	11.4545(8)	11.3133	-0.00642	0.0001	20	3.000	0.000	2.000	0.000	0.000	0.000	0.000	3.000	0.000	0.000
80	8139	11.3846(8)	11.1074	0.00931	3.48	20	3.000	0.000	2.000	0.000	0.000	0.000	0.000	3.000	0.000	0.000

80	8140	11.2893(7)	10.8308	0.01737	8.57	20	3.000	0.000	2.000	0.000	0.000	0.000	0.000	3.000	0.000	0.000
80	8141	11.2353(7)	10.6762	0.01105	11.53	20	3.000	0.000	2.000	0.000	0.000	0.000	0.000	3.000	0.000	0.000
80	8142	11.1717(8)	10.4959	0.00397	15.28	20	3.000	0.000	2.000	0.000	0.000	0.000	0.000	3.000	0.000	0.000
80	8143	11.0335(8)	10.1112	-0.02601	24.07	20	3.000	0.000	2.000	0.000	0.000	0.000	0.000	3.000	0.000	0.000
80	8144	10.9339(9)	9.8398	-0.00927	32.47	20	3.000	0.000	2.000	0.000	0.000	0.000	0.000	3.000	0.000	0.000
80	-	11.1576(9)	10.4562	-0.00202	16.1	25	3.000	0.000	2.000	0.000	0.000	0.000	0.000	3.000	0.000	0.000
80	-	11.1258(8)	10.3670	-0.01248	17.95	25	3.000	0.000	2.000	0.000	0.000	0.000	0.000	3.000	0.000	0.000
80	-	11.0894(9)	10.2656	-0.00440	20.65	25	3.000	0.000	2.000	0.000	0.000	0.000	0.000	3.000	0.000	0.000
80	-	11.0672(8)	10.2041	-0.00456	22.23	25	3.000	0.000	2.000	0.000	0.000	0.000	0.000	3.000	0.000	0.000
80	-	11.0594(8)	10.1825	-0.01925	22.41	25	3.000	0.000	2.000	0.000	0.000	0.000	0.000	3.000	0.000	0.000
80	-	11.0540(14)	10.1676	-0.01105	23.02	25	3.000	0.000	2.000	0.000	0.000	0.000	0.000	3.000	0.000	0.000
80	-	11.0455(9)	10.1442	-0.00606	23.78	25	3.000	0.000	2.000	0.000	0.000	0.000	0.000	3.000	0.000	0.000
80	-	11.0208(9)	10.0763	-0.01039	25.52	25	3.000	0.000	2.000	0.000	0.000	0.000	0.000	3.000	0.000	0.000
80	-	11.0062(7)	10.0363	-0.00419	26.82	25	3.000	0.000	2.000	0.000	0.000	0.000	0.000	3.000	0.000	0.000
80	-	10.9821(10)	9.9705	-0.00299	28.76	25	3.000	0.000	2.000	0.000	0.000	0.000	0.000	3.000	0.000	0.000
80	-	10.9665(9)	9.9281	-0.00776	29.88	25	3.000	0.000	2.000	0.000	0.000	0.000	0.000	3.000	0.000	0.000
80	-	10.9549(8)	9.8966	-0.00522	30.91	25	3.000	0.000	2.000	0.000	0.000	0.000	0.000	3.000	0.000	0.000
80	-	10.9259(8)	9.8182	-0.00437	33.38	25	3.000	0.000	2.000	0.000	0.000	0.000	0.000	3.000	0.000	0.000
80	-	11.3991(8)	11.1499	-0.02188	2.3	25	3.000	0.000	2.000	0.000	0.000	0.000	0.000	3.000	0.000	0.000
80	-	11.3954(7)	11.1391	-0.02093	2.49	25	3.000	0.000	2.000	0.000	0.000	0.000	0.000	3.000	0.000	0.000
80	-	11.3794(7)	11.0922	-0.01943	3.28	25	3.000	0.000	2.000	0.000	0.000	0.000	0.000	3.000	0.000	0.000
80	-	11.3499(8)	11.0062	-0.01279	4.85	25	3.000	0.000	2.000	0.000	0.000	0.000	0.000	3.000	0.000	0.000
80	-	11.3230(7)	10.9281	-0.02564	6	25	3.000	0.000	2.000	0.000	0.000	0.000	0.000	3.000	0.000	0.000
80	-	11.3106(6)	10.8923	-0.01302	6.88	25	3.000	0.000	2.000	0.000	0.000	0.000	0.000	3.000	0.000	0.000
80	-	11.2898(7)	10.8323	-0.01139	8.03	25	3.000	0.000	2.000	0.000	0.000	0.000	0.000	3.000	0.000	0.000
80	-	11.2669(7)	10.7665	-0.00823	9.36	25	3.000	0.000	2.000	0.000	0.000	0.000	0.000	3.000	0.000	0.000
80	-	11.2434(9)	10.6993	-0.00590	10.75	25	3.000	0.000	2.000	0.000	0.000	0.000	0.000	3.000	0.000	0.000

80	-	11.2302(10)	10.6616	-0.00990	11.44	25	3.000	0.000	2.000	0.000	0.000	0.000	0.000	3.000	0.000	0.000
80	-	11.2208(8)	10.6349	-0.00833	12.03	25	3.000	0.000	2.000	0.000	0.000	0.000	0.000	3.000	0.000	0.000
80	-	11.1997(11)	10.5750	-0.00583	13.36	25	3.000	0.000	2.000	0.000	0.000	0.000	0.000	3.000	0.000	0.000
80	-	11.1888(11)	10.5441	-0.01236	13.89	25	3.000	0.000	2.000	0.000	0.000	0.000	0.000	3.000	0.000	0.000
80	-	11.177(1)	10.511	-0.01357	14.6	25	3.000	0.000	2.000	0.000	0.000	0.000	0.000	3.000	0.000	0.000
80	-	11.163(2)	10.471	-0.00821	15.61	25	3.000	0.000	2.000	0.000	0.000	0.000	0.000	3.000	0.000	0.000
80	-	11.144(3)	10.418	-0.01263	16.74	25	3.000	0.000	2.000	0.000	0.000	0.000	0.000	3.000	0.000	0.000
80	-	11.133(4)	10.387	-0.01077	17.51	25	3.000	0.000	2.000	0.000	0.000	0.000	0.000	3.000	0.000	0.000
80	-	11.107(3)	10.315	-0.01187	19.24	25	3.000	0.000	2.000	0.000	0.000	0.000	0.000	3.000	0.000	0.000
80	-	11.087(4)	10.259	0.02529	21.58	25	3.000	0.000	2.000	0.000	0.000	0.000	0.000	3.000	0.000	0.000
81	-	11.5195(8)	11.5070	-0.02383	0.0001	25	3.000	0.000	2.000	0.000	0.000	3.000	0.000	0.000	0.000	0.000
81	-	11.4757(9)	11.3762	-0.01771	2.3	25	3.000	0.000	2.000	0.000	0.000	3.000	0.000	0.000	0.000	0.000
81	-	11.4713(7)	11.3632	-0.01983	2.49	25	3.000	0.000	2.000	0.000	0.000	3.000	0.000	0.000	0.000	0.000
81	-	11.4561(8)	11.3180	-0.01990	3.28	25	3.000	0.000	2.000	0.000	0.000	3.000	0.000	0.000	0.000	0.000
81	-	11.4276(7)	11.2338	-0.01715	4.85	25	3.000	0.000	2.000	0.000	0.000	3.000	0.000	0.000	0.000	0.000
81	-	11.4003(10)	11.1535	-0.03624	5.99	25	3.000	0.000	2.000	0.000	0.000	3.000	0.000	0.000	0.000	0.000
81	-	11.3906(9)	11.1250	-0.01797	6.88	25	3.000	0.000	2.000	0.000	0.000	3.000	0.000	0.000	0.000	0.000
81	-	11.3683(10)	11.0598	-0.02314	8.05	25	3.000	0.000	2.000	0.000	0.000	3.000	0.000	0.000	0.000	0.000
81	-	11.3461(10)	10.9951	-0.02236	9.36	25	3.000	0.000	2.000	0.000	0.000	3.000	0.000	0.000	0.000	0.000
81	-	11.3227(8)	10.9273	-0.02273	10.75	25	3.000	0.000	2.000	0.000	0.000	3.000	0.000	0.000	0.000	0.000
81	-	11.3062(8)	10.8796	-0.02069	11.8	25	3.000	0.000	2.000	0.000	0.000	3.000	0.000	0.000	0.000	0.000
81	-	11.2880(10)	10.8271	-0.01755	13	25	3.000	0.000	2.000	0.000	0.000	3.000	0.000	0.000	0.000	0.000
81	-	11.2694(10)	10.7737	-0.02429	14.03	25	3.000	0.000	2.000	0.000	0.000	3.000	0.000	0.000	0.000	0.000
81	-	11.3072(8)	10.8824	-0.02719	11.6	25	3.000	0.000	2.000	0.000	0.000	3.000	0.000	0.000	0.000	0.000
81	-	11.2890(3)	10.8300	-0.02983	12.67	25	3.000	0.000	2.000	0.000	0.000	3.000	0.000	0.000	0.000	0.000
81	-	11.2563(7)	10.7361	-0.02309	14.9	25	3.000	0.000	2.000	0.000	0.000	3.000	0.000	0.000	0.000	0.000
81	-	11.2216(8)	10.6372	-0.01844	17.3	25	3.000	0.000	2.000	0.000	0.000	3.000	0.000	0.000	0.000	0.000

81	-	11.1885(13)	10.5433	-0.02522	19.4	25	3.000	0.000	2.000	0.000	0.000	3.000	0.000	0.000	0.000	0.000
81	-	11.1630(13)	10.4714	-0.02106	21.3	25	3.000	0.000	2.000	0.000	0.000	3.000	0.000	0.000	0.000	0.000
81	-	11.6068(8)	11.7706	-0.02467	0.0001	25	3.000	0.000	2.000	0.000	0.000	0.000	3.000	0.000	0.000	0.000
81	-	11.5631(8)	11.6381	-0.01540	2.3	25	3.000	0.000	2.000	0.000	0.000	0.000	3.000	0.000	0.000	0.000
81	-	11.5577(8)	11.6218	-0.02044	2.49	25	3.000	0.000	2.000	0.000	0.000	0.000	3.000	0.000	0.000	0.000
81	-	11.5433(9)	11.5785	-0.01770	3.28	25	3.000	0.000	2.000	0.000	0.000	0.000	3.000	0.000	0.000	0.000
81	-	11.5139(8)	11.4902	-0.01741	4.85	25	3.000	0.000	2.000	0.000	0.000	0.000	3.000	0.000	0.000	0.000
81	-	11.4874(9)	11.4111	-0.02512	6.17	25	3.000	0.000	2.000	0.000	0.000	0.000	3.000	0.000	0.000	0.000
81	-	11.4765(8)	11.3786	-0.02019	6.88	25	3.000	0.000	2.000	0.000	0.000	0.000	3.000	0.000	0.000	0.000
81	-	11.4556(10)	11.3166	-0.02217	8.05	25	3.000	0.000	2.000	0.000	0.000	0.000	3.000	0.000	0.000	0.000
81	-	11.4326(10)	11.2485	-0.02506	9.36	25	3.000	0.000	2.000	0.000	0.000	0.000	3.000	0.000	0.000	0.000
81	-	11.4087(9)	11.1781	-0.02862	10.75	25	3.000	0.000	2.000	0.000	0.000	0.000	3.000	0.000	0.000	0.000
81	-	11.3905(9)	11.1247	-0.02382	12	25	3.000	0.000	2.000	0.000	0.000	0.000	3.000	0.000	0.000	0.000
81	-	11.3722(10)	11.0712	-0.01859	13.3	25	3.000	0.000	2.000	0.000	0.000	0.000	3.000	0.000	0.000	0.000
81	-	11.3509(12)	11.0091	-0.02362	14.6	25	3.000	0.000	2.000	0.000	0.000	0.000	3.000	0.000	0.000	0.000
81	-	11.8410(8)	12.4976	-0.02993	0.0001	25	3.000	0.000	2.000	0.000	0.000	0.000	0.000	0.000	3.000	0.000
81	-	11.7910(7)	12.3399	-0.02393	2.3	25	3.000	0.000	2.000	0.000	0.000	0.000	0.000	0.000	3.000	0.000
81	-	11.7859(8)	12.3239	-0.02707	2.49	25	3.000	0.000	2.000	0.000	0.000	0.000	0.000	0.000	3.000	0.000
81	-	11.7691(9)	12.2713	-0.02719	3.28	25	3.000	0.000	2.000	0.000	0.000	0.000	0.000	0.000	3.000	0.000
81	-	11.7386(9)	12.1761	-0.02240	4.85	25	3.000	0.000	2.000	0.000	0.000	0.000	0.000	0.000	3.000	0.000
81	-	11.7351(9)	12.1653	-0.02588	4.97	25	3.000	0.000	2.000	0.000	0.000	0.000	0.000	0.000	3.000	0.000
81	-	11.7099(7)	12.0871	-0.03160	6.17	25	3.000	0.000	2.000	0.000	0.000	0.000	0.000	0.000	3.000	0.000
81	-	11.6982(8)	12.0509	-0.02625	6.88	25	3.000	0.000	2.000	0.000	0.000	0.000	0.000	0.000	3.000	0.000
81	-	11.6752(9)	11.9799	-0.03077	8.05	25	3.000	0.000	2.000	0.000	0.000	0.000	0.000	0.000	3.000	0.000
81	-	11.6516(9)	11.9074	-0.03172	9.36	25	3.000	0.000	2.000	0.000	0.000	0.000	0.000	0.000	3.000	0.000
81	-	11.6260(8)	11.8291	-0.03709	10.75	25	3.000	0.000	2.000	0.000	0.000	0.000	0.000	0.000	3.000	0.000
81	-	11.6110(12)	11.7834	-0.02962	11.8	25	3.000	0.000	2.000	0.000	0.000	0.000	0.000	0.000	3.000	0.000

81	-	12.0537(9)	13.1832	-0.02445	0.0001	25	3.000	0.000	0.000	2.000	0.000	0.000	0.000	0.000	3.000	0.000
81	-	12.0012(7)	13.0117	-0.01446	2.3	25	3.000	0.000	0.000	2.000	0.000	0.000	0.000	0.000	3.000	0.000
81	-	11.9947(8)	12.9906	-0.02134	2.49	25	3.000	0.000	0.000	2.000	0.000	0.000	0.000	0.000	3.000	0.000
81	-	11.9775(8)	12.9348	-0.01896	3.28	25	3.000	0.000	0.000	2.000	0.000	0.000	0.000	0.000	3.000	0.000
81	-	11.9432(7)	12.8240	-0.01908	4.85	25	3.000	0.000	0.000	2.000	0.000	0.000	0.000	0.000	3.000	0.000
81	-	11.9361(9)	12.8011	-0.03374	4.97	25	3.000	0.000	0.000	2.000	0.000	0.000	0.000	0.000	3.000	0.000
81	-	11.9129(10)	12.7266	-0.03985	5.99	25	3.000	0.000	0.000	2.000	0.000	0.000	0.000	0.000	3.000	0.000
81	-	11.9002(9)	12.6860	-0.02274	6.88	25	3.000	0.000	0.000	2.000	0.000	0.000	0.000	0.000	3.000	0.000
81	-	11.8764(10)	12.6100	-0.02528	8.05	25	3.000	0.000	0.000	2.000	0.000	0.000	0.000	0.000	3.000	0.000
81	-	11.8508(12)	12.5286	-0.02758	9.36	25	3.000	0.000	0.000	2.000	0.000	0.000	0.000	0.000	3.000	0.000
81	-	11.8232(10)	12.4413	-0.03438	10.75	25	3.000	0.000	0.000	2.000	0.000	0.000	0.000	0.000	3.000	0.000
81	-	11.8009(10)	12.3710	-0.04593	11.8	25	3.000	0.000	0.000	2.000	0.000	0.000	0.000	0.000	3.000	0.000
81	-	11.7822(10)	12.3123	-0.03963	13	25	3.000	0.000	0.000	2.000	0.000	0.000	0.000	0.000	3.000	0.000
81	-	11.7611(10)	12.2463	-0.05308	14	25	3.000	0.000	0.000	2.000	0.000	0.000	0.000	0.000	3.000	0.000

[a] American Mineralogist Crystal Structure Database (Downs and Hall-Wallace 2003) identification number

Supplement 3. Unconstrained standard deviation of fit parameters

	$1\sigma^*$	
$W_{grs\text{-}pyr}$	6.8688	(J/bar/mol)
$W_{grs\text{-}alm}$	0.7088	
$W_{grs\text{-}knr}$	39.4974	
$W_{grs\text{-}maj}$	1.9888	
$W_{grs\text{-}nag}$	11.8925	
$W_{grs\text{-}mmr}$	4.3177	
$W_{grs\text{-}sps}$	0.7102	
$W_{pyr\text{-}knr}$	40.8569	
$W_{pyr\text{-}maj}$	0.2379	
$W_{pyr\text{-}kho}$	5.3615	
$W_{pyr\text{-}mmr}$	6.2227	
$W_{alm\text{-}kho}$	25.0387	
$W_{knr\text{-}kho}$	8.2109	
$W_{kho\text{-}sps}$	7.8349	
$dW_{grs\text{-}pyr}$	9.3804	
$dW_{grs\text{-}alm}$	0.2898	
$dW_{grs\text{-}nag}$	24.7981	
$dW_{pyr\text{-}knr}$	88.0329	
$dW_{pyr\text{-}kho}$	10.3325	
V^{grs}_{o}	0.0014	

V^{pyr}_o	0.0016
V^{alm}_o	0.0024
V^{knr}_o	279.9645
V^{sps}_o	0.2312

*Bootstrap estimation of s.d. for each parameter, varying all other fit parameters

Supplement 4. Correlation matrix

	$W_{grs\text{-}pyr}$	$W_{grs\text{-}alm}$	$W_{grs\text{-}knr}$	$W_{grs\text{-}maj}$	$W_{grs\text{-}nag}$	$W_{grs\text{-}mmr}$	$W_{grs\text{-}sps}$	$W_{pyr\text{-}knr}$	$W_{pyr\text{-}maj}$	$W_{pyr\text{-}kho}$	$W_{pyr\text{-}mmr}$	$W_{alm\text{-}kho}$	$W_{knr\text{-}kho}$	$W_{kho\text{-}sps}$	$dW_{grs\text{-}pyr}$	$dW_{grs\text{-}alm}$	$dW_{grs\text{-}nag}$	$dW_{pyr\text{-}knr}$	$dW_{pyr\text{-}kho}$	$V^{grs}{}_o$	$V^{pyr}{}_o$	$V^{alm}{}_o$	$V^{knr}{}_o$	$V^{sps}{}_o$
$W_{grs\text{-}pyr}$	1.0000	-0.5583	0.9733	-0.0116	-0.0091	0.2106	-0.0130	0.9329	-0.0130	0.6599	0.1536	0.9366	0.5960	0.0837	0.8839	0.1769	0.0004	0.9730	0.9636	0.0042	0.0185	0.0193	0.9691	0.0007
$W_{grs\text{-}alm}$	-0.5583	1.0000	-0.6210	0.0425	0.0047	-0.2294	0.0450	-0.7005	0.0336	-0.7922	-0.1088	-0.6724	-0.0961	-0.1061	-0.6930	-0.0110	-0.0035	-0.6312	-0.6091	0.0006	-0.0269	-0.0205	-0.6469	-0.0073
$W_{grs\text{-}knr}$	0.9733	-0.6210	1.0000	-0.0126	-0.0075	0.2160	-0.0158	0.9743	-0.0116	0.7694	0.1525	0.9876	0.4589	-0.0841	0.9617	0.1590	-0.0005	0.9911	0.9970	-0.0038	0.0207	0.0227	0.9949	0.0007
$W_{grs\text{-}maj}$	-0.0116	0.0425	-0.0126	1.0000	0.1808	-0.0639	0.0110	-0.0039	0.0281	-0.0230	-0.0107	-0.0057	-0.0348	-0.1005	-0.0033	-0.0180	-0.0265	-0.0121	-0.0128	-0.0053	0.0103	-0.0352	-0.0104	-0.0056
$W_{grs\text{-}nag}$	-0.0091	0.0047	-0.0075	0.1808	1.0000	-0.1435	0.0113	-0.0055	0.0252	-0.0003	-0.0898	-0.0056	-0.0151	-0.0100	-0.0041	-0.0080	-0.4812	-0.0081	-0.0066	-0.0019	-0.0123	-0.0035	-0.0075	-0.0073
$W_{grs\text{-}mmr}$	-0.2106	0.2294	-0.2160	0.0639	0.1435	1.0000	-0.0332	-0.2217	0.0386	-0.2198	-0.7048	-0.2199	-0.0479	0.1574	-0.2164	-0.0696	-0.1259	-0.2122	-0.2094	-0.0095	-0.0166	-0.0190	-0.2160	-0.0233
$W_{grs\text{-}sps}$	-0.0130	0.0450	-0.0158	0.0110	0.0113	-0.0332	1.0000	-0.0224	-0.0010	-0.0533	-0.0395	-0.0230	-0.0239	-0.0495	-0.0259	-0.0216	-0.0008	-0.0145	-0.0141	-0.0224	-0.0145	-0.0119	-0.0167	-0.9114
$W_{pyr\text{-}knr}$	-0.9329	0.7005	-0.9743	0.0039	0.0055	-0.2217	0.0224	1.0000	-0.0310	0.8427	0.1454	0.9859	0.3200	-0.0867	0.9743	0.1258	-0.0005	0.9746	0.9760	-0.0067	0.0226	-0.0274	0.9845	-0.0004
$W_{pyr\text{-}maj}$	-0.0130	0.0336	-0.0116	0.0281	0.0252	-0.0386	0.0010	-0.0310	1.0000	-0.0709	-0.0227	-0.0326	-0.1131	-0.0186	-0.0484	-0.0091	-0.0008	-0.0067	-0.0212	-0.0374	-0.0233	-0.0102	-0.0133	-0.0123
$W_{pyr\text{-}kho}$	-0.6599	0.7922	-0.7694	0.0230	0.0003	-0.2198	0.0533	-0.8427	0.0709	1.0000	0.1087	-0.8516	-0.1593	-0.0687	-0.8949	-0.0009	-0.0035	-0.7448	-0.7723	-0.0083	-0.0356	-0.0338	-0.7761	-0.0105
$W_{pyr\text{-}mmr}$	-0.1536	0.1088	-0.1525	0.0107	0.0898	-0.7048	0.0395	-0.1454	0.0227	-0.1087	1.0000	-0.1441	-0.0882	-0.0700	-0.1360	-0.0967	-0.1461	-0.1531	-0.1464	-0.0027	-0.0125	-0.0218	-0.1519	-0.0199
$W_{alm\text{-}kho}$	-0.9366	0.6724	-0.9876	0.0057	0.0056	-0.2199	0.0230	-0.9859	0.0326	-0.8516	-0.1441	1.0000	0.3283	-0.0809	0.9917	0.1264	-0.0003	0.9758	0.9907	-0.0059	0.0239	-0.0257	0.9863	-0.0004
$W_{knr\text{-}kho}$	-0.5960	0.0961	-0.4589	0.0348	0.0151	-0.0479	0.0239	-0.3200	0.1131	-0.1593	-0.0882	-0.3283	1.0000	-0.0410	0.2200	0.2269	-0.0021	0.4902	0.4391	-0.0016	0.0021	-0.0055	0.4491	-0.0001
$W_{kho\text{-}sps}$	-0.0837	0.1061	-0.0841	0.1005	0.0100	-0.1574	0.0495	-0.0867	0.0186	-0.0687	-0.0700	-0.0809	-0.0410	1.0000	-0.0773	-0.0100	-0.0267	-0.0902	-0.0802	-0.0006	-0.0129	-0.0024	-0.0885	-0.0201
$dW_{grs\text{-}pyr}$	-0.8839	0.6930	-0.9617	0.0033	0.0041	-0.2164	0.0259	-0.9743	0.0484	-0.8949	-0.1360	-0.9917	-0.2200	-0.0773	1.0000	-0.1040	-0.0002	-0.9461	-0.9694	-0.0064	-0.0251	-0.0274	-0.9615	-0.0008
$dW_{grs\text{-}alm}$	-0.1769	0.0110	-0.1590	0.0180	0.0080	-0.0696	0.0216	-0.1258	0.0091	-0.0009	-0.0967	-0.1264	-0.2269	-0.0100	-0.1040	1.0000	-0.0103	-0.1606	-0.1534	-0.0381	-0.0301	-0.0077	-0.1531	-0.0091
$dW_{grs\text{-}nag}$	-0.0004	0.0035	-0.0005	0.0265	0.4812	-0.1259	0.0008	-0.0005	0.0008	-0.0035	-0.1461	-0.0003	-0.0021	-0.0267	-0.0002	-0.0103	1.0000	-0.0004	-0.0012	-0.0151	-0.0167	-0.0108	-0.0003	-0.0000
$dW_{pyr\text{-}knr}$	-0.9730	0.6312	-0.9911	0.0121	0.0081	-0.2122	0.0145	-0.9746	0.0067	-0.7448	-0.1531	-0.9758	-0.4902	-0.0902	-0.9461	-0.1606	-0.0004	1.0000	-0.9891	-0.0053	-0.0169	-0.0209	-0.9982	-0.0013
$dW_{pyr\text{-}kho}$	-0.9636	0.6091	-0.9970	0.0128	0.0066	-0.2094	0.0141	-0.9760	0.0212	-0.7723	-0.1464	-0.9907	-0.4391	-0.0802	-0.9694	-0.1534	-0.0012	-0.9891	1.0000	-0.0050	-0.0197	-0.0225	-0.9937	-0.0023
$V^{grs}{}_o$	-0.0042	0.0006	-0.0038	0.0053	0.0019	-0.0095	0.0224	-0.0067	0.0374	-0.0083	-0.0027	-0.0059	-0.0016	-0.0006	-0.0064	-0.0381	-0.0151	-0.0053	-0.0050	1.0000	-0.0093	-0.0065	-0.0054	-0.0336
$V^{pyr}{}_o$	-0.0185	0.0269	-0.0207	0.0103	0.0123	-0.0166	0.0145	-0.0226	0.0233	-0.0356	-0.0125	-0.0239	-0.0021	-0.0129	-0.0251	-0.0301	-0.0167	-0.0169	-0.0197	-0.0093	1.0000	-0.0195	-0.0190	-0.0155
$V^{alm}{}_o$	-0.0193	0.0205	-0.0227	0.0352	0.0035	-0.0190	0.0119	-0.0274	0.0102	-0.0338	-0.0218	-0.0257	-0.0055	-0.0024	-0.0274	-0.0077	-0.0108	-0.0209	-0.0225	-0.0065	-0.0195	1.0000	-0.0227	-0.0063
$V^{knr}{}_o$	-0.9691	0.6469	-0.9949	0.0104	0.0075	-0.2160	0.0167	-0.9845	0.0133	-0.7761	-0.1519	-0.9863	-0.4491	-0.0885	-0.9615	-0.1531	-0.0003	-0.9982	-0.9937	-0.0054	-0.0190	-0.0227	1.0000	-0.0009
$V^{sps}{}_o$	-0.0007	0.0073	-0.0007	0.0056	0.0073	-0.0233	0.9114	-0.0004	0.0123	-0.0105	-0.0199	-0.0004	-0.0001	-0.0201	-0.0008	-0.0091	-0.0000	-0.0013	-0.0023	-0.0336	-0.0155	-0.0063	-0.0009	1.0000

Chapter 3

NUCLEAR RESONANT INELASTIC X-RAY SCATTERING OF $(Mg,Fe)SiO_3$ ORTHOENSTATITES

Emily A. Hamecher

Jennifer M. Jackson

Wolfgang Sturhahn

This chapter is taken from sections of Jackson JM, Hamecher EA, Sturhahn W (2009) Nuclear resonant X-ray spectroscopy of $(Mg,Fe)SiO_3$ orthoenstatites. Eur J Mineral 21:551-560. doi:10.1127/0935-1221/2009/0021-1932

ABSTRACT

We present nuclear resonant inelastic X-ray scattering (NRIXS) measurements on synthetic samples of orthoenstatite-structured $(Mg,^{57}Fe)SiO_3$, a representative component in Earth's upper mantle. All measurements were performed at ambient conditions. NRIXS spectra were measured for three samples of orthoenstatite containing 20, 13, and 7 mol% $FeSiO_3$. The Debye sound velocities were determined from the low-energy region of the partial phonon density of states (PDOS). With known density and bulk modulus, the shear modulus (μ), compressional (v_P) and shear (v_S) wave velocities have been computed. The sound velocities obtained from NRIXS are in good agreement with sound velocities obtained using Brillouin spectroscopy and ultrasonic methods for similar compositions. An important advantage of NRIXS is access to additional thermodynamic information, such as the average force constant, mean-square displacement, obtained from the PDOS. We discuss the contribution of the vibrational spectra to these quantities.

INTRODUCTION

Some of the best-resolved properties throughout Earth's interior are seismologically determined sound velocities, which probe the in situ state of crustal, mantle, and core material with high spatial resolution. Accurate determination of the sound velocities of deep Earth materials is therefore essential for mapping chemical and thermal properties of Earth's interior to seismic observations (e.g., Bass and Anderson 1984; Wagner et al. 2008). Experimental methods to determine the compressional and shear sound velocities of materials include: ultrasonic interferometry (US), impulsively stimulated light scattering (ISLS), Brillouin inelastic light scattering (BS), inelastic neutron scattering (INS), momentum-resolved inelastic X-ray scattering (IXS), and nuclear resonant inelastic X-ray scattering (NRIXS). All of the above-mentioned methods can be applied to single-crystal or polycrystalline specimens. Selective vibrational quantities are obtained for each method. For example, US, BS, and ISLS provide access to the low-energy (long-wavelength) vibrational states: the sound velocities. The neutron-weighted density of states (DOS) obtained by INS requires larger samples, which in turn strongly limits the highest pressure that can be obtained. IXS provides experimental access to specific phonon branches under extreme pressures (e.g., Antonangeli et al. 2004) and has been successfully combined with theoretical phonon calculations (e.g., Ghose et al. 2006). However, in the case of IXS, one must measure over all momentum-space to determine the DOS, which often requires months of data collection. Under extreme conditions (e.g., confined systems, magnetic fields, high-pressures, high-temperatures), the DOS obtained from NRIXS is much more accessible than other methods and provides

access to thermodynamic quantities. The importance in determining accurate thermodynamic quantities from measured vibrational spectra is imperative for accurate modeling of Earth's interior (e.g., Kieffer 1982). Further comparisons and descriptions of these methods can be found in Angel et al. (2009) and references therein. NRIXS requires a sample bearing a nuclear resonant isotope and has been applied to single-crystals or powdered samples as small as 10 mm laterally (and 1 mm thick).

NRIXS is a high-resolution X-ray spectroscopic method that provides direct access to the partial phonon density of states (PDOS) of the nuclear resonant isotope, ^{57}Fe in this case. That is, all lattice vibrations involving ^{57}Fe-nuclei contribute to the measured PDOS, and one may obtain averaged thermodynamic quantities related to the ^{57}Fe-participating nuclei, including: vibrational specific heat per atom at constant volume (c_V), vibrational entropy per atom (S_{vib}), Lamb-Mössbauer factor (f_{LM}), mean force constant (D), vibrational kinetic energy (E_K), and vibrational kinetic energy at 0 K (E_Z) (Sturhahn 2004). From the kinetic energy of the ^{57}Fe-nuclei, one can calculate the β-factor, which relates the equilibrium iron isotope fractionation between two substances (e.g., Polyakov et al. 2007). With known density, the Debye sound velocity is obtained from the low-energy portion of the PDOS. If the bulk modulus of the material is known, the compressional and shear wave velocities and shear modulus can be computed. NRIXS studies related to geophysical applications have primarily been conducted on high symmetry and/or iron-rich materials (Giefers et al. 2000; Mao et al. 2001; Struzhkin et al. 2001; Hu et al. 2003; Mao et al. 2004; Lin et al. 2005; Lin et al. 2006; Gao et al. 2008),

but far fewer measurements have been conducted on low symmetry phases (Mao et al. 2006; Gao et al. 2008). We discuss the relevance of symmetry to the PDOS below.

In this contribution, we present NRIXS measurements for three powdered synthetic samples of orthorhombic-structured (Mg,^{57}Fe)SiO_3 orthoenstatite containing representative upper mantle iron concentrations of 20, 13, and 7 mole percent $FeSiO_3$. We show that the sound velocities of orthoenstatite determined from NRIXS are in good agreement with previous ultrasonic (Kumazawa 1969; Frisillo and Barsch 1972; Webb and Jackson 1993; Flesch et al. 1998; Kung et al. 2004) and Brillouin scattering studies (Weidner et al. 1978; Bass and Weidner 1984; Duffy and Vaughan 1988; Jackson et al. 1999, 2007) on similar compositions. Analysis of the raw NRIXS data and interpretation of results were completed as part of the author's first-year graduate work and were published in Jackson et al. (2009). These sections have been extracted from that work and are presented here.

SAMPLE DESCRIPTION

Three powdered samples of (Mg,^{57}Fe)SiO_3 orthoenstatite containing 20, 13, and 7 mole percent $FeSiO_3$ were prepared for the NRIXS measurements. The ^{57}Fe-enriched polycrystalline samples were synthesized from oxides in a piston-cylinder apparatus at the Geophysical Laboratory of the Carnegie Institution of Washington. The starting material consisted of 95% enriched $^{57}Fe_2O_3$, SiO_2, and MgO. The $^{57}Fe_2O_3$ was reduced to FeO in a gas-mixing furnace. SiO_2 and MgO were furnace-fired in an effort to dehydrate the starting materials. Synthesis conditions in the piston cylinder were 1.5 GPa and

1000 °C for a duration of 48 hours. Verification of the structure (space group: *Pbca*) and chemistry of the samples were obtained via powder X-ray diffraction (XRD) and electron microprobe analysis (EMPA), respectively. $(Mg,^{57}Fe)SiO_3$ was identified as the only phase present at the resolution of the above-mentioned techniques (XRD: 5 volume % and EMPA: 5 μm).

NRIXS EXPERIMENTS

The NRIXS experiments were performed at sector 3 ID-B of the Advanced Photon Source (APS) at Argonne National Laboratory under ambient conditions. The energy bandwidth of the incident X-rays determines the resolution of the phonon spectra of the samples. The X-rays were prepared with bandwidths of 1 meV using a multiple-crystal Bragg reflection monochromator (Toellner 2000). We used a Kirkpatrick-Baez mirror system to obtain a focal spot size of 6×6 μm^2 at the full width at half maximum (Zhao et al. 2004). The X-ray flux in this spot was 8×10^8 ph/s, and the resulting spectral flux density was 2×10^{16} ph/s/eV/mm^2 (Sturhahn 2004). The storage ring was operated in low-emittance top-up mode with 24 bunches that were separated by 153 ns. The ~2 mm thick samples were mounted in air on holders for the NRIXS measurements. For each spectrum, the monochromator was tuned from -80 to +100 meV (in 0.25 meV step size with 5 s collection time per energy point) around the nuclear resonance energy of ^{57}Fe, 14.4125 keV. The radiation emitted from the samples was observed with two avalanche photodiode detectors. One detector was placed close to the sample (~2 mm away) to collect the incoherent inelastic scattered photons, and the other detector was placed

downstream (100 cm) in the forward scattering direction, in order to obtain the resolution function independently (Fig. 1). High counting rates were achieved due to the thickness and enrichment of the samples. Therefore, one spectrum per composition was collected. The raw NRIXS spectra are shown in Fig. 2.

DETERMINATION OF THE PDOS AND SOUND VELOCITIES

The NRIXS method directly provides the Fourier-transformed self-intermediate scattering function, $S(\mathbf{k},E) = \frac{1}{2\pi\hbar}\int \left\langle e^{i\mathbf{k}r(t)}e^{-i\mathbf{k}r(0)}\right\rangle e^{iEt/\hbar}dt$, where $\hbar$ is Plank's constant, **k** is the wave vector of the X-rays incident on the sample, and r(t) is the displacement operator of the resonant nucleus (Sturhahn 2004). The quasi-harmonic model of lattice vibrations is then used to extract the partial (due to information about motions of the resonant nuclei only) and projected (due to a potential angular dependence on **k**) phonon DOS from $S(\mathbf{k},E)$ (Sturhahn et al. 1998; Sturhahn 2000) for each composition (Fig. 3). The dependence of $S(\mathbf{k},E)$ on the direction of the incident X-rays is implicitly contained in $S(\mathbf{k},E)$ and is expressed via the directional dependence of the phonon DOS. The description of the anisotropy of the PDOS is given by a symmetric second-rank tensor (e.g., Sturhahn and Kohn 1999), whereas the elastic anisotropy requires a symmetric fourth-rank tensor. For a sample characterized with symmetry lower than cubic, direct inversion of the measured NRIXS spectrum provides a reliable value of the averaged PDOS, if the Lamb-Mössbauer factor remains high (see Sturhahn and Jackson 2007, for a detailed discussion). In the case of orthoenstatite, the Lamb-Mössbauer factor remains high for all three compositions, ~0.7 (see following section).

As explained in previous reports, the energy of an acoustic mode a (E_a) with a small wave number q (long wavelength) that propagates in the direction **q** is given by $E_a = \hbar q v_a(\mathbf{q})$, where v_a is the sound velocity of mode a. The number of phonon states (N_a) in momentum space is then $dN_a = V\int k_a^2 dk_a d\Omega_q$, where $k_a = E_a/(\hbar v)$, V is a normalization volume, and the integration is performed over all directions **q,** symbolized by "$d\Omega_q$". The linear phonon dispersion leads to a Debye-like phonon DOS:

$$D(E) = \frac{m}{2\pi^2\hbar^3\rho}\frac{1}{v_D^3}E^2, \tag{1}$$

$$\text{with } \frac{1}{v_D^3} = \frac{1}{3}\sum_a \int \frac{1}{v_a^3(\mathbf{q})}\frac{d\Omega_q}{4\pi}, \tag{2}$$

where v_D is the Debye sound velocity, ρ is the density of the material, and m is the mass of the nuclear resonant isotope, ^{57}Fe in this case. This relationship is exact for sufficiently small energies (long phonon wavelengths).

The quantitative description of the low-energy region of the phonon DOS provides the Debye sound velocity, v_D. However, the derivation of the Debye sound velocity relies on a linear dispersion that will only be accurate within a limited energy range. Obtaining high-resolution data at low energies is crucial for studies like the present case, where iron is the heavy element in a relatively light matrix of Mg, Si, and O, thereby providing only a small window of accessible low-energy phonon-energies to evaluate the sound velocities. A systematic evaluation of the errors resulting in the selective energy interval (E_1, E_2) of the low-energy portion of the PDOS is therefore necessary in the present case, where E_1 and E_2 represent the low- and high-energy cut-offs in the PDOS. The energy interval (E_1, E_2) for each PDOS is as follows: En80 (2.8, 10.8 meV), En87: (3.8, 12.8 meV), and En93 (6.8, 12 meV). The ranges were selected so that the elastic contribution was less than 10% over the selected energy range, therefore ensuring that the influence of elastic scattering is small compared to the total scattering. Using these selective energy intervals and an improved empirical relation for the dispersion of the acoustic phonons at low-energy (Sturhahn and Jackson 2007), the Debye sound velocity has been determined from the PDOS of each composition. We show a representative fit procedure in Fig. 4 for En80.

For an isotropic solid, the relationship of the Debye sound velocity to the compressional, v_P, and shear, v_S, velocities is determined from Eqs. 1 and 2 (Sturhahn and Jackson 2007):

$$\left(\frac{3}{v_D^3}\right) = \left(\frac{1}{v_P^3}\right) + \left(\frac{2}{v_S^3}\right). \quad (3)$$

One can see from the above relationship that the Debye sound velocity is heavily weighted toward the shear sound velocity. With known density (ρ) and adiabatic bulk modulus (K_S), the isotropic v_P and v_S and shear modulus (μ) follow the additional relationships:

$$\frac{K_S}{\rho} = v_\phi^2 = v_P^2 - \frac{4}{3}v_S^2, \quad (4)$$

$$\frac{\mu}{\rho} = v_S^2 . \quad (5)$$

Combining Eqs. 3 and 4, one obtains the approximate general solutions for v_S and v_P (within 0.1% error, see Sturhahn and Jackson 2007):

$$v_S = 0.952v_D - 0.041v_\phi \quad (6)$$

and

$$v_P = 0.908v_\phi + 0.297v_D + (0.243v_D{}^2/v_\phi). \quad (7)$$

The density of our samples was determined from their measured volumes and chemistry and corrected for their natural iron-enrichment. The K_S values for this study were determined from a linear regression of the Brillouin scattering results for the Mg- (Weidner et al. 1978; Jackson et al. 1999, 2007) and Fe- (Bass and Weidner 1984) end members. In Figs. 5 and 6, we plot our determined sound velocities and elasticity of $(Mg,Fe)SiO_3$ orthoenstatites from NRIXS (Table 1) along with results from previous ultrasonic and Brillouin scattering measurements. In the cases where the full elastic tensor was available, the v_D values were determined from the Christoffel equation and Eqs. 1 and 2. If only the isotropic values of v_S and v_P were given, Eq. 3 was used to determine v_D. We find good agreement with the results from NRIXS in comparison with Brillouin (Weidner et al. 1978; Bass and Weidner 1984; Duffy and Vaughan 1988; Jackson et al. 1999, 2007) and ultrasonic measurements (Kumazawa 1969; Frisillo and

Barsch 1972; Webb and Jackson 1993; Flesch et al. 1998; Kung et al. 2004) on similar compositions. Within the experimental uncertainties of our NRIXS data, all three iron-bearing compositions exhibit the same Debye sound velocity. Reports from ultrasonic measurements on similar compositions also appear independent of iron content for some elastic parameters (Kumazawa 1969; Frisillo and Barsch 1972; Webb and Jackson 1993; Kung et al. 2004). In Fig. 6, we also include the bulk modulus obtained on a suite of synthetic (Mg,Fe)SiO_3 samples determined from single-crystal X-ray diffraction measurements (Hugh-Jones and Angel 1994, 1997), using the isothermal to adiabatic bulk modulus conversion of $K_{0S} = K_{0T}(1 + \alpha\gamma T)$ at 300 K, where $\alpha = 3.2 \times 10^{-5}$ K^{-1} and $\gamma = 1.009$ (Angel and Jackson 2002). Natural orthopyroxenes (OPX) are known to contain minor amounts of Al and Ca, in addition to iron. The substitution of small amounts of Ca into the M2 octahedral site in OPX does not significantly affect its elasticity (Nestola et al. 2006; Perrillat et al. 2007). However, either the coupled substitution of Al into the tetrahedral and octahedral sites or simply the substitution of Al into the tetrahedral site of OPX appears to stiffen the bulk modulus of OPX, in comparison to the Mg end-member (Chai et al. 1997). The v_D values calculated from the measured elastic tensors of the (Al,Fe)- (Chai et al. 1997) and Ca-bearing (Perrillat et al. 2007) orthopyroxenes are 5.37 km/s and 5.31 km/s, respectively, compared to a v_D values of 5.40 km/s for $MgSiO_3$ (Jackson et al. 2007) and 5.20 km/s for $(Mg_{0.8}Fe_{0.2})SiO_3$ (Frisillo and Barsch 1972) orthoenstatites.

THERMODYNAMIC PARAMETERS EXTRACTED FROM THE PDOS

The PDOS provides access to several thermodynamic quantities of the material (Sturhahn 2004). For the orthoenstatite samples measured, we determined the following from the PDOS: c_V, vibrational specific heat per atom at constant volume (k_B/atom); S_{vib}, the vibrational entropy per atom (k_B/atom); f_{LM}, the average Lamb-Mössbauer factor; D (N/m), the mean force constant; E_K, the vibrational kinetic energy; E_Z, the vibrational

kinetic energy at 0 K of the ^{57}Fe nucleus (Table 2; Fig. 7). These are thermodynamic parameters of the ^{57}Fe-participating vibrations. It is interesting to note that although the sound velocities of orthoenstatite do not show an obvious trend within the low iron-concentration region of the solid-solution, quantities derived from the whole spectrum (the PDOS) do show trends. The shape of the PDOS indeed changes as a function of iron content (Fig. 3). This can be understood quantitatively by analyzing the contributions of the vibrational spectrum to the individual thermodynamic quantities. The energy dependence of the PDOS, *g(E),* of the contribution to the mean force constant (*D*) is proportional to $g(E)*E^2$ (Fig. 8). The higher energy regions (E > 10 meV) of the spectra differ significantly as a function of iron content.

In Fig. 9 we plot the energy dependence of the vibrational contributions to the vibrational specific heat per atom at constant volume (c_V) for En80:

$$c_V = 3k_B \int E^2 \left[2k_B T \sinh(E/2k_B T)\right]^{-2} g(E)dE . \quad (8)$$

One can see that all energies are essentially weighted equally at 300 K, which results in minimal effects from c_V to the shapes of the PDOS. The differences will decrease even further at higher temperatures. This effect is the same for En87 and En93. The relationship between the PDOS, *g(E)*, and the Lamb-Mössbauer factor (f_{LM}) (Chumakov and Sturhahn 1999) is as follows:

$$-\ln f_{LM} = E_R \int \left(\frac{1+e^{-\beta E}}{1-e^{-\beta E}}\right)\frac{g(E)}{E}dE = k^2\left\langle x^2\right\rangle, \quad (9)$$

where k is the incident wave vector and $\langle x^2 \rangle$ is the mean-square-displacement of the ^{57}Fe atoms. For vibrational entropy, the relationship is as follows (Sturhahn 2004):

$$S_{vib} = 3k_B \int \left\{\frac{\beta E}{2}\left(\frac{e^{\beta E}+1}{e^{\beta E}-1}\right) - \ln\left[e^{\frac{\beta E}{2}} - e^{-\frac{\beta E}{2}}\right]\right\} g(E)dE . \quad (10)$$

CONCLUDING REMARKS

We have shown that the sound velocities of a suite of orthoenstatite samples measured by NRIXS are in good agreement with sound velocities obtained using ultrasonic and Brillouin scattering methods. More importantly, the lattice vibrations pertaining to the ^{57}Fe-nuclei have been measured. The quantities derived from NRIXS measurements of the PDOS for orthoenstatites offer unique insights into the behavior of iron in materials. The nature of the PDOS obtained from NRIXS involving only ^{57}Fe participating vibrations suggests that these measurements should be complemented with the total phonon density of states to obtain representative thermodynamic behavior of the entire sample.

ACKNOWLEDGEMENTS

We thank Y. Fei (Carnegie Institution of Washington) for synthesizing the orthoenstatite samples, J. Zhao (ANL) for technical assistance at sector 3, D. Zhang (Caltech) for discussions, and two anonymous reviewers for their positive comments and suggestions. Support for this work was provided by the National Science Foundation (NSF) EAR #0711542 (awarded to JMJ). Use of the Advanced Photon Source was supported by the U. S. DOE, Office of Science, and BES (DE-AC02-06CH11357). This research was partially supported by COMPRES under NSF Cooperative Agreement EAR 06-49658.

REFERENCES

Angel RJ, Jackson JM (2002) Elasticity and equation of state of orthoenstatite, $MgSiO_3$. Am Mineral 87:558–561

Angel RJ, Jackson JM, Reichmann HJ, Speziale S (2009) Elasticity measurements of minerals: a review. Eur J Mineral 21:525-550

Antonangeli D, Occelli F, Requardt H, Badro J, Fiquet G, Krisch M (2004) Elastic anisotropy in textured hcp-iron to 112 GPa from sound wave propagation measurements. Earth Planet Sci Lett 225:243–251

Bass JD, Anderson DL (1984) Composition of the upper mantle: geophysical tests of two petrological models. Geophys Res Lett 11:237–250

Bass JD, Weidner DJ (1984) Elasticity of single-crystal orthoferrosilite. J Geophys Res 89:4359–4371

Chai M, Brown M, Slutsky LJ (1997) The elastic constants of an aluminous orthopyroxene to 12.5 GPa. J Geophys Res 102:14779–14785

Chumakov AI, Sturhahn W (1999) Experimental aspects of inelastic nuclear resonant scattering. Hyperfine Interact 123–124:781–808

Duffy TS, Vaughan MT (1988) Elasticity of enstatite and its relationship to crystal-structure. J Geophys Res 93:383–391

Flesch LM, Li BS, Liebermann RC (1998) Sound velocities of polycrystalline $MgSiO_3$-orthopyroxene to 10 GPa at room temperature. Am Mineral 83:444–450

Frisillo AL, Barsch GR (1972) Measurement of single-crystal elastic-constants of bronzite as a function of pressure and temperature. J Geophys Res 77:6360–6384

Gao L, Chen B, Wang J, Alp EE, Zhao J, Lerche M, Sturhahn W, Scott H, Huang F, Ding Y, Sinogeikin SV, Lundstrom CC, Bass JD, Li J (2008) Pressure-induced magnetic transition and sound velocities of Fe_3C: Implications for carbon in the Earth's inner core. Geophys Res Lett 35:L17306. doi:10.1029/2008GL03481

Ghose S, Krisch M, Oganov AR, Beraud A, Bosak A, Gulve R, Seelaboyina R, Yang H, Saxena SK (2006) Lattic dynamics of MgO at high pressure: theory and experiment. Phys Rev Lett 96:035507

Giefers H, Lubbers R, Rupprecht K, Wortmann G, Alfe D, Chumakov AI (2000) Phonon spectroscopy of oriented hcp iron. High P Res 22:501–506

Hu MY, Sturhahn W, Toellner TS, Mannheim PD, Brown DE, Zhao J, Alp EE (2003) Measuring velocity of sound with nuclear resonant inelastic X-ray scattering. Phys Rev B 67:094304. doi:10.1103/PhysRevB.1167.094304

Hugh-Jones DA, Angel RJ (1994) A compressional study of $MgSiO_3$ orthoenstatite up to 8.5 GPa. Am Mineral 79:405–410

Hugh-Jones DA, Angel RJ (1997) Effect of Ca^{2+} and Fe^{2+} on the equation of state of $MgSiO_3$ orthopyroxene. J Geophys Res 102:12333–12340

Jackson JM, Sinogeikin SV, Bass JD (1999) Elasticity of $MgSiO_3$ orthoenstatite. Am Mineral 84:677–680

Jackson JM, Sinogeikin SV, Bass JD (2007) Sound velocities and single-crystal elasticity of orthoenstatite to 1073 K at ambient pressure. Phys Earth Planet Inter 161**:**1–12

Jackson JM, Hamecher EA, Sturhahn W (2009) Nuclear resonant X-ray spectroscopy of $(Mg,Fe)SiO_3$ orthoenstatites. Eur J Mineral 21:551-560. doi:10.1127/0935-1221/2009/0021-1932

Kieffer SW (1982) Thermodynamics and lattice vibrations of minerals: 5. Applications to phase equilibria, isotopic fractionation, and high-pressure thermodynamic properties. Rev Geophys 20:827–849

Kumazawa M (1969) Elastic constants of single-crystal orthopyroxene. J Geophys Res 74:5973–5980

Kung J, Li BS, Uchida T, Wang YB, Neuville D, Liebermann RC (2004) In-situ measurements of sound velocities and densities across the orthopyroxene -> high-pressure clinopyroxene transition in $MgSiO_3$ at high pressure. Phys Earth Planet Inter 147:27–44

Lin JF, Sturhahn W, Zhao J, Shen G, Mao HK, Hemley RJ (2005) Sound velocities of hot dense iron. Science 308:1892–1894

Lin JF, Jacobsen SD, Sturhahn W, Jackson JM, Zhao J, Yoo CS (2006) Sound velocities of ferropericlase in the Earth's lower mantle. Geophys Res Lett 33. doi:10.1029/2006GL028099

Mao HK, Xu J, Struzhkin VV, Shu J, Hemley RJ, Sturhahn W, Hu MY, Alp EE, Vacadlo L, Alfè D, Price GD, Gillan MJ, Schwoerer-Böhning M, Häusermann D, Eng P, Shen G, Geifers H, Lübbers R, Wortman G (2001) Phonon density of states of iron to 153 gigapascals. Science, 292:914–916

Mao WL, Sturhahn W, Heinz DL, Mao HK, Shu J, Hemley RJ (2004) Nuclear resonant X-ray scattering of iron hydride at high pressure. Geophys Res Lett 31:LI5618. doi:10.1029/2004GL020541

Mao WL, Mao HK, Sturhahn W, Zhao J, Prakapenka VB, Meng Y, Shu J, Fei Y, Hemley RJ (2006) Iron-rich post-perovskite and the origin of the ultra low velocity zone. Science 312:564–565

Nestola F, Gatta GD, Boffa Ballaran T (2006) The effect of Ca substitution of the elastic and structural behavior of orthoenstatite. Am Mineral 91:809–815

Perrillat JP, Nestola F, Sinogeikin SV, Bass JD (2007) Single-crystal elastic properties of $Ca_{0.07}Mg_{1.93}Si_2O_6$ orthopyroxenes. Am Mineral 92:109–113

Polyakov VB, Clayton RN, Horita J, Mineev SD (2007) Equilibrium iron isotope fractionation factors of minerals: Reevaluation from the data of nuclear inelastic resonant X-ray scattering and Mössbauer spectroscopy. Geochim Cosmochim Acta 71:3833–3846

Struzhkin VV, Mao HK, Hu J, Schwoere-Bohning M, Shu J, Hemley RJ, Sturhahn W, Hu MY, Alp EE, Eng P, Shen G (2001) Nuclear inelastic X-ray scattering of FeO to 48 GPa. Phys Rev Lett 87:255501

Sturhahn W (2000) CONUSS and PHOENIX: Evaluation of nuclear resonant scattering data. Hyperfine Interact 125:149–172

Sturhahn W (2004) Nuclear resonant spectroscopy. J Phys: Condens Matter 16:5497–5530

Sturhahn W, Jackson JM (2007) Geophysical applications of nuclear resonant spectroscopy. In: Ohtani, E (ed) Advances in High-Pressure Mineralogy, Geological Society of America, pp 157–174

Sturhahn W, Kohn V (1999) Theoretical aspects of inelastic nuclear resonant scattering. Hyperfine Interact 123–124:367–399

Sturhahn W, Alp EE, Toellner TS, Hession P, Hu M, Sutter J (1998) Introduction to nuclear resonant scattering with synchrotron radiation. Hyperfine Interact 113:47–58

Toellner TS (2000) Monochromatization of synchrotron radiation for nuclear resonant scattering experiments. Hyperfine Interact 125:3–28

Wagner LS, Anderson ML, Jackson JM, Beck, SL, Zandt Z (2008) Seismic evidence for orthopyroxene enrichment in the continental lithosphere. Geol 36:935–938

Webb SL, Jackson I (1993) The pressure-dependence of the elastic-moduli of single-crystal orthopyroxene $(Mg_{0.8}Fe_{0.2})SiO_3$. Eur J Mineral 5:1111–1119

Weidner DJ, Wang H, Ito J (1978) Elasticity of orthoenstatite. Phys Earth Planet Inter 17:7–13

Zhao J, Sturhahn W, Lin JF, Shen G, Alp EE, Mao HK (2004) Nuclear resonant scattering at high pressure and high temperatures. High P Res 24:447–457

TABLES

Table 1. Debye sound velocities and other elastic parameters of orthoenstatites determined from the low-energy region of the PDOS.

	Density (g/cc)	v_D (km/s)	v_S (km/s)	v_P (km/s)	K_{0S}^* (GPa)	μ (GPa)
En93	3.26(1)	5.12(20)	4.62(2)	7.83(20)	107.2	70(6)
En87	3.31(1)	5.11(5)	4.62(5)	7.79(10)	106.8	71(2)
Em80	3.36(1)	5.08(7)	4.59(7)	7.23(11)	106.4	71(2)

Notes: (*) fixed values obtained from a linear regression of previous Brillouin scattering results for $MgSiO_3$ and $FeSiO_3$ orthopyroxene as a function of density. A density correction (<1%) to account for natural iron-enrichment was applied to our data. Values in parentheses represent the error in the last significant digit(s).

Table 2. The ^{57}Fe weighted thermodynamic parameters of orthoenstatites determined from the PDOS.

	c_V (k_B/atom)	S_{vib} (k_B/atom)	f_{LM}	D (N/m)	E_Z (meV/atom)	E_K (meV/atom)
En93	2.74(2)	3.61(2)	0.723(3)	195(5)	6.38(8)	14.7(1)
En87	2.75(1)	3.60(1)	0.730(2)	170(3)	6.15(6)	14.01(7)
En80	2.77(2)	3.71(2)	0.709(3)	165(5)	6.11(8)	15.1(1)

Notes: c_V - specific heat per atom at constant volume; S_{vib} - the vibrational entropy per atom; f_{LM} - the average Lamb-Mössbauer factor; D - the mean force constant; E_Z, E_K - vibrational kinetic energy of the nucleus at 0 K and room-temperature, respectively.

FIGURE CAPTIONS

Fig. 1 Typical experimental set-up for NRIXS experiments at third generation synchrotron sources. For high-pressure experiments, focusing mirrors are placed after the monochromator and a diamond anvil cell contains the sample. The "SMS" detector is placed in the forward scattering direction and hence, measures the resolution function (RF) of the NRIXS spectrum independently (modified from Sturhahn and Jackson 2007).

Fig. 2 Raw NRIXS energy spectra, *S(E)*, of (Mg,^{57}Fe)SiO_3 orthoenstatites. The elastic peak has not been removed. Data for En87 and En93 are shifted vertically. The errors in *S(E)* for En87 and En93 are similar to those of En80, but are not plotted for clarity.

Fig. 3 Partial phonon density of states of iron in (Mg,^{57}Fe)SiO_3 orthoenstatites. The PDOS for En87 and En93 are shifted vertically by 100 ev^{-1} and 200 ev^{-1}, respectively.

Fig. 4 Debye velocity (v_D) determination for En80 using an improved method for extracting the sound velocity (see text). The fit was performed on the data (open circles) starting from 2.8 meV (E_1) and ending at 10.8 meV (E_2) (solid line), then extrapolated to $E = 0$ to determine v_D (dashed line). This fit produced a χ^2 of 0.33.

Fig. 5 Debye (v_D, circles), compressional (v_P, diamonds), and shear (v_S, squares) velocities from this experiment (open symbols) along with previous measurements of the enstatite-ferrosilite solid solution series (filled symbols). The dashed lines represent a

linear regression of the enstatite and ferrosilite end-members from Brillouin scattering. Sources of data: 1 = Weidner et al. 1978; 2 = Flesch et al. 1998; 3 = Jackson et al. 1999; 4 = Kung et al. 2004; 5 = Jackson et al. 2007; 6 = Duffy and Vaughan 1988; 7 = Kumazawa 1969; 8 = Frisillo and Barsch 1972; 9 = Webb and Jackson 1993; 10 = Bass and Weidner 1984. A density correction (<1%) to account for natural iron-enrichment was applied to our data. In the cases where the full elastic tensor was available, the v_D values were determined from the Christoffel equation and Eqs. 1 and 2.

Fig. 6 Adiabatic bulk and shear elastic moduli determined from this experiment (triangles) along with previous results (squares) for the orthoenstatite-orthoferrosilite solid solution series. Note that K_S was fixed in our study (see text). Symbols and reference numbers have the same meaning as in Fig. 5. Additionally, 11 = $(Mg,Fe)SiO_3$ orthoenstatite (Hugh-Jones and Angel 1997); 12 = $MgSiO_3$ orthoenstatite (Hugh-Jones and Angel 1994).

Fig. 7 Selected thermodynamic parameters extracted from the PDOS of the orthoenstatites measured with NRIXS in this study: (a) c_V: vibrational specific heat per atom at constant volume (k_B/atom), (b) S_{vib}: the vibrational entropy per atom (k_B/atom), (c) f_{LM}: the Lamb-Mössbauer factor, and (d) the mean force constant, D (N/m).

Fig. 8 The energy dependence of the vibrational contributions to the mean force constant (D). One can see that the higher energy regions of the spectra differ significantly as a function of iron content.

Fig. 9 The energy dependence of the vibrational contributions to the vibrational specific heat at constant volume (c_V), where k_B is the Boltzman factor and T = 300 K for En80. One can see that all energies are essentially weighted equal at this temperature, which results in minimal effects on the shape of the PDOS. This effect is the same for the two other compositions.

FIGURES

Fig. 1

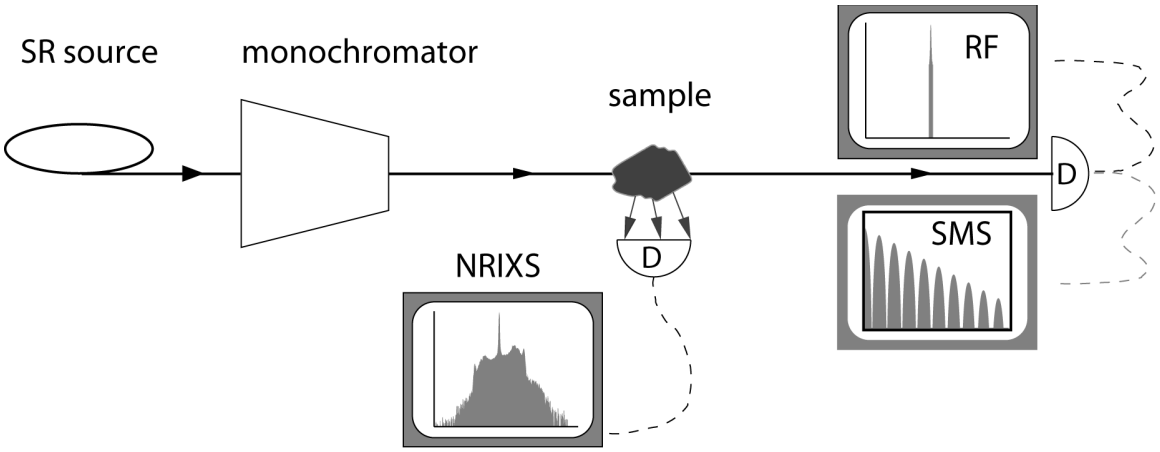

Fig. 2

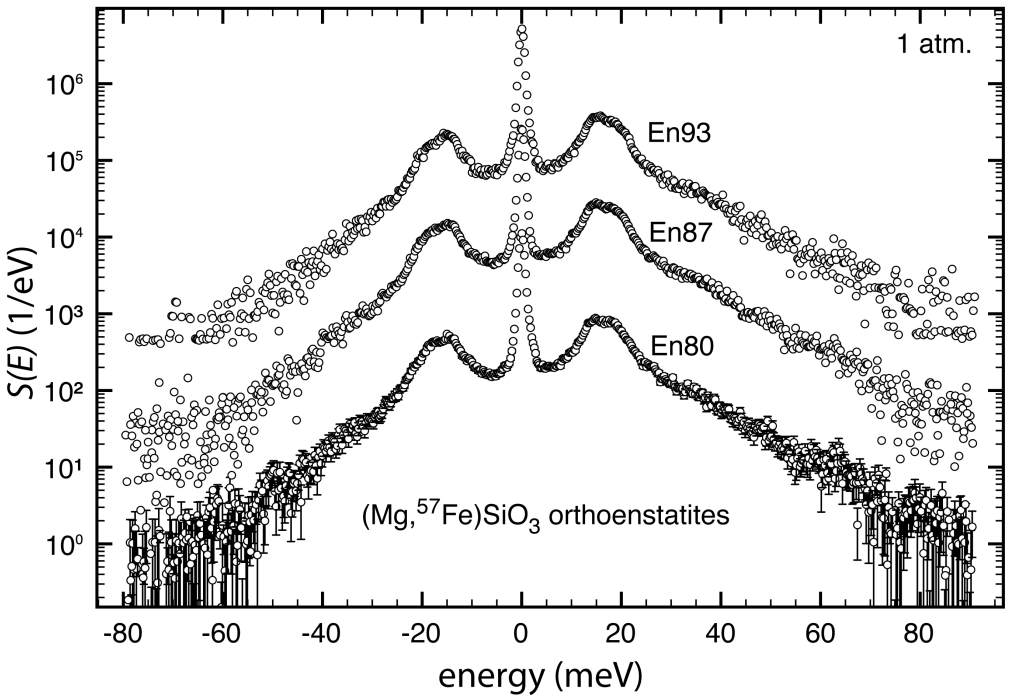
1 atm.
En93
En87
En80
(Mg,57Fe)SiO3 orthoenstatites
S(E) (1/eV)
energy (meV)
10⁶
10⁵
10⁴
10³
10²
10¹
10⁰
-80
-60
-40
-20
0
20
40
60
80

Fig. 3

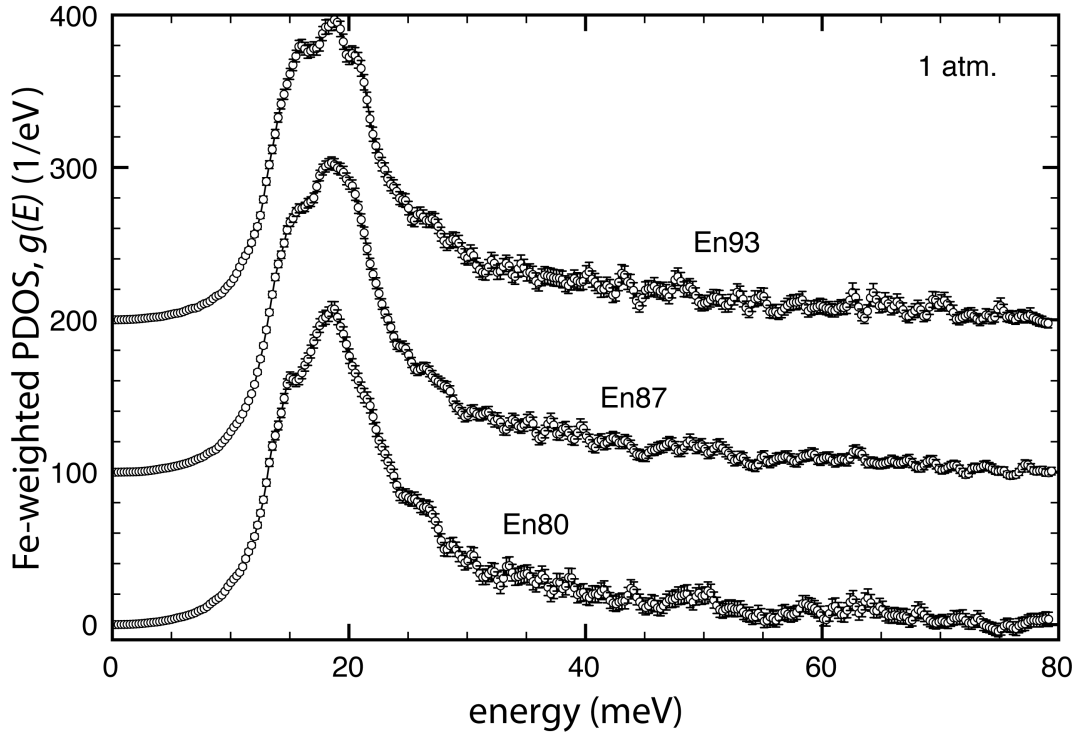
1 atm.
En93
En87
En80
Fe-weighted PDOS, g(E) (1/eV)
energy (meV)
0
100
200
300
400
0
20
40
60
80

Fig. 4

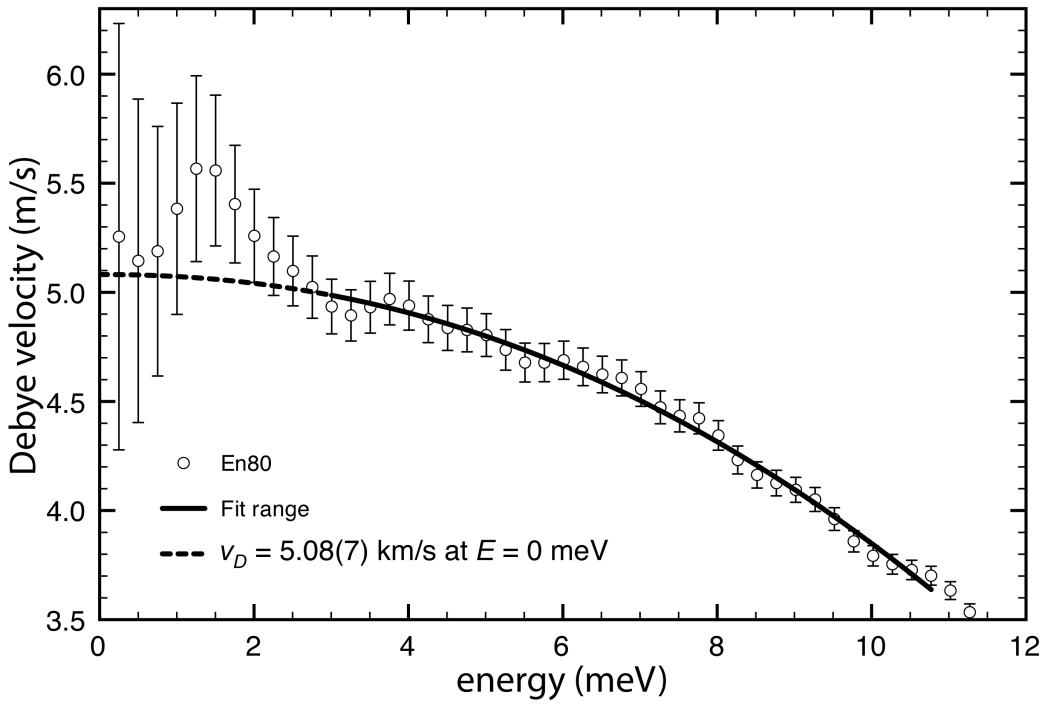
Debye velocity (m/s)
energy (meV)
En80
Fit range
v_D = 5.08(7) km/s at E = 0 meV
6.0
5.5
5.0
4.5
4.0
3.5
0
2
4
6
8
10
12

Fig. 5

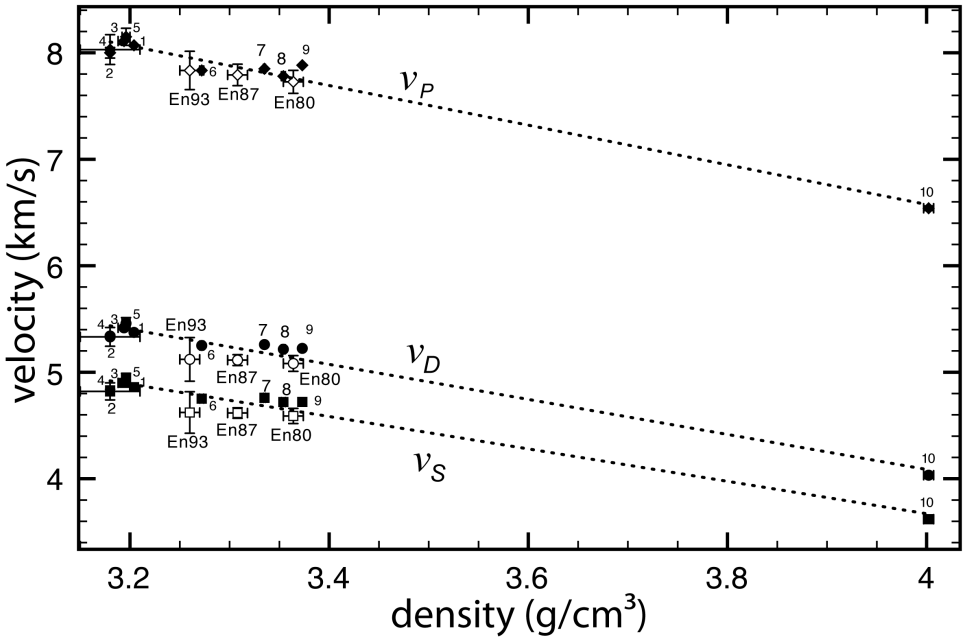
velocity (km/s)
density (g/cm³)
v_P
v_D
v_S
En93
En87
En80
8
7
6
5
4
3.2
3.4
3.6
3.8
4

Fig. 6

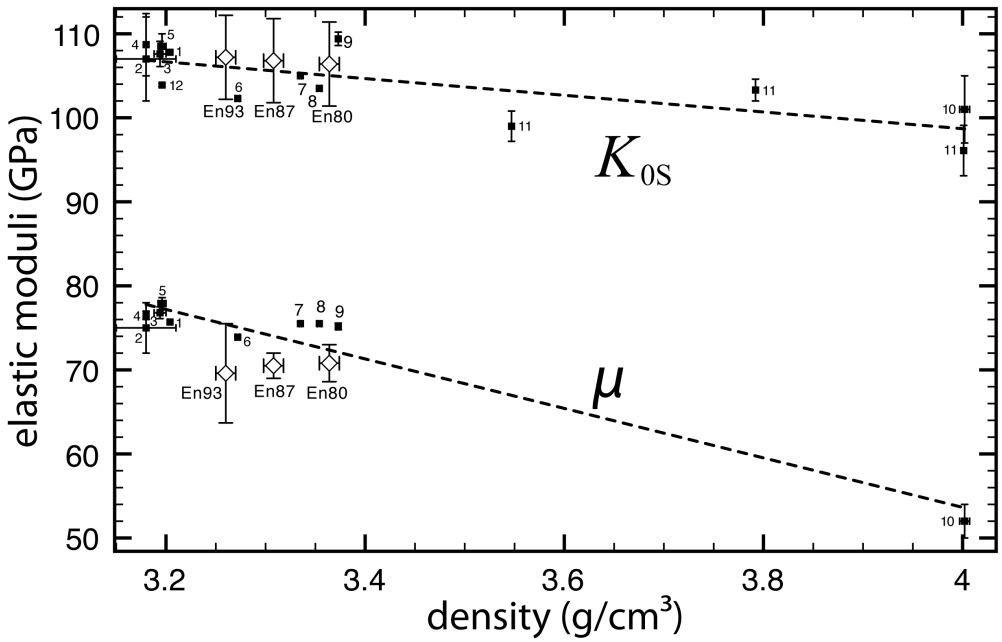
elastic moduli (GPa)
density (g/cm³)
K_{0S}
μ
En93
En87
En80
110
100
90
80
70
60
50
3.2
3.4
3.6
3.8
4

Fig. 7

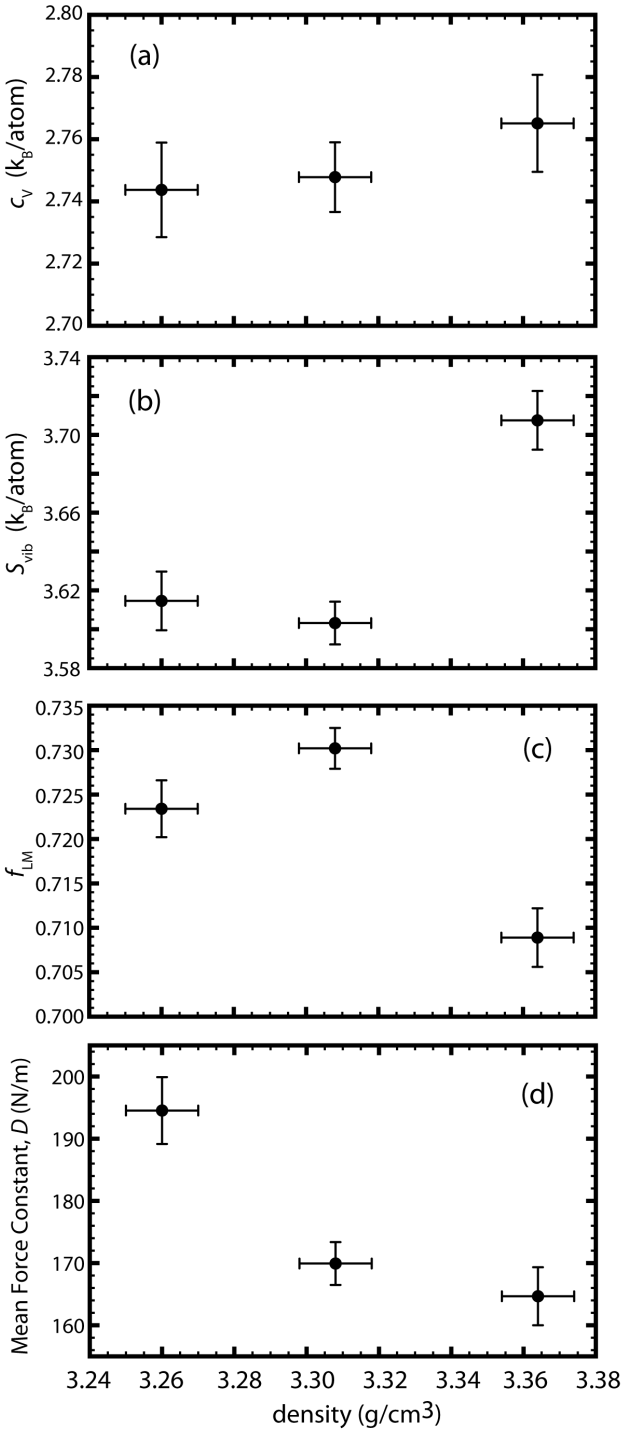
(a)
(b)
(c)
(d)
c_V (k_B/atom)
S_{vib} (k_B/atom)
f_{LM}
Mean Force Constant, D (N/m)
density (g/cm3)
2.80
2.78
2.76
2.74
2.72
2.70
3.74
3.70
3.66
3.62
3.58
0.735
0.730
0.725
0.720
0.715
0.710
0.705
0.700
200
190
180
170
160
3.24
3.26
3.28
3.30
3.32
3.34
3.36
3.38

Fig. 8

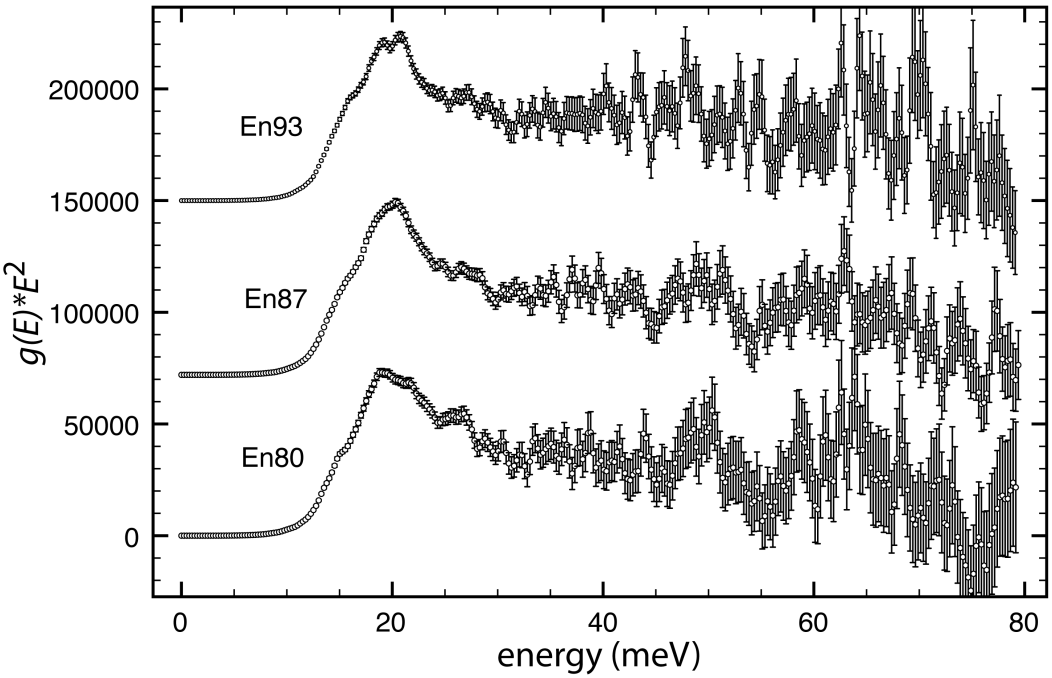
200000
150000
100000
50000
0
g(E)*E2
En93
En87
En80
0
20
40
60
80
energy (meV)

Fig. 9

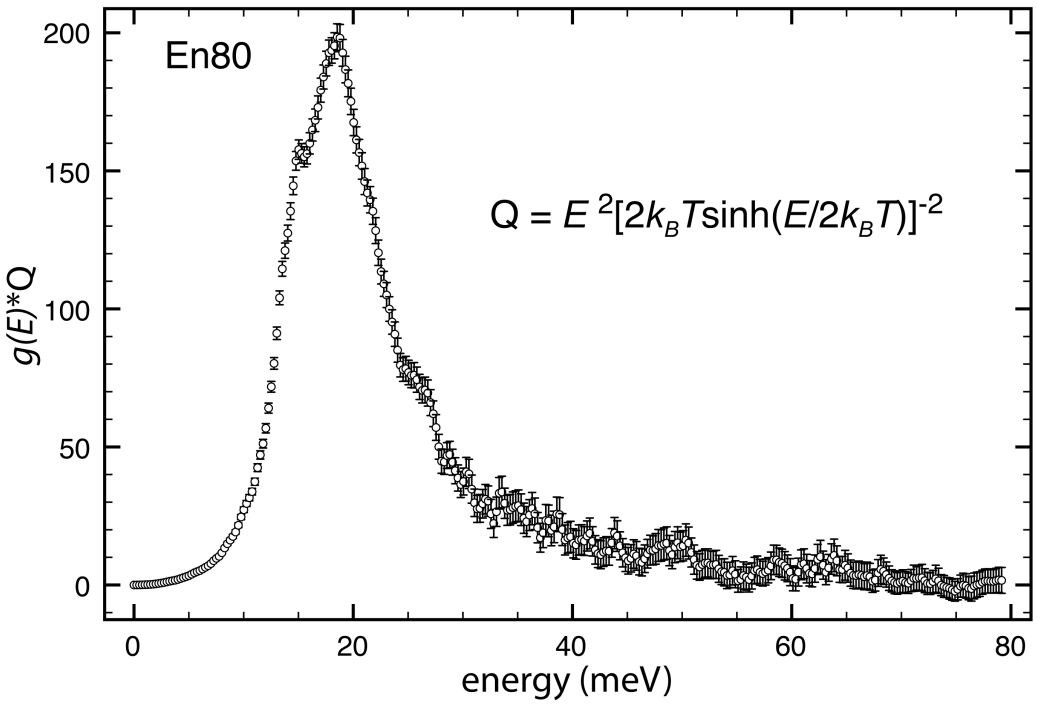
En80
Q = E 2[2kBTsinh(E/2kBT)]-2
g(E)*Q
energy (meV)
0
50
100
150
200
0
20
40
60
80